UNIVERSITÀ DEGLI STUDI DELL'INSUBRIA

SEDE DI COMO

FACOLTÀ DI SCIENZE MATEMATICHE FISICHE E NATURALI

CORSO DI DOTTORATO IN SCIENZE CHIMICHE – CICLO XXI

UNIVERSITÉ PARIS-SUD 11

FACULTÉ DE PHARMACIE

CO-TUTORED PHD THESIS
PRESENTED BY:

ANA SOFIA MARQUES DA RESSURREIÇÃO

TITLE:

SYNTHESIS, CONFORMATIONAL ANALYSIS AND BIOLOGICAL EVALUATION OF PEPTIDOMIMETICS ACTING AS β-SHEET INDUCERS

PHD SUPERVISORS:

PROFESSOR UMBERTO PIARULLI
(UNIVERSITÀ DEGLI STUDI DELL'INSUBRIA)

PROFESSOR SAMES SICSIC
(UNIVERSITÉ PARIS-SUD 11)

ACADEMIC YEAR: 2007-2008

THESIS DEFENCE: December 12th, 2008 (Como, Italy)

JURY MEMBERS:	Professor Umberto Piarulli	Università degli Studi dell'Insubria
	Professor Sames Sicsic	Université Paris 11
	Dr. Sandrine Ongeri	Université Paris 11
	Professor Tiziana Benincori	Università degli Studi dell'Insubria
	Professor Oliver Reiser	Universität Regensburg

For my parents and sister,
to whom I owe everything.

For Tiago,
who was always there for me.

ACKNOWLEDGEMENTS

Firstly, I would like to thank my PhD supervisors: Prof. Umberto Piarulli ("*il capo buono*"), Prof. Sames Sicsic and Dr. Sandrine Ongeri for giving me the opportunity to participate in this research project. I am extremely grateful for their ongoing support, leadership, availability and critical spirit during this thesis, that helped me to grow as a chemist!

In terms of collaborations, I would like to thank:

- Prof. Cesare Gennari (Università degli Sudi di Milano) for his advices and criticism;
- Dr. Laura Belvisi and Monica Civera (Università degli Sudi di Milano) for their precious molecular modelling studies;
- Dr. Leonardo Manzoni (C.N.R. - Istituto di Scienze e Tecnologie Molecolari c/o CISI - Centro Interdisciplinare Studi biomolecolari e applicazioni Industriali);
- and Prof. Michèle Reboud-Ravaux and Laure Dufau (Laboratoire Enzymologie Moléculaire et Fonctionnelle, FRE2852, CNRS – Université Paris 6).

For the financial support, I am grateful to the European Community that financed this project (Contract MEST-CT-2004-515968), granting me a "Marie Curie Early Stage Training Fellowship".

I sincerely thank Angelo and Enrica (Como) and Claire (Paris) for all the NMR spectra and all the patience they demonstrated with me. I also thank Sonia (Como) and Karine (Paris) for the microanalysis.

A special thanks to Patrizia, Barbara, Daminano, Gianni (in Como) and Jean-Louis, Julia, Cyril, Jordi (in Paris), for being so nice to me and for the pleasant and warm atmosphere in the laboratory.

I would like to thank all the members of this project: Karine, Lucia, Chiara, Anamaria, Bertrand, Hans, Andrea and Regis. A special thank to "*the girls*": mes petites Karine and Chiara who shared with me the adventures of living in Italy, and Lucia and Anamaria for their presence and support during the last months in France.

To all my colleagues and friends in Italy and France: Mitch, Collo, Giorgio, Borsini, Silvia ("gruppo Broggini"), Chicco, Nathan, Gerardo, Francesca and, specially, "*Steffffano*", Alice and Marco ("gruppo Piarulli"); thank you for all the fun that we had together, inside and outside the laboratory. To Marco (or "*Duru*" in Italian with a Portuguese accent) I have to dedicate a special thanks, because it is definitely not easy to be co-tutored by someone like me…thank you for this fulfilling experience!

A warm thank you to all my friends in Portugal (the best ones in the world), that supported me at distance.

My parents and sister receive my greatest wholeheartedly thank you for their support, understanding, helpfulness and encouragement they gave me all through this experience.

Last but not least, I thank Tiago who always understood and supported my choices, and that helped me believe that it was possible. Thank you for all the stupid things that make me laugh, even in the difficult moments, for all the adventures, and especially thank you for always being there for me.

Grazie mille a tutti!

TABLE OF CONTENTS

ABSTRACT

There is no doubt that without the ability of nature to form very stable aggregates of small molecules, or to form well-defined secondary, tertiary and even quaternary structures of macromolecules, life as we know it could not exist. The folding of polypeptide chains into secondary and eventually a bewildering array of tertiary structures results in protein molecules that are responsible for most of the biological interactions and functions found in nature.

A logical next step is to mimic nature and to create nonbiological structures, involving intramolecular folding of unnatural molecules that are capable of mimicking or antagonizing the biological action(s) of a natural parent peptide, the so called: **PEPTIDOMIMETICS**.

The development of these chemical model systems provides valuable insights into biomolecular structure and interactions by allowing researchers to simplify, isolate, and manipulate aspects of the complex molecular machinery of living systems.

This thesis reports our efforts towards the design and synthesis of new peptidomimetics that act as secondary structure inducing elements with respect to the growing peptide chain (such as the β-hairpin mimics, discussed in Chapter II) or that are able to establish a defined secondary structure with biological targets. (*i.e.* the molecular tongs discussed in Chapter III).

In Chapter II, a practical synthesis of a new bifunctional diketopiperazine scaffold, formally derived from the cyclization of L-aspartic acid and (*S*)-2,3-diaminopropionic acid, is reported. The scaffold bears a carboxylic acid functionality and an amino functionality in a *cis* relationship, which were used to grow peptide sequences. Conformational analysis of these peptidomimetic sequences reveals the formation of β-hairpin mimics and a reverse turn of the peptide chain.

Synthetic peptides and peptidomimetics, containing the arginine-glycine-aspartate (RGD) sequence, have been used as inhibitors of integrin-ligand interactions. In many cases, the RGD sequence is combined with a secondary structure inducing element to form cyclic peptidomimetics. Therefore, the diketopiperazine scaffold was used to synthesise a cyclic peptidomimetic containing the RGD sequence that was tested as a selective ligand for the $\alpha_v\beta_3$ integrin receptor.

In Chapter III, new peptidomimetics were introduced in molecular tongs for inhibiting HIV-1 protease dimerization.

HIV-1 protease (PR) is a homodimer of two identical 99-amino acid subunits in which the active site is generated by self-assembly of these subunits. Remarkably, the antiparallel β-sheet formed by interdigitation of N- and C-terminal strands of each protease monomer,

which contributes over 75% to the stabilization force of the dimer, is found relatively free of mutations. By targeting this highly conserved dimerization interface, we demonstrated that HIV-1 protease dimer is disrupted with loss of activity by constrained molecular tongs that are able to establish a stable β-sheet structure with the N- and C-terminal of one PR monomer, mimicking the 4-stranded β-sheet structure of the protease dimer. Herein, we describe the design, synthesis, and enzyme inhibitory activity against wild-type HIV-1 PR, of new molecular tongs containing hydrazide-based peptidomimetic fragments in both arms, as well as, new naphthalene-based scaffolds bearing hydrophilic groups.

KEYWORDS: peptidomimetics, diketopiperazine, reverse turn mimic, β-turn, β-peptides, β-hairpin, RGD, integrin, inhibitors, dimerization, β-sheet, HIV-1 protease, molecular tongs, hydrazide.

Part of this thesis was published in:

1. PUBLICATIONS:

Ressurreição, Ana Sofia M.; Bordessa, A.; Civera, M.; Belvisi, L.; Gennari, C.; Piarulli, U. "Synthesis and Conformational Studies of Peptidomimetics Containing a New Bifunctional Diketopiperazine Scaffold Acting as a β-Hairpin Inducer" *J. Org. Chem.* **2008**, *73*, 652-660.

2. POSTERS:

"Synthesis and biological evaluation of new hydrophilic peptidomimetic molecular tongs as inhibitors of HIV-1 protease dimerization", (III.2/P-042).
Ressurreiçao, A.; Vidu, A.; Dufau, L.; Soulier, J.-L.; Sicsic, S.; Reboud-Ravaux, M.; Ongeri, S.; *2nd EuChems Chemistry Congress*, Torino, Italy, September 16-20, 2008.

"Synthesis and biological evaluation of new peptidomimetic molecular tongs as inhibitors of HIV-1 protease dimerization", (D19).
Ressurreiçao, A.; Vidu, A.; Bauvais, C.; Dufau, L.; Sicsic, S.; Reboud-Ravaux, M.; Ongeri, S.; *International Conference in Medicinal Chemistry: Interfacing Chemical Biology, Natural Products and Drug* Discovery, Angers, France, July 2-4, 2008.

"Synthesis and Conformational Analysis of β-Harpin Mimics Containing Bifunctional Diketopiperazine Scaffolds", (P49).
Ana Sofia Ressurreiçao, Monica Civera, Laura Belvisi, Cesare Gennari, Umberto Piarulli, *7th Portuguese National Meeting of Organic Chemistry - Portuguese Chemical Society*, Lisbon, Portugal, July 16-18, 2007.

"Synthesis and Conformational Analysis of β-Harpin Mimics Containing Bifunctional Diketopiperazine Scaffolds", (P25).
Ana Sofia Ressurreiçao, Monica Civera, Laura Belvisi, Cesare Gennari, Umberto Piarulli, *XXXII th Corso Estivo "A. Corbella" Seminari di Sintesi Organica, Gargnano*, Italy, June 18-22, 2007.

"Functionalized Diketopiperazine Scaffolds as Inducers of the Secondary Structure of Proteins", (P51).
Ana Ressurreiçao, Andrea Bordessa, Cesare Gennari, Umberto Piarulli, *Ischia Advanced School of Organic Chemistry – Organic Chemistry from Synthesis to the Interfaces of Life Sciences (IASOC 2006),* Ischia, Italy, September 16-21, 2006.

ABBREVIATIONS

AA	Amino acid
Ac	Acetyl
AcCN	Acetonitrile
AIDS	Acquired Immunodeficiency Syndrome
APCI	Atmospheric Pressure Chemical Ionization
BIV	Bovine Immunodeficiency Virus
Bn	Benzyl
Boc	*tert*-Butyloxycarbonyl
Boc_2O	Di-*tert*-butyldicarbonate
Boc-ON	2-(*tert*-Butoxycarbonyloxyimino)-2-phenylacetonitrile
Cbz	Benzyloxycarbonyl
CD	Circular Dichroism
CHA	Cyclohexylamine
COSY	Correlation Spectroscopy
DABCYL	4-(4-Dimethylaminophenylazo)-benzoic acid
DIAD	Diethyl azodicarboxylate
DIPEA	Diisopropylethylamine
DMEDA	*N*,*N*'-Dimethylethylamine
DMSO	Dimethylsulfoxide
DMSO-d_6	Deuterated dimethylsulfoxide
DMF	*N,N*-Dimethylformamide
DKP	Diketopiperazine
ECM	Extracellular Matrix
EDANS	5-[(2-Aminoethyl)amino]naphthalene-1-sulfonic acid
EDC	*N*-Ethyl-*N*'-[3-(dimethylamino)propyl]-carbodiimide
Equiv	Equivalents
ESI	Electrospray Ionization
Et	Ethyl
EtOAc	Ethyl acetate
FAB	Fast Atom Bombardment
FRET	Fluorescence Resonance Energy Transfer
HAART	Highly Active Antiretroviral Therapy
HATU	*O*-(7-Azabenzotriazol-1-yl)-*N*,*N*,*N*',*N*'-tetramethyluronium hexafluorophosphate

HBTU	*O*-Benzotriazolyl-*N*,*N*,*N*',*N*'-tetramethyluronium hexafluorophosphate
HIV-1	Human Immunodeficiency Virus-1
HOAt	1-Hydroxy-7-azabenzotriazole
HOBt	*N*-Hydroxybenzotriazole
HPLC	High Performance Liquid Chromatography
HRMS	High Resolution Mass Spectroscopy
ICAM	Intercellular Adhesion Molecule
IN	Integrase
IR	Infrared Spectroscopy
M	Molar
Me	Methyl
MeOD	Deuterated methanol
MeOH	Methanol
Mp	Melting point
MS	Mass Spectroscopy
Mtr	4-Methoxy-2,3,6-trimethylbenzenesulfonyl
NMM	*N*-Methyl morpholine
NMR	Nuclear Magnetic Resonance
nNRTI	Non-nucleoside reverse transcriptase inhibitor
NOE	Nuclear Overhauser Effect
NOESY	Nuclear Overhauser Enhancement Spectroscopy
NRTI	Nucleoside Reverse Transcriptase Inhibitor
Ph	Phenyl
ppb	Part per billion
PR	Protease
p-TsOH	*para*-Toluene sulfonic acid
RGD	Arginine-Glycine-Aspartic sequence
ROESY	Rotating frame Overhause Effect Spectroscopy
RT	Reverse Transcriptase
r.t.	Room temperature
Sat.	Saturated
SIV	Simian Immunodeficiency Virus
*t*Bu	*tert*-Butyl
TES	Triethylsilane
TFA	Trifluoroacetic acid
THF	Tetrahydrofuran

NATURAL AMINO ACIDS:

AMINO ACID	ONE-LETTER CODE	THREE-LETTER CODE
Alanine	A	Ala
Arginine	R	Arg
Asparagine	N	Asn
Aspartic acid	D	Asp
Cysteine	C	Cys
Glutamine	Q	Gln
Glutamic acid	E	Glu
Glycine	G	Gly
Histidine	H	His
Isoleucine	I	Ile
Leucine	L	Leu
Lysine	K	Lys
Methionine	M	Met
Phenylalanine	F	Phe
Proline	P	Pro
Serine	S	Ser
Threonine	T	Thr
Tryptophan	W	Trp
Tyrosine	Y	Tyr
Valine	V	Val

UNNATURAL AMINO ACIDS:

Dab	Diaminobutyric acid
Orn	Ornithine
Aib	Aminoisobutyric acid

CHAPTER I:

INTRODUCTION

I. PROTEIN STRUCTURE: OVERVIEW

Proteins play crucial roles in virtually all biological processes. Their significance and the remarkable scope of their activity are exemplified in the following functions: enzymatic catalysis, transport and storage, coordinated motion, mechanical support, immune protection, generation and transmission of nerve impulses and growth control, and differentiation.

Despite the enormous functional diversity, all proteins are built of a single repertoire of 20 amino acids ("building blocks"), meaning that all proteins consist of a linear arrangement of these "building blocks" assembled together into a polypeptide chain. However the flat "two-dimensional" representation of the polypeptide chain fails to convey the beautiful three-dimensional arrangement of proteins. In fact, it is the formation of regular secondary structures into complicated patterns of protein folding that ultimately leads to the characteristic functional properties of proteins: *function arises from conformation.*

Four levels of protein structure are commonly defined (Figure I.1):

(a) Primary structure: is the amino acid sequence of the protein. It arises from covalent linkage of individual amino acids via peptide bonds. Every protein is defined by a unique sequence of residues and all subsequent levels of organization rely on this primary level of structure.

(b) Secondary structure: it is the local conformation of the polypeptide chain or the spatial relationship of amino acid residues that are close together in the primary sequence. In globular proteins the three basic units of secondary structure are the: α-helix, β-sheet and turns.

(c) Tertiary structure: it represents the folded polypeptide chain. It is defined as the spatial arrangement of amino acid residues that are widely separated in the primary sequence. The formation of stable tertiary folds relies on interactions that differ in their relative strengths and frequency in proteins, like: disulfide bonds, hydrophobic effect, charge-charge interactions, hydrogen bonding and Van der Waals interactions.

(d) Quaternary structure: it happens in proteins that have more than one polypeptide chain (also called, subunit). The interaction between these subunits underscores the quaternary structure. The interactions responsible for this kind of protein structure are exactly the same as those responsible for tertiary structure, with the exception that they occur between one or more polypeptide chain.

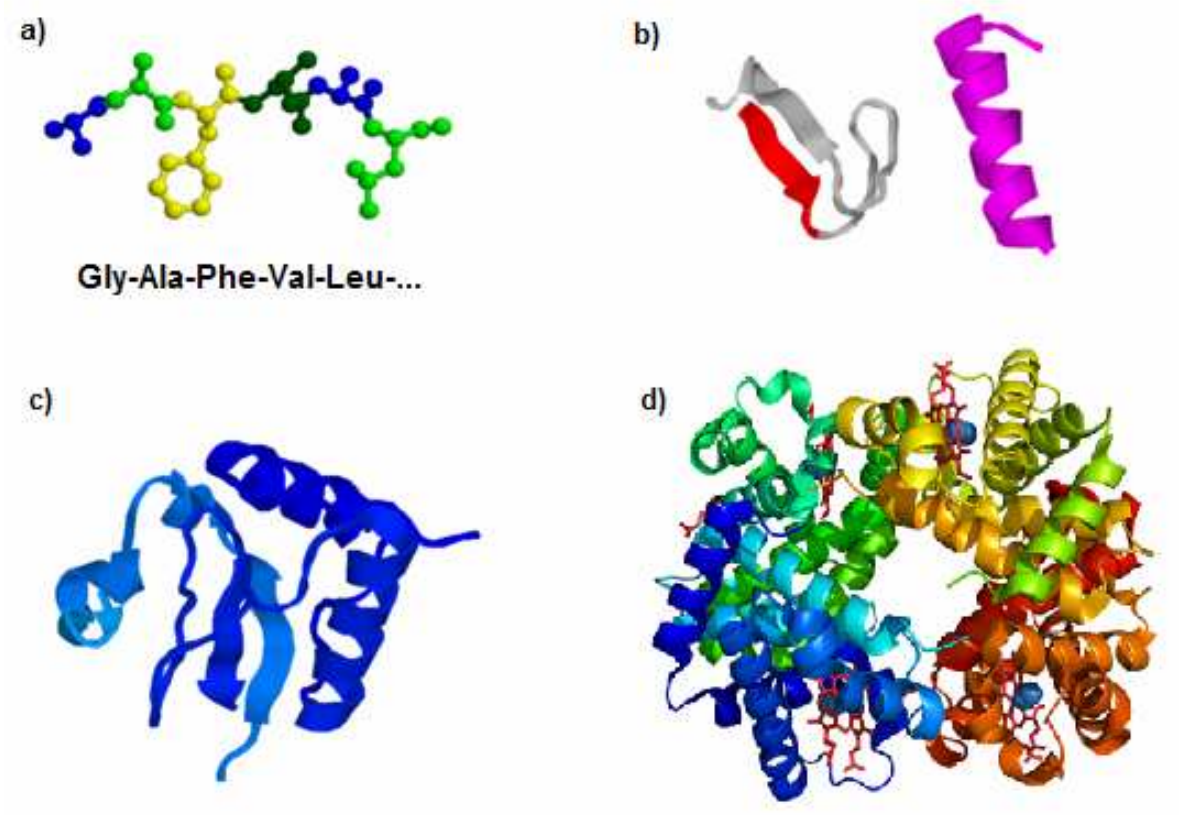

Figure I.1. Four levels of organization within proteins: a) primary, b) secondary, c) tertiary, and d) quaternary.

II. SECONDARY STRUCTURES

II.1 α-HELIX

The α-helix is the most common structural motif found in proteins, in fact, in globular proteins over 30% of all residues are found in helices.

The α-helix is a "rodlike" structure in which the tightly coiled polypeptide main chain forms the inner part of the rod, and the side chains extend outwards. The regular α-helix (Figure I.2) has 3.6 residues per turn with each residue offset from the preceding residue by 0.15 nm (this parameter is called the translation per residue distance). With a translation distance of 0.15 nm and 3.6 residues per turn the pitch (translation distance between any two corresponding atoms on the helix) of the α-helix is simply 0.54 nm (*i.e.* 3.6 x 0.15 nm).

The values of ϕ and ψ (torsion or dihedral angles) adopted in the α-helix allow the backbone atoms to pack close together with few unfavourable contacts. More importantly this arrangement allows some of the backbone atoms to form hydrogen bonds that occur

between the carbonyl oxygen (acceptor) of one residue and the amide hydrogen (donor) of a residue four ahead in the polypeptide chain. In a regular helix the H-bonds are 0.286 nm long from oxygen to nitrogen atoms, linear and lie parallel to the helical axis.

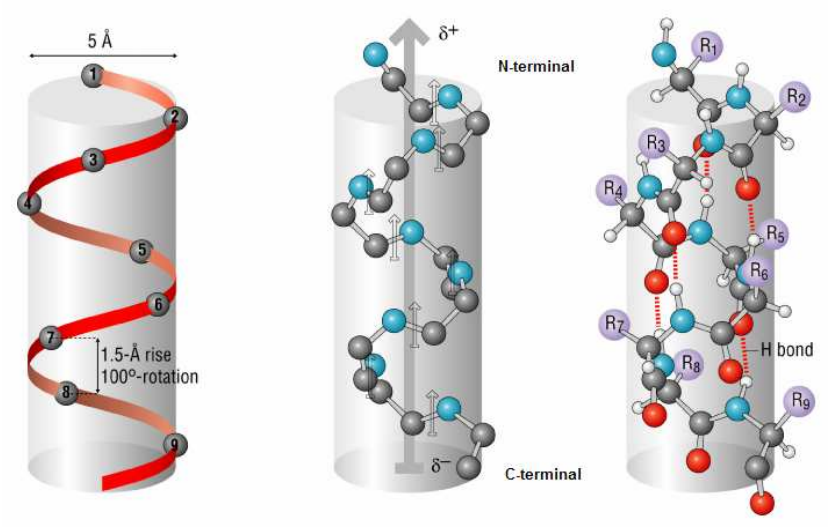

Figure I.2. Regular α-helix.[1]

Hydrogen bonds have directionality that reflects the intrinsic polarization of the H-bond due to the electronegative oxygen atom. In a similar fashion the peptide bond also has polarity and the combined effect of these two parameters gives α-helix pronounced dipole moments. On average the amino end is positive whilst the carbonyl end is negative.

II.2. β-STRAND AND β-SHEETS

The β-strand is the second type of periodic secondary structure and is an extended conformation when compared with the α-helix. In this kind of "zig-zag" conformation (labelled E on the Ramachandran plot, Figure I.3) the translation distance between similar atoms in neighbouring residues is of 0.34 nm, which leads to a pitch of repeated distance of nearly 0.7 nm in a regular β-strand.[2]

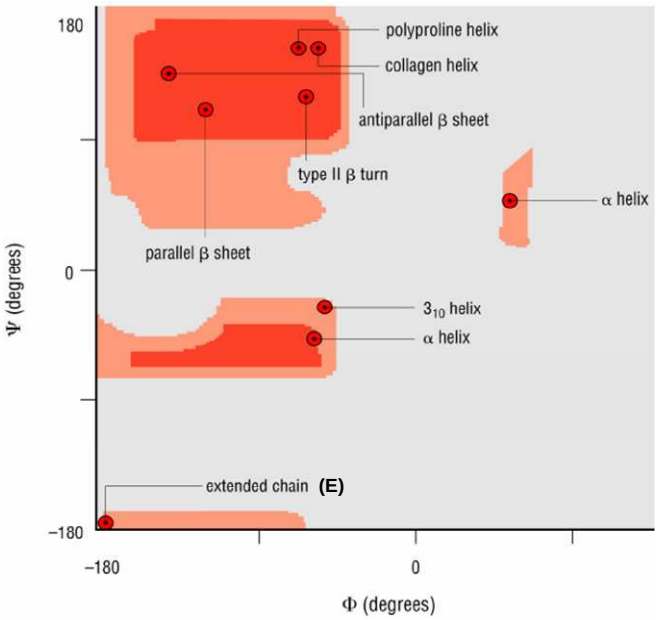

Figure I.3. Ramachandran plot.[3]

A single β-strand (Figure I.4a) is not stable largely because of the limited number of local stabilizing interactions. However, the backbone of N–H and C=O groups are oriented approximately perpendicular to the direction of the chain and therefore these groups are available for interstrand hydrogen bonding. Consequently, hydrogen bonds can be formed between two or more β-strands leading to a stable sheet arrangement. These β-sheets result in significant increase in the overall stability and in the formation of backbone H-bonds between adjacent stands that may involve residues widely separated in the primary sequence. Adjacent strands can align in antiparallel or parallel arrangements with the orientation established by determining the direction of the polypeptide from the N- to the C-terminal. Antiparallel association of β-strands leads to colinear N–H ••• O=C hydrogen bonds and, consequently, to a network of 10- and 14-membered H-bonded rings, while a parallel association of strands leads to deviation from colinearity and to a network of 12-membered H-bonded rings (Figure I.4b and I.4c, respectively). On average β-sheets containing antiparallel strands are more common than sheets made up entirely of parallel strands. Antiparallel sheets are often formed from just two β-strands running in opposite directions whilst it is observed that at least four β-strands are required to form parallel sheets.

Another amazing characteristic of β-sheets is the ability to produce amphipathic structures. This ability arises from the fact that the residues side chains in β-strands point at right angles alternately above and below the plane of the propagating polypeptide chain. As a consequence, patterns in amino acid character in the primary sequence of a segment that

adopts a β-structure can lead to sidedness in the character of a β-sheet. Alternating polar and nonpolar residues will create an amphipathic sheet.

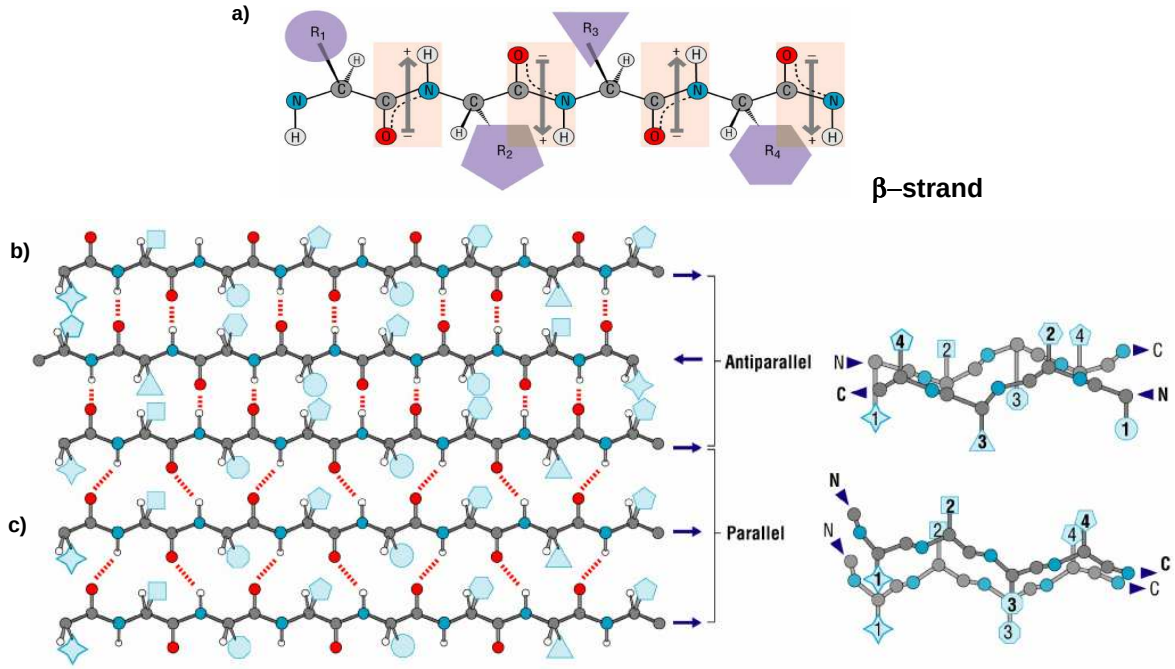

Figure I.4. a) β-strand, b) antiparallel β-sheet and c) parallel β-sheet.[1]

II.3. TURNS AS ELEMENTS OF SECONDARY STRUCTURE

Reverse turns constitute one of the most common structural features in globular proteins. Turns have the universal role of enabling the polypeptide to change direction and in some cases to reverse back on itself. Besides its structural role in the protein fold, turns play also a key role in many of the molecular recognition events in biological systems. These events include interactions between peptide hormones and their receptors, antibodies and antigens, and regulatory enzymes and their corresponding substrates.[4]

Reverse turns comprise the widely distributed β-turns, as well as the less prevalent γ-turns and α-turns, and may include well-defined loops, such as Ω-loops.[5] In current practice, the classification of a turn is based on the preferred torsion angles (ϕ and ψ) of the backbone chain, the position of the stabilizing hydrogen bond, and the length of the chain where the turn occurs.[6] Analysis of the amino acid composition of turns reveals that bulky or branched side chains occur at very low frequencies. Instead, residues with small side chains as: glycine, aspartate, asparagine, serine, cysteine and proline are found preferentially.[5]

A γ-turn (Figure I.5) contains three residues and frequently links adjacent stands of antiparallel β-sheets. This kind of turn is characterized by the fact that the middle residue (*i*+1) does not participate in H-bonding whilst the first and third residues can form the final and initial H-bonds of the antiparallel β-stands, resulting in a 7-membered hydrogen-bonded ring. The change in direction of the polypeptide chain caused by a γ-turn is reflected in the values of ϕ and ψ for the central residue. As result of the size and conformational flexibility, glycine is a favoured residue in this position although other amino acids can be found.

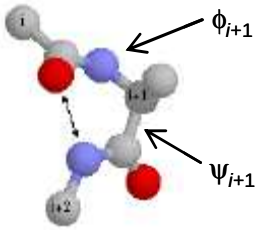

TURN TYPE	ϕ_{i+1}	ψ_{i+1}
CLASSIC γ-TURN	70º to 85º	-60º to -70º
INVERSE γ-TURN	-70º to -85º	60º to 70º

Figure I.5. Torsion angles of classic and inverse γ-turns.[7]

More commonly found in proteins and both linear and cyclic peptides are four residue turns, meaning β-turns. According to the last revaluation of the β-turn classification, nine distinct structural types were suggested based on the ϕ and ψ torsion angles in residues *i*+1 and *i*+2 (Figure I.6).[8] β-turns, may (classical β-turn) or may not (open β-turn) be stabilised by an intramolecular H-bond formed between the C=O of the first residue (*i*) and the N–H of the fourth residue (*i*+3) (abbreviated as 4 → 1 H-bond), giving rise to a 10-membered H-bonded ring.

Two major classes of β-turns meet the stereochemical criteria with all peptide bonds *trans*: type I and type II (Figure I.6).[2] These turns differ in the orientation of the peptide bond between the *i*+1 and *i*+2 residues, and consequently in the preferred side chain dispositions in these positions. In a type I turn, both the *i*+1 and *i*+2 positions accommodate L-residues, however proline preferentially fits in the *i*+2 position. Type I turns are the most prevalent in naturally occurring proteins. In a type II turn, the *i*+1 position can accommodate an L-residue (usually proline) and the *i*+2 position favours a glycine, small polar L-residues, or a D-residue because of steric clash with a side chain in the L-configuration. Proline in the *i*+1 position is a

strong sequence determinant for either a type I or II turn because of the restriction on the ϕ angle from the cyclic side chain.[2]

Other turn geometries are also found. For example, the mirror images of types I and II are known respectively as types I' and II', and are energetically equivalent if residues of the opposite chirality occupy corresponding sequence positions. This means that, for example, a D-Pro residue would be favoured in position *i*+1 of a type I' turn or in position *i*+2 of a type II' turn. On the other hand, the intervening peptide bond (between residue *i*+1 and *i*+2) can adopt a *cis* conformation and still allow the turn to form an *i* to *i*+3 hydrogen bond and link to two β-strands. The resulting turn is called a type VI turn.

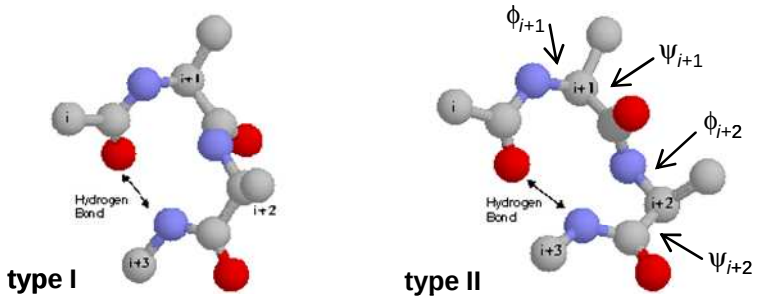

TURN TYPE	ϕ_{i+1}	ψ_{i+1}	ϕ_{i+2}	ψ_{i+2}
I	-60	-30	-90	0
I'	60	30	90	0
II	-60	120	80	0
II'	60	-120	-80	0
IV	-61	10	-53	17
VIa1	-60	120	-90	0
VIa2	-120	120	-60	0
VIb	-135	135	-75	160
VIII	-60	-30	-120	120

Figure I.6. Torsion angles of classic β-turns.[7]

II.4 β-HAIRPIN

β-Hairpins (Figure I.7) are the simplest units that can be constructed from β-strands and β-turns. These occur widely in proteins and make up the fundamental building blocks of antiparallel β-sheet. They are also structures found in many naturally occurring bioactive cyclic peptides such as gramicidin S and the peptide hormones oxytocin and vasopressin.[2]

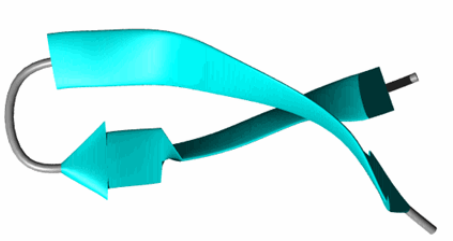

Figure I.7. Ribbon representation of a β-hairpin.[9]

β-hairpins are stabilised by virtue of turn propensities of amino acid residues as well cross-strand interactions between the sequences flaking the turn. Favourable energetic contributions to the stability of these structural features have been demonstrate to include cross-strand aromatic-aromatic, aromatic-polar, H-bonding and salt-bridge interactions in combination with loop conformational propensity and entropy terms dependent on loop length.[10]

A tetrapeptide can adopt a “minimal β-hairpin” conformation (Figure I.8) with residues *i*+1 and *i*+2 involved in the β-turn. This structure is characterized by the presence of 10- and 14-membered H-bonded rings.

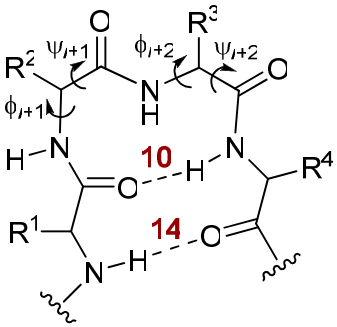

Figure I.8. Minimal β-hairpin.

III. PEPTIDOMIMETICS OF PROTEIN SECONDARY STRUCTURES IN THE β-REGION

There is no doubt that without the ability of nature to form very stable aggregates of small molecules, or to form well-defined secondary, tertiary and even quaternary structures of macromolecules, life as we know it could not exist. The folding of polypeptide chains into secondary and eventually a bewildering array of tertiary structures results in protein molecules that are responsible for most of the biological interactions and functions found in nature.

A logical next step is evidently to mimic nature and to create nonbiologically derived molecules that fold into well-defined structures. Since the early 1990's, a great deal of literature has been devoted to these types of biomimetic structures,[11-17] involving intramolecular folding of unnatural molecules that are capable of mimicking or antagonizing the biological action(s) of a natural parent peptide, the so called: **PEPTIDOMIMETICS**.

The development of these chemical model systems provides valuable insights into biomolecular structure and interactions by allowing researchers to simplify, isolate, and manipulate aspects of the complex molecular machinery of living systems.

III.1. β-AMINO ACIDS AND β-PEPTIDES

Oligomers composed exclusively of β-amino acids (so-called β-peptides) are probably the most thoroughly investigated peptidomimetics.[11,12,14,15,18-20] They have the advantage of being: **(i)** stable to metabolism (exhibit slow microbial degradation, and are inherently stable to proteases and peptidases) and **(ii)** able to mimic α-peptides in peptide-protein and protein-protein interactions; they also fold into well-ordered secondary structures (helices, turns, and sheets) in solution even with short chain lengths.[21]

β-Amino acids represent the smallest step away from α-amino acids in "backbone space", and they can be subdivided into β^3-, β^2-, and $\beta^{2,3}$-amino acids, depending upon the position of the side chain(s) on the 3-aminoalkanoic acid skeleton (Figure I.9).[21]

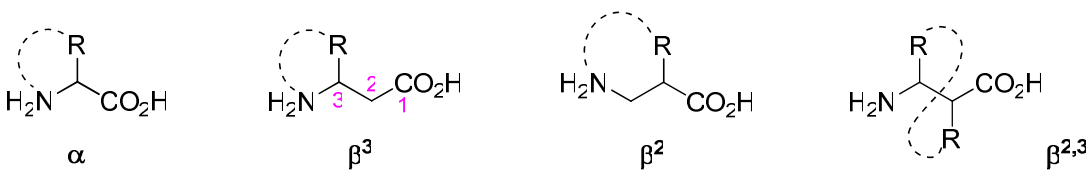

Figure I.9. β-Amino acid classification.

The conformations of β-peptides can be analysed in terms of the main chain torsional angles, which are assigned the ω, ϕ, θ, and ψ angles (Figure I.10) in the convention of Balaram.[22] Folded helical or turnlike conformations of β-peptides require a *gauche* conformation about the θ torsion angle defined by the C^2–C^3 bond. A *trans* rotamer leads to a fully extended conformation, provided the values of ϕ and ψ are appropriate.

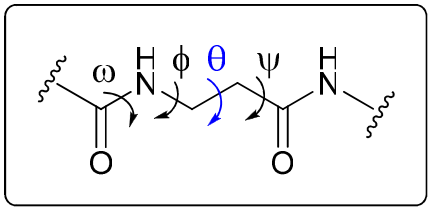

Figure I.10. Definition for torsion angles in β-peptides.

The effects of substituents on the local conformation of a β-amino acid are summarised in Figure I.11. The unsubstituted β-amino acid, β-alanine, is highly flexible, analogous to Gly in the α-amino acids. Alkyl substituents at positions 2 and 3 favour a *gauche* conformation about the C^2–C^3 bond.[23] C^2,C^3-disubstituted amino acids are even more conformationally constrained and favour *gauche* conformers when the substituents are *anti* (aldol convention). When substituents at C^2 and C^3 are *syn*, a *trans* conformation about the C^2–C^3 bond is favoured, which encourages the formation of sheet-like structures.[23-25] It is interesting to consider $C^{2,2}$- and $C^{3,3}$-disubstituted β-amino acids in light of the well-known tendency of dialkyl α-amino acids such as α-aminoisobutyric acid to induce helical and turn-like conformations in α-peptides.[26] In β-peptides, this constraint stabilizes reverse turns.[27,28]

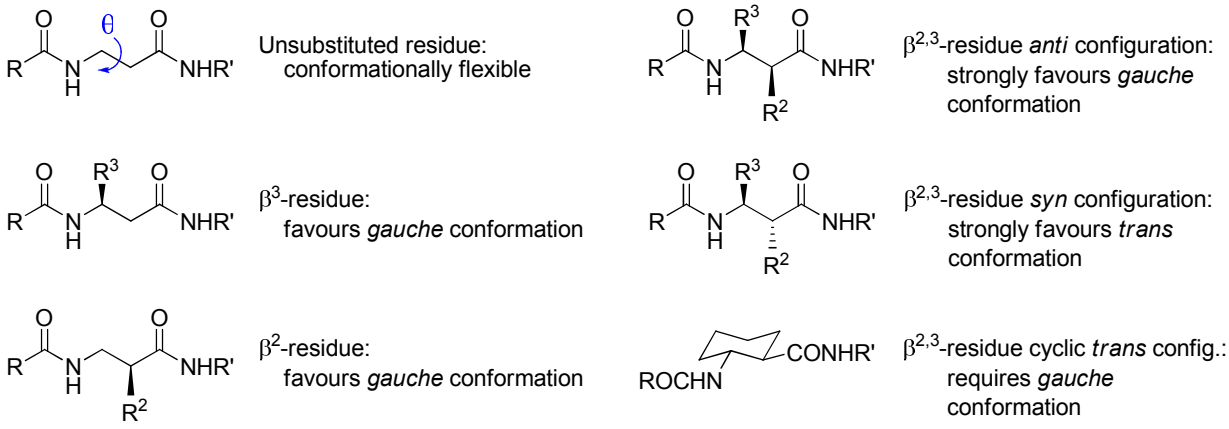

Figure I.11. Effect of substituents on the torsional angle, θ.[15]

β-SHEET-LIKE CONFORMATIONS OF β-PEPTIDES

Besides helical arrangements,[29] β-peptides, like the α-peptidic prototypes, can also adopt non-aggregating extended-chain structures,[30] can assemble to parallel[25,31,32] (Figure I.12a) and antiparallel[24,25,32-34] pleated sheets (the latter being inherently part of a hairpin turn, Figure I.12b), and stack in crystals.[19]

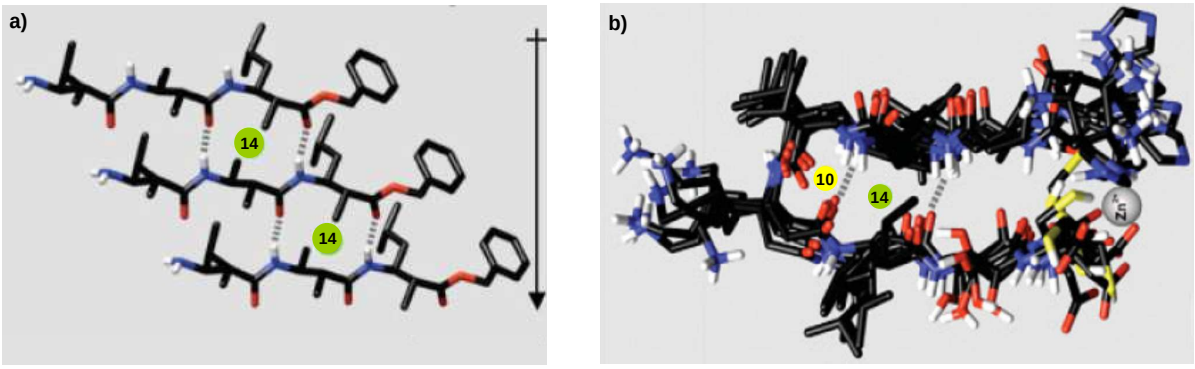

Figure I.12. a) Parallel pleated sheet of a β-tripeptide,[25] b) a β-octapeptide folded into a hairpin-like conformation with antiparallel β-sheet-type H-bonding interaction (Zn^{2+}-enforced turn structure).[33]

There are in principle two types of sheet secondary structure available to β-peptides, one in which each residue has an *anti* C^2–C^3 torsion angle and another in which each residue has a *gauche* C^2–C^3 torsion angle.[24] The "*anti*" type of β-peptide sheet is distinctive since all backbone carbonyls are oriented in approximately the same direction, which would endow the resulting sheet with a net dipole, rendering the β-peptidic sheet polar. In contrast, β-sheets formed by α-peptides have little or no net dipole because the backbone carbonyls alternate in direction along each strand. β-Peptide sheets formed by residues with *gauche* C^2–C^3 torsion angles would lack a net dipole for the same reason.

In the last decade significant progresses have been made toward the goal of preparing β-peptides with sheet-like conformations.

Initial studies performed in Gellman's laboratory led to the identification of an optimal β-amino acid substitution pattern for the strand residues in an antiparallel sheet through the use of hairpin-forming molecules containing non-β-peptide loop segments.[24] It was demonstrated that disubstituted β-amino acid residues with *syn* configuration (*syn* $\beta^{2,3}$-amino acids) favours *anti* C^2–C^3 torsion angles because the alkyl substituents at these positions can adopt an energetically favourable *anti*-orientation only when the N–C^3–C^2–C torsion angle is 180°, and therefore these residues have the highest sheet-forming propensity. Later on, the

same group has also described a loop segment containing a heterochiral dipeptide, composed of the Pro analogue nipecotic acid residues, that adopts a reverse turn conformation and promotes hairpin formation.[35] The resulting tetrapeptide **1** (Figure I.13), contains exclusively β-amino acid residues, and represented the first autonomously folded β-peptide sheet. It was also demonstrated that homochiral dinipecotic acid segments (*i.e.*, both nipecotic acid residues with the same absolute configuration) prevented sheet interactions between the terminal residues.

Seebach's group used a similar strategy to stabilize the formation of β-peptide hairpins in organic solvent.[25] They prepared hexapeptide **2** (also Figure I.13) with the first two and last two residues being *syn*-C^2,C^3-disubstituted β-amino acids. Significantly, Seebach *et al.* found that a dipeptide sequence containing a β^2- followed by a β^3-amino acid stabilised a reverse turn that is different from the reverse turn formed by Gellman's heterochiral dinipecotic acid segment (10-membered ring hydrogen bond in the former *vs* 12-membered ring hydrogen bond in the latter).

The availability of two distinct types of reverse turn among β-peptides highlights the greater conformational diversity in this foldamer family relative to α-peptides in which only a single type of reverse turn (β-turn) is commonly observed.

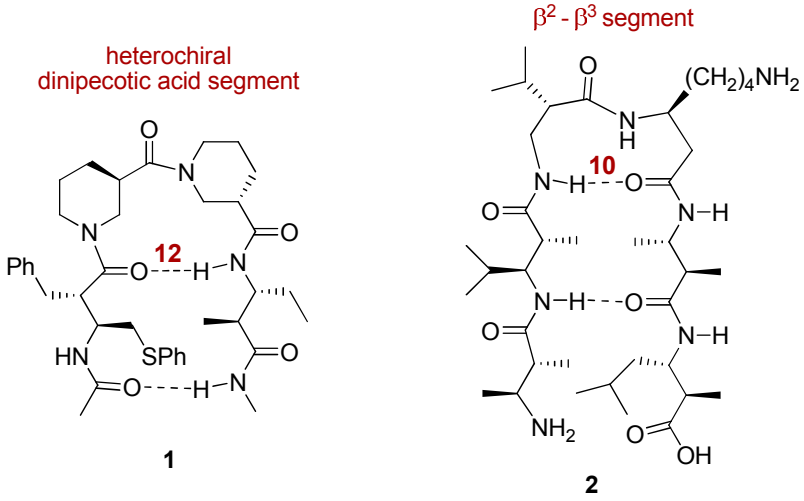

Figure I.13. Different hydrogen-bond patterns in β-peptide hairpins.

Stable β-hairpins generated from hybrid peptide sequences containing both α- and β-amino acids have also been reported.

Balaram and co-workers were the first to describe hairpin-turn formation involving mixed α/β-peptides. They reported an α/β-hybrid octapeptide **3** containing the conventional

D-Pro-Gly α-peptidic turn motif and carrying β-amino acid residues (β^{3}Val or β^{3}Leu)[i] on opposite sides of the antiparallel sheet part of the hairpin.[36] In this case, a hydrogen bond between the C=O of residue *i* and the N–H of residue *i*+3 of the β-turn is formed resulting in a 10-membered H-bonded ring (Figure I.14).

Seebach and co-workers have also reported hairpin-turn secondary structures of mixed α/β-peptides containing novel types of turn structures with 9- and 10-membered H-bonded rings.[37] The hexapeptide **4** consists of β^3-homo-amino, β^2-homo-amino, and α-amino acids with a central β^2–β^3 segment, whereas heptapeptide **5** is composed of β^2-homo-amino and α-amino acids in alternating positions. Despite their small size, these two peptides showed stable hairpin structures showing a turn with a 10-membered H-bonded ring induced by the β^2/β^3 unit, for **4**, and a turn involving the β^{2}Met[ii] and Lys units with a (formally) 9-membered H-bonded ring, for **5** (also Figure I.14).

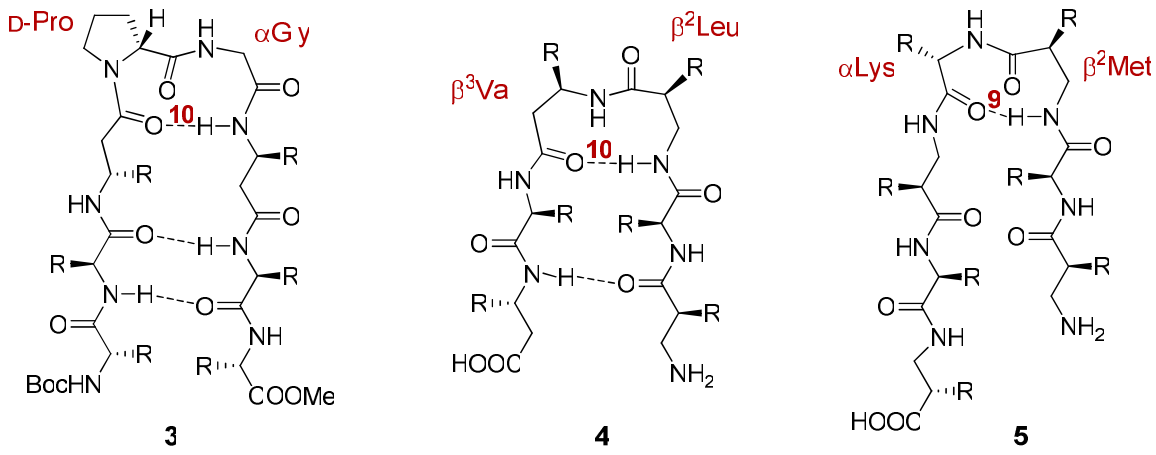

Figure I.14. Schematic representation of hairpin structures involving mixed α/β-peptides.

The enzymatic stability and the variety of secondary structures discovered push the door wide open for the application of β-peptides as peptidomimetics in medicinal chemistry. Once again, Seebach's group synthesised cyclic β-tetrapeptide **6**[38] (Figure I.15) that was able to mimic the α-peptide hormone somatostatin, a peptide responsible for several important biological functions, like the regulation of the release of growth hormone and insulin. Compound **6** also displayed biological activity and micromolar affinity for human receptors.[38]

[i] β^{3}Val: β^3-(*R*)-homovaline and β^{3}Leu: β^3-(*S*)-homoleucine.
[ii] β^{2}Met: β^2-(*S*)-homomethionine.

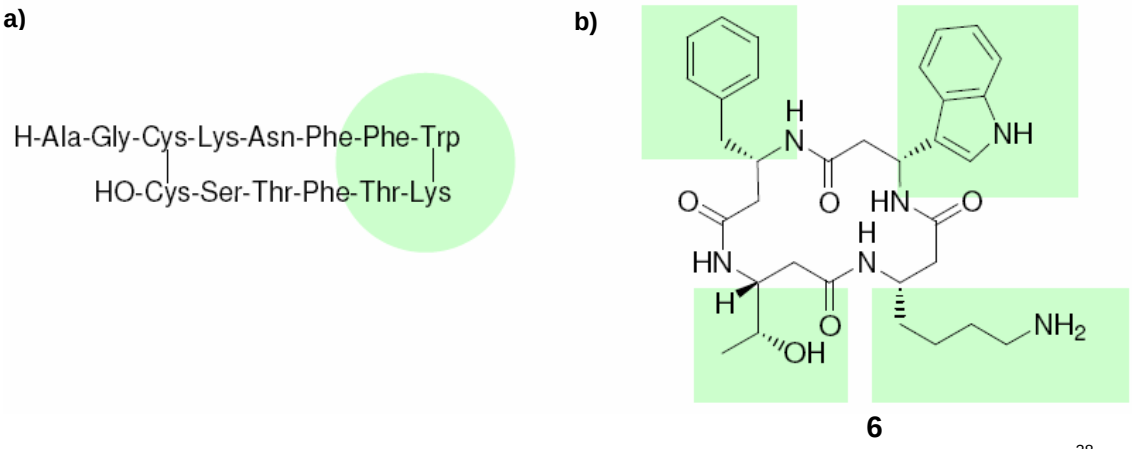

6

Figure I.15. a) The α-peptide hormone somatostatin and b) loop analogue, cyclic β-tetrapeptide **6**.[38]

III.2. β-TURN MIMETICS

In the previous section the role of specific β-amino acids in the nucleation of secondary structure systems was discussed. However, this function may also be performed by synthetic organic templates. Molecular templates may be used in two distinct ways in generating folded polypeptides.[39] First, the designed templates may provide a preorganized folding nucleus which can position hydrogen-bonding groups in a manner that permits propagation of a regular secondary structure. Second, templates may be used to organize prefabricated modules of secondary structure in order to generate compact tertiary folds. Regarding the first case, considerable efforts have been devoted towards the development of structures able to mimic or stabilize β-turns, either in linear or cyclic peptides.

β-turn mimetics can be categorized into two distinct groups: internal and external.[40] Internal mimetics are constructed upon skeletons that lie within the pseudo 10-membered ring framework of the turn motif, and place an emphasis on side chain presentation as displayed by the pioneering structures of Kahn[41] (**7**, Figure I.16). On the other hand, the external mimetics are often constructed on dipeptide isostere skeletons that do not display side chain functionality at the central *i*+1 and *i*+2 positions. These structures reduce the conformational flexibility of a peptide with a rigidified skeleton that lies outside of the turn's general framework, and are primarily employed to orientate the surrounding peptide chain into a turn conformation. Structures **8** and **9** developed by Freidinger[42] and Nagai,[43] respectively, are examples of external turn mimetics (also Figure I.16).

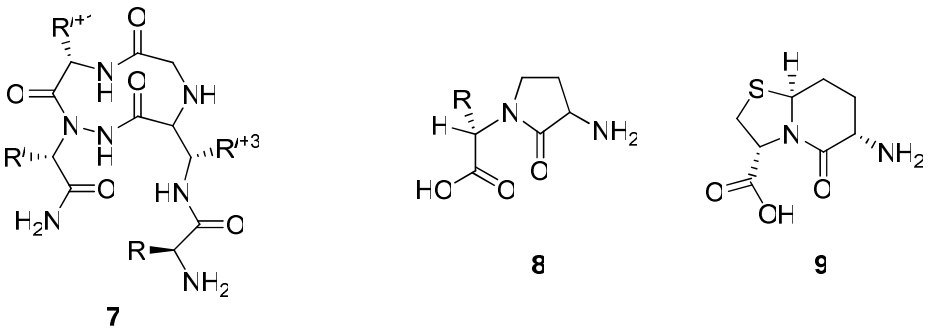

Figure I.16. Internal (**7**) and external (**8** and **9**) turn mimetics.

In the last two decades a considerable amount or work has been published in terms of β-turn mimetics leading to an enormous structural diversity. Figure I.17 shows a representative set of these structures that can include: spirocyclic β-lactams **10**,[44,45] spirobarbiturates **11**,[46] piperidinone derivatives **12**,[47] sugar amino acids (**13**[48] and **14**[49]), BTAa (**B**icycles from **T**artaric Acid and **A**mino **a**cids) scaffolds **15**,[50] aza-, thiaza-, and oxaza-bicycloalkane amino acids (**16**,[51-53] **17**,[54,55] and **18**,[56-58] respectively), other bicyclic lactams **19**,[59,60] saturated (**20**[61]) and unsaturated (**21**[62]) 10-membered lactams, bicyclic diketopiperazines **22**,[60,63] and benzodiazepines **23**.[64]

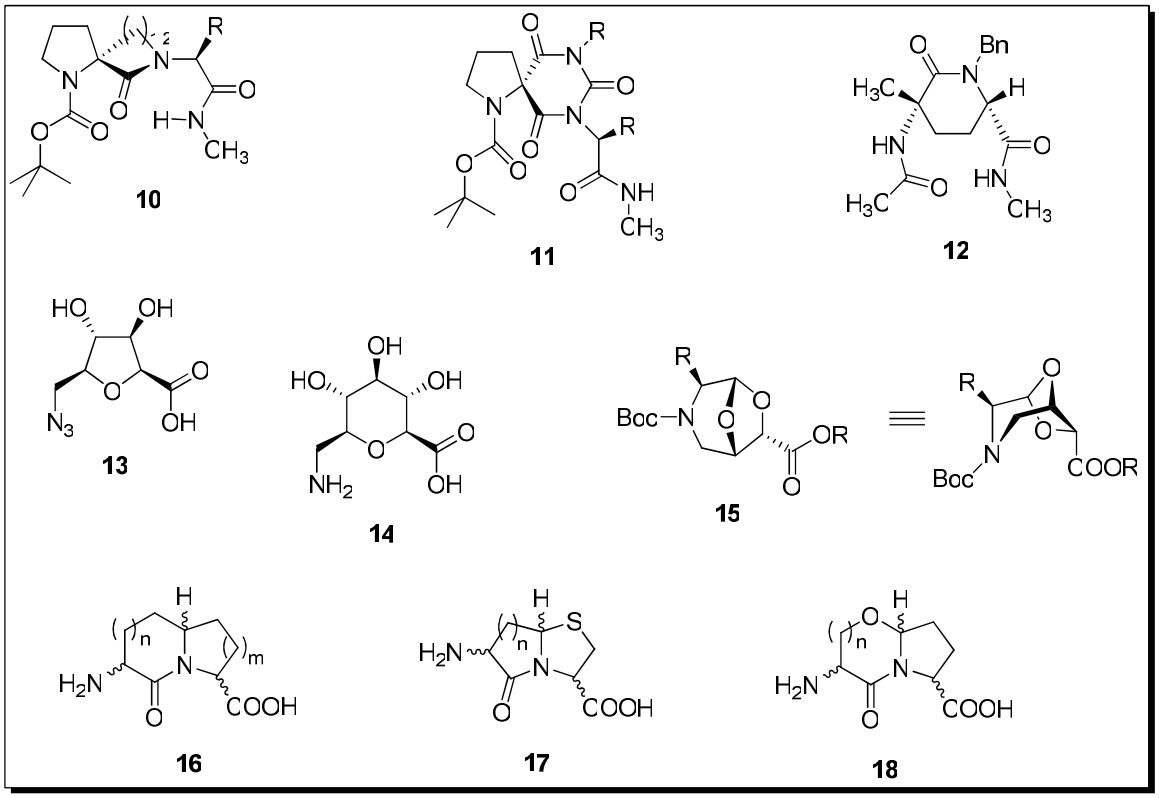

Figure I.17. Examples of β-turn mimetics (Part I).

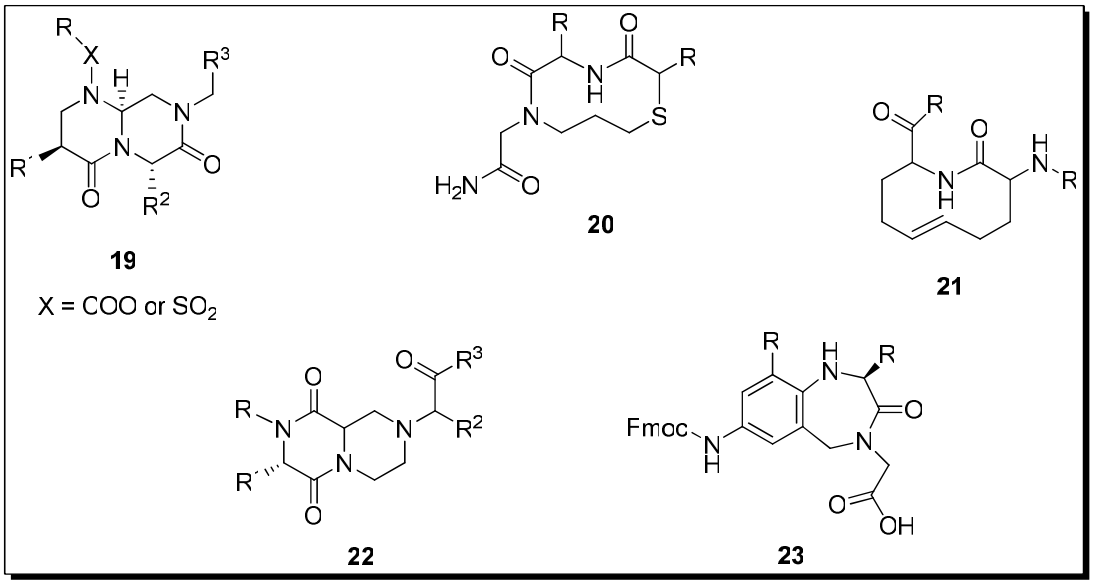

Figure I.17. Examples of β-turn mimetics (Part II).

III.3. β-STRAND MIMETICS

Mimicking β-strands to antagonize β-sheet formation or recognition may represent a viable therapeutic strategy toward the prevention or treatment of diseases associated with β-sheet structures.

With respect to conformational stability, the arrangement of peptides into β-strands for recognition by biomolecular targets is either a chance event in which the receptor captures the small percentage of peptide present in a β-strand conformation, or in alternative the receptor plays an active role in contorting the peptide into the preferred strand shape.[65] It is known that molecules, which are conformationally preorganized or fixed into a shape that is recognized by a receptor, can have higher affinity for that receptor due to the reduced entropy penalty for adopting the receptor-binding shape. It is therefore surprising that, unlike the case for turns and helices, there are relatively few reported conformationally restricted, surrogates for the β-strand.

One minimalist approach to conformational stability involves restricting peptide freedom though cyclization,[66] either via side chain to side chain, side chain to main chain, or main chain to main chain linkages, to form macrocycles. Nature frequently uses cyclization to force peptides into bioactive conformations.[67] Cyclic peptides also have the advantages over linear peptides of being more resistant to amide bond cleavage by proteolytic enzymes and of being more conformationally restrained or less flexible.[65]

Alternatively, conformational constraints can be incorporated in peptide sequences. Nature frequently moulds peptides into turn shapes by replacing amino acid components with a wide variety of constraints such as disulfides, double bonds, *N*-methyl amino acids, D-amino acids, aromatic and heterocyclic rings, often in conjunction with cyclization.[67,68] Similar conformational constraints could be used to synthetically mimic the peptide β-strand. For example, one or more amino acid residues could be replaced in a peptide sequence by one or more rigid organic units.

Schrader *et al.* were the first to report an artificial template (3-aminopyrazole derivative) able to stabilize the β-sheet conformation in N/C-protected dipeptides by purely intermolecular interactions.[69] In the complex reported (**24**, Figure I.18a). two aminopyrazole molecules laid exactly above and below the peptide backbone. Binding to the top face of the peptide is strongly favoured because it forms three cooperative hydrogen bonds simultaneously to the receptor molecule, whereas the bottom face has only two. Later on, they introduced an additional carboxylate into the aminopyrazole structure that allowed them to produce aminopyrazole oligomers (**25**, Figure I.18b), with a hydrogen pattern complementary to the top and bottom face of a peptide in β-sheet conformation.[70,71]

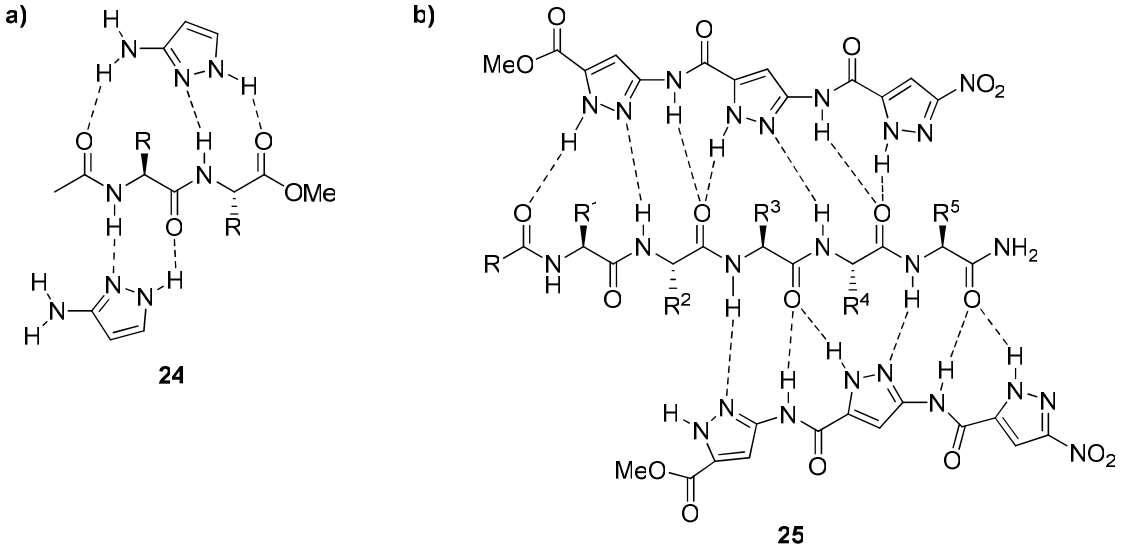

Figure I.18. a) First generation of 3-aminopyrazole derivatives, b) aminopyrazole oligomers for β-sheet stabilization of peptides.

A single-strand mimic was introduced by Hirschmann and co-workers, based on the pyrrolinone scaffold, which mimics both the functionality and the side chain orientation of a peptide in the extended conformation (**26**, Figure I.19).[72,73]

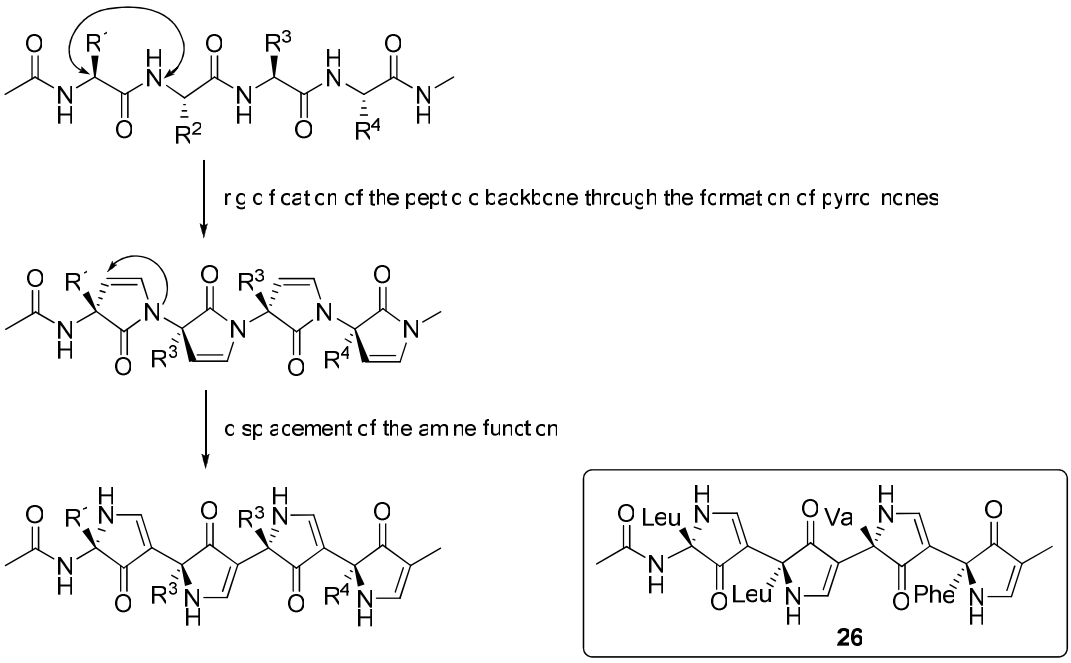

Figure I.19. Design of a pyrrolinone-based peptidomimetic possessing the conformation of a β-strand.

Bartlett and co-workers have developed a cyclic amino acid surrogate (1,2-dihydro-3(*6H*)-pyridinone or "@"-unit, Figure I.20) that was designed to mimic the extended conformation of a peptide unit and to provide hydrogen bond donor and acceptor functions conducive to β-sheet formation.[74,75] The "@"-unit has then incorporated into oligomers alternating with peptide units. The resulting "@-tides" (**27**, Figure I.20) revealed an enhanced propensity to dimerize in comparison to a related peptide.

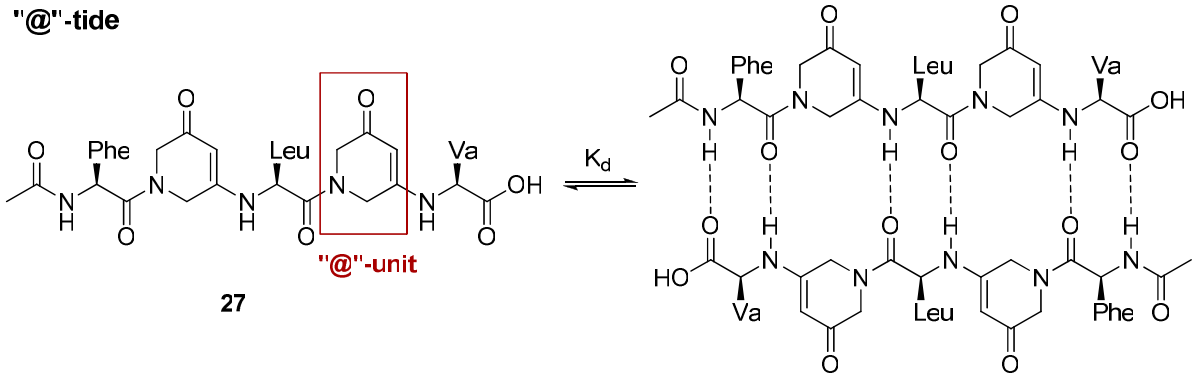

Figure I.20. Dimerization of linear "@-tides".

III.4. β-HAIRPIN AND β-SHEET MIMETICS

Although β-sheets are key structural elements in the three dimensional structure and biological activity of proteins, the factors that contribute to β-sheet structure and stability are still not as well understood as in the case of α-helices. Unlike helices, where local conformational effects and amino acids not further apart than 3–4 residues play a decisive role in dictating structural stability, the β-sheet can be viewed partly as a tertiary structure, with complex geometry and interactions between residues far apart in primary sequence. This implies that a scale for the intrinsic sheet-forming propensities of residues is not as easily obtained as for the α-helices, and therefore it is difficult to predict the pattern of protein folding from the sequence of amino acids.

Generally, preparation of chemical models of β-sheet is difficult due to the complexity of their folding and their propensity for self-association, therefore, several researchers have developed chimeric peptides that display β-hairpin-like or β-sheet-like conformations in which a strand or a loop is replaced by a peptidomimetic segment.

In 1988, Kemp *et al.* reported the first example of antiparallel β-sheet formation with urea functionalized peptide conjugates of 2,8-diaminoepindolidione[76] (Figure I.21). The presence of two D-Ala-Pro loops led to the three-stranded antiparallel **28** sheet in which two β-hairpins share a common peptidomimetic strand.[77]

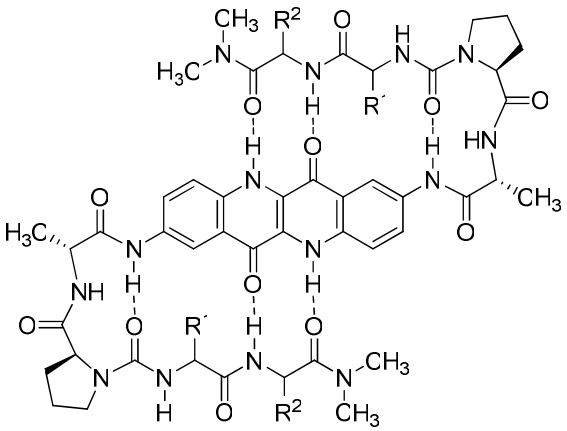

28

Figure I.21. First example of β-sheet mimics containing a peptidomimetic strand by Kemp et al.

In 1993, Kelly *et al.* reported the first model system in which a molecular scaffold was employed to create the β-sheet-like structure of attached peptide chains and serve as

substitute for the β-turn.[78] The authors used a dibenzofuran-based amino acid **29**[79] to induced β-hairpin-like antiparallel pairing of two short peptide strands (**30**, Figure I.22) in aqueous solution. It is noteworthy that this achievement was coincident with the discovery by Blanco *et al.*[80] of the first water-soluble peptide that forms a β-hairpin in aqueous solution.

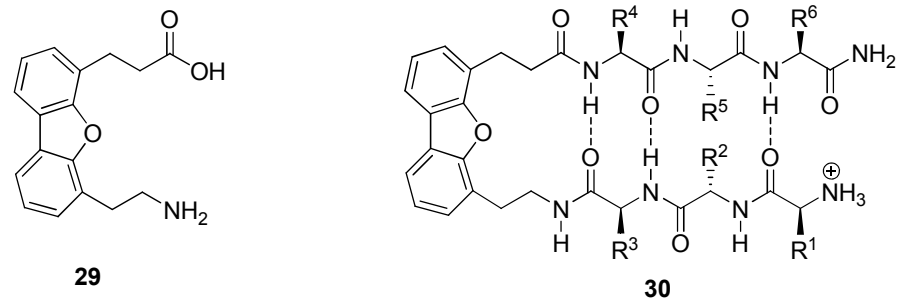

Figure I.22. Kelly's dibenzofuran peptidomimetic acting as β-hairpin inducer.

Kelly's studies on related peptides containing residue **29** suggested that **29** needs to be flanked by two α-amino acid residues bearing relatively large hydrophobic side chains (*e.g.* Leu, Val, Phe, etc.). In this case the aromatic template and the side chains of the flanking α-amino acids form a hydrophobic cluster which appears to be sufficient to nucleate β-sheet folding in aqueous medium. Based on this conclusion, template **29** was used to create an acyclic β-sheet peptidomimetic **31**[81] with sufficient structural integrity to exhibit antimicrobial activity equivalent to that of gramicidin S (Figure I.23), a cyclic peptide that adopts an antiparallel β-sheet structure in aqueous buffers known to be critical for its antimicrobial activity.[82]

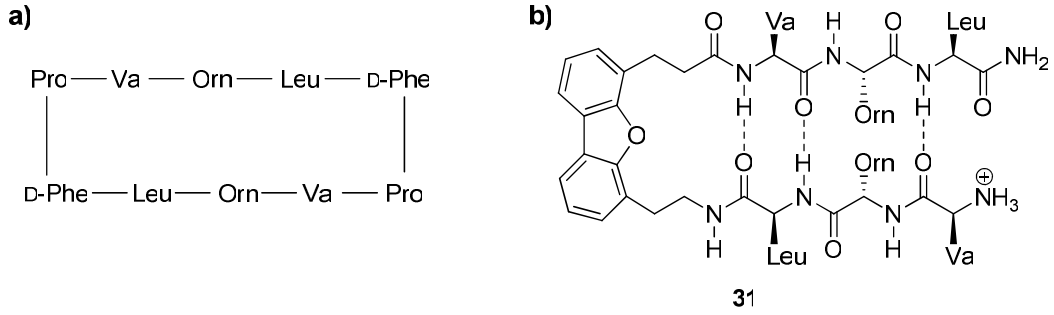

Figure I.23. a) Gramicidin S and b) acyclic peptidomimetic analogue.

These initial studies push the door wide open for the application of peptidomimetics in chemical models of β-hairpins and β-sheets. Encouraged by the success of Kemp and Kelly, several research groups have dedicated their efforts to continue the development of such peptidomimetic systems. For example, König and co-workers have developed a model system containing Gellman's β-turn fragment (D-Pro-Gly), a peptidic and a peptidomimetic β-strand formed by methoxypyrrole amino acids - MOPAS[83] (Figure I.24). System **32** adopts a hairpin structure and the observed hydrogen bonding pattern is complementary to a peptide β-sheet.

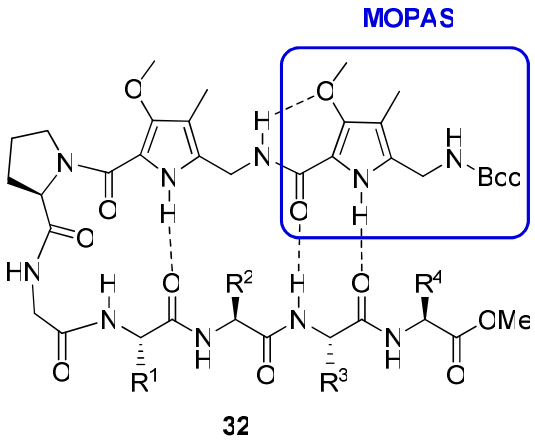

Figure I.24. Konig's model system containing methoxypyrrole amino acids.

Bartlett and co-workers have demonstrated that the presence of a 1,6-dihydro-3(2*H*)-pyridinone moiety (the @-unit, previously described in Section III.3, page 19) as an amino acid replacement at the *i*-1 or *i*+4 positions relative to a β-turn (in this case, D-Pro-Ala) strongly stabilizes the β-hairpin conformation (**33**, Figure I.25) in a variety of short peptides in both nonpolar and hydroxylic solvents.[84,85] Moreover, the vinylogous amide moiety of the @-unit produces a distinctive CD signal at 280 nm that is sensitive to conformational changes, providing a convenient spectroscopic handle for investigating sequence and side-chain effects on β-hairpin folding.[86]

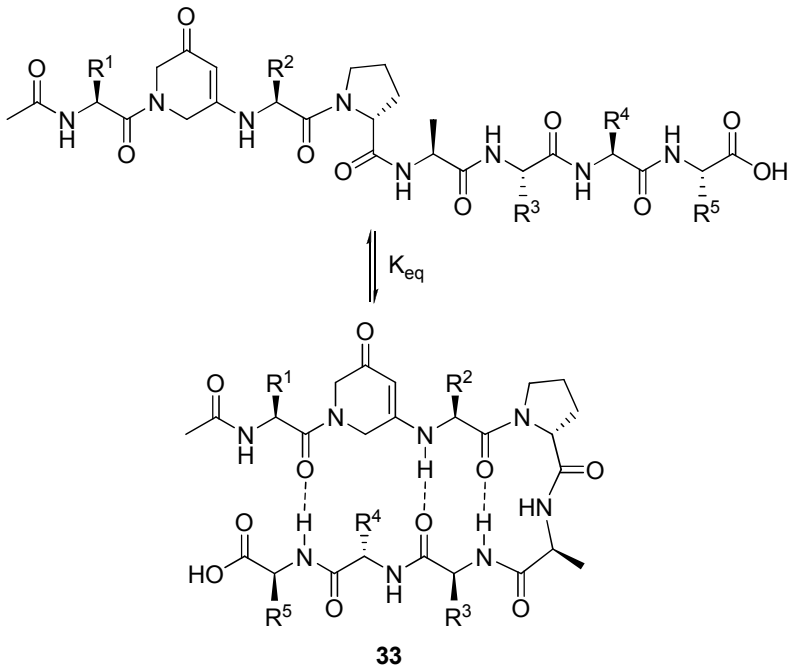

Figure I.25. Folding of @-tide-peptide into β-hairpin structures.

Scolastico and co-workers have incorporated different bicyclic lactam in *N*-acetylated hexapeptide mimics. They have demonstrated that the nature of the bicyclic lactam determines not only the turn motifs but also the folding patterns of these constrained peptides. For example, the (5,6)-bicyclic lactam derivative **34** is characterized by a type-II' β-turn (C=O^3 ••• H^6–N) and is a very compact intramolecularly H-bonded structure (Figure I.26). On the other hand, the (5,7)-bicyclic lactam derivative **35** is characterized by an inverse γ-turn (C=O^4 ••• H^6–N) and is a quite flexible "tweezer-like" structure[87] (Figure I.26).

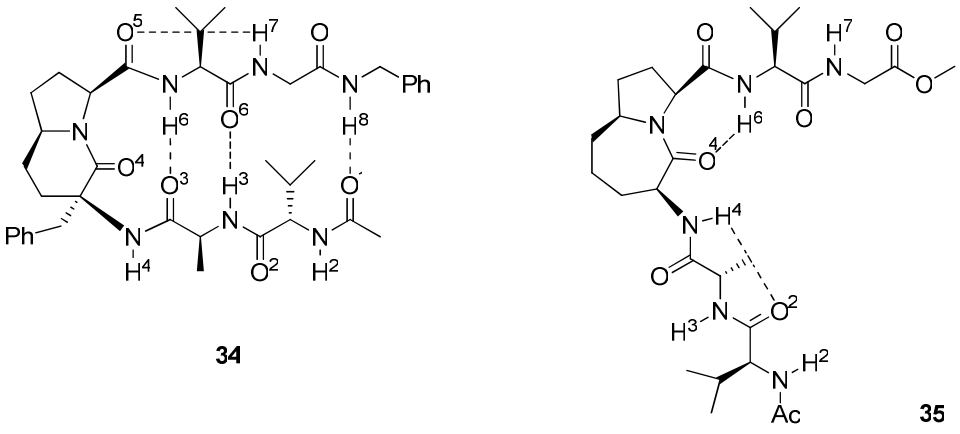

Figure I.26. Different hydrogen-bonding patterns in *N*-acetylated hexapeptide mimics.

In the last years two groups have reported the incorporation of a photoswitchable azobenzene as a turn mimic. Both groups found that the *cis*-azobenzene maintained a β-hairpin structure, but that the *trans* isomer disrupted folding (Figure I.27). The system designed by Hilvert and co-workers[88,89] was found to aggregate in the *trans* configuration, whereas no aggregation was observed for either isomer in the system designed by Renner and co-workers.[90] This fact was attributed to differences in the strand sequences.

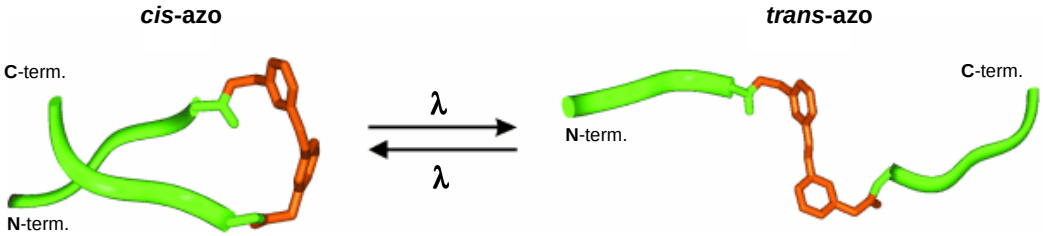

Figure I.27. Light-induced isomerisation of azobenzene-based peptides.[90]

In a similar manner, Gogoll and co-workers developed a stilbene-type β-hairpin mimetic capable of light-triggered conformational changes between an unfolded structure and a folded β-hairpin structure (Figure I.28).[91]

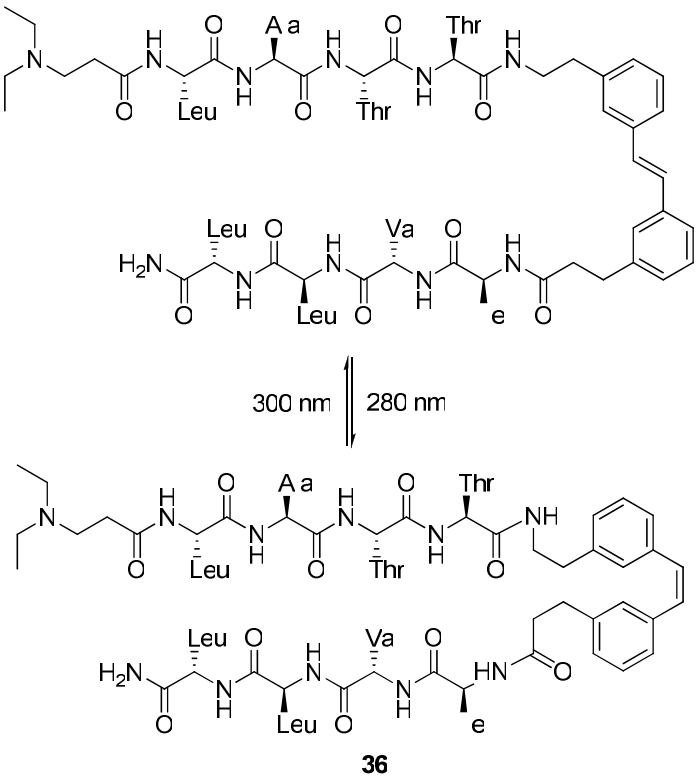

36

Figure I.28. Photoswitchable stilbene-type β-hairpin mimetic.

According to the authors, stilbene derivatives **36** are in many ways superior to azobenzenes compounds, which are known to undergo *cis-trans* isomerisation and are more sensitive to reducing agents, whilst the separation of their isomers is often complicated, if not impossible.

In terms of cyclic β-hairpin peptidomimetics, a considerable amount of work has been developed by Robinson and co-workers. Since the end of the 90's they have designed, synthesised, and studied the conformational preferences of several β-hairpin mimetics containing different templates, like, bicyclic diketopiperazine-based templates[92,93] and the heterochiral D-Pro-L-Pro dipeptide unit.[94-97]

In particular the mimetics containing the β-hairpin-inducing template, D-Pro-L-Pro dipeptide, revealed very interesting biological applications as: trypsin inhibitors,[98] antibacterial agents against Gram-positive and Gram-negative bacteria,[95,99] BIV and HIV-1 Tat–TAR RNA (Tat-Transactivator Response Element RNA) inhibitors,[96] HIV-1 RRE (Rev Response Element) inhibitors,[97] and CXCR4[iii] antagonists.[100]

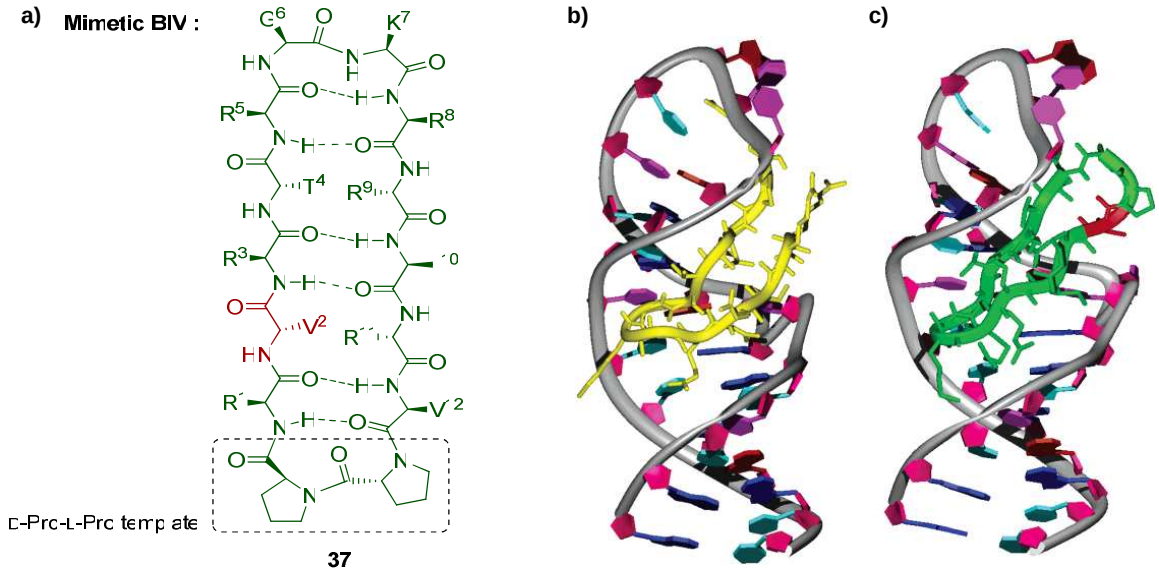

Figure I.29. a) Structure of the β-hairpin mimetic **37** (Val^2 in red); b) BIV Tat peptide (yellow) adopts a β-hairpin conformation upon binding to the TAR RNA; c) model of the **37**-TAR complex (green with Val^2 in red), with β-hairpin mimetic **37** bound in the major groove of BIV TAR RNA.[96]

[iii] CXCR4 is an α-chemokine receptor specific for stromal-derived-factor-1 (SDF-1). This receptor is one of several chemokine receptors that HIV isolates can use to infect CD4+ T-cells.

Finally, it is not possible to close this section without mentioning the enormous work developed by Nowick and co-workers in β-sheet mimetics field, during the last 16 years. Their first paper, published in 1992, described an intramolecularly hydrogen-bonded oligourea molecular scaffold that presents a series of amino acids or other groups in an orderly fashion.[101] This achievement represented one of the first examples of synthetic "foldamers". Later on, the attachment of two peptide strands to a urea-based scaffold led to Nowick's first artificial β-sheet **38** (Figure I.30), which folded in chloroform solution to mimic the structure and H-bonding pattern of a parallel β-sheet.[102]

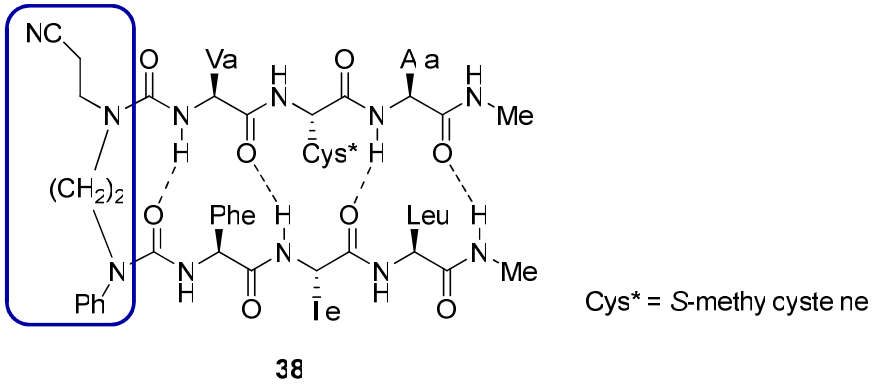

38

Figure I.30. Nowick's first artificial β-sheet showing the urea-based scaffold (blue box).

Nowick and co-workers also developed a series of molecular templates based on 5-amino-2-methoxybenzoic acid, and related hydrazine derivatives, to mimic and complement the hydrogen-bonding functionality of peptide strands and block unfilled hydrogen-bonding valences. The 2-methoxy group played the dual roles of blocking a H-bond donor group and providing organization through intramolecular hydrogen bonding within these β-strand mimics. By combining the urea-based molecular scaffold with these β-strand mimics, they created a variety of artificial β-sheets (*e.g.*, **39**, Figure I.31) that fold into well-defined structures in chloroform and other non-competitive organic solvents.[103-107] Singly-templated structure **38** (Figure I.30) exhibits a parallel β-sheet, while doubly-templated structure **39** (Figure I.31) mimics the structure and hydrogen-bonding pattern of an antiparallel β-sheet.

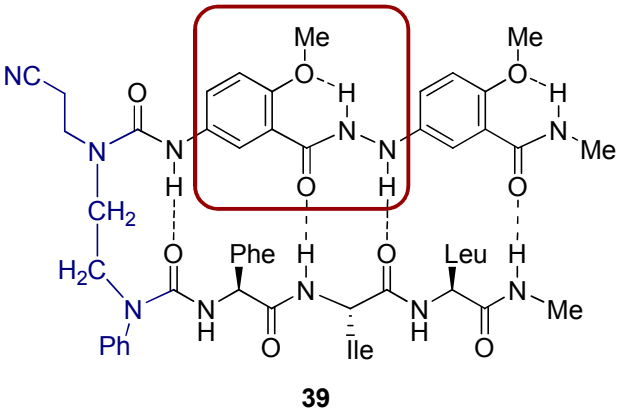

39

Figure I.31. Artificial β-sheet showing the 5-amino-2-methoxybenzoic hydrazide unit (red box).

Aiming to create larger and more complex artificial β-sheets, Nowick and co-workers combined oligourea molecular scaffolds and β-strand mimics to make molecules that mimic the structure and hydrogen-bonding patterns of protein β-sheets. Three- and four-stranded artificial β-sheets were then created. These structures combine features of doubly-templated artificial β-sheet **39** (Figure I.31) with features of singly-templated artificial β-sheet **38** (Figure I.30), meaning that they are mixed β-sheets, exhibiting both parallel and antiparallel hydrogen-bonding patterns (**40,** Figure I.32).[108,109]

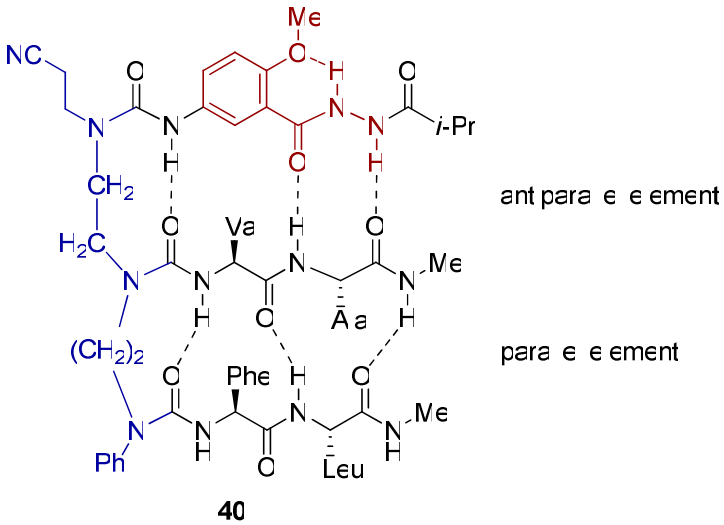

40

Figure I.32. Three-stranded artificial β-sheets, exhibiting antiparallel and parallel H-bonding patterns.

More recently, Nowick's laboratory has developed a new class of cyclic models of protein β-sheets (**41**, Figure I.33). These "cyclic modular β-sheets" are 42-membered rings

that contain a pentapeptide in the "upper" strand, the amino acid Hao[110,111] and two α-amino acids in the "lower" strand, and two δ-linked ornithine β-turn mimics.[112] Hao is a relatively rigid tripeptide β-strand mimic that serves as a template for the folding of the upper strand and blocks the lower strand to minimize edge-to-edge aggregation. The two α-amino acids in the lower strand permit tuning the folding and solubility of the cyclic modular β-sheets without changing the upper strand. The two δ-linked ornithine ($^{\delta}$Orn) residues form hairpin turns and have free α-amino groups that serve as sites for linking other cyclic modular β-sheets to form multivalent structures.[113]

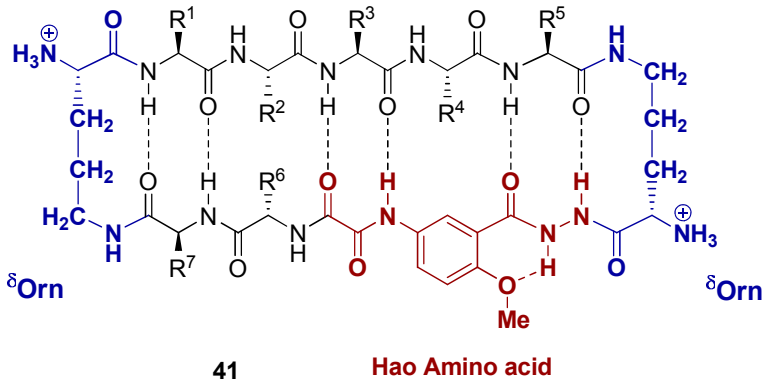

Figure I.33. Cyclic modular β-sheets.

CHAPTER I BIBLIOGRAPHIC REFERENCES:

[1] http://wiz2.pharm.wayne.edu/biochem/prot.html.

[2] Rotondi, K. S.; Gierasch, L. M. *Biopolymers* **2006**, *84*, 13-22.

[3] www.new-science-press.com.

[4] Rose, G. D.; Gierasch, L. M.; Smith, J. A. *Advances in Protein Chemistry* **1985**, *37*, 1-109.

[5] Marcelino, A. M. C.; Gierasch, L. M. *Biopolymers* **2008**, *89*, 380-390.

[6] Sibanda, B. L.; Blundell, T. P.; Thornton, J. M. *J. Mol. Biol.* **1989**, *206*, 1425-1436.

[7] http://www.imtech.res.in/raghava/betaturns/turn.html.

[8] Hutchinson, G.; Thornton, J. M. *Protein Sci.* **1994**, *3*, 2207-2216.

[9] http://en.citizendium.org/wiki/Protein_structure.

[10] Ball, J. B.; Hughes, R. A.; Alewood, P. F.; Andrews, P. R. *Tetrahedron* **1993**, *49*, 3467-3478.

[11] Seebach, D.; Matthews, J. L. *Chem. Commun.* **1997**, 2015-2022.

[12] Gellman, S. H. *Acc. Chem. Res.* **1998**, *31*, 173-180.

[13] Stigers, K. D.; Soth, M. J.; Nowick, J. S. *Curr. Opin. Chem. Biol.* **1999**, *3*, 714-723.

[14] Hill, D. J.; Mio, M. J.; Prince, R. B.; Hughes, T. S.; Moore, J. S. *Chem. Rev.* **2001**, *101*, 3893-4011.

[15] Cheng, R. P.; Gellman, S. H.; DeGrado, W. F. *Chem. Rev.* **2001**, *101*, 3219-3232.

[16] Patch, J. A.; Barron, A. E. *Curr. Opin. Chem. Biol.* **2002**, *6*, 872-877.

[17] Stanford, A. R.; Gong, B. *Curr. Org. Chem.* **2003**, *7*, 1649-1659.

[18] DeGrado, W. F.; Schneider, J. P.; Hamuro, Y. *J. Pept. Res.* **1999**, *54*, 206-217.

[19] Gademann, K.; Hintermann, T.; Schreiber, J. V. *Curr. Med. Chem.* **1999**, *6*, 905-925.

[20] Seebach, D.; Beck, A. K.; Bierbaum, D. *Chem. Biodiver.* **2004**, *1*, 1111-1239.

[21] Lelais, G.; Seebach, D. *Biopolymers* **2004**, *76*, 206-243.

[22] Banerjee, A.; Balaram, P. *Curr. Science* **1997**, *73*, 1067-1077.

[23] Seebach, D.; Abele, S.; Gademann, K.; Guichard, G.; Hintermann, T.; Jaun, B.; Matthews, J. L.; Schreiber, J. V. *Helv. Chim. Acta* **1998**, *81*, 932-982.

[24] Krauthauser, S.; Christianson, L. A.; Powell, D. R.; Gellman, S. H. *J. Am. Chem. Soc.* **1997**, *119*, 11719-11720.

[25] Seebach, D.; Abele, S.; Gademann, K.; Jaun, B. *Angew. Chem., Int. Ed.* **1999**, *38*, 1595-1597.

[26] Balaram, P. J. *Pept. Res.* **1999**, *54*, 195-199.

[27] Abele, S.; Seebach, D. *Eur. J. Org. Chem.* **2000**, 1-15.

[28] Seebach, D.; Abele, S.; Sifferlen, T.; Hanggi, M.; Gruner, S.; Seiler, P. *Helv. Chim. Acta* **1998**, *81*, 2218-2243.

[29] Seebach, D.; Hook, D. F.; Glättli, A. *Biopolymers* **2006**, *84*, 23-37.

[30] Seebach, D.; Sifferlen, T.; Bierbaum, D. J.; Rueping, M.; Jaun, B.; Schweizer, B.; Schaefer, J.; Mehta, A. K.; O'Connor, R. D.; Meier, B. H.; Ernst, M.; Glättli, A. *Helv. Chim. Acta* **2002**, *85*, 2877–2917.

[31] Seebach, D.; Sifferlen, T.; Mathieu, P. A.; Häne, A. M.; Krell, C. M.; Bierbaum, D. J.; Abele, S. *Helv. Chim. Acta* **2000**, *83*, 2849-2864.

[32] Chung, Y. J.; Huck, B. R.; Christianson, L. A.; Stanger, H. E.; Krauthäuser, S.; Powell, D. R.; Gellman, S. H. *J. Am. Chem. Soc.* **2000**, *122*, 3995-4004.

[33] Lelais, G.; Seebach, D.; Jaun, B.; Mathad, R. I.; Flögel, O.; Rossi, F.; Campo, M. A. *Helv. Chim. Acta* **2006**, *89*, 361-403.

[34] Daura, X.; Gademann, K.; Schäfer, H.; Jaun, B.; Seebach, D.; van Gunsteren, W. F. *J. Am. Chem. Soc.* **2001**, *123*, 2393-2404.

[35] Chung, Y. J.; Christianson, L. A.; Stanger, H. E.; Powell, D. R.; Gellman, S. H. *J. Am. Chem. Soc.* **1998**, *120*, 10555-10556.

[36] Gopi, H. N.; Roy, R. S.; Raghothama, S. R.; Karle, I. L.; Balaram, P. *Helv. Chim. Acta* **2002** *85*, 3313-3330.

[37] Seebach, D.; Jaun, B.; Sebesta, R.; Mathad, R. I.; Flogel, O.; Limbach, M.; Sellner, H.; Cottens, S. *Helv. Chim. Acta* **2006**, *89*, 1801-1825.

[38] Gademann, K.; Ernst, M.; Hoyer, D.; Seebach, D. *Angew. Chem., Int. Ed.* **1999**, *38*, 1223-1226.

[39] Venkatraman, J.; Shankaramma, S. C.; Balaram, P. *Chem. Rev.* **2001**, *101*, 3131-3152.

[40] Souers, A. J.; Ellman, J. A. *Tetrahedron* **2001**, *57*, 7431-7448.

[41] Gardner, B.; Nakanishi, H.; Kahn, M. *Tetrahedron* **1993**, *49*, 3433-3448.

[42] Freidinger, R. M.; Veber, D. F.; Perlow, D. S.; Brooks, J. R.; Saperstein, R. *Science* **1980**, *210*, 656-658.

[43] Nagai, U.; Sato, K. *Tetrahedron Lett.* **1985**, *26*, 647-650.

[44] Bittermann, H.; Gmeiner, P. *J. Org. Chem.* **2006**, *71*, 97-102.

[45] Bittermann, H.; Böckler, F.; Einsiedel, J.; P., G. *Chem. Eur. J.* **2006**, *12*, 6315-6322.

[46] Lomlim, L.; Einsiedel, J.; Heinemann, F. W.; Meyer, K.; Gmeiner, P. *J. Org. Chem.* **2008**, *73*, 3608-3611.

[47] De Borggraeve, W. M.; Verbist, B. M. P.; Rombouts, F. J. R.; Pawar, V. G.; Smets, W. J.; Kamoune, L.; Alen, J.; Van der Eycken, E. V.; Compernolle, F.; Hoornaert, G. J. *Tetrahedron* **2004**, *60*, 11597-11612.

[48] Grotenbreg, G. M.; Buizert, A. E. M.; Llamas-Saiz, A. L.; Spalburg, E.; van Hooft, P. A. V.; de Neeling, A. J.; Noort, D.; van Raaij, M. J.; van der Marel, G. A.; Overkleeft, H. S.; Overhand, M. *J. Am. Chem. Soc.* **2006**, *128*, 7559-7565.

[49] Graf von Roedern, E.; Lohof, E.; Hessler, G.; Hoffmann, M.; Kessler, H. *J. Am. Chem. Soc.* **1996**, *118*, 10156-10167.

[50] Trabocchi, A.; Menchi, G.; Guarna, F.; Machetti, F.; Scarpi, D.; Guarna, A. *Synlett* **2006**, 331-353.

[51] Mueller, R.; Revesz, L. *Tetrahedron Lett.* **1994**, *35*, 4091-4092.

[52] Belvisi, L.; Gennari, G.; Mielgo, A.; Potenza, D.; Scolastico, C. *Eur. J. Org. Chem.* **1999**, 389-400.

[53] Hanessian, S.; Sailes, H.; Munro, A.; Therrien, E. *J. Org. Chem.* **2003**, *68*, 7219-7233.

[54] Nagai, U.; Kato, R.; Sato, K.; Nakamura, R. *Tetrahedron* **1993**, *49*, 3577-3592.

[55] Qiu, W.; Gu, X.; Soloshonok, V. A.; Carducci, M. D.; Hruby, V. J. *Tetrahedron Lett.* **2001**, *42*, 145-148.

[56] Baldwin, J. E.; Hulme, C.; Schofield, C. J.; Edwards, A. J. *J. Chem. Soc., Chem. Commun.* **1993**, 935-936.

[57] Slomczynska, U.; Chalmers, D. K.; Cornille, F.; Smythe, M. L.; Beusen, D. D.; Moeller, K. D.; Marshall, G. R. *J. Org. Chem.* **1996**, *61*, 1198-1204.

[58] Cornille, F.; Slomczynska, U.; Smythe, M. L.; Beusen, D. D.; Moeller, K. D.; Marshall, G. R. *J. Am. Chem. Soc.* **1995**, *117*, 909-917.

[59] Eguchi, M.; Lee, M. S.; Nakanishi, H.; Stasiak, M.; Lovell, S.; Kahn, M. *J. Am. Chem. Soc.* **1999**, *121*, 12204-12205.

[60] Kim, H.-O.; Nakanishi, H.; Lee, M. S.; Kahn, M. *Org. Lett.* **2000**, *2*, 301-302.

[61] Virgilio, A. A.; Schfirer, S. C.; Ellman, J. A. *Tetrahedron Lett.* **1996**, *37*, 6961-6964.

[62] Fink, B. E.; Kym, P. R.; Katzenellenbogen, J. A. *J. Am. Chem. Soc.* **1998**, *120*, 4334-4344.

[63] Golebiowski, A.; Klopfenstein, S. R.; Chen, J. J.; Shao, X. *Tetrahedron Lett.* **2000**, *41*, 4841-4844.

[64] Rosenström, U.; Sköld, C.; Lindeberg, G.; Botros, M.; Nyberg, F.; Karlén, A.; Hallberg, A. *J. Med. Chem.* **2006**, *49*, 6133-6137.

[65] Loughlin, W. A.; Tyndall, J. D. A.; Glenn, M. P.; Fairlie, D. P. *Chem. Rev.* **2004**, *104*, 6085-6117.

[66] Abbenante, G.; March, D. R.; Bergman, D. A.; Hunt, P. A.; Garnham, B.; Dancer, R. J.; Martin, J. L.; Fairlie, D. P. *J. Am. Chem. Soc.* **1995**, *117*, 10220-10226.

[67] Fairlie, D. P.; Abbenante, G.; March, D. R. *Curr. Med. Chem.* **1995**, *2*, 654-686.

[68] Fairlie, D. P.; West, M. L.; Wong, A. K. *Curr. Med. Chem.* **1998**, *5*, 29-62.

[69] Kirsten, C. N.; Schrader, T. H. *J. Am. Chem. Soc.* **1997**, *119*, 12061-12068.

[70] Rzepecki, P.; Wehner, M.; Molt, O.; Zadmard, R.; Harms, K.; Schrader, T. *Synthesis* **2003**, *12*, 1815-1826.

[71] Rzepecki, P.; Gallmeier, H.; Greib, N.; Cernovska, K.; König, B.; Schrader, T. *J. Org. Chem.* **2004**, *69*, 5168-5178.

[72] Smith, A. B.; Keenan, T. P.; Holcomb, R. C.; Sprengeler, P. A.; Guzman, M. C.; Wood, J. L.; Carroll, P. J.; Hirschmann, R. *J. Am. Chem. Soc.* **1992**, *114*, 10672-10674.

[73] Smith, A. B.; Liu, H.; Hirschmann, R. *Org. Lett.* **2000**, *2*, 2037-2040.

[74] Phillips, S. T.; Rezac, M.; Abel, U.; Kossenjans, M.; Bartlett, P. A. *J. Am. Chem. Soc.* **2002**, *124*, 58-66.

[75] Phillips, S. T.; Piersanti, H.; Ruth, M.; Gubernator, N.; vanLengerich, B.; Bartlett, P. A. *Org. Lett.* **2004**, *6*, 4483-4485.

[76] Kemp, D. S.; Bowen, B. R. *Tetrahedron Lett.* **1988**, *29*, 5077-5080.

[77] Kemp, D. S.; Bowen, B. R. *Tetrahedron Lett.* **1988**, *29*, 5081-5082.

[78] Díaz, H.; Tsang, K. Y.; Choo, D.; Espina, J. R.; Kelly, J. W. *J. Am. Chem. Soc.* **1993**, *115*, 3790-3791.

[79] Díaz, H.; Kelly, J. W. *Tetrahedron Lett.* **1991**, *32*, 5725-5728.

[80] Blanco, F. J.; Jimenez, M. A.; Herranz, J.; Rico, M.; Santoro, J.; Nieto, J. L. *J. Am. Chem. Soc.* **1993**, *115*, 5887-5888.

[81] Graciani, N. R.; Tsang, K. Y.; McCutchen, S. L.; Kelly, J. W. *Bioorg. Med. Chem.* **1994**, *2*, 999-1006.

[82] Ovchinnikov, Y. A.; Ivanov, V. T. *Tetrahedron* **1975**, *31*, 2177-2209.

[83] Bonauer, C.; Zabel, M.; König, B. *Org. Lett.* **2004**, *6*, 1349-1352.

[84] Phillips, S. T.; Blasdel, L. K.; Bartlett, P. A. *J. Am. Chem. Soc.* **2005**, *127*, 4193-4198.

[85] Phillips, S. T.; Blasdel, L. K.; Bartlett, P. A. *J. Org. Chem.* **2005**, *70*, 1865-1871.

[86] Phillips, S. T.; Blasdel, L. K.; Bartlett, P. A. *Proc. Natl. Acad. Sci. USA* **2005**, *102*, 13737-13742.

[87] Belvisi, L.; Gennari, C.; Madder, A.; Mielgo, A.; Potenza, D.; Scolastico, C. *Eur. J. Org. Chem.* **2000**, 695-699.

[88] Aemissegger, A.; Krautler, V.; van Gunsteren, W. F.; Hilvert, D. *J. Am. Chem. Soc.* **2005**, *127*, 2929-2936.

[89] Kräutler, V.; Aemissegger, A.; Hünenberger, P. H.; Hilvert, D.; Hansson, T.; van Gunsteren, W. F. *J. Am. Chem. Soc.* **2005**, *127*, 4935-4942.

[90] Dong, S.-L.; Löweneck, M.; Schrader, T. E.; Schreier, W. J.; Zinth, W.; Moroder, L.; Renner, C. *Chem. Eur. J.* **2006**, *12*, 1114-1120.

[91] Erdélyi, M.; Karlén, A.; Gogoll, A. *Chem. Eur. J.* **2006**, *12*, 403-412.

[92] Bisang, C.; Weber, C.; Robinson, J. A. *Helv. Chim. Acta* **1996**, *79*, 1825-1842.

[93] Pfeifer, M. E.; Moehle, K.; Linden, A.; Robinson, J. A. *Helv. Chim. Acta* **2000**, *83*, 444-464.

[94] Späth, J.; Stuart, F.; Jiang, L.; Robinson, J. A. *Helv. Chim. Acta* **1998**, *81*, 1726-1738.

[95] Shankaramma, S. C.; Athanassiou, Z.; Zerbe, O.; Moehle, K.; Mouton, C.; Bernardini, F.; Vrijbloed, J. W.; Obrecht, D.; Robinson, J. A. *ChemBioChem* **2002**, *3*, 1126-1133.

[96] Athanassiou, Z.; Dias, R. L. A.; Moehle, K.; Dobson, N.; Varani, G.; Robinson, J. A. *J. Am. Chem. Soc.* **2004**, *126*, 6906-6913.

[97] Moehle, K.; Athanassiou, Z.; Patora, K.; Davidson, A.; Varani, G.; Robinson, J. A. *Angew. Chem., Int. Ed.* **2007**, *46*, 9101-9104.

[98] Descours, A.; Moehle, K.; Renard, A.; Robinson, J. A. *ChemBioChem* **2002**, *3*, 318-323.

[99] Robinson, J. A.; Shankaramma, S. C.; Jetter, P.; Kienzl, U.; Schwendener, R. A.; Vrijbloedc, J. W.; Obrechtc, D. *Bioorg. Med. Chem.* **2005**, *13*, 2055-2064.

[100] DeMarco, S. J.; Henze, H.; Lederer, A.; Moehle, K.; Mukherjee, R.; Romagnoli, B.; Robinson, J. A.; Brianza, F.; Gombert, F. O.; Lociuro, S.; Ludin, C.; Vrijbloed, J. W.; Zumbrunn, J.; Obrecht, J.-P.; Obrecht, D.; Brondani, V.; Hamyc, F.; Klimkaitc, T. *Bioorg. Med. Chem.* **2006**, *14*, 8396-8404.

[101] Nowick, J. S.; Powell, N. A.; Martinez, E. J.; Smith, E. M.; Noronha, G. *J. Org. Chem.* **1992**, *57*, 3763-3765.

[102] Nowick, J. S.; Smith, E. M.; Noronha, G. *J. Org. Chem.* **1995**, *60*, 7386-7387.

[103] Nowick, J. S.; Holmes, D. L.; Mackin, G.; Noronha, G.; Shaka, A. J.; Smith, E. M. *J. Am. Chem. Soc.* **1996**, *118*, 2764-2765.

[104] Smith, E. M.; Holmes, D. L.; Shaka, A. J.; Nowick, J. S. *J. Org. Chem.* **1997**, *62*, 7906-7907.

[105] Nowick, J. S.; Pairish, M.; Lee, I. Q.; Holmes, D. L.; Ziller, J. W. *J. Am. Chem. Soc.* **1997**, *119*, 5413-5424.

[106] Tsai, J. H.; Waldman, A. S.; Nowick, J. S. *Bioorg. Med. Chem.* **1999**, *7*, 29-38.

[107] Junquera, E.; Nowick, J. S. *J. Org. Chem.* **1999**, *64*, 2527-2531.

[108] Nowick, J. S.; Cary, J. M.; Tsai, J. H. *J. Am. Chem. Soc.* **2001**, *123*, 5176-5180.

[109] Nowick, J. S.; Smith, E. M.; Ziller, J. W.; Shaka, A. J. *Tetrahedron* **2002**, *58*, 727-739.

[110] Nowick, J. S.; Chung, D. M.; Maitra, K.; Maitra, S.; Stigers, K. D.; Sun, Y. *J. Am. Chem. Soc.* **2000**, *122*, 7654-7661.

[111] Nowick, J. S.; Lam, K. S.; Khasanova, T. V.; Kemnitzer, W. E.; Maitra, S.; Mee, H. T.; Liu, R. *J. Am. Chem. Soc.* **2002**, *124*, 4972-4973.

[112] Nowick, J. S.; Brower, J. O. *J. Am. Chem. Soc.* **2003**, *125*, 876-877.

[113] Woods, R. J.; Brower, J. O.; Castellanos, E.; Hashemzadeh, M.; Khakshoor, O.; Russu, W. A.; Nowick, J. S. *J. Am. Chem. Soc.* **2007**, *129*, 2548-2558.

CHAPTER II:

SYNTHESIS AND CONFORMATIONAL ANALYSIS OF PEPTIDOMIMETICS CONTAINING A NEW DIKETOPIPERAZINE SCAFFOLD

I. DIKETOPIPERAZINES (DKPS)

I.1. INTRODUCTION

Although diketopiperazines (DKPs) have been known since the beginning of the century, only now they have attracted considerable interest with respect to their biological properties.[1] As result of the structural similarity of diketopiperazines to peptides, their appearance in biologically active natural products has inspired medicinal chemists to use DKPs to circumvent the limitations of peptides. Constraining the nitrogen atoms of an α-amino amide into a DKP ring (Figure II.1) alters its physical properties, reduces the susceptibility to metabolic amide bond cleavage reactions and induce conformational rigidity. These changes in structural and physical properties, as well as the presence of groups that can act as donors and acceptors of hydrogen bonds enhance favourable interactions with biological targets. Moreover, diketopiperazines are simple heterocyclic scaffolds in which diversity can be introduced and stereochemically controlled at up to four positions and they can be prepared from readily available α-amino acids using conventional synthetic procedures. In view of all these properties it is understandable why DKPs are seen as privileged structures for the discovery of new lead compounds and they have been exploited in combinatorial chemistry strategies aimed at accelerating the drug discovery process.[2] In addition, DKPs have been used as organic catalysts for asymmetric hydrocyanation of aldehydes[3] and imines,[4] and have been shown to be useful scaffolds for the rational design of drugs and peptidomimetics.[5-7]

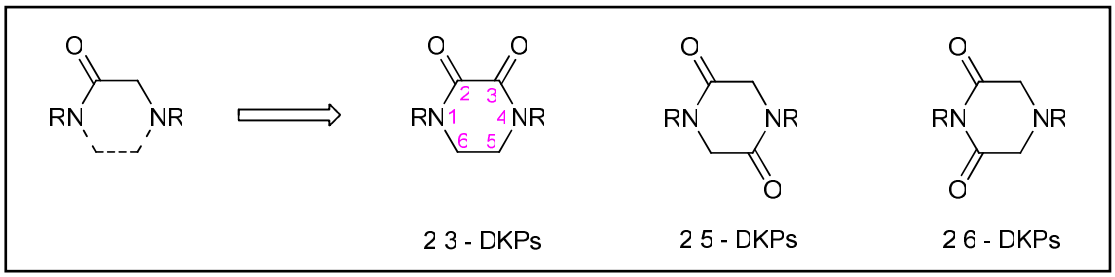

Figure II.1. Diketopiperazine isomers.

Diketopiperazines, the smallest cyclic peptides known, are commonly biosynthesised from amino acids by different organisms, including mammals, and are considered to be secondary functional metabolites or side products of terminal peptide cleavage. Cyclic

dipeptides are extensively obtained by extraction from natural sources, but may be easily synthesised as it will be discussed in Section I.3.2 (page 40).

I.2. BIOLOGICAL ACTIVITIES

Some of the most important biological activities of diketopiperazines are related to the inhibition of Plasminogen Activator Inhibitor-1 (PAI-1)[8-11] and alteration of cardiovascular and blood-clotting functions.[1]

PAI-1 is the main physiological inhibitor of serine proteases, urokinase plasminogen activator (uPA) and tissue plasminogen activator (tPA). The plasminogen-converting enzymes generate active plasmin, which proteolytically degrades fibrin and components of the extracellular matrix; while tPA is an essential element in the fibrinolytic system, regulating the formation and degradation of clots, uPA is linked to extracellular proteolytic homeostasis and consequently related to detachment and cell migration events inherent in metastasis, invasion and angiogenesis processes.[8-11]

When PAI-1 is quantitatively disrupted, a variety of modulated functions are implicated in several pathological situations such as thromboembolic disease due to highly active PAI-1,[11] coronary heart disease, atherosclerosis, thrombosis[10] and cancer progression[8] associated with increase levels of circulating PAI-1. The correlation between PAI-1 and cancer has been demonstrated in mice, by showing that the administration of exogenous PAI-1 leads to an increasing number of metastases in animals previously injected with malignant cells, while the introduction of monoclonal antibodies to this macromolecular inhibitor reduces the metastatic potential.

The inhibitory capacity of PAI-1 is dependent on the conformation of the reactive centre loop (RCL) and on its availability to bind tPA or uPA, so its potential to be explored as a therapeutic macromolecular target for the treatment of cardiovascular diseases and cancer emphasises the importance of developing drugs as specific inhibitors.[9] Diketopiperazines are the most potent PAI-1 inhibitors known,[10] acting through a mechanism involving conformational changes, which inactivate PAI-1 RCL-complementarity, preventing its binding to the target protein.

Metabolite **42** isolated from *Streptomyces sp.*, as the first low-molecular-weight PAI-1 inhibitor, was the model for designing structural changes in order to obtain more active products (Figure II.2). Using bioisosteric substitutions and combinatorial chemistry approaches, DKP **43** and **44** containing different side chains connected by exocyclic double

bonds were synthesised and showed both *in vivo* and *in vitro* PAI-1 inhibitory activity (IC_{50} 3.5 μM and 0.2 μM, respectively).[11] Other strategies, such as introduction of structural rigidity, were also applied to metabolite **42**, leading to compounds like **45** that also shows an interesting PAI-1 inhibitory activity (IC_{50} 0.3 μM).[8]

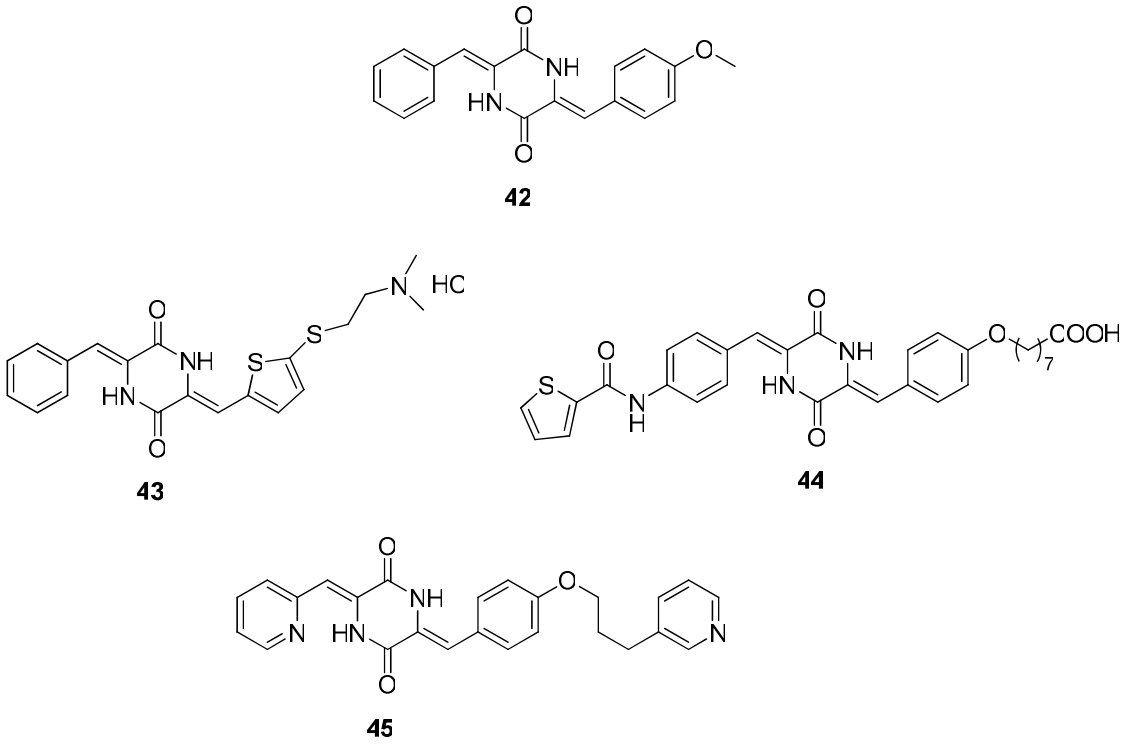

Figure II.2. Diketopiperazines as PAI-1 inhibitors.

Tumour cell pro-coagulant activity has been considered to favour metastatic processes by encasing malignant cells in a fibrin coat, which protects them from the host immunological system. Thus, components of the blood-clotting system are potential targets for a new class of therapeutic agents designed to selectively inhibit tumour growth and prevent metastasis. Haematological studies showed that *cyclo*(L-His-L-Tyr) DKP **46** (Figure II.3) significantly increases clotting time and prevents platelet adhesion and aggregation induced by adenosine diphosphate.[1] *Cyclo*(L-His-L-Phe) DKP **47** (Figure II.3) showed antitumour activity by significantly reducing the viability of HeLa, WHCO3 and MCF-7 cells, respectively from, cervical, oesophageal and mammary carcinoma.[1]

In relation to cardiac effects, compound **46** increased the heart rate in isolated rodent hearts, while compound **47** decreased cardiac output and the level of coronary blood flow. In a similar manner to several cyclic dipeptides that display potential activity for the treatment of

cardiovascular dysfunctions, compounds **46** and **47** could be employed as antiarrhythmic agents, thus reducing mortality by ventricular fibrillation in myocardial infarction.[1]

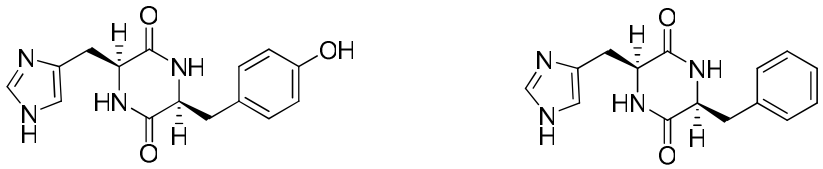

46 **47**

Figure II.3. DKPs which interfere in cardiovascular and blood-coagulation functions.

Some DKP-based compounds show a different antitumor mechanism. Phenylahistin **48** (Figure II.4), structurally similar to **47** (Figure II.3), is a metabolite isolated from *Aspergillus ustus*, which is involved in microtubule depolymerisation in human A549 lung carcinoma cells and is cytotoxic to several lines of tumour cells. Although structurally distinct from colchicine, compound **48** interacts at the same site in tubulin causing depolymerisation and inhibiting progression of the cellular cycle.[12]

Diketopiperazine **49** (also Figure II.4), a synthetic non-chiral analogue of the natural product **48**, also binds to microtubules, as colchicine, and shows antitumour activity in vitro against human tumour cell lines from prostate, breast, lung, leukaemia and colorectal tumours with IC_{50} values varying from 4.3 to 18 nM. A similar activity was reported against multidrug-resistant lines.[13] More potent than colchicine and vincristine and active in concentrations as low as 10 nM, compound **49** was able to rapidly induce microtubule depolymerisation in proliferating human umbilical vein endothelial cells (HUVECs), an in vitro model for vascular endothelial tumour cells. Since these cells lack a well-developed actin filament structure, the microtubule network is essential to structure integrity and may thus be explored as a selective therapeutic target. Compound **49** at 20 nM was able to increase permeability in a proliferating HUVEC monolayer, eventually causing vascular collapse. Considering that vasculature is very important to tumour survival and growth, the property of selective rupture of tumour vessels makes compound **49** a promising agent for cancer treatment and, for this reason, it is being tested in preclinical studies.[13]

Other compounds inhibiting cellular division were prepared from diketopiperazines with phenylalanine side chains. Some cyclic dipeptides were converted into dehydrogenated derivatives at the α-β positions of the amino acids generating exocyclic double bonds, using enzyme catalysis from strains of *Streptomyces albulus*. The unsaturated functions allow the molecule to assume a planar structure, important for the inhibition of cellular division. Among

the tetradehydro derivatives evaluated, compound **50** (also Figure II.4) was the most potent with an MIC value of 0.8 μg/mL.[14]

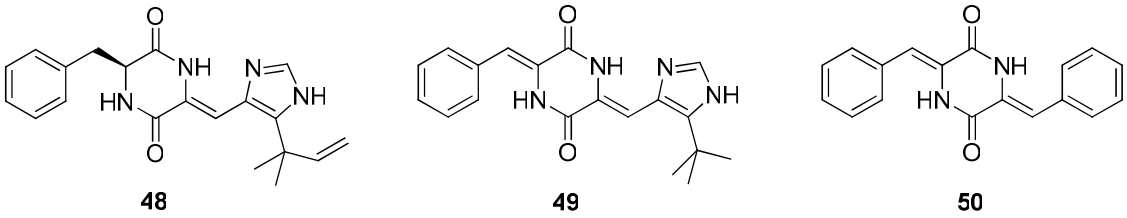

Figure II.4. Cytotoxic diketopiperazines.

Other examples in literature have also demonstrated that diketopiperazines show activities as antiviral,[15] antifungal,[16-18] antibacterial,[19-24] and antihyperglycaemic[25-27] agents and affinities for calcium channels and opioid,[28] GABAergic,[29] serotoninergic 5-HT_{1A}[30] and oxytocin[31] receptors. Figure II.5 shows a representative set of DKP-based molecules exhibiting the afore mentioned activities.

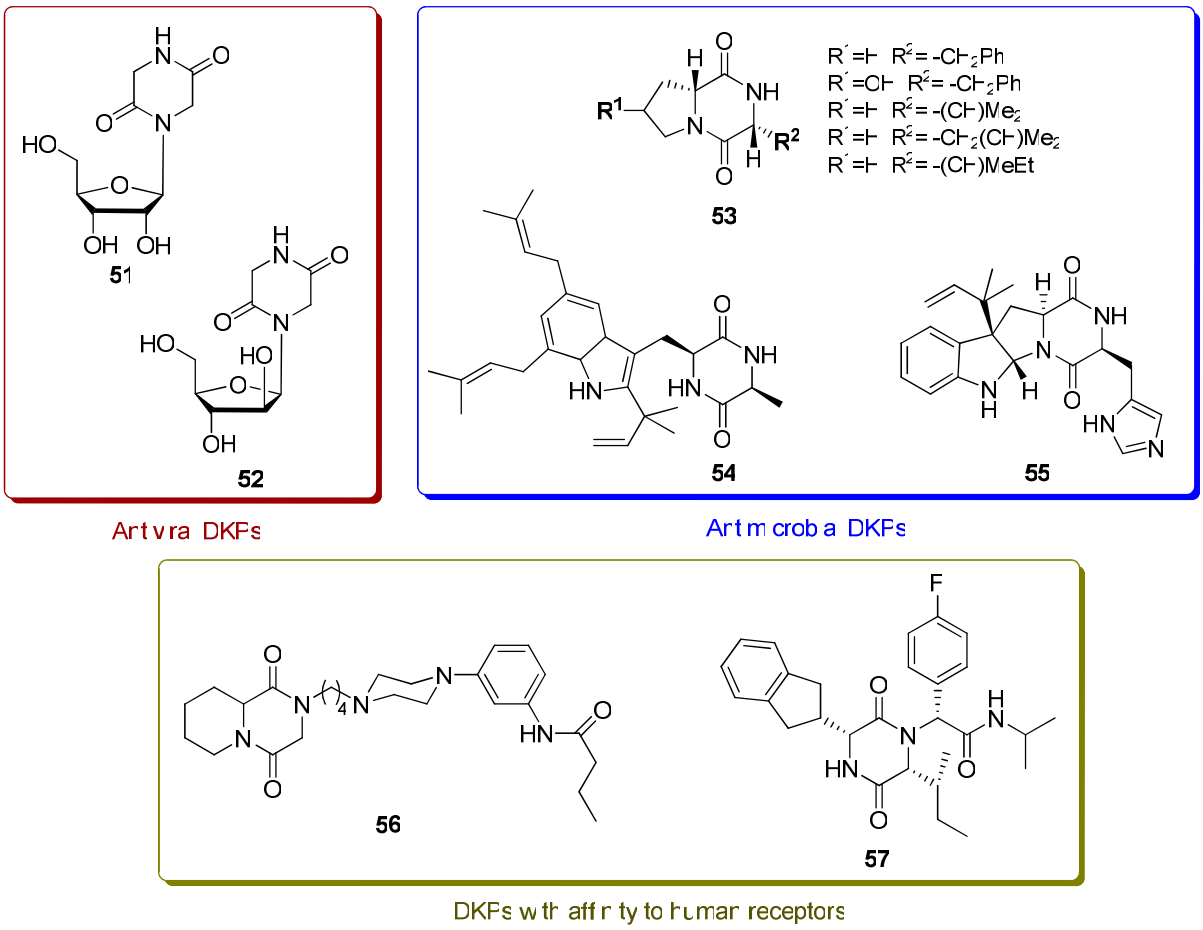

Figure II.5. Biological activities of 2,5-diketopiperazines (Part I).

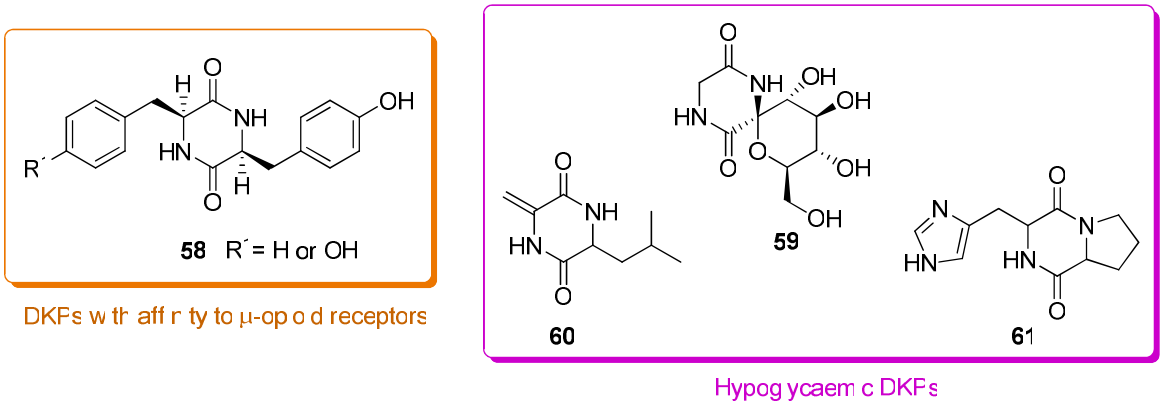

Figure II.5. Biological activities of 2,5-diketopiperazines (Part II).

I.3. SYNTHESIS OF DIKETOPIPERAZINES

I.3.1 MECHANISM OF DIKETOPIPERAZINE FORMATION

The planar backbone amide bonds in polypeptides are known to occur predominantly in the *trans* conformation. Planarity is maintained through a rotational energy barrier because of the partial double bond character of the peptide bond. On average, the energy difference between *trans* and *cis* peptide bond isomers is in the order of 2.5 kcal/mol (Scheme II.1).

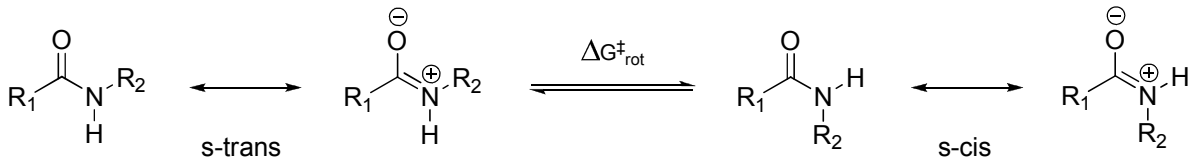

Scheme II.1

Such isomerism is relevant to DKP formation because in a dipeptide derivative the intramolecular attack of the amino group on the terminal carboxylic group is possible only from a folded conformation containing a *cis* peptide bond (Scheme II.2).

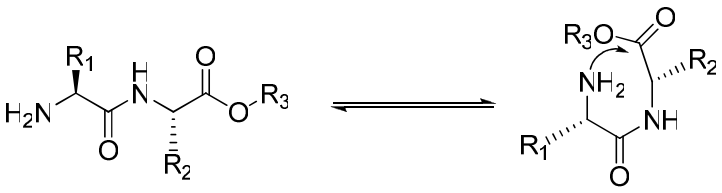

Scheme II.2

The low abundance of *cis* peptide bonds in naturally occurring polypeptides is thought to be mostly due to steric conflict between neighbouring C^{α}-substituents in the *cis* conformation. However, the actual frequencies of occurrence of *cis* peptide bonds in known protein structures do not correlate well with residue side-chain bulk. In a similar way, the relative ease of DKP formation from a number of dipeptide derivatives can not be explained sufficiently by steric interactions between the side chains in the *trans* and *cis* isomers. Particularly noteworthy in this respect are dipeptides involving α-alkyl amino acid residues. For such compounds one would predict large energy differences between *trans* and *cis* isomers on the basis of steric crowding in the *cis* isomer, whereas in fact such peptides have been observed to cyclise quite readily. It is likely that the conformational constrains (on backbone torsional angles) introduced into a peptide by, for example Aib residues, result in amide bond isomerisation/cyclization mechanisms with low energy barriers that are favoured. Possibly such factors as overall proximity between terminal amino and carbonyl groups, as well as stabilizing intramolecular interactions may be involved.[32]

I.3.2. CONVENTIONAL SYNTHETIC PROCEDURES

The 2,5-diketopiperazines, head-to-tail dipeptide dimers, are a common naturally occurring structural motif and consequently most biologically active DKPs are isolated from natural sources. They are also frequently generated as unwanted by-products or degradation products in the synthesis of oligopeptides.[33] However, due to the relative structural simplicity of its basic nucleus, several synthetic methods are also available mainly based on reactions of dipeptides, easily prepared from α-amino acids by conventional methodology.

Most symmetrical DKPs can be prepared simply by heating the free amino acid methyl esters in a sealed tube and this method can even be effective for DKPs derived from amino acids with reactive side chains. However, it is generally advisable to use protected precursors since for example, Dab, Orn, and Lys derivatives can give rise do the corresponding pyrrolidone, piperidone and homopiperidone by-products. In the case of unsymmetrical DKPs, the oldest synthetic procedure consists in the dipeptide ester treatment with methanolic ammonia, but the strongly basic conditions in this procedure can lead to epimerization. A method less prone to loss of chiral integrity consists of Boc-dipeptidyl methyl ester *N*-deprotection with formic acid, followed by reflux of the dipeptidyl ester formate salt in 2-butanol/toluene and removal of formic acid through azeotropic distillation.[34] However, for many DKPs, simple reflux of dipeptidyl methyl esters in low-boiling solvents, particularly methanol, is normally effective (Scheme II.3).[35]

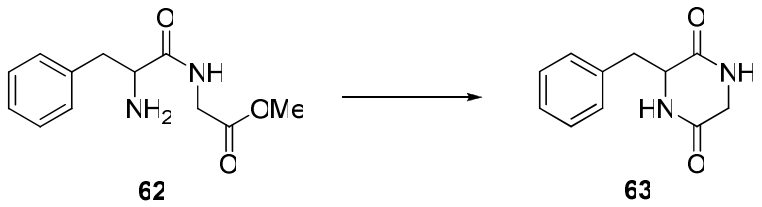

Scheme II.3. Solution-layer synthesis: (i) MeOH, reflux, 14 h.

Diketopiperazines can also be obtained by the Ugi reaction, a synthesis containing a small number of multicomponent steps, which allows substitutions on the secondary amino group.[5] The stereospecific synthesis illustrated in Scheme II.4 was proposed as an alternative in the preparation of trisubstituted DKPs. However, it was not possible to control the stereochemistry of the chiral centre located in the α carbon of the tertiary amine.[36]

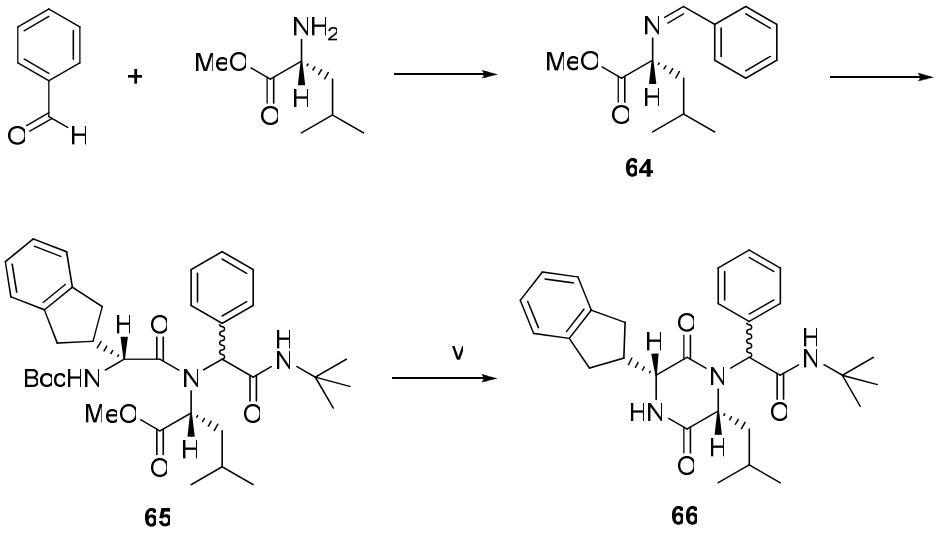

Scheme II.4. Ugi reaction: (i) 1 equiv Et_3N, MeOH; (ii) *t*-Bu-isonitrile, *N*-Boc-*R*-indanylglycine; (iii) 4 N HCl/dioxane, 4 h; (iv) Et_3N.

As an alternative, the glycine cyclic dipeptide has been used as the starting material for the solution-layer synthesis of substituted diketopiperazines. The protocol outlined in Scheme II.5 was used in the synthesis of several active compounds.[11] A similar strategy was employed to generate olefin derivatives of *N*-acetylated diketopiperazines with exocyclic double bonds.[35]

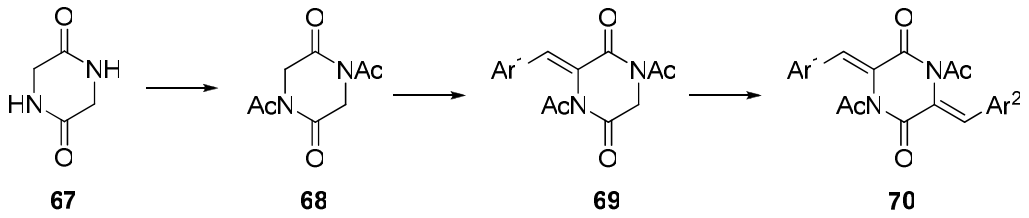

Scheme II.5. Synthesis of substituted diketopiperazines starting from *cyclo*(Gly-Gly): (i) Ac_2O, reflux; (ii) *t*-BuOH, *t*-BuOK, Ar^1CHO, THF, r.t.; (iii) Ar^2CHO, Cs_2CO_3, DMF, 80-100ºC.

An innovating strategy employing microwave heating was used to couple peptides intramolecularly, resulting in symmetrical dimeric DKP, without epimerisation in the α-position of the amino acids. N^{α}-benzoyl-Arg(NO_2)-Leu-NH_2 **71**, a PAR-2 receptor antagonist, was prepared by classical solution-layer synthesis. To the C-terminal end of this dipeptide pharmacophore, a glycine residue was introduced and activated for auto-condensation, resulting in the DKP *cyclo*(Gly-Gly) **72** *N*-substituted by the selected dipeptide. The cyclization reaction is exemplified in Scheme II.6 and, compared to conventional heating, the microwave synthesis provides the desired compounds in higher yields and shorter reaction times.[37]

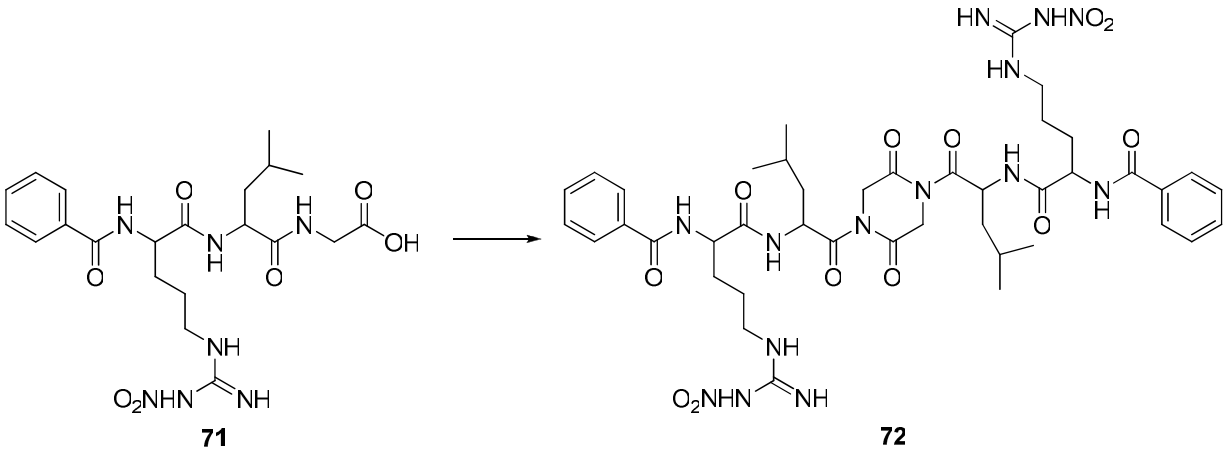

Scheme II.6. Dipeptide dimers obtained by microwave heating: (i) HBTU/DMAP, DMF, 5 min, 40 ºC, 400 W.

A microwave-assisted stereoselective one-pot synthesis of symmetrical and unsymmetrical 2,5-DKPs from unprotected amino acids, through a phosphite-promoted one step coupling reaction (Scheme II.7), was recently reported. This method is characterized by overall good yields, scalability, and tolerance to several base-stable protecting groups. Simple filtration through a pad of silica provides the pure compounds.[38]

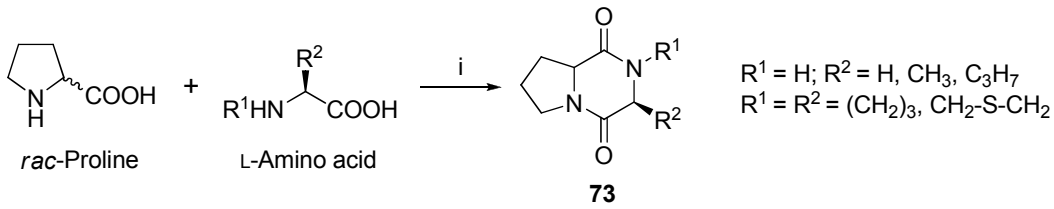

Scheme II.7. P^{III}-promoted coupling of amino acids: (i) $MeOPCl_2$, Et_3N, toluene, MW.

DKP formation can also occur even when it is not desired. In fact, parallel DKP formation in reactions involving amino acids is a quite common side reaction. For example, attempts to perform nucleophilic substitutions in substituted pyrimidinic rings, by ethyl glycine chloride in the presence of a strong base, DABCO (1,4-diaza-bicyclo[2.2.2]octane), resulted in the glycine DKP produced by predominant auto-condensation of ethyl glycine.[39]

Although solution-layer synthesis presents the advantage of requiring a smaller number of reaction steps, solid-layer synthesis has been the most used method to synthesise DKPs, with variations in the type of resin, protecting groups and type of cleavage among others. In multistep protocols, a dipeptide having the first peptide bond generated *in situ* is attached to the solid support, and it remains bound through the carboxylic extremity up to the cycling step, that is then followed by separation from the matrix or release of the *N*-protective group of the amino acid (cyclative cleavage).[40-42] A generic solid-layer protocol is shown in Scheme II.8 for obtaining DKPs under mild conditions, using the phenacyl ester (*O*-Pac) bond to attach the carboxylic amino acid terminal to the resin. Deprotection of the Boc-amino group and coupling with the next amino acid afforded dipeptide **77**, which was subsequently deprotected and cyclized by intramolecular aminolysis to DKP **78**.[41]

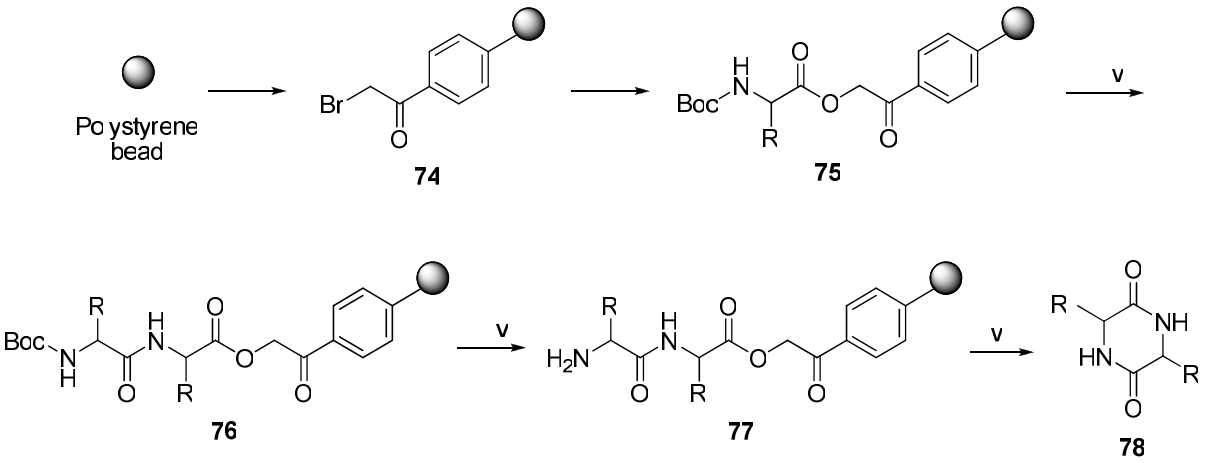

Scheme II.8. Solid-layer synthesis: (i) $BrCH_2COBr$, $AlCl_3$, nitrobenzene/DCM (1:1); (ii) Boc-AA'-OH, Et_3N, DMF; (iii) 3.5 N HCl/AcOH; (iv) Boc-AA''-OH, HOBt, DCC, NMM, DMF; (v) 10% DIPEA/EtOAc; (vi) 5% Et_3N/THF-H_2O.

Solid-layer synthesis of unsaturated 3-substituted DKP, employing a carbamate bond between the dipeptide N-terminal and the resin, was also described.[40]

Notwithstanding the successful use of activated ligands such *O*-Pac, the bond susceptible to nucleophilic attack requires amino acid side-chain group protection. Small losses of the elongating peptides are usually associated with this relative lability. Peptide attachment to the resin by the safety-catch technique circumvents this problem, because the stable bond is conveniently activated only after ending the peptide synthesis, allowing cleavage and cyclization. The strategy outlined in Scheme II.9 permits the removal of protecting groups before cleavage, facilitating further workup.[5] The use of safety-catch ligands allowed the solid-layer generation of bicyclic and tricyclic DKP, which show even greater structural diversity.

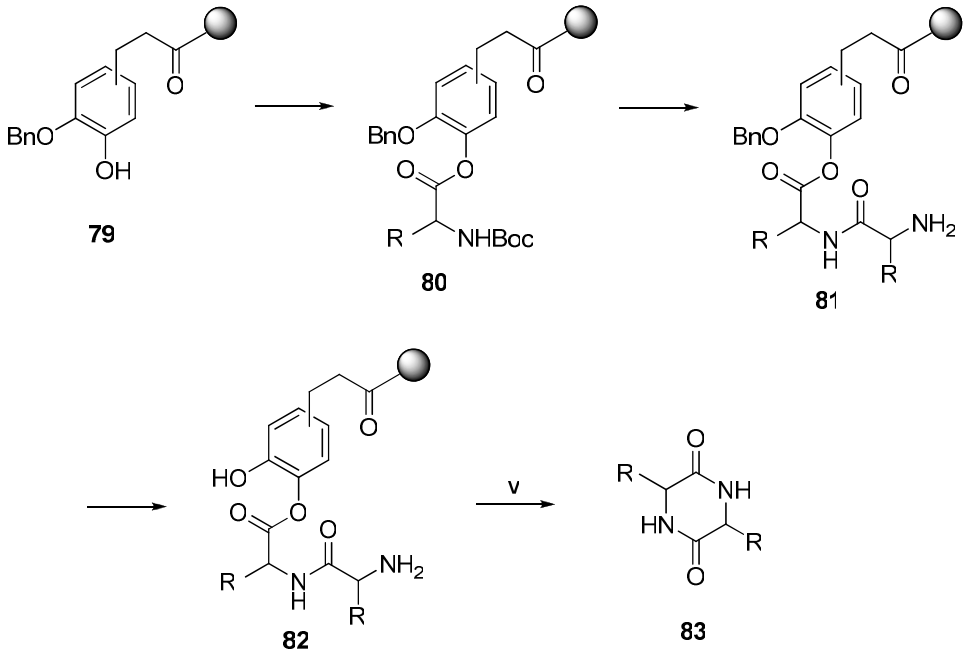

Scheme II.9. Solid-layer synthesis by safety-catch approach: (i) Boc-AA'-OH, DIC, DIPEA; (ii) Boc-based solid-layer peptide synthesis; (iii) TFMSA, TFA; (iv) DIPEA.

II. DKPS AS TEMPLATES THAT INDUCE A DEFINED SECONDARY STRUCTURE

II.1. DKP-BASED TEMPLATES IN LITERATURE

A relevant application of DKPs, which has gained importance in the last decade, is its use as templates capable of inducing a defined secondary structure in peptide sequences. In

these cases, advantage can be taken from the synthesis of symmetrical and unsymmetrical DKP bearing reactive functionalities in the lateral chains of the amino acids.

For instance, Wennemers and co-workers have prepared a few symmetrical diketopiperazine two-armed receptors derived from 4-amino-proline where the two amino groups (with a *cis* disposition) were functionalized with two tripeptide side chains (**84**, Figure II.6). The resulting two-armed receptors were screened towards a tripeptide library and showed highly selective binding properties which were attributed to the specific turn geometry of the receptor.[43-46] Later on, the same group reported the synthesis of water soluble diketopiperazine receptors (**85**, Figure II.6) and their selective binding properties to arginine containing peptides in aqueous solution.[47] To provide for arginine binding sites and water solubility the authors equipped the receptor arms of the DKP receptors with aspartic acids. The termini of the arms were either acetylated (receptor **85a**) or functionalized with succinic acid which provided for an additional carboxylic acid functional group (receptor **85b**).

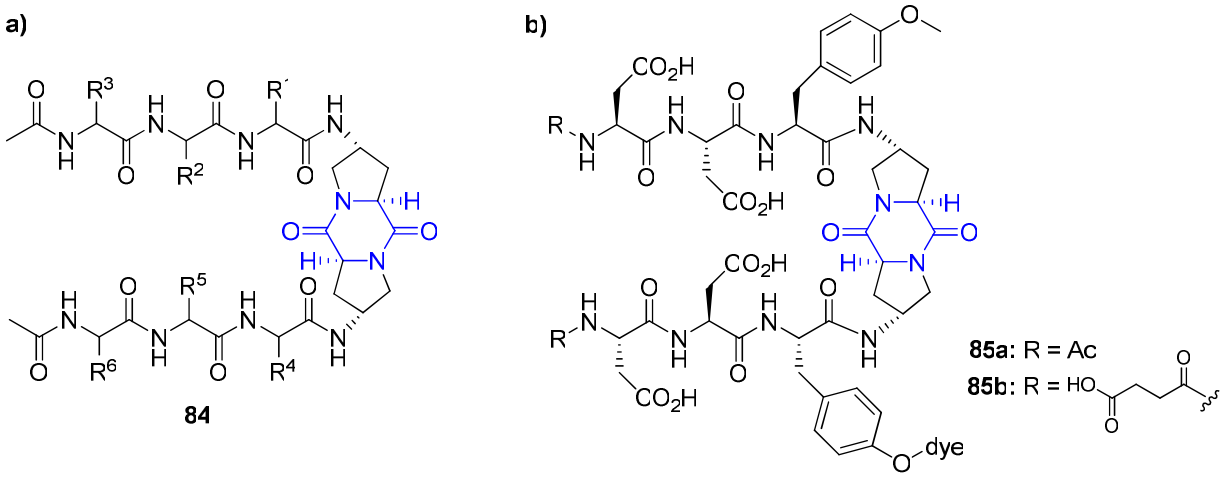

Figure II.6. a) General structure of diketopiperazine receptors and b) water-soluble DKP receptors.

Alternatively, two different functionalities can be created in the lateral chains of the two amino acids forming the DKP core, such as an amine (*e.g.* derived from Lys, Orn or diaminobutyric acid) and a carboxylic acid (*e.g.* derived from Asp or Glu). In this case, a new peptidomimetic structure is formed, possessing a fixed conformation (due to the cyclic DKP core and the configuration of the two amino acids), and which can now be used as molecular templates, scaffolds or spacers in molecular design.[48]

Davies and co-workers reported the synthesis of diketopiperazine scaffold **86** (Figure II.7), capable of mimicking a β-turn, although no synthesis or conformational studies of peptides containing scaffold **86** have been reported.[49]

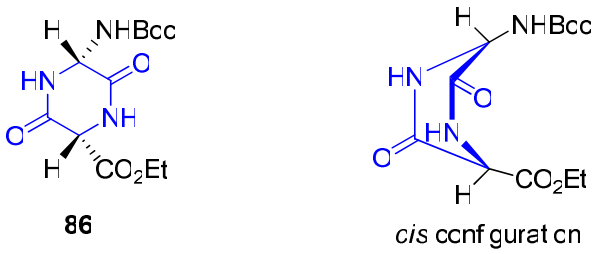

Figure II.7. Diketopiperazines as β-turn mimetics.

Golebiowski and co-workers have developed a high-throughput organic synthesis protocol for the efficient preparation of bicyclic DKP-containing systems (**87**, Figure II.8).that could be seen as a β-turn mimetic.[50] In a similar way, Kahn and co-workers have also reported the synthesis of conformationally restricted reverse turn mimetic based on a bicyclic diketopiperazine scaffold.[51]

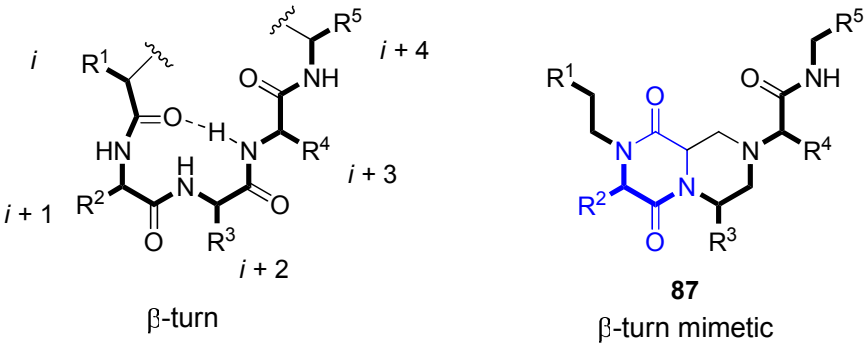

Figure II.8. Bicyclic diketopiperazines as β-turn mimetics.

Robinson and co-workers have synthesised a novel bicyclic template (**88**, Figure II.9), comprising a diketopiperazine derived from L-aspartic acid and (2*S*,3*R*,4*R*)-diaminoproline,[52] that was then incorporated by solid-layer peptide synthesis into a cyclic loop mimetic containing the sequence [-Ala^1-Asn^2-Pro^3-Asn^4-Ala^5-Ala^6-template-] (**89**, Figure II.9). It was demonstrated by NMR analysis that the mimic adopted a stable β-hairpin conformation in DMSO-d_6 solutions.[53]

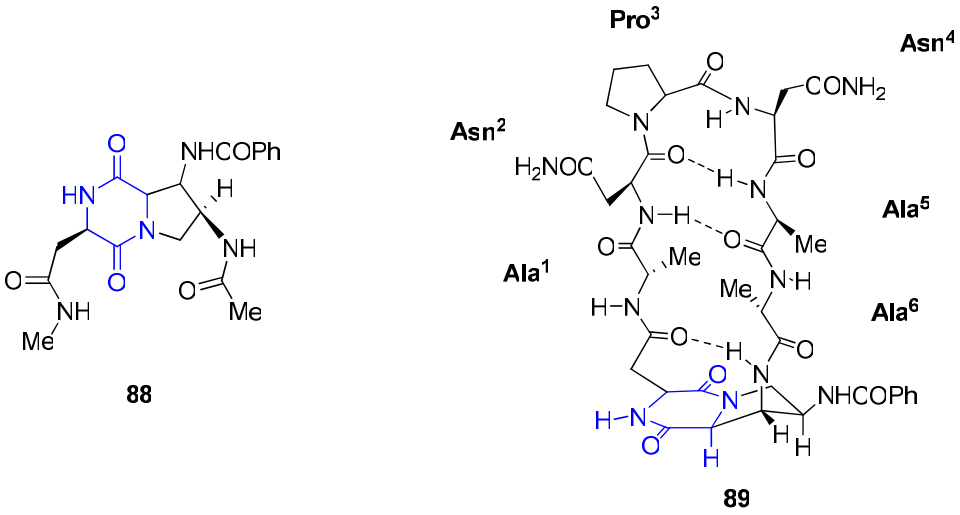

Figure II.9. DKP-based template **88** stabilizes loop conformations in cyclic peptides.

II.2. CONCEPTION OF OUR DKP-BASED MOLECULES

II.2.1. CONCEPTION OF THE DKP SCAFFOLD 90 (DKP-90)

Capitalizing on the interesting properties of diketopiperazines discussed above, we decided to synthesise a new bifunctional DKP scaffold **90** (DKP-**90**, Figure II.10), formally derived from L-aspartic acid and (*S*)-2,3-diaminopropionic acid, bearing a carboxylic acid and an amino functionalities. As a consequence of the absolute configuration of the two α-amino acids forming the cyclic dipeptide unit, the two reactive functionalities (amino and carboxylic acid) are locked in a *cis* configuration. Furthermore, these functionalities allow the introduction of peptide or peptidomimetic sequences and, therefore, we can foresee the use of DKP scaffold **90** as a secondary structure inducing element in biologically active peptides.

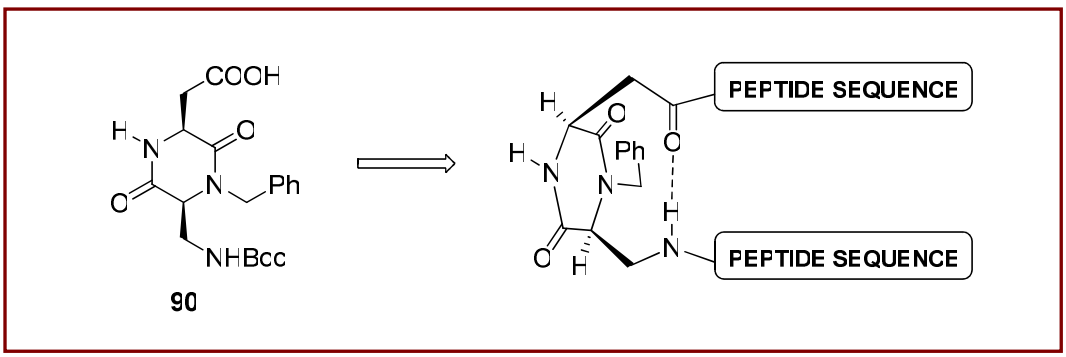

Figure II.10. DKP scaffold **90** as a reverse turn inducer.

II.2.2. CONCEPTION OF PEPTIDOMIMETICS CONTAINING DKP-90

Although DKP scaffold **90** is derived from α-amino acids, it can be seen as a conformationally constrained β-peptide formed by two β-amino acids (Figure II.11), in particular a β^2- and a β^3-amino acids (according to Seebach's nomenclature, the superscripted number after β specifies the position of the side-chain in the corresponding β-amino acid).[54]

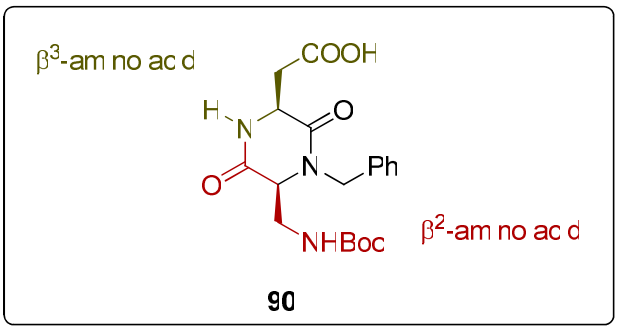

Figure II.11. Structure of the bifunctional diketopiperazine scaffold **90** (DKP-**90**) highlighting the conformationally constrained β^2-β^3 dipeptide sequence.

As it was extensively described in Chapter I (Section III.1, page 10), investigation on β-peptides indicated that these are able to adopt stable secondary structures such as helices and sheets. The stabilization of β-peptide-hairpins sequences was also studied, and in particular Seebach and co-workers described the formation of turn-like secondary structures in oligo-β-peptides containing a dipeptide sequence formed by a β^2-amino acid (C^2-substituted) followed by a β^3-amino acid (C^3-substituted)[55] (**2**, Figure II.12). Gellman and co-workers reported the formation of a hairpin conformation when a heterochiral dinipecotic acid β-peptide unit was introduced into tetrapeptide **1**[56] (also Figure II.12).

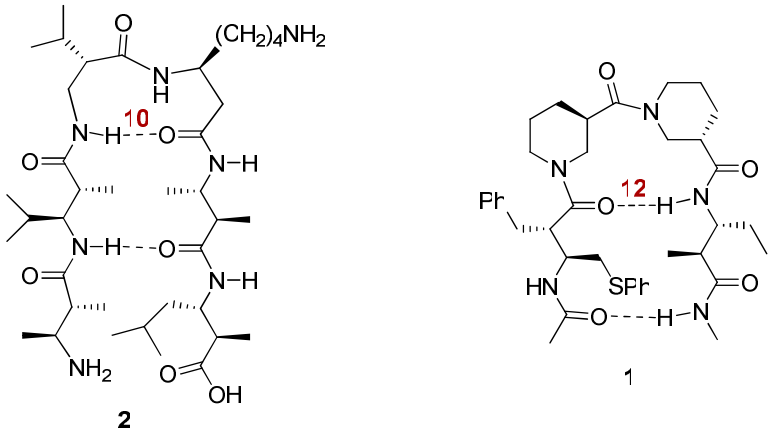

Figure II.12. Different hydrogen-bond patterns in β-peptide hairpins.

The intramolecular hydrogen bonding pattern in these two cases is different (Figure II.12): in the first case a 10-membered H-bonded ring is formed involving the C=O of the β^3-amino acid and the NH of the β^2-amino acid, while, in the second case a 12-membered H-bonded ring can be identified, which is a two-term homolog of the β-turn structure formed by α-amino acids. β-Hairpins containing both α- and β-amino acids have also been reported to be very stable.[57]

In view of these potential properties, we decided to study the ability of DKP-**90** to form well-defined folded structures, when introduced in peptide sequences. Therefore, several peptidomimetics containing DKP scaffold **90**, were synthesised (Figure II.13).

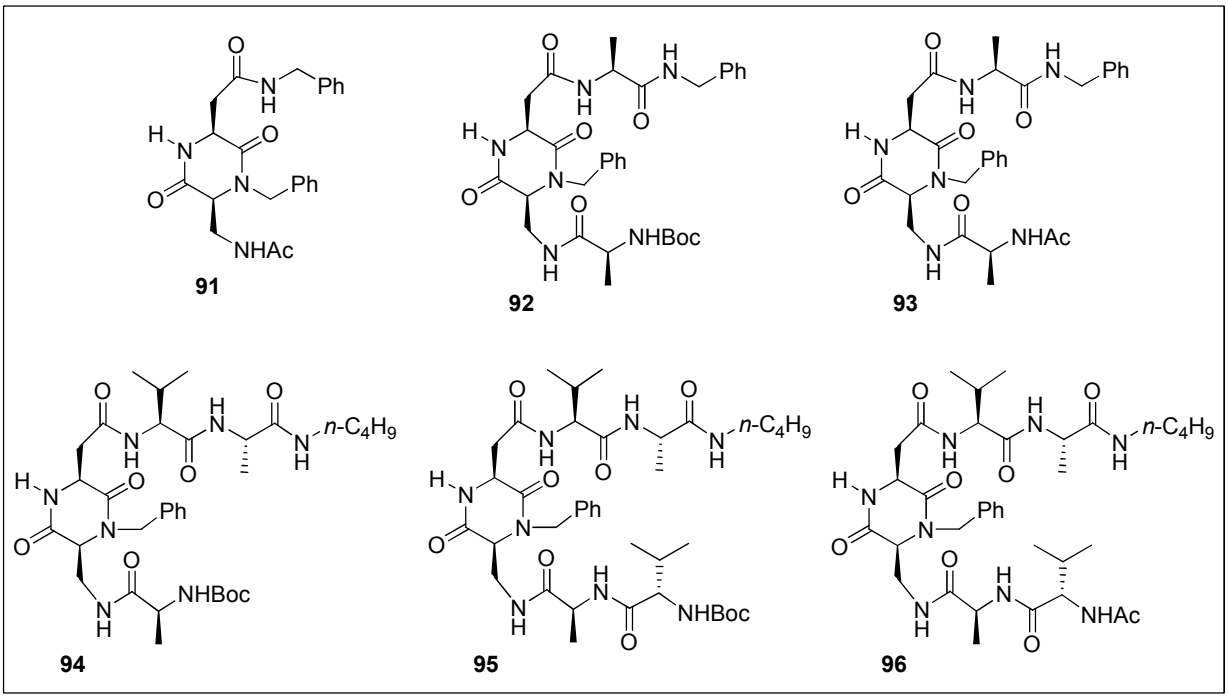

Figure II.13. Peptidomimetics containing DKP-**90**.

II.3. SYNTHESIS OF THE DKP-BASED MOLECULES

II.3.1. SYNTHESIS OF THE DKP SCAFFOLD 90

The synthetic procedure to obtain DKP-**90** involved the cyclization of the corresponding dipeptide, bearing a tertiary amide (namely the central one), in turn prepared starting from two α-amino acids namely, (2*S*)-aspartic acid and (*S*)-serine (Figure II.14).

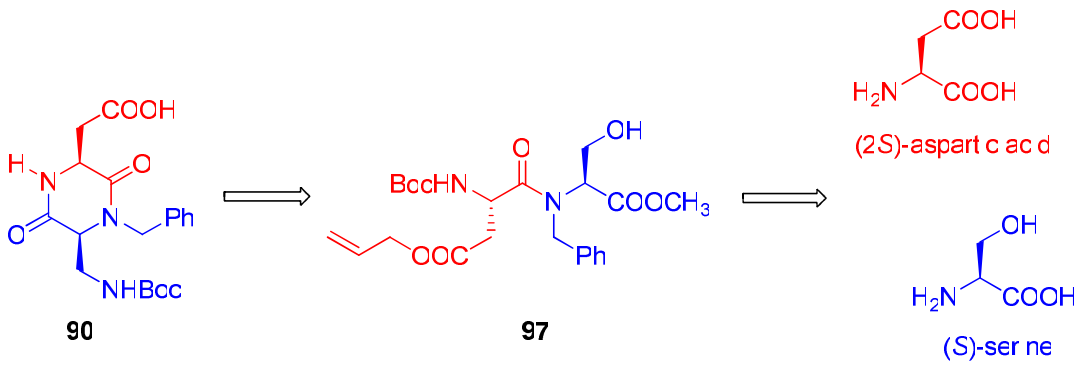

Figure II.14. Strategy designed to obtain DKP scaffold **90**.

The success of the strategy designed hinged on the availability of an ester protecting group which would be orthogonal to the Boc and methyl ester. We decided, therefore, to protect the β-carboxylic acid group of the (2*S*)-aspartic acid as its allyl ester. Accordingly, (2*S*)-aspartic acid was esterified by treatment with acetyl chloride in allyl alcohol to give (2*S*)-aspartic acid β-allyl ester hydrochloride **98** (Scheme II.10). In this procedure, the reaction of acetyl chloride with an alcohol (allyl alcohol here) is used to generate HCl *in situ* leading to allyl acetate formation that, if necessary, can be removed by evaporation under reduced pressure. This procedure is reported to be selective for the β-carboxylic group esterification but some bis-allylation can still take place.[58] In order to minimize the α-carboxylic acid esterification the reaction was performed at low temperature (0–10 ºC). The amino group was then protected as its *N*-*tert*-butoxycarbonyl derivative, under standard conditions, to give *N*-(*tert*-butoxycarbonyl)-(2*S*)-aspartic acid β-allyl ester **99** (Scheme II.10).

On the other hand, the OH group in the (*S*)-serine side-chain does not interfere with the subsequent coupling reaction, therefore, it is only necessary to protect the α-carboxylic acid group, in this case, as its methyl ester. (*S*)-serine methyl ester hydrochloride **100** was obtained by esterification of the corresponding free amino acid in refluxing methanol, in the presence of acetyl chloride. The serine α-amino group was then alkylated because, as we noted previously (see Section I.3.1, page 39), the presence of a tertiary amine decreases the energy difference between *cis* and *trans* peptide bond isomers and, therefore, facilitates the cyclization step and DKP formation. The (*S*)-*N*-benzylserine methyl ester **101** was then obtained through a reductive amination. The hydrochloride salt **100** was treated with benzaldehyde in methanol, in the presence of triethylamine to obtain the corresponding imine, that was subsequently reduced with sodium borohydride (Scheme II.10). In order to minimize racemisation during this last step, special attention should be given to both temperature and reaction time.[59]

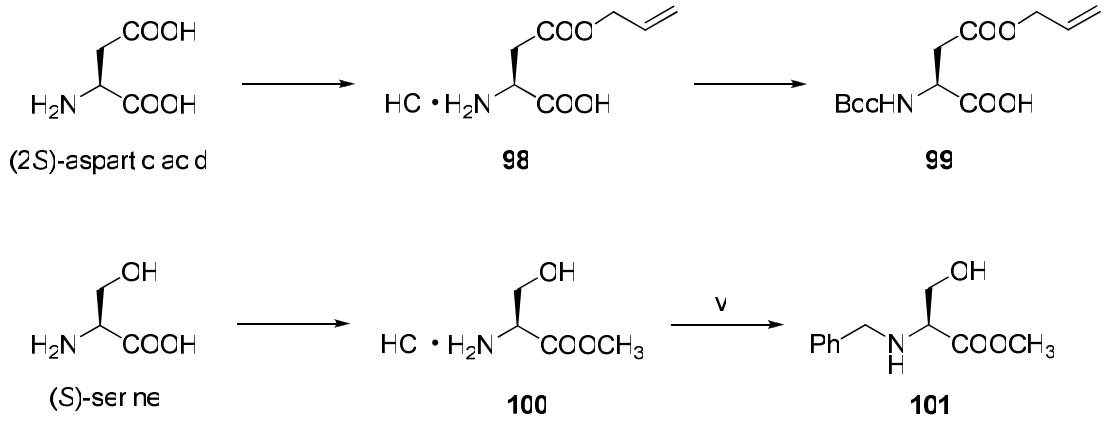

Scheme II.10. (i) CH_3COCl, $CH_2=CHCH_2OH$: 90%; (ii) Et_3N, Boc_2O, H_2O/Dioxane: 96%; (iii) CH_3COCl, CH_3OH: 82%; (iv) Et_3N, PhCHO, CH_3OH, then $NaBH_4$: 86% over two steps.

The suitably protected amino acids were then coupled to form dipeptide **101**. However, this coupling step proved to be difficult, possibly because it involves the formation of a tertiary amine. Different coupling reagents (EDC, HOAt, HATU) and reaction conditions (solvent, temperature, inert atmosphere) were tried. The best yield (72%) was obtained using HATU as coupling reagent and DIPEA as base in dichloromethane under nitrogen atmosphere (Scheme II.11). Dipeptide **101** was fully characterized and it was possible to observe two set of signals in the ^{13}C spectrum due to the presence of two rotational isomers (20:1 ratio).

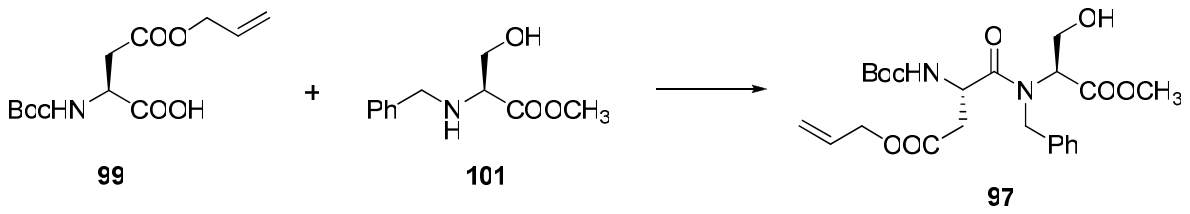

Scheme II.11. (i) HATU, DIPEA, CH_2Cl_2: 72%.

Intramolecular aminolysis of dipeptide esters with DKP formation is thermodynamically favoured due to the 6-membered ring formation and, in this particular case, also due to the presence of the tertiary amide that favours the folded conformation containing a *cis* peptide bond necessary in the ring-closing step. In order to proceed to the cyclization step, dipeptide **101** was deprotected with neat TFA and its trifluoroacetate salt cyclized, in good yield, to diketopiperazine **102** (Scheme II.12), in a basic biphasic system ($NaHCO_{3\ aq}$ / EtOAc).[60] These conditions were selected to minimize the epimerization of the serine methyl ester and

the formation of the diastereomeric *trans*-DKP **103** (< 10%), which could, however, be separated by a chromatographic purification.

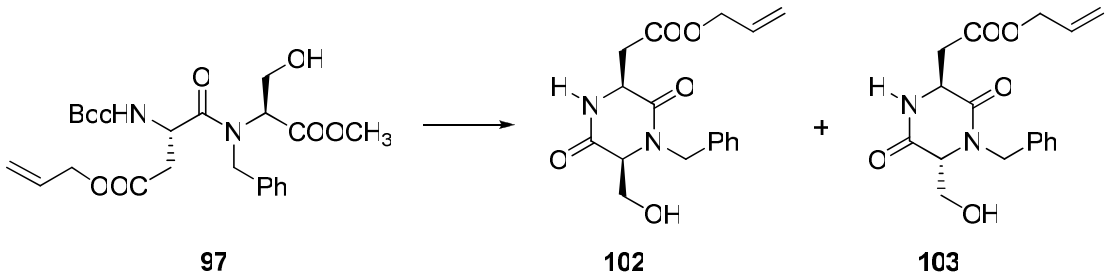

Scheme II.12. (i) TFA and (ii) saturated aqueous. $NaHCO_3$/EtOAc (1:1, v/v): 81% over two steps.

These reaction conditions represent the final step of a long series of tests to optimize the cyclization step both in terms of yield as well as proportion of epimeric *trans*-DKP **103**. Table 2.1 summarizes the conditions tried.

Table II.1- Optimization of the cyclization step.

REACTION CONDITIONS	**TOTAL YIELD**	**RATIO *cis* : *trans***
DIPEA (4 equiv), CH_2Cl_2, 48 h, r.t.	47 %	8 : 2
DIPEA (6 equiv), CH_2Cl_2, 48 h, r.t.	63 %	7 : 3
DIPEA (6 equiv), CH_2Cl_2, 24 h, reflux	80 %	3 : 7
Sat. aq. $NaHCO_3$/EtOAc (0.1 M, 1:1, v/v), 24-48 h, r.t.	90 %	9 : 1

A single crystal X-ray structure of DKP **102** was obtained, confirming its relative stereochemistry (Figure II.15).

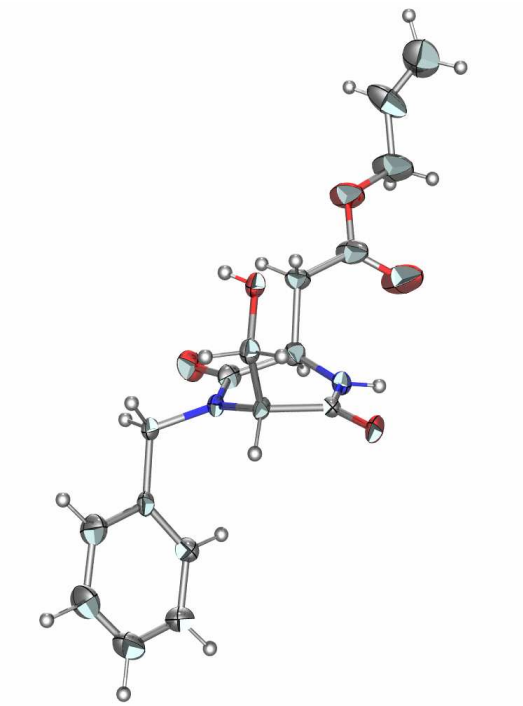

Figure II.15. X-ray crystallographic data of **102**: Crystal data: $C_{17}H_{20}N_2O_5$; MW = 332.35 g.mol^{-1}; T = 293 K; λ(Mo, Kα) = 0.71073 Å, monoclinic, space group $P2_1$, a = 7.394(4) Å, b = 10.764(19) Å, c = 10.800(5) Å, β = 99.71(4)°, V = 847(2) Å^3, ρ_{calc} = 1.303 g.cm^{-3}, Z = 2; μ(Mo, Kα) = 1.0 cm^{-1}. R and wR2 0.086 and 0.155, respectively, for 1230 unique data collected in the 3 - 25.3°2 θ range.

The introduction of the nitrogen functionality (the amino group precursor) proved to be the most difficult step of the synthetic strategy. Several methodologies were tested but they were always hampered by the concurrent elimination reaction yielding the unsaturated diketopiperazine with the exocyclic double bond. Initial trials involved the activation of the hydroxyl group of **102** in the form of a mesylate.[61]

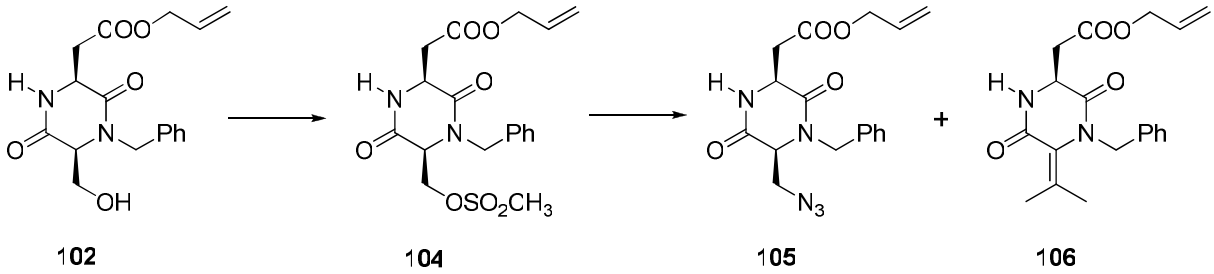

102 **104** **105** **106**

Scheme II.13. (i) Et_3N, CH_3SO_2Cl, CH_2Cl_2, 0 ºC: quantitative yield; (ii) NaN_3 (2 equiv), DMF: 30%.

Reaction of alcohol **102** with methanesulfonyl chloride, in the presence of triethylamine led to the corresponding mesylate **104** in quantitative yield (Scheme II.13). However the

subsequent reaction with sodium azide at room temperature resulted to be quite disappointing. The desired azide **105** was obtained, but in a low yield (30%) and, the elimination product **106** was obtained as the major product (44 %). Similar results were obtained even when the reaction was performed at low temperature (0 ºC).

On the other hand, when the hydroxyl group was activated as its triflate, the concurrent elimination reaction did not occur (Scheme II.14). The same observation had been already reported in literature, using the same reaction conditions.[62] Nonetheless, the yield of isolated azide **105** was in the same range (31%), probably due to decomposition of the triflate derivative prior to substitution. The same reaction in different solvents (THF and THF/DMF, 2/1) led to similar results.

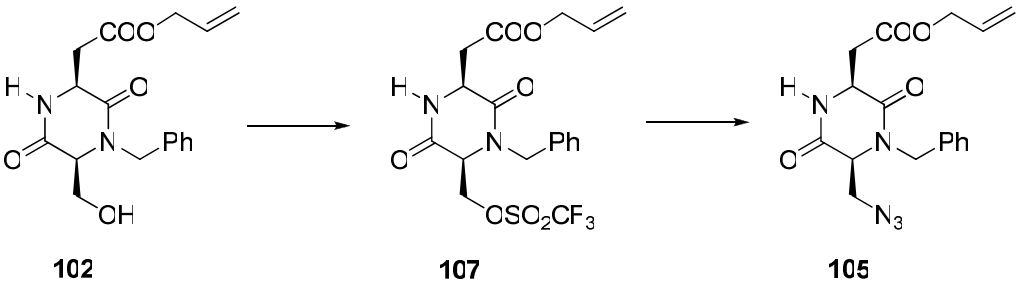

102 107 105

Scheme II.14. (i) Pyridine, $(CF_3SO_2)_2O$, CH_2Cl_2, -20 ºC; (ii) NaN_3 (4 equiv), DMF, 0 ºC to r.t.: 31%.

Finally, the introduction of the azide group was attempted through a Mitsunobu-type reaction using a solution of hydrazoic acid (HN_3) in toluene.[63]. This procedure has been reported for the successful synthesis of 2,3-diamino propionic acid starting from serine derivatives.[64,65] Unfortunately, in our case even the Mitsunobu-type conditions led to significant amounts of elimination product. By decreasing the temperature reaction it was possible to increase the yield of the desired product and reduce the formation of the elimination product. Eventually, it was necessary to change solvent due to the insolubility of DKP **102** in toluene at temperatures lower than 0 ºC. Scheme II.15 summarizes the optimized Mitsunobu-type conditions which afforded azide **105** in a moderate yield (48%).

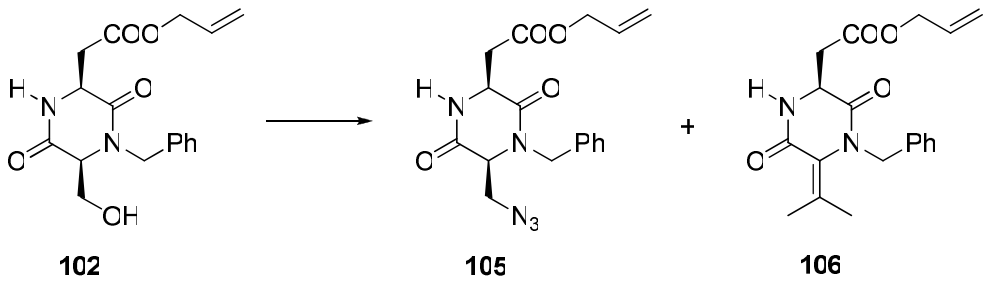

102 105 106

Scheme II.15. (i) PPh_3, DIAD, HN_3·Tol, Toluene/CH_2Cl_2 (2/1), -20 ºC: 48%.

The same Mitsunobu-HN_3 reaction run on dipeptide **101** gave a higher yield of the azide derivative, but, unfortunately, all attempts to cyclise this derivative met with no success.

The next step involved a one pot Staudinger – Boc protection. The Staudinger reaction, a very mild azide reduction, involves the reaction of the azide with a phosphine to generate a phosphazide, which loses N_2 to form an iminophosphorane. Hydrolysis of this intermediate leads to the amine and the very stable phosphine oxide (Scheme II.16).

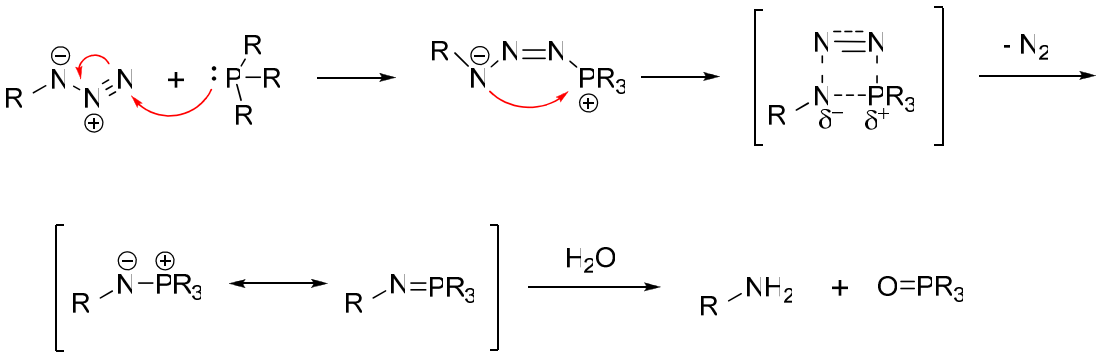

Scheme II.16. Mechanism of the Staudinger reaction.

In our case the intermediate iminophosphorane reacted directly with 2-(*t*-butoxycarbonyloxyimino)-2-phenylacetonitrile (Boc-ON),[66] present in the reaction medium, affording the desired Boc-protected amine in very good yield (Scheme II.17). Finally the DKP scaffold allyl ester **108**, was de-allylated in the presence of a catalytic amount of palladium *tetrakis*(triphenylphosphine) [$Pd(PPh_3)_4$] and pyrrolidine, *i.e.* a nucleophile acting as an allyl scavenger to give the amino acid derivative **90** in quantitative yield (Scheme II.17). Such methodology is of special interest for peptide synthesis because the deprotection conditions are usually mild enough to be compatible with the presence of acid labile *t*-Bu and Boc protections.[67]

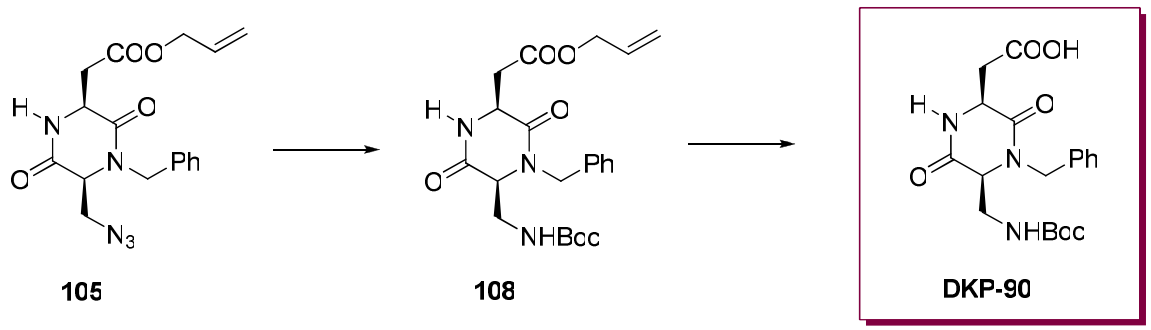

Scheme II.17. (i) Me_3P, Boc-ON, Toluene, -20 ºC to r.t.: 90%; (ii) pyrrolidine, PPh_3, $[Pd(PPh_3)_4]$, CH_2Cl_2, 0 ºC: quantitative yield.

II.3.2. SYNTHESIS OF THE PEPTIDOMIMETICS CONTAINING DKP-90

Several peptidomimetics: di- (Ac-DKP-NH-CH_2Ph), tri- (AA^1-DKP), tetra- (AA^1-DKP-AA^2), penta- (AA^1-AA^2-DKP-AA^3) and hexa-peptide mimics (AA^1-AA^2-DKP-AA^3-AA^4), were synthesised by solution layer peptide synthesis (Boc strategy) starting from the C-terminus.[68] Good yields were obtained in the coupling of the amino acids to the N-terminus of DKP-**90**, using HOBt [*N*-hydroxybenzotriazole] / EDC [*N*-ethyl-*N'*-(3-(dimethylamino)propyl)carbodiimide] in dichloromethane (Procedure A) or HATU [*O*-(7-azabenzotriazol-1-yl)-*N,N,N',N'*-tetramethyluronium hexafluorophosphate] in dimethylformamide (Procedure B), always in the presence of a tertiary amine (in this case, *N,N*-diisopropylethylamine).[68]

SYNTHESIS OF THE DIPEPTIDE MIMIC 91

In a first instance dipeptide **109** was synthesised by coupling benzylamine to the C-terminus of DKP-**90**, using general procedure A. The N-terminus was deprotected using TFA and then acetylated, affording dipeptide **91** in good yield (Scheme II.18).

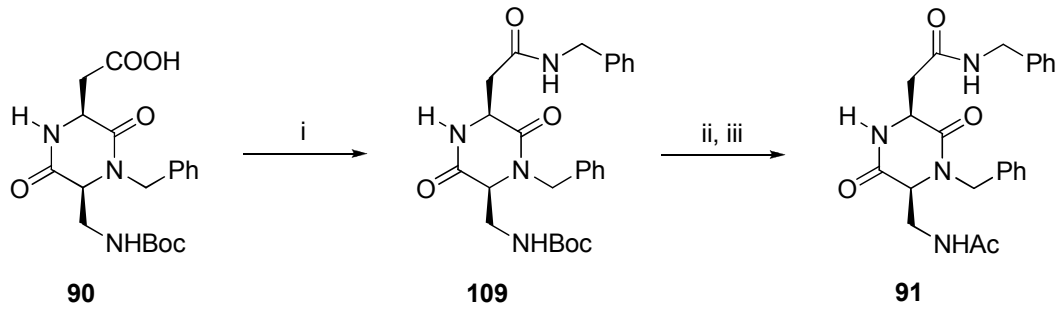

Scheme II.18. (i) $PhCH_2NH_2$, HOBt, DIPEA, DMF then EDC, 0 ºC to r.t.: 90%; (ii) TFA/CH_2Cl_2 (1:1, v/v) and (iii) Ac_2O, DIPEA, CH_2Cl_2: 92% over two steps.

SYNTHESIS OF THE TETRAPEPTIDE MIMICS 92 AND 93

Tetrapeptide mimics **92** and **93**, were obtained by initially coupling the TFA salt of **110** to the C-terminus of DKP-**90**, using general procedure A. Boc-(*S*)-Ala-OH was then coupled to the N-terminus of the tripeptide mimic **111**, yielding the *N*-Boc-tetrapeptide mimic **92**. Alternatively, when Ac-(*S*)-Ala-OH was reacted, the *N*-Ac-tetrapeptide mimic **93** was obtained (Scheme II.19). In both cases general procedure B was used for the attachment of amino acid derivatives to the N-terminus of DKP-**90**.

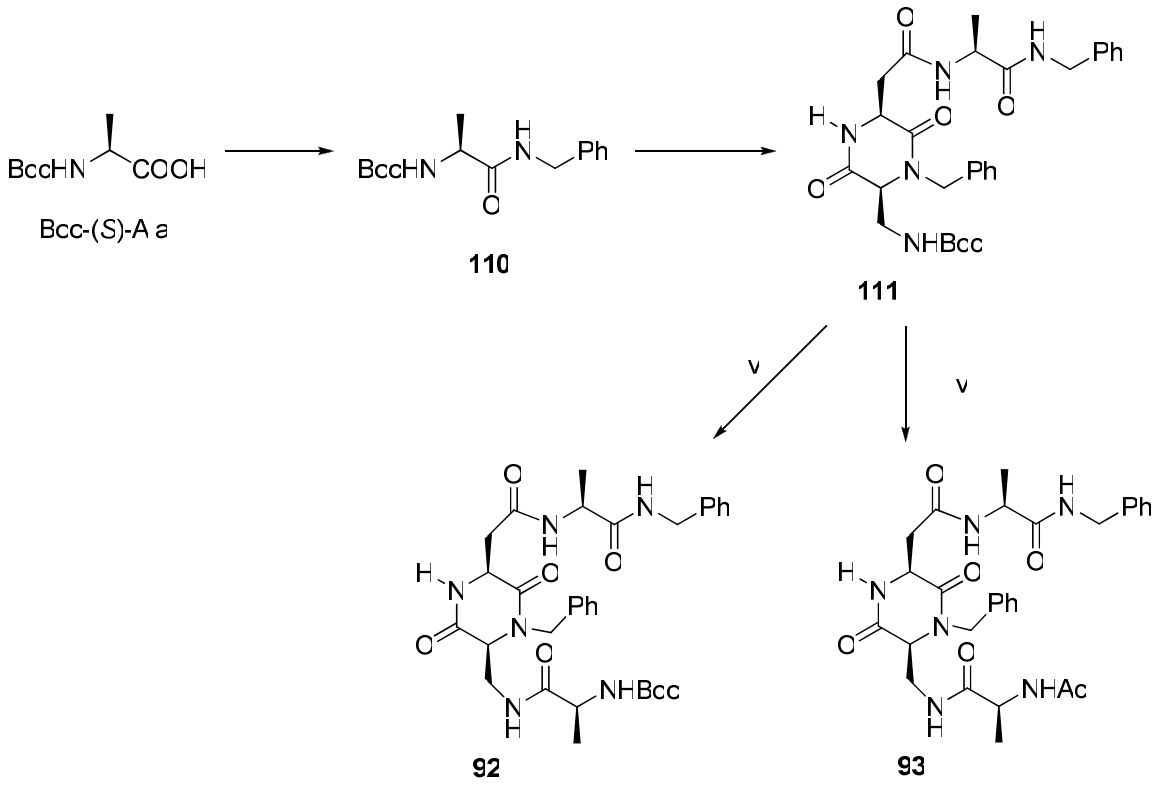

Scheme II.19. (i) $PhCH_2NH_2$, HOBt, DIPEA, DMF then EDC, 0 ºC to r.t.: quantitative yield; (ii) TFA/CH_2Cl_2 (1:1, v/v) and (iii) DKP-**90**, HOBt, DIPEA, DMF then EDC, 0 ºC to r.t.: 92% over two steps; (ii) and (iv) Boc-(*S*)-Ala-OH, HATU, DIPEA, CH_2Cl_2, 0 ºC to r.t.: 82% over two steps; (ii) and (v) Ac-(*S*)-Ala-OH, HATU, DIPEA, CH_2Cl_2, 0 ºC to r.t.: 76% over two steps.

SYNTHESIS OF THE PENTAPEPTIDE AND HEXAPEPTIDE MIMICS 95 AND 96

The synthesis of the longer hexapeptide mimics was obtained starting form the dipeptide fragment **113** (Scheme II.20), which was then attached to the C-terminus of DKP-**90**. Dipeptide **113** was synthesised from Boc-(*S*)-Ala-O*n*Bu **112** and Boc-(*S*)-Val-OH, using procedure A. According to the same general procedure, coupling of the deprotected dipeptide **113** to the C-terminus of DKP-**90**, afforded compound **114**. After Boc deprotection with TFA, another Ala residue was coupled to the N-terminus of DKP-**90**. In this case general procedure B was necessarily used to obtain the pentapeptide mimic **94** in good yield (85%).

Finally, coupling of either Boc-(*S*)-Val-OH or Ac-(*S*)-Val-OH to the N-terminus of **94** (again with general procedure B), afforded the *N*-Boc-hexapeptide mimic **95** and *N*-Ac-hexapeptide mimic **96**, respectively, both in satisfactory yields (Scheme II.20).

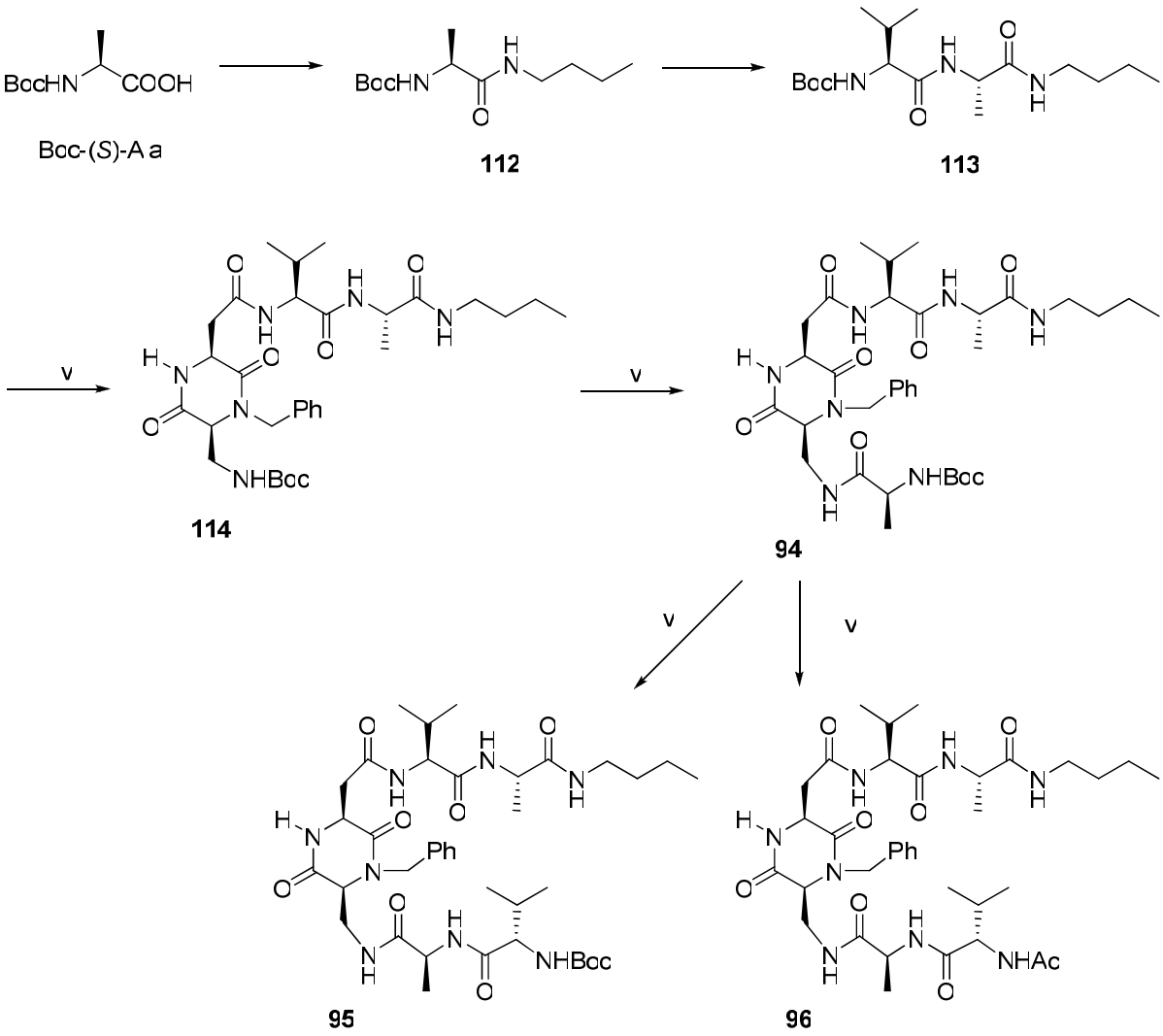

Scheme II.20. *n*-$BuNH_2$, HOBt, DIPEA, DMF then EDC, 0 ºC to r.t.: 95%; (ii) TFA/CH_2Cl_2 (1:1, v/v) and (iii) Boc-(*S*)-Val-OH, HOBt, DIPEA, DMF then EDC, 0 ºC to r.t.: 96% over two steps; (ii) and (iv) DKP-**90**, HOBt, DIPEA, DMF then EDC, 0 ºC to r.t.: 80% over two steps; (ii) and (v) Boc-(*S*)-Ala-OH, HATU, DIPEA, CH_2Cl_2, 0 ºC to r.t.: 85% over two steps; (ii) and (vi) Boc-(*S*)-Val-OH, HATU, DIPEA, CH_2Cl_2, 0 ºC to r.t.: 70% over two steps; (ii) and (vii) Ac-(*S*)-Val-OH, HATU, DIPEA, CH_2Cl_2, 0 ºC to r.t.: 60% over two steps.

II.4. CONFORMATIONAL STUDIES

II.4.1. CONFORMATIONAL STUDIES OF CONSTRAINED PEPTIDES: AN OVERVIEW

The conformational preferences of peptides are commonly carried out by means of NMR spectroscopy, IR spectroscopy, as well as, molecular modelling techniques.

Characteristic differences in the NMR spectral parameters for unstructured peptides and peptides in extended and intramolecularly hydrogen bonded conformations have been widely reported in organic solvents.[69-72] Chemical shifts and coupling constants for the C_α hydrogens reflect the average conformations of individual amino acid residues, while the chemical shifts of the amide protons and their temperature dependence reveal whether they are solvent exposed or intramolecularly hydrogen bonded.

Insights into hydrogen bonding can be gained from the chemical shifts of amide NHs: signals of protons that are H-bonded, either intramolecularly or to the solvent, appear downfield of those that are not H-bonded. In solvents that do not form strong hydrogen bonds (*e.g.* $CDCl_3$), significantly deshielded amide protons often indicate that they are involved in intramolecular hydrogen bonding.[73] However, the same conclusion is not true in the case of strongly H-bonding solvents (e. g. MeOD, DMSO-d_6). In, such cases each amide proton is either locked in an intramolecular H-bond or engaged in an intermolecular H-bonding with the solvent.

Peptide amide protons involved in H-bonding, or otherwise shielded from solvent, can be identified by their relatively slow rate of H/D exchange. It is generally accepted that intramolecular hydrogen-bonds in proteins must break before exchange with the solvent can occur.[74] Therefore, amide proton-deuterium exchange rates permit the identification of amide protons that are involved in intramolecular hydrogen-bonding. The $\Delta\delta$(NH) upon addition of a solvent able to compete for the formation of H-bonds (MeOH, DMSO) can also provide information regarding the possible participation of an amide proton in a stable intramolecular H-bond.

On the ^{1}H-NMR timescale, equilibration between hydrogen-bonded and non-hydrogen-bonded states for a given amide proton is rapid; therefore the observed amide resonances are weight averages of the contributing states. IR spectroscopy is, in principle, more useful for detecting amide H-bonding equilibrium, as the much shorter timescale of IR measurements permits the observation of distinct N-H stretching absorptions for equilibrating H-bonded and non-H-bonded states.[75] However, the use of this technique to elucidate H-bonding behaviour in peptides is limited, because the presence of multiple NH groups (specially, the resulting band overlap) often renders IR data inconclusive in such cases.

Another powerful tool for understanding the extent of H-bonding is the temperature dependence of the chemical shifts of amide protons [$\Delta\delta$(NH)/ΔT]. In non-competitive solvents (like $CDCl_3$), different ways of interpreting these data have been proposed. According to some authors, peptide NH protons that are either non-H-bonded or locked in a H-bonded conformation exhibit a small temperature dependence (typically 0 to -3 ppb/K), while protons that participate in an equilibrium between a H-bonded and a non-H-bonded state exhibit a large temperature dependence (typically -4 to -8 ppb/K).[76,77] However, other authors consider that NH protons with a $\Delta\delta$(NH)/ΔT smaller in absolute value than -2.6 ppb/K are intramolecularly H-bonded, irrespective of the chemical shift value or other parameters, while protons with a $\Delta\delta$(NH)/ΔT larger in absolute value than -2.6 ppb/K are non-H-bonded.[78] In the case of competitive solvents, like water and DMSO, the consensus is higher and, it is generally accepted that solvent-exposed protons exhibit a large temperature dependence, while intramolecular H-bonded (solvent-shielded) protons exhibit only a small temperature dependence.

Finally, molecular mechanics calculations are usually performed to corroborate NMR data. Monte Carlo conformational search and molecular dynamics calculations are often carried out to investigate the conformational preferences of peptides and peptidomimetics.

II.4.2. CONFORMATIONAL STUDIES OF PEPTIDOMIMETICS CONTAINING DKP-90

The tendency of the DKP-**90**-containing peptidomimetics **91**–**96** to adopt a defined secondary structure was then evaluated by a combination of ^{1}H-NMR spectroscopy, IR spectroscopy, CD spectroscopy, and computer modelling.

The dipeptide mimic **91**, in $CDCl_3$, showed some degree of concentration dependence and a strong temperature dependence of the chemical shifts of all the NH's (> 20 ppb/K) at a 2 mM concentration, while the chemical shift values were only slightly deshielded (6.25–7.02 ppm) with respect to the average values for non-hydrogen-bonded NH protons (*ca* 6.0 ppm). These data are in agreement with an equilibrium between a non-hydrogen-bonded and an intermolecularly H-bonded status (aggregation).

In the case of the longer peptidomimetics (tetra-, penta-, and hexa-peptides), the chemical shift of the amide protons was essentially invariant over the concentration range 0.5 – 10 mM at 298 K, indicating an absence of significant aggregation in this concentration range, and 0.5 – 2 mM solutions were employed for all conformational analysis. In all cases, all the proton resonances could be assigned by means of COSY and ROESY spectra.

The NMR studies for tetrapeptide mimics **92** and **93** were performed in $CDCl_3$. From the NMR data summarised in Table II.2 it appears that the amide protons NH^4 are in an intramolecularly hydrogen-bonded status. In fact: (a) their resonance is shifted substantially downfield (8.10 and 8.18 for **92** and **93**, respectively); (b) the temperature dependence of the NH^4 chemical shift falls within the typical values for intramolecularly hydrogen bonded protons: 2.7 ppb/K for **93** and slightly higher (4.1 ppb/K) for **92**; (c) the $\Delta\delta$ (NH^4) upon addition of CH_3OH (obtained measuring the spectrum in a $CDCl_3/CH_3OH$, 4/1 mixture), is small (0.03 in the case of **93**), and the rate of exchange H^4/D upon addition of CD_3OD is quite slow (*ca.* 960 min). In the case of proton NH^1, the same parameters (*i.e.* values of chemical shift, temperature dependence, $\Delta\delta$ upon addition of CH_3OH and rate of exchange H^1/D upon addition of CD_3OD), are indicative of an equilibrium between an intramolecularly hydrogen-bonded and a non-hydrogen-bonded status for both **92** and **93**. A similar equilibrium is also partially displayed by proton NH^2, although in this case the NMR parameters reflect a looser intramolecular hydrogen-bond.

Table II.2. ^{1}H-NMR data for the amide protons in compounds **92** and **93**.

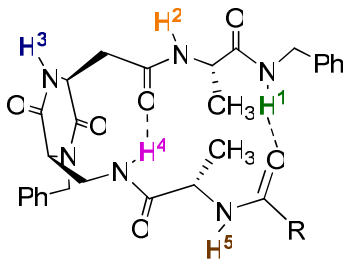

92 R = C-*t*Bu
93 R = CH_3

	92		**93**			
	$\delta^{a,c}$ (ppm)	$\Delta\delta/\Delta T^{a,d}$ (ppb/K)	$\delta^{b,c}$ (ppm)	$\Delta\delta/\Delta T^{b,d}$ (ppb/K)	$\Delta\delta^{b,e}$ (added CH_3OH)	NH/ND exchange^{b,f} (min)
NH^1	**7.81**	**-7.6**	**8.21**	**-4.6**	**-0.07**	**300**
NH^2	7.03	-8.2	7.21	-5.3	0.53	160
NH^3	6.28	-9.1	6.61	-15.5	1.25	< 10
NH^4	**8.10**	**-4.1**	**8.18**	**-2.7**	**0.03**	**960**
NH^5	5.41	-1.8	6.40	-2.3	≥ 0.7	-^{g}

a) Concentration 0.5 mM in $CDCl_3$; b) Concentration 2.0 mM in $CDCl_3$; c) at 298 K; d) determined between 238 and 288 K; e) measured in $CDCl_3/CH_3OH$ 4/1; f) measured in $CDCl_3/CD_3OD$ 4/1; g) not determined due to overlap with other resonances.

NOE contacts can be highly indicative of the formation of a β-hairpin mimic when inter-strand contacts are visible. Unfortunately, in the case of the tetrapeptide mimics **92** and **93** we could not detect this kind of contacts, and only strong intra-strand contacts were observed, which are indicative of an extended conformation for the amino acid residues.

The FT-IR spectrum of the tetrapeptide mimic **92** (2 mM solution in $CHCl_3$), is characterized by two bands, at 3427 and 3395 cm^{-1} (free NH groups) and two prominent bands at 3321 and 3291 cm^{-1} (H-bonded NH groups), respectively.[75] In the case of **93**, only two bands can be recognized, one in the free NH region (3410 cm^{-1}), and one at 3291 cm^{-1} indicative of H-bonded NH's.

The NMR and IR data collected support the formation of a β-hairpin mimic involving a 10-membered and a 18-membered H-bonded rings and a reverse turn of the growing peptide chain. The weak hydrogen-bonded character of NH^2 might indicate that a different β-hairpin mimic involving a 12-membered and a 16-membered H-bonded rings (*vide infra* the molecular modelling discussion) is present as a minor conformer at the equilibrium.

Computational studies designed to investigate the ability of the DKP-**90** scaffold to induce β-hairpin conformations were performed on the tetrapeptide mimic **93**. The molecule was subjected to an extensive, unconstrained Monte Carlo/Energy Minimization (MC/EM) conformational search[79] by molecular mechanics methods using the AMBER* force field[80] and the implicit $CHCl_3$ GB/SA solvent model.[81]

Only two types of conformations, both featuring a β-hairpin-like arrangement, are predominant among the structures found within 3 kcal/mol from the global minimum. The lowest energy conformer features an intramolecular hydrogen bonding pattern involving the formation of a 10-membered and a 18-membered H-bonded rings (Figure II.16, **93a**). The 10-membered ring of this conformer features a *gauche* orientation of the NH and C=O groups around the C^2–C^3 bond (β-amino acid numbering), with the β^2 and β^3 amino acid torsion angles (θ) of -87° and 81°, respectively. This cross-strand hydrogen bonding pattern is in agreement with the structure proposed on the basis of the NMR experiments, summarised in Table II.2.

A second β-hairpin-like conformer was found at 1.09 kcal/mol from the global minimum, involving the formation of a 12-membered and a 16-membered H-bonded rings (Figure II.16, **93b**). The 12-membered ring requires *anti* C^2–C^3 torsion angles, with θ values of -171° and -177° for the corresponding β^2 and β^3 amino acids. As also suggested by the NMR data reported in Table II.2, this second type of β-hairpin structure, or at least its 12-membered H-bonded ring portion, might participate as a minor conformer to the conformational equilibrium.

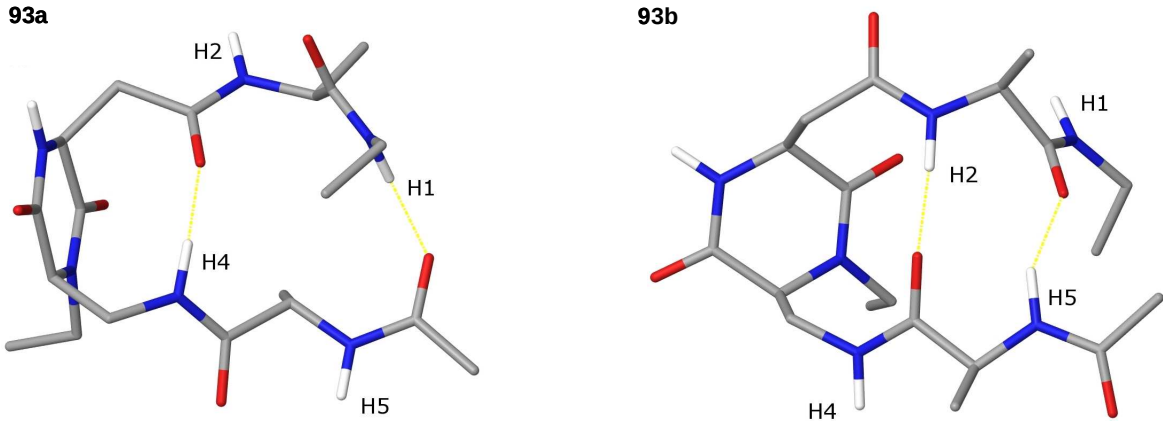

Figure II.16. Structures of low-energy conformers (MC/EM, AMBER*, $CHCl_3$ GB/SA) calculated for compound **93**: left, global minimum (**93a**); right, conformer with relative energy of 1.09 kcal/mol (**93b**). Hydrogen bonds are indicated with dotted lines and for clarity all non-polar hydrogen atoms and phenyl groups have been omitted.

The solution structure of the pentapeptide mimic **94** was also studied by determining the temperature dependence of the NH chemical shifts at 2 mM in $CDCl_3$ (Table II.3).

Table II.3. ^{1}H-NMR data for the amide protons in compound **94**.

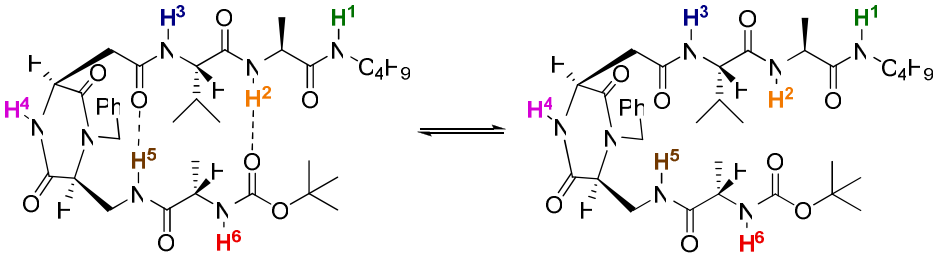

	94	
	$\delta^{a,b}$ (ppm)	$\Delta\delta/\Delta T$ ^{a,c} (ppb/K)
NH^1	6.47	-2.5
NH^2	7.71	-8.3
NH^3	7.21	-14.3
NH^4	7.14	-16.0
NH^5	7.77	-6.8
NH^6	5.27	-4.8

a) Concentration 2.0 mM in $CDCl_3$; b) at 298 K; c) determined between 258 and 298 K.

An equilibrium between an intramolecularly hydrogen-bonded and a non-hydrogen-bonded status is suggested by the various parameters for protons NH^2 and NH^5 (δ= 7.71 and 7.77; $\Delta\delta/\Delta T$= -8.3 and -6.8 ppb/K, respectively, Table II.3), which might be indicative of the presence of a β-hairpin conformation with a 10-membered and a 18-membered H-bonded rings, in analogy to the tetrapeptide mimics **92** and **93**.

Finally, the conformational preferences of hexapeptide mimics **95** and **96** were studied. The first dramatic difference with respect to the shorter homologues was the insolubility of these products, in particular the hexapeptide mimic **96**. In fact compound **96** was only soluble in DMSO and in hot methanol, while compound **95** was also sparingly soluble in $CHCl_3$ and soluble in methanol. For this reason the NMR studies of these compounds were performed in DMSO-d_6 and, in the case of **95**, also in 5% CD_3OH-$CDCl_3$. All the proton resonances could be assigned by means of COSY and ROESY spectra.

The analysis of the ^{1}H-NMR spectrum of hexapeptide mimic **95** in 5% CD_3OH-$CDCl_3$ (Table II.4) showed that protons NH^2 and NH^5 are notably shifted downfield with respect to the other NH protons (δ= 8.24 and 7.97; respectively). The temperature dependency is indicative of a hydrogen-bonded status for both NH^2 and NH^5 ($\Delta\delta/\Delta T$= -2.5 and -1.3 ppb/K, respectively), and of an equilibrium between an intramolecularly hydrogen-bonded and a non-hydrogen-bonded status for NH^7 ($\Delta\delta/\Delta T$= -6.0 ppb/K).

The ^3J values for the NH-C_αH in DMSO-d_6 for both compounds **95** and **96** (Table II.4) are in agreement with the typical values for peptides showing a β-hairpin secondary structure (7.5–8.5 Hz).[70] Similar values were also found for the spectrum of **95** in 5% CD_3OH-$CDCl_3$, also shown in Table II.4.

Table II.4. ^{1}H-NMR data for the amide protons in compounds **95** and **96**.

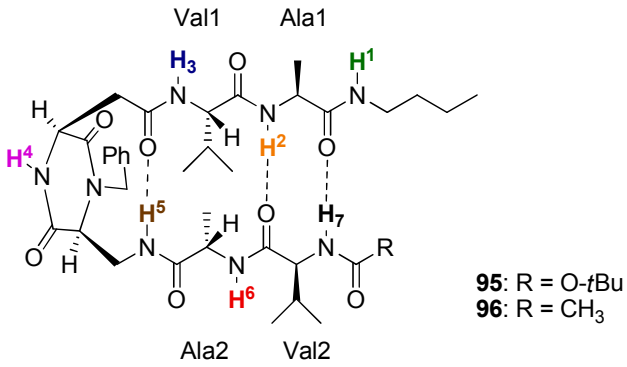

	95				**96**	
	$\delta^{a,b}$ (ppm)	$\Delta\delta/\Delta T^{a,c}$ (ppb/K)	$^{3}J_{NHC\alpha H}{}^{a,d}$	$^{3}J_{NHC\alpha H}{}^{e,f}$	$\delta^{e,f}$ (ppm)	$^{3}J_{NHC\alpha H}{}^{e,f}$
NH^1	6.99	-8.0	5.7	5.6	7.83	5.6
NH^2	**8.24**	**-2.5**	**7.7**	**7.4**	**8.19**	**7.9**
NH^3	7.61	-15.5	8.0	8.1	8.29	7.2
NH^4	7.68	-16.5	-[g]	-[g]	8.28	-[g]
NH^5	**7.97**	**-1.3**	**-[g]**	**-[g]**	**8.25**	**-[g]**
NH^6	7.42	-8.5	8.0	7.8	8.18	7.8
NH^7	5.76	-6.0	6.8	9.1	7.96	8.9

a) Concentration 2.0 mM in 5% CD_3OH-$CDCl_3$; b) at 288 K; c) determined between 248 and 288 K; d) at 278 K; e) Concentration 2.0 mM in DMSO-d_6; f) at 298 K; g) broad signal.

The 2D-NMR analysis in DMSO-d_6 suggests that both compounds **95** and **96** adopt a β-hairpin-type conformation with a 10-membered H-bonded ring similar to that observed in the previous structures. In fact, the ROESY spectrum shows a set of NOE cross-peaks that support this conclusion (Figure II.17). In particular, in the case of **95**, several interstrand NOE contacts were observed: a strong contact between the $C_\alpha H$ of the Val1 and $C_\alpha H$ of the Ala2 residue (see also Figure II.18a); a medium contact between NH^2 and the $C_\alpha H$ of the Ala2 residue (see also Figure II.18b) and a weak contact between NH^2 and NH^7 (see also Figure II.18c). The same contacts were also observed when the ROESY spectrum of **95** was collected in 5% CD_3OH-$CDCl_3$ (Figure II.19). A similar pattern is also shown by the spectrum of **96** in DMSO-d_6 (Figure II.20), with the exception of the cross peak between NH^2 and NH^7 which is too weak to be detected in this case.

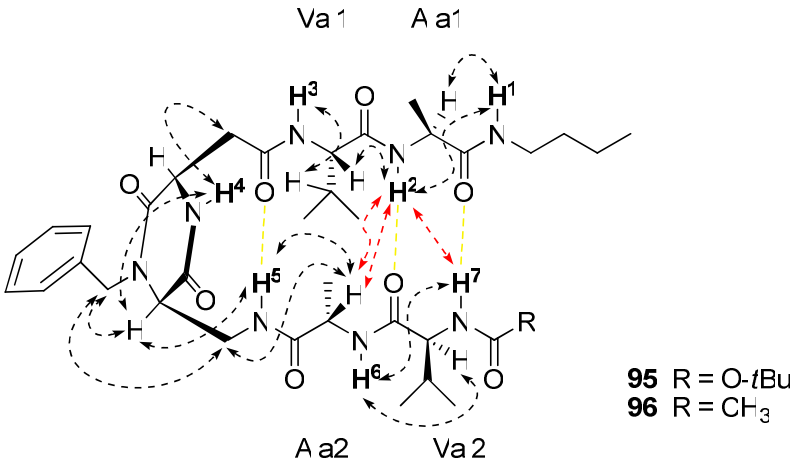

Figure II.17. Selected intrastrand (dashed black arrows) and interstrand (dashed red arrows) NOE contacts for hexapeptide mimics **95** and **96**.

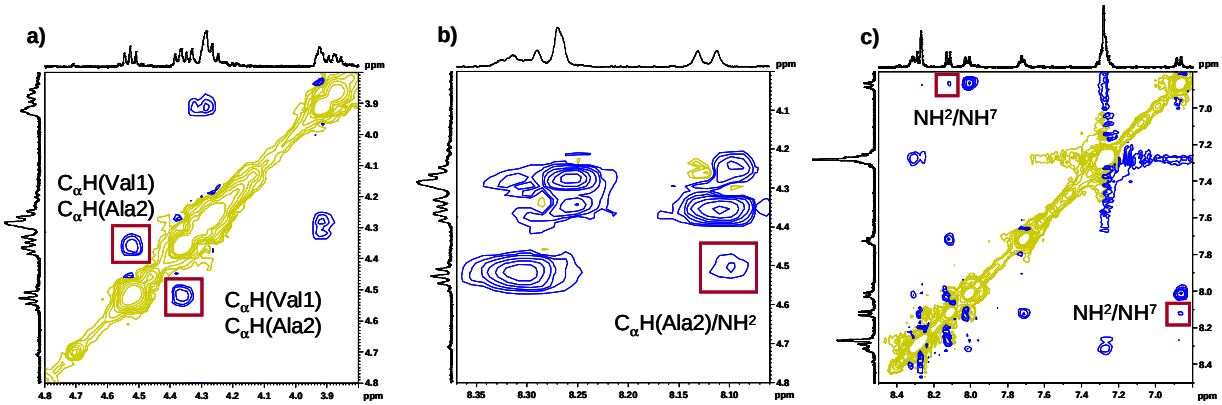

Figure II.18. Sections of the ROESY spectrum of **95** (2 mM in DMSO-d_6, p15=400 ms) showing: a) interstrand NOE's in the $C_\alpha H$ region, b) interstrand NOE's for $C_\alpha H$ and NH, and c) interstrand NOE's for the NH.

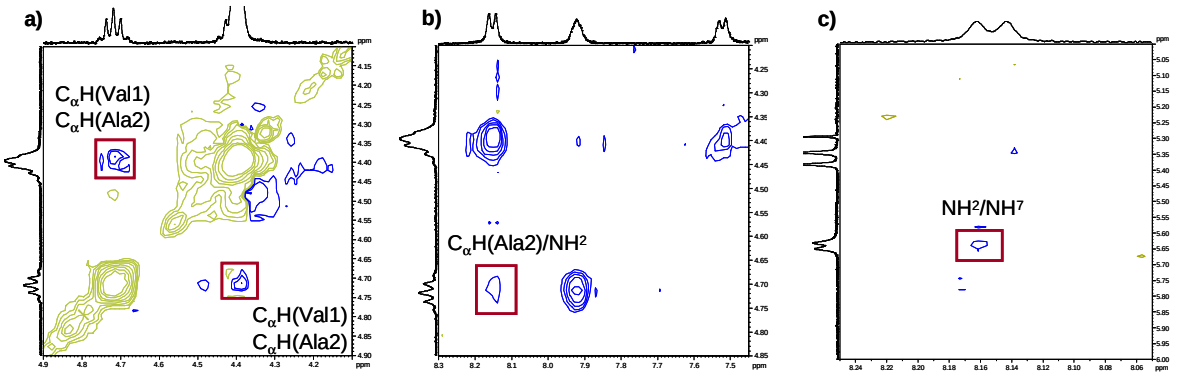

Figure II.19. Sections of the ROESY spectrum of **95** (2 mM in 5% CD_3OH-$CDCl_3$, p15=400 ms) showing: a) interstrand NOE's in the $C_\alpha H$ region, b) interstrand NOE's for $C_\alpha H$ and NH, and c) interstrand NOE's for the NH.

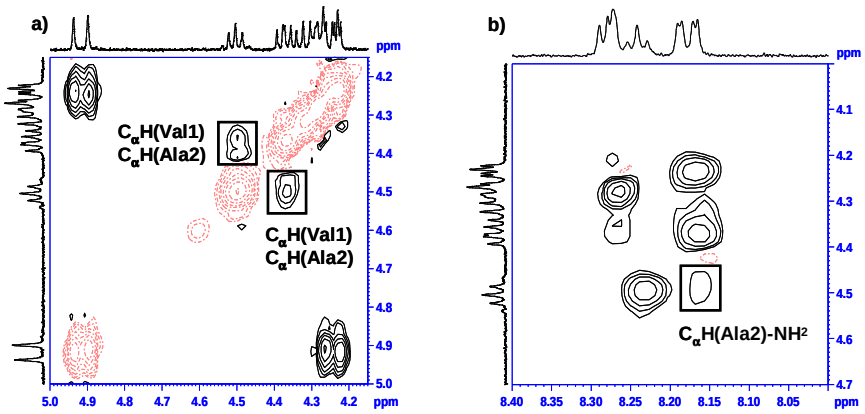

Figure II.20. Sections of the ROESY spectrum of **96** (2 mM in DMSO-d_6, p15=400 ms) showing: a) interstrand NOE's in the $C_\alpha H$ region, b) interstrand NOE's for $C_\alpha H$ and NH.

Molecular mechanics calculations were performed on the hexapeptide mimic **96,** similarly to the tetrapeptide mimic **93**, to investigate the ability of the DKP-**90** scaffold to induce β-hairpin conformations. The molecule was subjected to an unconstrained Monte Carlo/Energy Minimization (MC/EM) conformational search[79] *in vacuo* (the implicit DMSO solvation model is not available in the software employed) with a distance dependent dielectric constant of *4r*, to generate a suitable starting conformation for the following restrained simulation in explicit DMSO solvent (see below). Two different, energetically equivalent, β-hairpin conformations were found within 3 kcal/mol from the global minimum (Figure II.21). The lowest energy conformer is characterized by the presence of hydrogen bonds involving the amide protons NH^3, NH^6 and NH^1 and forming, respectively, a 12-membered, a 16-membered and a 24-membered rings (Figure II.21, **96a**). However, no experimental evidence is provided by the NMR data in solution (Table II.4, Figure II.17) for such intramolecular hydrogen bonding pattern (resembling conformer **93b** of the tetrapeptide mimic **93**, Figure II.16). The second conformer (Figure II.21, **96b**) shows a β-hairpin conformation in agreement with the structure proposed on the basis of the spectroscopic data (Table II.4, Figure II.17). This conformer features a 10-membered and a 18-membered H-bonded rings that resemble the hydrogen bonding pattern observed in conformer **93a** of the tetrapeptide mimic **93** (Figure II.16), and an additional 22-membered H-bonded ring involving the NH^7 amide proton and the Ala1 carbonyl group.

Furthermore, comparing the calculated interstrand distances in conformers **96a** and **96b** between protons $C_\alpha H$ of the Val1 and $C_\alpha H$ of the Ala2 residues and between the proton $C_\alpha H$ of the Ala2 residue and the NH^2 amide proton (Table II.5), only the **96b** conformer

shows distance values consistent with the NOE contacts observed in DMSO-d_6 solution (Figure II.17).

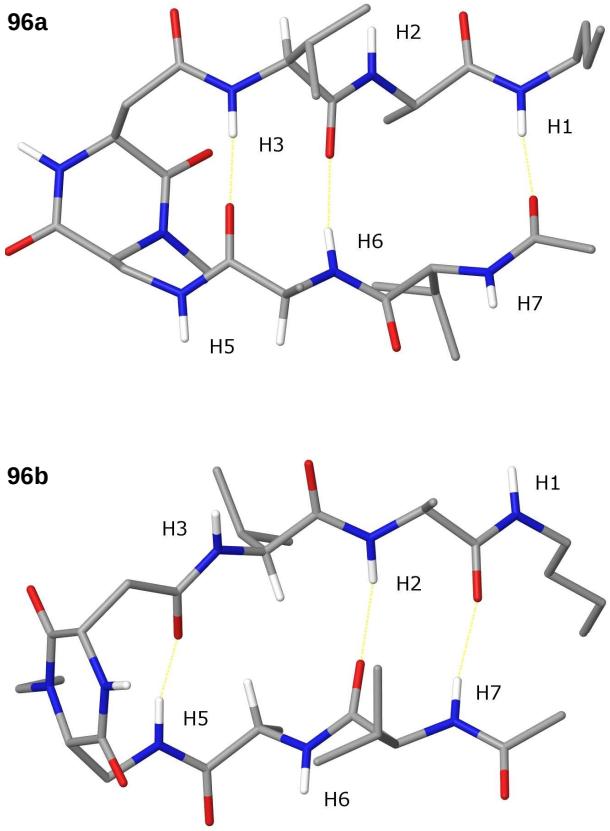

Figure II.21. Structures of the lowest energy conformers (MC/EM, AMBER*, *in vacuo*) calculated for **96**: left, global minimum (**96a**); right: conformer with relative energy of 0.26 kcal/mol (**96b**). Hydrogen bonds are indicated with dotted lines and for clarity all non-polar hydrogen atoms (except $C_\alpha H$ of Val1 and Ala2 residues) and the phenyl residues, have been omitted.

Table II.5. Relevant proton distances of the low-energy conformers (MC/EM, AMBER*, *in vacuo*) calculated for compound **96**.

Conformer	ΔE (kcal/mol)	Proton distance (Å)	
		$C_\alpha H$(Val1)-$C_\alpha H$(Ala2)	$C_\alpha H$(Ala2)-NH^2
96a	0.0	7.56	7.92
96b	0.26	2.49	3.95

A simulated annealing protocol in explicit DMSO solvent[82] using the ff03 force field[83] and the SANDER module of the AMBER7 package,[84] was performed starting from conformer **96b**. According to the NOE data, two distance restraints were imposed between the protons $C_\alpha H$ of the Val1 and $C_\alpha H$ of the Ala2 residues (upper bound of 3.0 Å and force constant of 20 kcal/mol Å) and between the proton $C_\alpha H$ of the Ala2 residue and NH_2 amide (upper bound of 4.0 Å and force constant of 20 kcal/mol Å). The simulation converged to a unique β-hairpin structure (Figure II.22). Consistent with the NMR analysis, this β-hairpin arrangement features a 10-membered and a 18-membered H-bonded rings involving the NH^5 and NH^2 amide protons, respectively, while the NH^7 amide proton does not form any intramolecular hydrogen bond.

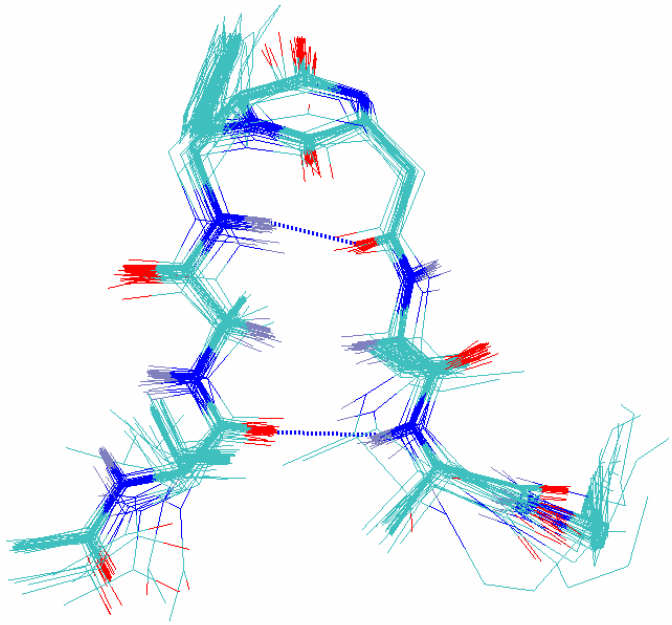

Figure II.22. Simulated annealing superimposed solutions for **96b**. Hydrogen bonds are indicated with dotted lines and all non-polar hydrogen atoms, except $C_\alpha H$ of Val1 and Ala2 residues, have been omitted for clarity.

Finally, the ability of peptidomimetics **92**, **93**, **95** and **96** to adopt an ordered secondary structure in solution was also evaluated by CD spectroscopy (Figure II.23). The spectra were measured in methanol (0.5 mM) and showed a similar behaviour: two negative minima, one at 200-205 nm (201 nm for compound **96**) and a second one at about 220 nm (220 nm for compound **96**), and a negative maximum at 209-215 nm (209 nm for **96**) were displayed by all these compounds.

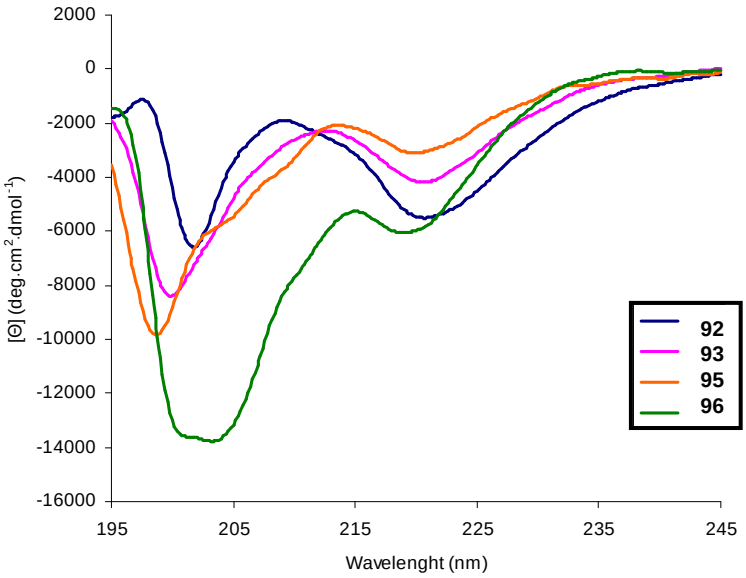

Figure II.23. CD spectra of peptidomimetics **92**, **93**, **95**, and **96** (0.5 mM in methanol). The data are normalized for peptide concentration and number of residue.

Unfortunately, while several CD studies have been reported for β-peptides adopting helical conformations (and in particular 12- and 14-helices),[85-87] no conclusive data on β-peptides assuming hairpin-type conformations have appeared in the literature. A hexapeptide **115** (Figure II.24) consisting of β^3-homo-amino, β^2-homo-amino and α-amino acids with a central β^2-β^3 segment, was recently reported by Seebach and co-workers to adopt a turn-like conformation with a 10-membered H-bonded ring induced by the β^2-β^3 unit.[57] Its CD spectrum (0.2 μM in CH_3OH) displayed a similar behaviour with respect to our derivatives, with a minimum at 197 nm, a shoulder at 205 nm, a negative maximum at about 215 nm and a less pronounced minimum at *ca* 220 nm (Figure II.24). In addition, both minima and the maximum showed negative molar ellipticities of comparable intensity to our compounds.

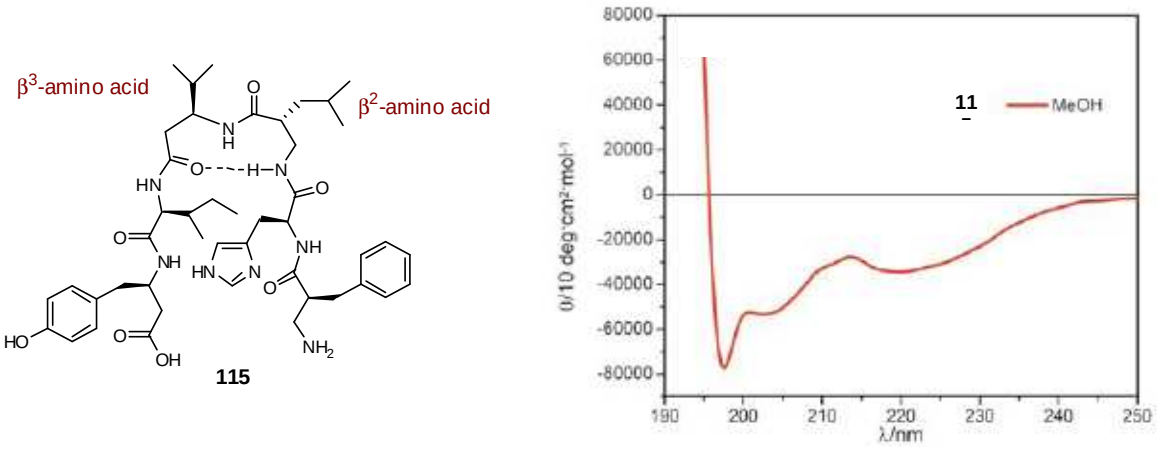

Figure II.24. CD spectra of peptidomimetic **115** (0.2 μM in methanol).

III. TARGETING INTEGRINS: DKP AS RIGID SCAFFOLDS FOR RGD SEQUENCES

III.1. INTEGRINS: FAMILY, FUNCTION AND STRUCTURE

The integrin family is an extensive group of structurally related receptors for ECM (Extracellular Matrix) proteins and immunoglobulin superfamily molecules. Integrins are divalent cation dependent heterodimeric membrane glycoproteins composed of non-covalently associated α and β subunits that promote cell attachment and migration on the surrounding ECM. These heterodimeric proteins are expressed by all multicellular animals, but their diversity varies widely among species; for example, in mammals, one of 18 possible α subunits heterodimerises with one of the 8 β subunits to form more than 24 distinct integrin proteins, whereas the Drosophila and Caenorhabditis genomes encode only five and two integrin α subunits respectively.[88] Each integrin subunit consists of a large extracellular domain (approximately 80–150 kDa), a single transmembrane α-helix and a short (~30–40 amino acids) largely unstructured cytoplasmic region.

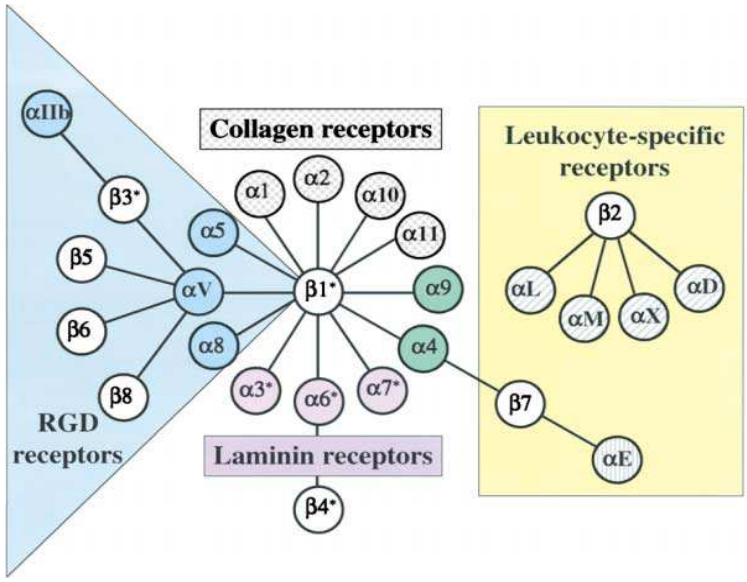

Figure II.25. The Integrin Receptor Family. The figure depicts the mammalian subunits and their αβ associations; 8 β can assort with 18 α subunits to form 24 distinct integrins. These can be considered in several subfamilies based on evolutionary relationships (coloring of α subunits), ligand specificity and, in the case of β_2 and β_7 integrins, restricted expression on white blood cells. α subunits with gray hatching or stippling have inserted I/A domains.[88]

Some integrins, such as $\alpha_5\beta_1$, primarily recognize a single ligand, whereas others, such as $\alpha_v\beta_3$, can bind several ligands. Many integrins, including $\alpha_v\beta_3$, $\alpha_5\beta_1$, $\alpha_{IIb}\beta_3$, $\alpha_v\beta_6$ and $\alpha_3\beta_1$, recognize the tripeptide Arg–Gly–Asp (RGD) in their ligands. Sequences flanking the RGD peptide are also important for integrin selectivity.[89] Other integrins recognize alternative short peptide sequences; for example, integrin $\alpha_4\beta_1$ recognizes Glu–Ile–Leu–Asp–Val (EILDV) and Arg–Glu–Asp–Val (REDV) in the alternatively spliced fibronectin domain known as IIICS. Some integrins, such as $\alpha_4\beta_1$, can also bind cell surface receptors, such as vascular cell adhesion molecule 1 (VCAM-1), to promote cell–cell adhesion.

Table II.6. Integrin extracellular ligands and recognition sequences.[90]

INTEGRIN		LIGAND	RECOGNITION SEQUENCES
β_1	α_1	Collagens, laminins	GFOGER[a]
	α_2	Collagens, laminins, chondroadherin	GFOGER[a]
	α_3	Laminins, fibronectin, thrombospondin, TIMP-2, uPAR, collagen, epiligrin, entactin	RGD
	α_4	Fibronectin, VCAM	IDAPS, EILDV, REDV, QIDS
	α_5	Fibronectin, fibrinogen, uPAR	RGD
	α_6	Laminins, merosin, kalinin	
	α_7	Laminins, merosin	
	α_8	Fibronectin, vitronectin, tenascin-C, osteopontin, and nephronectin	RGD
	α_9	Angiostatin, tenascin-C, osteopontin, and ADAMs, VCAM-1, tTG	AEIDGIEL
	α_{10}	Collagens	
	α_{11}	Collagens	
	α_V	Fibronectin, vitronectin	RGD
β_2	α_L	ICAM-1, -2 and -3	ICAM peptides
	α_M	Fibrinogen (γ-chain), ICAMs, iC3b, factor-Xa, denatured ovalbumin	P1 and P2 peptide, ICAM peptides
	α_X	Fibrinogen (α-chain), iC3b	GPR
	α_D	VCAM, ICAMs	
β_3	α_{IIb}	Collagens, fibronectin, vitronectin, fibrinogen (γ-chain), vWf, thrombospondin	RGD, HHLGGAKQAGDV
	α_V	Fibronectin, vitronectin, fibrinogen, vWf, thrombospondin, FGF-2, MMP-2 and some	RGD

		ADAM proteins	
β_4	α_6	Laminins	
β_5	α_V	Vitronectin, uPAR	RGD
β_6	α_V	Fibronectin, tenascin	RGD, DL*XX*L
β_7	α_4	Fibronectin, VCAM, MAdCAM	CS-1 peptide, LDT
	α_E	E-cadherin	
	α_V	Collagens, laminins, fibronectin	
β_8	α_V	Vitronectin, fibronectin	

[a]O as hydroxyproline. Abbreviations used in Table II.6 are: TIMP-2: tissue inhibitor of metalloproteinase; uPAR: urokinase-type plasminogen activator (uPA) receptor; VCAM: vascular cell adhesion molecule; ADAMs: a disintegrin and metalloproteinase proteins; tTG: tissue-type transglutaminase; iC3b: inactivated complement component 3b; ICAM: intercellular cell adhesion molecule; vWf: von Willebrand factor; FGF-2: fibroblast growth factor 2; MMP: matrix metallo-proteinases and MAdCAM: mucosal addressin cell adhesion molecule.

Integrin ligation promotes integrin clustering and subsequent integrin-mediated intracellular signal transduction. Unlike growth factor receptors, integrins have no intrinsic enzymatic or kinase activities, but activate complex signalling pathways by co-clustering with kinases and adaptor proteins in focal adhesion complexes. A number of signalling moieties are activated by integrins and many of these are found within focal adhesion complexes. Focal adhesion complexes are composed of integrins, protein kinases, adaptor proteins, signalling intermediates such as Rho family GTPases, actin-binding cytoskeletal proteins such as talin, α-actinin, paxillin, tensin and other signalling proteins. Integrin signalling promotes cell migration, proliferation and survival. Loss of integrin ligation inhibits these events and unligated integrins can actively initiate apoptosis, even without loss of cell attachment. This form of cell death is stressresponse- and death-receptor-independent, but caspase 8-dependent, and has been called “integrin-mediated death”.[91]

INTEGRIN STRUCTURE

The crystal structure of the extracellular domains of $\alpha_v\beta_3$ integrin published in 2001[92] revealed that the α_v and β_3 subunits can be considered as a ‘head domain’, formed by the α_v subunit β-propeller domain, the β_3 subunit βA domain and an immunoglobulin (Ig)-like ‘hybrid’ domain, and two ‘legs’. The α_v ‘leg’ is comprised of the Ig-like ‘thigh’ domain and two β-sandwich ‘calf ’ domains. The β leg consists of a plexin/semaphorin/integrin (PSI) domain, four EGF domains and a β-tail domain (β-TD) (Figure II.26).

In the crystal structure, the legs are folded at the knee or 'genu' between the α_v thigh and calf-1domain and between the EGF domains 1 and 2, such that the head domain is in proximity with the lower leg; there is evidence to suggest that this represents the resting-state. Upon activation, the integrin is believed to move to a more extended form, accompanied by conformational changes within the head domain,[93] including a significant swing in the hybrid domain that facilitates ligand binding, the so-called 'switch-blade' mechanism. However, some of the details of this mechanism still remain controversial. What is ceratin is that, both the ligand and unliganded structures, have a metal ion (Ca^{2+} or Mn^{2+}) that occupies the α-genu. At the base of the propeller, blades 4-7 also contain a metal ion coordinated in a β-hairpin loop.

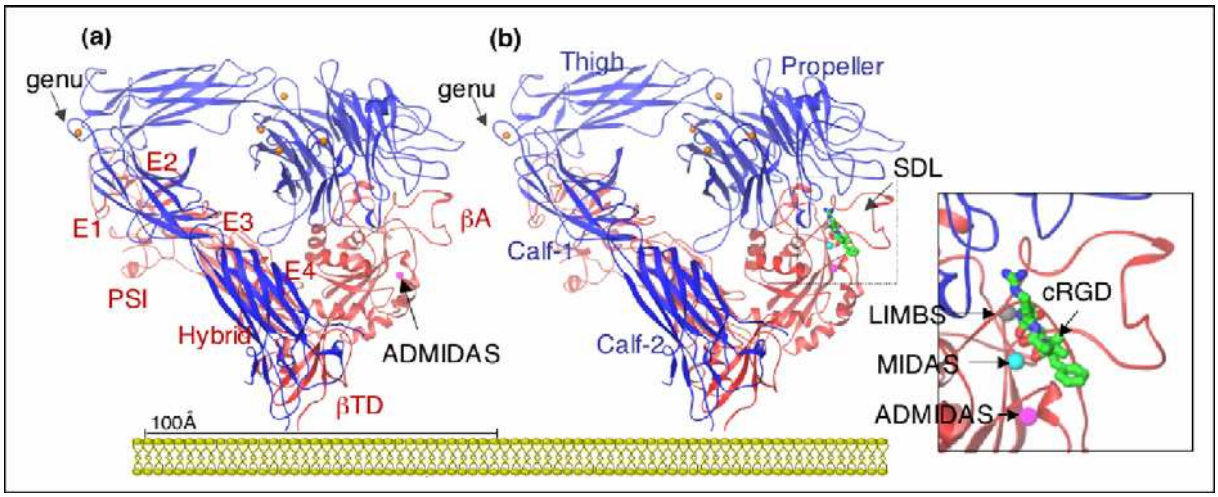

Figure II.26. Crystal structure of the integrin $\alpha_V\beta_3$ ectodomain. (a) Ribbon diagram of the structure of the unliganded $\alpha_V\beta_3$. The protein is bent at a flexible region (genu, arrow) occupied by a metal ion (orange sphere). Four metal ions occupy the base of the propeller (indicated in orange) and an ADMIDAS ion is found in βA (purple sphere). (b) Ribbon diagram of the same structure in complex with the high-affinity ligand cRGD; peptide is shown as a ball-and-stick model, with carbons in green, amides in blue and oxygens in red. The specificity-determining loop (SDL) is indicated. Two extra metal ions occupy MIDAS and LIMBS (indicated in the insert).[94]

III.2. INTEGRINS: THE KEYS TO UNLOCKING ANGIOGENESIS

Angiogenesis, the development of new blood vessels, is a fundamental physiological process that promotes embryonic development, tissue repair and fertility, yet that also promotes chronic inflammation, tumour growth and tumour metastasis. New blood vessels in tumours can grow by sprouting from pre-existing vessels or by recruitment of rare, circulating bone marrow-derived endothelial progenitor cells.[95] Tumour cells, macrophages and

fibroblasts within tumours can secrete factors, such as vascular endothelial growth factor (VEGF), that induce blood vessel growth in tumours.[95] Basic and clinical studies indicate that suppression of angiogenesis can inhibit tumour progression and metastasis.[96] Many lines of investigation implicate integrins, which are key regulators of endothelial cell migration and survival, as key regulators of tumour angiogenesis. As is shown in Figure II.27 tumour cells near pre-existing blood vessels secrete growth factors and chemokines, such as vascular endothelial growth factor A (VEGFA), basic fibroblast growth factor (bFGF) and tumour necrosis factor α (TNFα), that stimulate quiescent vascular endothelium to enter the cell cycle. Tumours also secrete factors such as VEGFC, VEGFA or hepatocyte growth factor (HGF) that stimulate the growth of new lymphatic vessels in the peritumoural space (Figure II.27a). These growth factors activate or upregulate expression of integrins such as $\alpha_1\beta_1$, $\alpha_2\beta_1$, $\alpha_4\beta_1$, $\alpha_5\beta_1$, and $\alpha_v\beta_3$ on blood vessels and $\alpha_1\beta_1$, $\alpha_2\beta_1$, $\alpha_4\beta_1$, and $\alpha_9\beta_1$ on lymphatic vessels (Figure II.27b). These integrins then promote endothelial cell migration and survival during invasion of tumour tissue, resulting in the creation of new vessel sprouts. The new blood vessels promote tumour growth by removing waste products and providing nutrients, and they also provide an avenue for tumour metastasis (Figure II.27c).

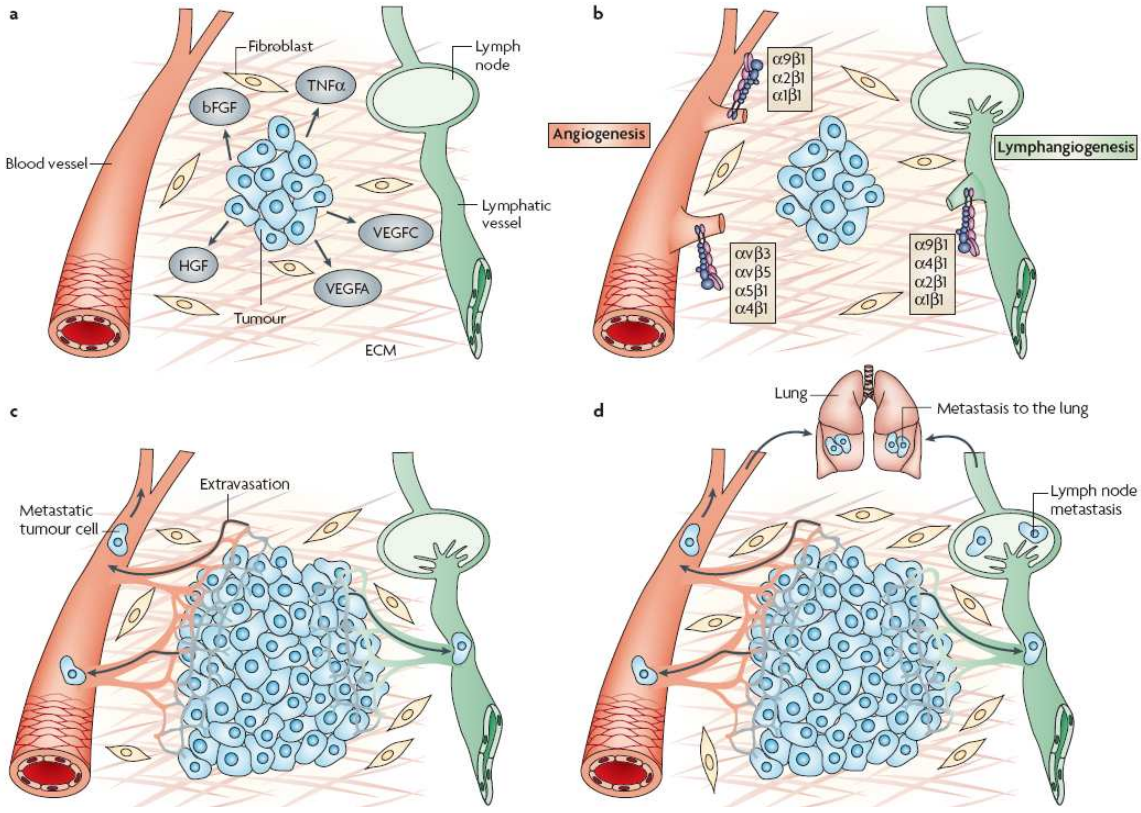

Figure II.27. Mechanisms regulating angiogenesis and lymphangiogenesis.[97]

Lymphangiogenesis promotes metastasis to lymph nodes and, sometimes, more distant tissues such as the lung, whereas angiogenesis promotes metastasis both to local and distant sites, such as the lung (Figure II.27d).[97]

In vitro and *in vivo* data have implicated a number of endothelial cell integrins in the regulation of cell growth, survival and migration during angiogenesis. These integrins include the heterodimers $\alpha_1\beta_1$, $\alpha_2\beta_1$, $\alpha_4\beta_1$, $\alpha_5\beta_1$, $\alpha_6\beta_1$, $\alpha_6\beta_4$, $\alpha_9\beta_1$, $\alpha_v\beta_3$ and $\alpha_v\beta_5$. Additionally, the glial cell integrin $\alpha_v\beta_8$ regulates blood vessel development in the brain. Although distinct experimental approaches, have led to conflicting theories of the roles of several integrins in angiogenesis (including α_v integrins and $\alpha_2\beta_1$ integrin), increasing molecular *in vivo* evidence points to major roles for key integrins in tumour angiogenesis.[97]

α_v INTEGRINS: As afore mentioned, the α_v integrin subunit can heterodimerize with several different β subunits (β_1, β_3, β_5, β_6 and β_8) to achieve unique ligand-binding profiles. The integrin $\alpha_v\beta_3$, a receptor for RGD-containing proteins such as vitronectin, fibronectin, fibrinogen and osteopontin, which are components of the ECM, was the first of the α_v integrins to be characterized. It was also the first α_v integrin to be shown to regulate angiogenesis.[98] This integrin is widely expressed on blood vessels in human tumour biopsy samples but not on vessels in normal human tissues. Its expression on endothelial cells is stimulated by angiogenic growth factors such as bFGF, TNFα and IL8 and it is upregulated on endothelium in tumours, wounds and sites of inflammation.[98] Whereas angiogenesis during wound healing is tightly regulated and self-limiting, angiogenesis associated with chronic inflammation and cancer is often persistent and abnormal.[99] However, many of the same molecules that regulate angiogenesis in wound healing, such as integrin $\alpha_v\beta_3$, also regulate pathological angiogenesis. Increasing evidence points to important causative links between inflammation and cancer and some evidence suggests that inflammation promotes the angiogenic switch in tumours.

Several experimental approaches indicate that $\alpha_v\beta_3$ has a key role in endothelial cell survival and migration during angiogenesis.[98] Antagonists of $\alpha_v\beta_3$ inhibited angiogenesis and tumour growth in a variety of animal models of cancer and blocked corneal as well as choroidal angiogenesis in animal models of ocular disease.[100]

Integrin $\alpha_v\beta_3$ antagonists induce endothelial cell apoptosis, increase the activity of the tumour suppressor p53, increase levels of the cell cycle inhibitor $p21^{WAF1/CIP1}$ and decrease levels of the antiapoptotic protein BAX.[101] Further studies show that $\alpha_v\beta_3$ antagonists activate a caspase 8-dependent cell death program.[102] Thus, a sizeable body of evidence indicates

that integrin $\alpha_v\beta_3$ promotes angiogenesis and endothelial cell survival and that antagonism of this integrin suppresses angiogenesis by inducing endothelial cell apoptosis *in vitro* and *in vivo*.

The related integrin $\alpha_v\beta_5$ promotes an angiogenic pathway that is distinct from that regulated by $\alpha_v\beta_3$. Anti-$\alpha_v\beta_3$ antibodies blocked angiogenesis induced by bFGF, whereas antibodies that target $\alpha_v\beta_5$ blocked the angiogenesis induced by VEGF. The VEGF-$\alpha_v\beta_5$ pathway, but not the bFGF-$\alpha_v\beta_3$ pathway, is dependent on Src kinase and protein kinase C.[103] *In vivo* angiogenesis assays showed that bFGF and TNFα depend on $\alpha_v\beta_3$ to initiate angiogenesis, whereas $\alpha_v\beta_5$ is required for TGFα- and VEGF-mediated angiogenesis. These data indicate unique roles for $\alpha_v\beta_3$ and $\alpha_v\beta_5$ integrins in angiogenesis and suggest that both could be important therapeutic targets.

FIBRONECTIN-BINDING INTEGRINS: Fibronectin is a key ECM protein that is deposited by endothelial cells during normal and tumour angiogenesis. Short fibronectin peptide loops containing the sequence Arg–Gly–Asp (RGD) interact with integrins such as $\alpha_5\beta_1$, $\alpha_v\beta_5$ and $\alpha_v\beta_3$.[90] Fibronectin secreted by endothelial cells also contains the alternatively spliced EIIIA, EIIIB and IIICS domains, which bind to integrins $\alpha_4\beta_1$ and $\alpha_9\beta_1$. Fibronectin is essential for developmental angiogenesis as early embryonic lethality, which occurs when all isoforms of fibronectin are deleted. Deletion of only EIIIA and EIIIB alternatively spliced variants is also embryonically lethal, owing to severe vascular defects that suppress placentation, yolk sac vessel formation and heart formation.[97] Thus fibronectin has a key role in angiogenesis, as do many of its receptors, the β_1 integrins.

III.3. $\alpha_v\beta_3$ INTEGRIN ANTAGONISTS

Preclinical studies suggested that antagonists of several integrins might be useful to suppress tumour angiogenesis and growth either alone or in combination with current cancer therapeutics. Although antagonists of several integrins are undergoing preclinical evaluation and development, only a handful of integrin-based drugs have so far been tested in the clinic. Integrin antagonists include function-blocking antibodies, peptides and organic small molecules. Function-blocking anti-integrin monoclonal antibodies typically have high affinity and specificity, and were the first integrin antagonists to reach the clinic. Cyclic peptide or peptidomimetics antagonists have also been evaluated in clinical trials. Small organic inhibitors, particularly orally active drugs, are the most cost-effective therapeutics but the

development of selective and high-affinity integrin inhibitors is time-consuming. Hence, no organic small-molecule antagonists of integrins have yet entered clinical trials.

Of the several integrin antagonists undergoing clinical evaluation for cancer treatment (Table II.7), all have proved to be non-toxic. These agents are probably non-toxic because the targeted integrins are only expressed or activated in remodelling tissues such as tumours.

Table II.7- Integrin antagonists tested in clinical trials for cancer therapy.[97]

DRUG NAME	TARGET	DRUG TYPE	TRIAL LAYER	TUMOUR TYPE	COMPANY
MEDI-522	$\alpha_v\beta_3$	Humanized	II	Metastatic melanoma	Medimmune
(Vitaxin,		antibody	II	Metastatic prostate cancer	
Abegrin)			II	Colorectal carcinoma	
M200	$\alpha_5\beta_1$	Chimeric	II	Metastatic melanoma	Protein
(volociximab)		mouse-human	II	Rena cell carcinoma	Design Labs
		antibody	II	Non-small-cell lung cancer	
CNTO 95	$\alpha_v\beta_3$	Human	I	Advanced refractory	Centocor
	$\alpha_v\beta_5$	antibody		cancers	
EMD121974	$\alpha_v\beta_3$	Peptide	II	Metastatic melanoma	Merck KGaA
(cilengitide)	$\alpha_v\beta_5$		II	Metastatic prostate cancer	
			II	Pancreatic cancer	
			II	Non-small-cell lung cancer	
			II	Glioblastoma multiforme	
ATN-161	$\alpha_5\beta_1$	Peptide	I/II	Malignant glioma	Attenuon, LLC

Concerning cyclic peptides or peptidomimetics $\alpha_v\beta_3$ antagonists a great amount of work was developed by Kessler and co-workers since the beginning of the 90's. Initially, an extensive ligand-based drug design study, using cyclic peptide libraries with constrained backbone conformations, led to the discovery of the $\alpha_v\beta_3$-selective first generation cyclic pentapeptide **116**, *cyclo*(-RGDfV-).[104-106] This peptide shows a βII'/γ-turn arrangement with D-Phe in the *i*+1 position of the βII'-turn (Figure II.28). The systematic derivatization of this peptide resulted in the N-alkylated cyclopeptide *cyclo*(-RGDf[NMe]V-)[107] (**117**, IC_{50} = 0.6 nM), which is in clinical layer II as anticancer drug (Cilengitide, EMD121974). This is the ligand for which the crystal structure of the complex has been reported.[93]

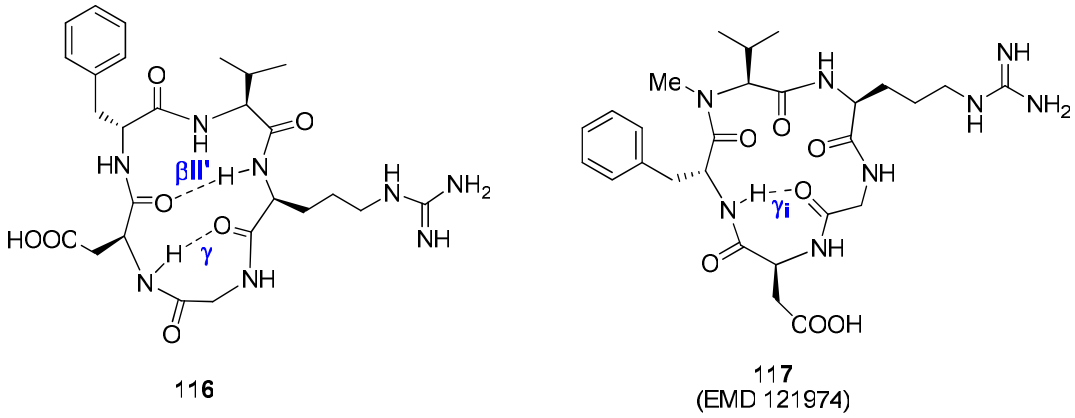

116 117 (EMD 121974)

Figure II.28. *Cyclo*(-RGDfV-) **116** and *cyclo*(-RGDf[NMe]V-) **117** (Cilengitide).

Compound **117** is different from the other cyclic pentapeptides prepared by Kessler *et al.* as the hydrogen bond formation between Arg^1-H^N and Asp^3-CO is blocked by the *N*-methyl group of the valine residue. Due to steric repulsion the amide groups Asp^3-D-Phe^4 and Val^5-Arg^1 turn into a more perpendicular orientation with respect to the plane of the peptide ring. The rotation of the peptide bonds Asp^3-D-Phe^4 and Val^5-Arg^1 moreover affects the side chains of Arg^1 and Asp^3 through allylic and vinylic strain, resulting in a pronounced conformational difference between **116** and **117** which certainly has an effect on the $\alpha_v\beta_3$ activity. Examination of the three-dimensional structure of **117** bound to $\alpha_v\beta_3$ integrin reveals a conformation characterized by an inverse γ-turn with Asp at position *i*+1 and by a distorted βII'-turn with Gly and Asp at the *i*+1 and *i*+2 positions (Figure II.28). A 8.9 Å distance between Asp and Arg C_β atoms is observed in this pentapeptide-bound conformation. The backbone conformations of the ligand in the integrin complex and in solution (as determined by nuclear magnetic resonance spectroscopy in water) are very similar.[108]

The same group also performed a systematic study of all retro-, inverso-, and retro-inverso isomers of the *cyclo*(-RGDFV-) containing one amino acid in the D-configuration. This study yielded the highly active compound *cyclo*(-vfdGR-) (IC_{50} = 40 nM).[109] Subsequently, novel nonpeptidic ligands have been designed by other groups.[110-114] Most of them contained an N-terminal guanidino, benzamidino, or aminopyridine group and a carboxyl group separated by a well-defined distance. From this RGD-mimetic libraries[115,116] derived some highly active compounds like the aza-Gly RGD mimics: **118a** (IC_{50} = 150 nM) and **118b** (IC_{50} = 2.6 nM), possessing a β^3-amino acid as the acidic C-terminal component of the molecule (Figure II.29), and **119** (IC_{50} = 6 nM) in which the C-terminal is replaced by a substituted glutaric acid group and the basic part of the molecule by an aminopyridine moiety (Figure II.29).

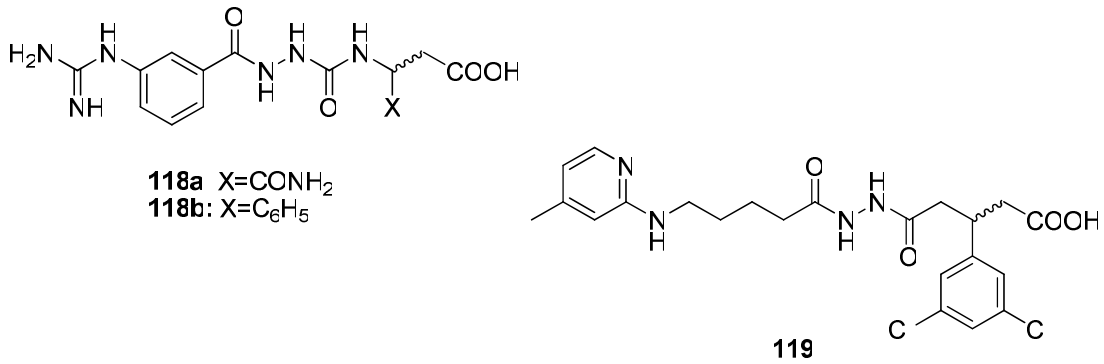

Figure II.29. Nonpeptidic inhibitors.

In order to reduce the accessible conformational space of the cyclic RGD pentapeptides, Kessler's group decided to incorporate several β-turn mimetics[117] and sugar amino acids[118] into the lead structure *cyclo*(-RGDfV-) **116** (Figure II.28), by replacing the D-Phe-Val dipeptide unit, meaning the *i*+1 and *i*+2 position of the βII'-turn (Figure II.30). Although, it was expected that this modifications would lead to a stabilization of the βII' turn simultaneously with a reduction of flexibility of the γ-turn region, it was observed that most of the peptidomimetic analogues contained the turn mimetic in the γ-turn region, and Gly was found in the *i*+1 position of a βII' turn (meaning that the achiral Gly residue can act as a D-amino acid residue). These investigations also led to several potent $\alpha_v\beta_3$ peptidomimetic ligands, among which the *cyclo*(-RGD"*R*-ANC"-) **120** (IC_{50} = 0.8 nM), containing a 3-amino pyrrolidin-2-one ring as turn mimetic.

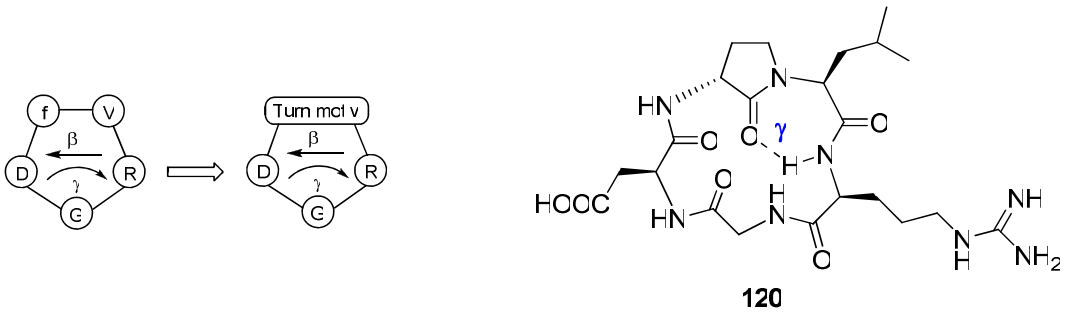

Figure II.30. *Cyclo*(-RGD"*R*-ANC"-).

The combination of the recognition epitope with a secondary-structure-inducing element, like for example, β-amino acids,[119] and cyclic or bicyclic templates was also used by other groups.[120,121]

Reiser *et al.*, have synthesised a pentapeptide *cyclo*(-RGD-(+)-β-Acc-) (IC_{50} = 20 nM), containing a (+)-β-Acc ((+)-*cis*-β-aminocyclopropanecarboxylic acid) adjacent to the RGD sequence. Structural analysis of this cyclic pentapeptide has shown that the RGD sequence occupies a γ turn with glycine in the central position, and that the restrained cyclopropane system occupies the *i*+1 position of a pseudo β-turn.[120]

Scolastico *et al.*, have reported a library of cyclic RGD pentapeptide mimics, based on azabicycloalkane amino acid scaffolds (**121**, Figure II.31).[121] Stereoisomeric 5,6- and 5,7-fused bicyclic lactams showing different reverse-turn mimetic properties[122] were exploited as dipeptide analogs for the synthesis of a library of general formula *cyclo*(-RGD-Lactam-) (**122**, Figure II.31). This library was found to contain specific high-affinity ligands of $\alpha_V\beta_3$ integrin, which are presently being evaluated as very promising antiangiogenic drugs. Among the peptides tested, compound ST1646 (**123**, Figure II.31) showed the highest affinity to $\alpha_V\beta_3$, inhibiting echistatin binding to $\alpha_V\beta_3$ with an IC_{50} of 4 nM.

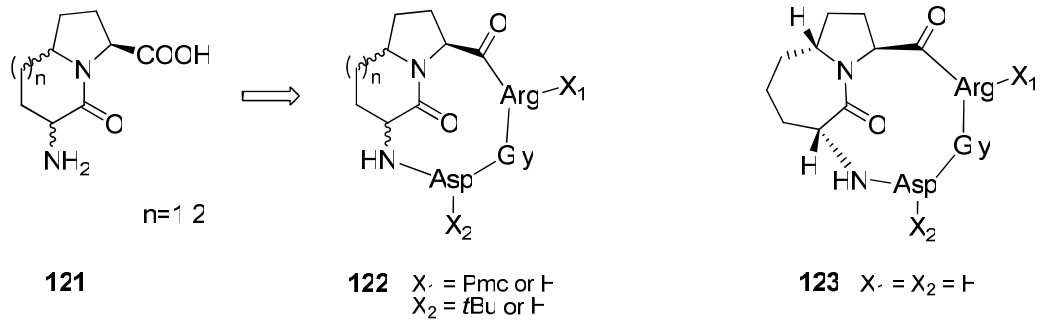

Figure II.31. Cyclic RGD pentapeptide mimics based on azabicycloalkane amino acid scaffolds.

DKPs were also used as rigid scaffolds to synthesise a small library of cyclic RGD peptidomimetics using solid-layer synthesis, where the RGD sequence was attached through the side chains of the DKP ring (*cyclo*-[Lys-Glu]).[123] In this study Royo, Albericio and co-workers have demonstrated that, in the case of the DKP analogues, the binding affinity to the $\alpha_v\beta_3$ receptor is affected by the size of the RGD-containing ring. Compound **124a** (Figure II.32), where the loop contains just the RGD sequence, shows the highest binding affinity but even so with a rather modest IC_{50} of 4 μM. In another work reported by Robinson and co-workers, a bicyclic template, comprising a diketopiperazine derived from L-aspartic acid and (2*S*,3*R*,4*R*)-diaminoproline, was incorporated into a cyclic four-residue loop mimetic containing the sequence [-Ala-Arg-Gly-Asp-template-] (**125**, Figure II.32). Structural analysis revealed that the peptide backbone of **125** is probably interconverting rapidly between two or

more conformational states in aqueous solution and, solid-layer binding assays reveal that compound **125** displays quite modest antagonist activity towards both the integrin receptor $\alpha_v\beta_3$ (IC_{50} = 100 nM) and $\alpha_{IIb}\beta_3$ (IC_{50} = 250 nM).[52]

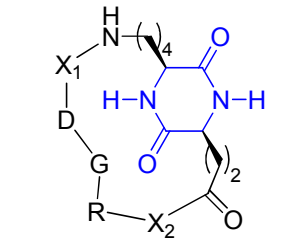

124a: $X_1 = X_2$ = not present
124b: X_1 = not present, X_2 = Gly
124c: $X_1 = X_2$ = Gly

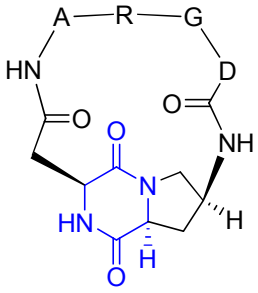

125

Figure II.32. Cyclic RGD peptidomimetics containing a DKP-based scaffold.

DKPs have also been used to synthesise linear peptidomimetics of the RGD sequence.[124] In this case, the DKP scaffold (possessing a carboxylic side chain that provides the acidic C-terminal component of the molecule) is linked to the basic function of the molecule (a guanidine, piperidone or benzamidino moiety), through a spacer of variable structure and length (Figure II.33). These RGD analogues were tested as inhibitors of platelet aggregation and of cell adhesion but only one showed a rather modest (IC_{50} = 27 μM) but selective inhibition of $\alpha_{IIb}\beta_3$ receptor.

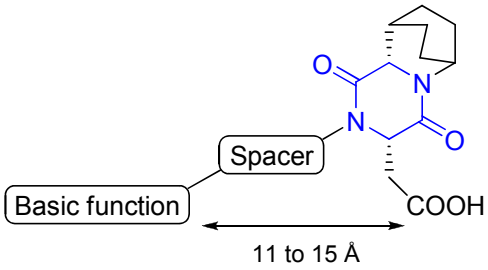

Figure II.33. Linear RGD peptidomimetics containing a DKP-based scaffold.

III. 4. CONFORMATIONAL STUDIES OF A CYCLIC RGD-DKP-90 PEPTIDOMIMETIC

As previously discussed the examples found in literature of cyclic-RGD peptidomimetics containing diketopiperazine-based templates were quite discouraging.

However the rather modest antagonist activity shown, is probably due to the large conformational liberty of the molecules synthesised. In fact as discussed before in order to obtain potent inhibitors it is often necessary to reduce the accessible conformational space, like for example by incorporating a turn mimetic. Therefore, in view of the good properties of DKP scaffold **90** as a secondary-structure-inducing element (see discussion in Section II.4.2, page 60) it seemed rather logic to use this scaffold as a template for the synthesis of cyclic-RGD peptidomimetics (**126**, Figure II.34).

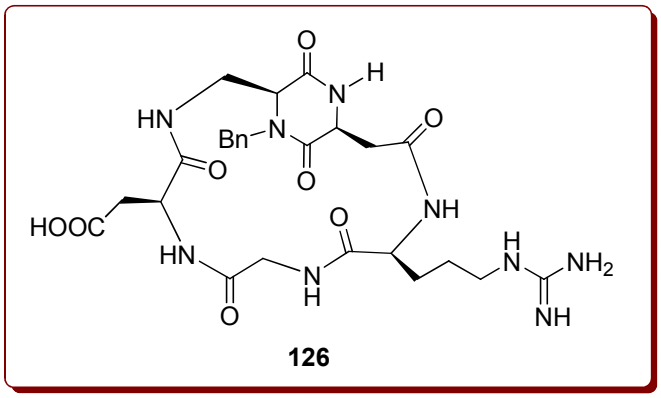

126

Figure II.34. *Cyclo*(-RGD-DKP-**90**-).

Before starting the synthetic part, computational studies aimed at investigate the effects of DKP scaffold **90** on the cyclopeptide conformation were performed on the *cyclo*(-Asp-Gly-Arg-DKP-**90**-) pentapeptide mimic **126**. The molecule was subjected to an extensive, unconstrained Monte Carlo/Energy Minimization (MC/EM) conformational search[79] by molecular mechanics methods using the AMBER* force field[80] and the implicit H_2O GB/SA solvent model.[81] A simplified model of the molecule, in which the Asp and Arg side chains were substituted by methyl groups, was chosen in a first instance. This computational choice had already been applied to study RGD pentapeptide mimics containing an azabicycloalkane amino acid scaffold,[125] due to the program limitation to treat charged systems using implicit solvent models.

Only one type of conformation, featuring a β-hairpin-like arrangement, was predominant among the structures found within 3 kcal/mol from the global minimum. The lowest energy conformer features an intramolecular hydrogen bonding pattern involving the formation of a 12-membered and a 16-membered hydrogen-bonded rings, in which the RGD sequence assumes a folded conformation (Figure II.35, **126a**). A second conformer was found at 4.20 kcal/mol from the global minimum, in which the RGD sequence assumes a more extended conformation showing an inverse γ-turn with Asp at the *i*+1 position (Figure

II.35, **126b**). This conformation is in fact more similar to the X-ray-binding conformation of EMD121974 (Figure II.36) than the minimum energy conformation **126a** (Figure II.35).

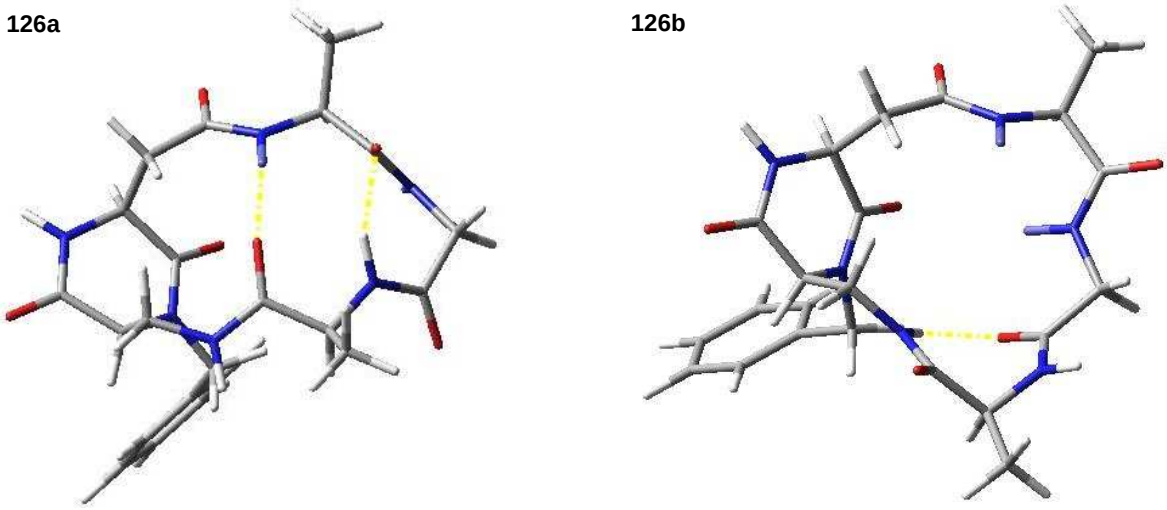

Figure II.35. Structures of low-energy conformers (MC/EM, AMBER*, H_2O GB/SA) calculated for compound **126**: left, global minimum (**126a**); right, conformer with relative energy of 4.20 kcal/mol (**126b**). Hydrogen bonds are indicated with dotted lines.

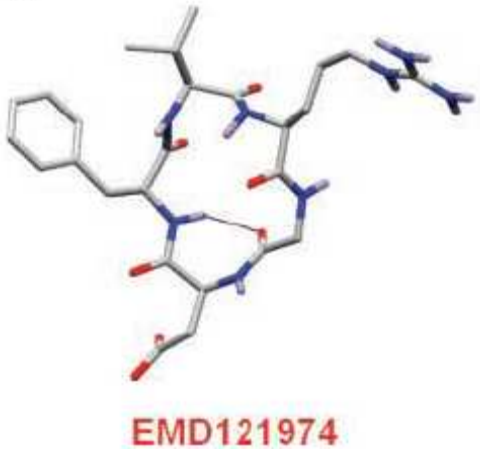

Figure II.36. X-ray conformation of $\alpha_v\beta_3$-bound EMD121974 (**117**).[93]

Docking studies of compound **126** in the ligand binding site of $\alpha_v\beta_3$ integrin were attempted starting from the crystal structure of the $\alpha_v\beta_3$ integrin-EMD121974 complex. The second conformer found (Figure II.35, **126b**) was docked in the ligand-bound integrin by superimposing the C_α atoms of the cyclopentapeptide mimic backbone and the guanidine and carboxy moieties of **126b** to the corresponding elements of EMD121974. The resulting

complex seemed to maintain almost the same ligand-receptor distances and interactions observed in the crystalline complex of EMD121974 with $\alpha_v\beta_3$ (Figure II.36). The main interactions observed are between the positively charged arginine of **126b** and the negatively charged side chain of Asp^{218} in the α subunit and between the anionic aspartic acid and the metal cation in the metal ion-dependent adhesion site region of the β subunit. Further stabilization occurs through hydrogen bonds between the Asp side chain and the NH group of Asn^{215} and of Tyr^{122} in the β subunit (Figure II.37). Unfortunately the good results obtained in the docking studies are probably not a good representation of the reality, since the conformer used has a relatively high energy (4.20 kcal/mol) and therefore is not representative of the molecule in question.

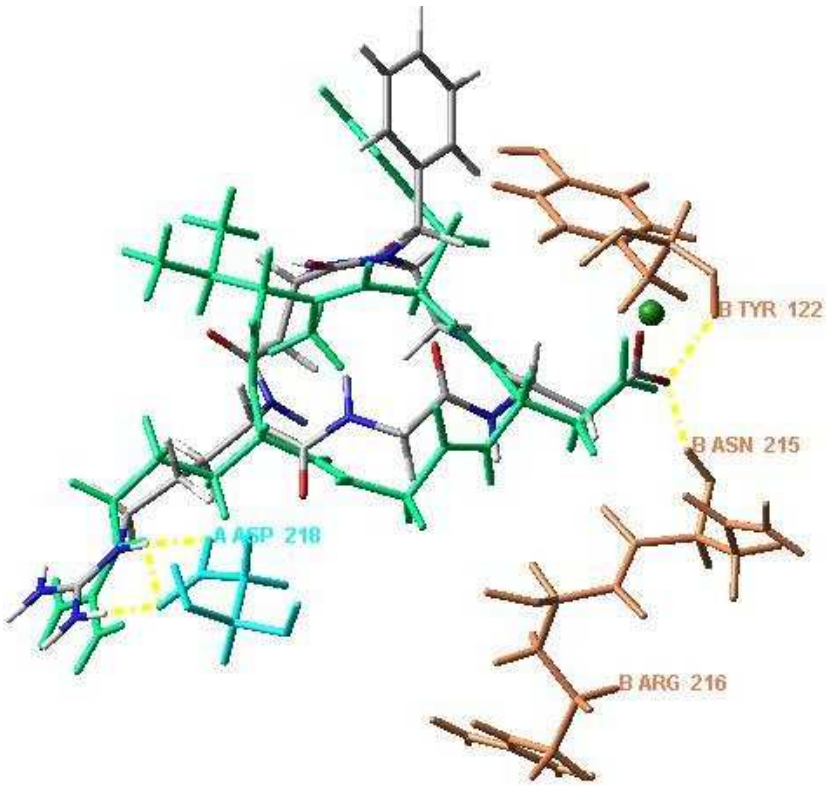

Figure II.37. Top-ranking binding mode of RGD-ligand **126b** into the crystal structure of the extracellular domain of $\alpha_v\beta_3$ integrin overlaid on the bound conformation of EMD121974 (green). Selected integrin residues involved in the interactions with the ligand (residues of the α subunit in blue, and those of the β subunit in brown) and crucial hydrogen bonds are shown.

III.5. SYNTHESIS OF THE CYCLIC-RGD-DKP-90 PEPTIDOMIMETIC

The synthetic procedure designed to obtain the *cyclo*(-RGD-DKP-**90**-) **126** involves the cyclization of the linear precursor Asp-DKP-**90**-Arg-Gly. In order to minimize steric hindrance at the cyclization site, cyclization between the Gly and Asp residues was envisaged. These conditions had been already used by other groups[121] and also present the advantage of minimizing the epimerization during the ring-closure step. In fact, since the glycine residue does not have a stereocentre in α, the activation of the carboxylic group and subsequent coupling does not present the risk of partial racemisation that eventually leads to the formation of the corresponding diastereomer.

The success of the strategy designed also relies on the adequate choice of the protecting groups, which must be orthogonal to the conditions applied during the peptide chain growth. Our idea was to develop a synthetic strategy based on commercially available amino acids or amino acids easily obtained from the commercial derivatives. Therefore we decided, to use a glycine *tert*-butyl ester derivative in the form of hydrochloride salt and an arginine derivative presenting the α- and ε-amino group protected respectively as a carbobenzyloxy (Cbz) and a 4-methoxy-2,3,6-trimethylbenzenesulfonyl (Mtr), and the carboxylic group in the form of a cyclohexylammonium salt. The acid-labile Mtr protecting group is normally removed with concentrate TFA in the presence of thioanisole (a carbocation scavenger) but it seems to be stable to the milder acidic conditions required to remove Boc protecting groups (TFA in dichloromethane in variable proportions).[126]

The suitably protected amino acids were coupled to form the dipeptide Cbz-Arg(Mtr)-Gly-O*t*Bu **127**, using HBTU/HOBt, EDC and DIPEA in dimethylformamide. Cleavage of the Cbz group through catalytic hydrogenolysis afforded the deprotected dipeptide **128** (Scheme II.21).

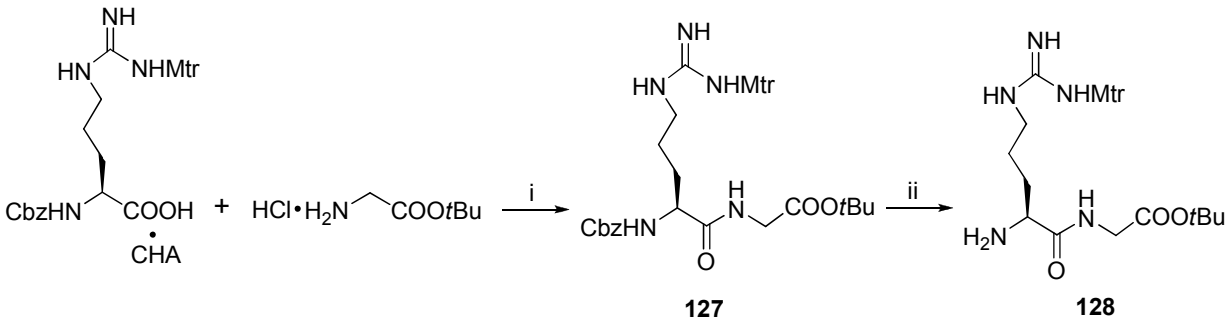

Scheme II.21. (i) HOBt, DIPEA, DMF then EDC, 0 ºC to r.t.: 87%; (ii) H_2, $Pd(OH)_2$/C, MeOH: quantitative yield.

Deprotected dipeptide **128** was then coupled to DKP-**90** (Scheme II.22), leading to compound **129** in satisfactory yield (67%).

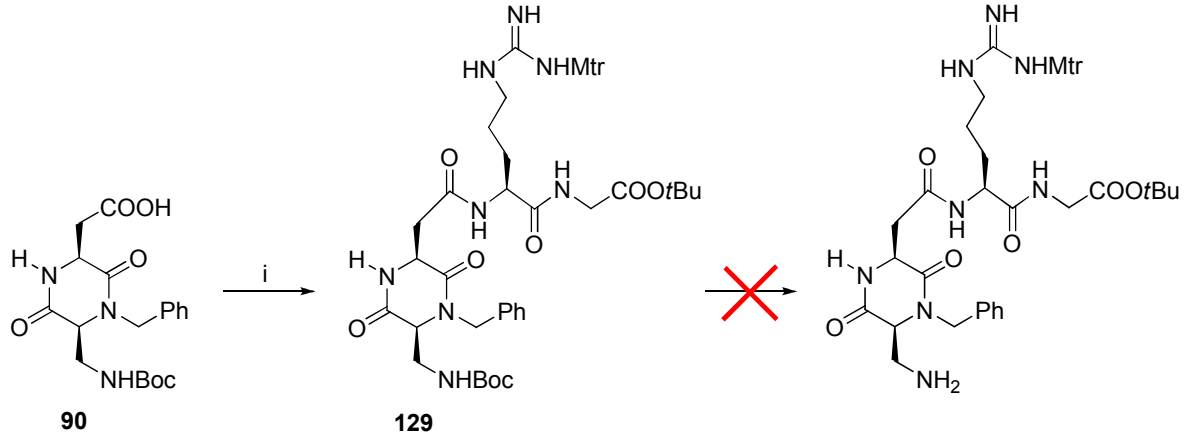

90 **129**

Scheme II.22. (i) H_2N-Arg(Mtr)-Gly-O*t*Bu **128**, HOBt, DIPEA, DMF then EDC, 0 ºC to r.t.: 67%.

At this point, in order to couple the last residue of the RGD sequence (Asp), the synthetic strategy designed relied in a selective removal of the Boc group while retaining the *tert*-butyl ester of the glycine residue. Some selective procedures based on the higher kinetic lability of *N*-Boc groups in respect to *tert*-butyl esters were reported in the literature.[127,128] An alternative strategy involved the deprotection of both groups followed by re-esterification *in situ* of the carboxylic group under acid-catalyzed conditions in the presence of a *t*-Butyl cation source.[129] In this last case, the authors claim that it is likely that the removal of a Boc group is an irreversible process due to protonation of the amine product and loss of CO_2, while the deprotection of a *tert*-butyl ester should be reversible under acidic conditions (Scheme II.23). Indeed, *tert*-butyl esters are generally prepared under acid-catalyzed conditions in the presence of a *t*-Butyl cation source (*e.g.* isobutylene, *t*BuOAc, *t*-butanol).

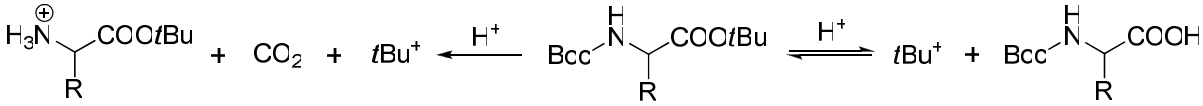

Scheme II.23

In our case, all attempts to selective remove the *N*-Boc group of derivative **129** in the presence of the *tert*-butyl ester using the described conditions were unsuccessful. The use of different protic acids in organic solvents (like EtOAc and CH_2Cl_2) led to a 1:1 mixture of the desired amino ester and the completely deprotected amino acid as a result of *tert*-butyl ester

removal. On the other hand when CH_3SO_3H was used in the presence of *t*BuOAc and CH_2Cl_2 as a co-solvent, a 2:1 mixture of the desired amino ester and the completely deprotected amino acid was obtained.

This failure obliged us to re-consider the original strategy and, as an alternative, we decided to start from glycine methyl ester which could be later transesterified to its benzyl counterpart. Using the Arg derivative described before and the commercially available Cbz-Asp(O*t*Bu)-OH, it would be possible to obtain the linear precursor Cbz-Asp(O*t*Bu)-DKP-**90**-Arg(Mtr)-Gly-OCH_2Ph, containing both extremities protected with groups susceptible to catalytic hydrogenolysis (Cbz and Bn) while the Arg and Asp side chains would be orthogonally protected with acid-labile groups (Mtr and *t*Bu groups, respectively).

As is exemplified in Scheme II.24 the alternative synthetic strategy started with the synthesis of dipeptide Cbz-Arg(Mtr)-Gly-OMe **130**. Cleavage of the Cbz group through catalytic hydrogenolysis afforded the deprotected dipeptide **131**. Deproteced dipeptide **131** was then coupled to the C-terminus of DKP-**90**, affording the desired Boc-DKP-**90**-Arg(Mtr)-Gly-OMe **132**. Removal of the Boc group using TFA in dichloromethane at 0 ºC allowed the coupling of Cbz-Asp(O*t*Bu)-OH to the N-terminus of DKP-**90**, leading to the desired Cbz-amino ester **133**.

The transformation of the methyl ester **133** to the corresponding benzyl derivative **134** was performed under smooth conditions using a large excess of benzyl alcohol, titanium isopropoxide [Ti(O*i*Pr)$_4$] and molecular sieves to trap the methanol formed.[130] Using this methodology the corresponding benzyl ester **134** was obtained with an excellent yield (97%).

Simultaneous deprotection of the benzyl ester and Cbz group, through catalytic hydrogenolysis, leaded to the desired linear precursor **135** in quantitative yield.

Finally the macrocyclization step was performed in dimethylformamide using HATU/HOAt as coupling agent and collidine as a base, under nitrogen atmosphere, affording *cyclo*(-RGD-DKP-**90**-) **136** in satisfactory yield (61%). Moderately high dilution conditions (20 mM) were used in order to favour the intramolecular condensation.

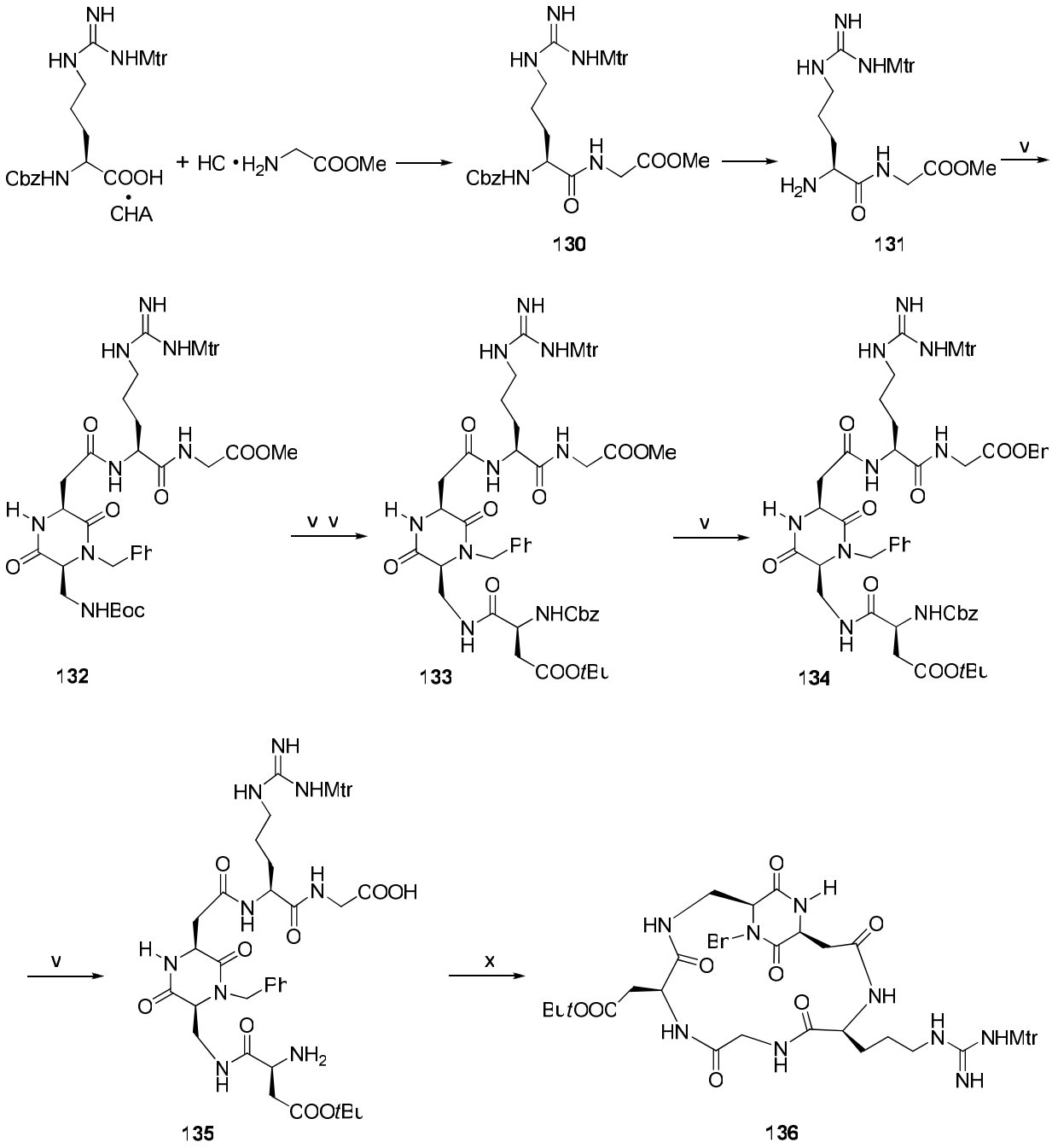

Scheme II.24. (i) $KHSO_4$ (1 M) and (ii) HBTU, HOBt, DIPEA, DMF: 78% over two steps; (iii) H_2, $Pd(OH)_2/C$, MeOH: quantitative yield; (iv) NH_2-Arg(Mtr)-Gly-OMe, DKP-**90**, HBTU, HOBt, DIPEA, DMF: 72%; (v) TFA/CH_2Cl_2 (1:1, v/v) and (vi) Cbz-Asp(*Ot*Bu)-OH, HATU, HOAt, DIPEA, DMF: 89% over two steps; (vii) BnOH, $Ti(OiPr)_4$, THF, MS 4 Å: 97%, (viii) H_2, Pd/C, MeOH: quantitative yield; (ix) HATU, HOAt, collidine, DMF: 61%.

Side-chain deprotection was achieved by treating **136** with TFA, in the presence of ion scavengers: triethylsilane (2.5%), ethanedithiol (5%), phenol (5%), thioanisole (5%), water (2.5%) (Scheme II.25).

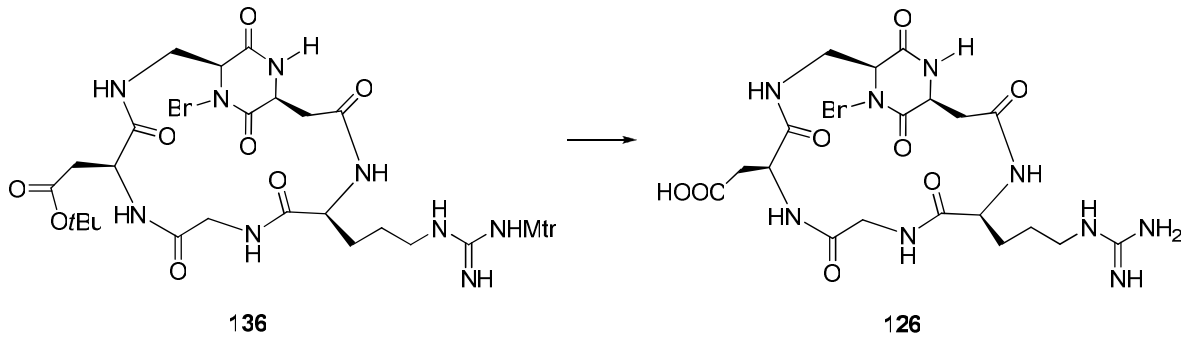

Scheme II.25. "Cleavage cocktail": TFA (80%), triethylsilane (2.5%), ethanedithiol (5%), phenol (5%), thioanisole (5%), H_2O (2.5%).

After TFA removal, under reduced pressure, the cyclic RGD peptide mimic **126** was precipitated with diisopropyl ether, centrifuged and the resulting pellet was washed, several times, with diisopropyl ether. Finally, the crude compound was purified by HPLC (Water's Atlantis 21 mm x 10 cm column, gradient: 95% H_2O / 5% acetonitrile to 80% H_2O / 20% acetonitrile).

III.6. BIOLOGICAL EVALUATION OF THE CYCLIC RGD-DKP-90 PEPTIDOMIMETIC

RECEPTOR BINDING ASSAY: the cyclic RGD peptide mimic **126** was examined *in vitro* for its ability to compete with biotinylated vitronectin for binding to the purified $\alpha_v\beta_3$ receptor (Table II.8). Screening assays were performed by measuring the effects of the RGD cyclopeptide on the interaction between immobilized integrin receptors and biotinylated soluble ligands. The ability of the new compound **126** to inhibit the binding of vitronectin to the isolated $\alpha_v\beta_3$ receptor was compared with that of the standard compound *cyclo*(RGDf[NMe]V) and are reported in Table II.8.

Table II.8. Inhibition of biotinylated vitronectin binding to $\alpha_v\beta_3$ receptor.

COMPOUND	**IC_{50} (nM) ± SD** [a]
cyclo(RGDf[NMe]V)	18.9 ± 3.1 (measured with ^{125}I-Echistatin)
126	3898 ± 418

[a] Values are the means ± standard deviation of triplicate determinations.

The high IC_{50} value of compound **126** is to be acribed to the folded conformation which has been found as a global minimum energy in the molecular mechanics calculations that we

discussed above. In fact the conformation that the highly active *cyclo*(RGDf[NMe]V) assumes both in the solid state and in water solution features an extended conformation of the RGD moiety which is thus able to interact with the active site of the receptors. Our efforts are now devoted to the synthesis and biological evaluation of other cyclic RGD-diketopiperazine peptidomimetics possessing a different configuration of the DKP-side arms (*e.g. R* and *S*).

IV. CONCLUSIONS AND PERSPECTIVES

There is no doubt that without the ability of nature to form very stable aggregates of small molecules, or to form well-defined secondary, tertiary and even quaternary structures of macromolecules, life as we know it could not exist. The folding of polypeptide chains into secondary and eventually a bewildering array of tertiary structures results in protein molecules that are responsible for most of the biological interactions and functions found in nature. A logical next step is evidently to mimic nature and to create nonbiologically derived molecules that fold into well-defined structures. Since the early 1990's, a great deal of literature has been devoted to these types of biomimetic structures, involving intramolecular folding of unnatural molecules that are capable of mimicking or antagonizing the biological action(s) of a natural parent peptide, the so called: **PEPTIDOMIMETICS**.

The development of these chemical model systems provides valuable insights into biomolecular structure and interactions by allowing researchers to simplify, isolate, and manipulate aspects of the complex molecular machinery of living systems.

Herein, we reported the synthesis of a new bifunctional diketopiperazine scaffold **90**, derived from L-aspartic acid and (*S*)-2,3-diaminopropionic acid. DKP-**90** bears an amino and a carboxylic acid functionalities in a *cis* relationship.

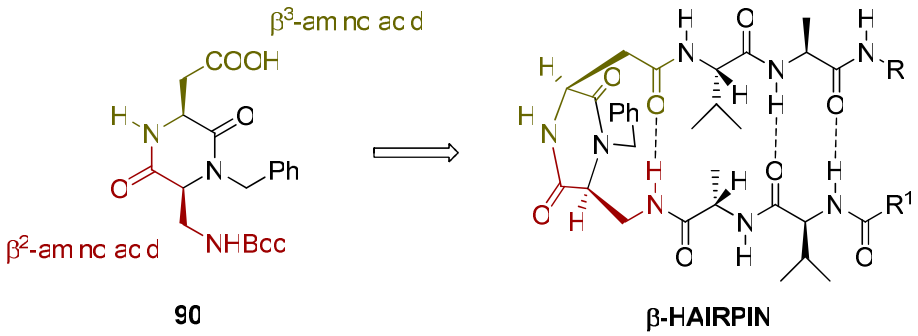

Figure II.38. β-Hairpins bearing DKP-**90** (a constrained β-dipeptide).

As a consequence, DKP scaffold **90** can be seen as a conformationally constrained mimic of a dipeptide formed by two β-amino acids (namely a β^2- and a β^3-amino acids, Figure II.38). When inserted into a peptidic sequence, involving α-amino acids, DKP-**90** is accommodated into the turn position of a β-hairpin (Figure II.38). IR, NMR and CD experiments provide strong support to this conclusion, strengthened by molecular modelling and molecular dynamics calculations.

Potential applications of the α_v integrin antagonists range from angiogenesis and vascular disorders to osteoporosis. A large amount of research has been especially devoted to ascertain the value of the α_v integrin antagonists in the cancer therapy. The expression of integrin adhesion molecules $\alpha_v\beta_3$ on sprouting capillary cells and their interaction with specific matrix ligands play a key role in angiogenesis, the formation of new blood vessels from pre-existing vasculature, that is essential for tumour growth, and formation of metastasis.

Herein we describe the synthesis, conformational analysis, and biological evaluation of a cyclic RGD-DKP-**90** peptidomimetic (**126**, Figure II.39). Its biological activity was examined in vitro for its ability to compete with biotinylated vitronectin in binding to the purified $\alpha_v\beta_3$ receptor. The biological results are in agreement with the conformational studies and show a low inhibitory activity for the compound **126** bearing DKP-**90** (IC_{50} = 3898 ± 418 nM).

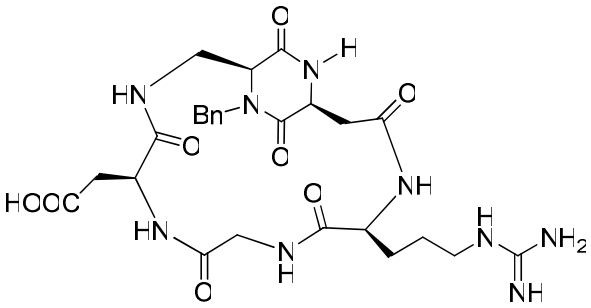

126

IC_{50} = 3898 ± 418 nM

Figure II.39. Cyclic RGD-DKP-90 peptidomimetic.

Our efforts are now devoted to the synthesis and biological evaluation of other cyclic RGD-diketopiperazine peptidomimetics possessing a different configuration of the DKP-side arms (*e.g. R* and *S*) as well as different functionalities in the DKP ring.

CHAPTER II BIBLIOGRAPHIC REFERENCES:

[1] McCleland, K.; Milne, P. J.; Lucieto, F. R.; Frost, C.; Brauns, S. C.; Van De Venter, M.; Du Plessis, J.; Dyason, K. *J. Pharm. Pharmacol.* **2004**, *56*, 1143-1153.

[2] Fischer, P. M. *J. Peptide Sci.* **2003**, *9*, 9-35.

[3] Tanaka, K.; Mori, A.; Inoue, S. *J. Org. Chem.* **1990**, *55*, 181-185.

[4] Iyer, M. S.; Gigstad, K. M.; Namdev, N. D.; Lipton, M. *J. Am. Chem. Soc.* **1996**, *18*, 4910-4911.

[5] Horton, D. A.; Bourne, G. T.; Smythe, M. L. *Mol. Divers.* **2000**, *5*, 289-304.

[6] Falorni, M.; Giacomelli, G.; Porcheddu, A.; Taddei, M. *Eur. J. Org. Chem.* **2000**, 1669-1675.

[7] del Fresno, M.; Alsina, J.; Royo, M.; Barany, G.; Albericio, F. *Tetrahedron Lett.* **1998**, *39*, 2639-2642.

[8] Brooks, T. D.; Wang, S. M. W.; Brunner, N.; Charlton, P. A. *Anti-Cancer Drugs* **2004**, *15*, 37-44.

[9] Einholm, A. P.; Pedersen, K. E.; Wind, T.; Kulig, P.; Overgaard, M. T.; Jensen, J. K.; Bodker, J. S.; Christensen, A.; Charlton, P.; Andreasen, P. A. *Biochem. J.* **2003**, *373*, 723-732.

[10] Wang, S. M.; Golec, J.; Miller, W.; Milutinovic, S.; Folkes, A.; Williams, S.; Brooks, T.; Hardman, K.; Charlton, P.; Wren, S.; Spencer, J. *Bioorg. Med. Chem. Lett.* **2002**, *12*, 2367-2370.

[11] Folkes, A.; Roe, M. B.; Sohal, S.; Golec, J.; Faint, R.; Brooks, T.; Charlton, P. *Bioorg. Med. Chem. Lett.* **2001**, *11*, 2589-2592.

[12] Kanoh, K.; Kohno, S.; Katada, J.; Takahashi, J.; Uno, I. *J. Antibiot.* **1999**, *52*, 134-141.

[13] Nicholson, B.; Lloyd, G. K.; Miller, B. R.; Palladino, M. A.; Kiso, Y.; Hayashi, Y.; Neuteboom, S. T. C. *Anti-Cancer Drugs* **2006**, *17*, 25-31.

[14] Kanzaki, H.; Imura, D.; Nitoda, T.; Kawazu, K. *J. Biosci. Bioeng.* **2000**, *90*, 86-89.

[15] Sinha, S.; Srivastava, R.; De Clereq, E.; Singh, R. K. *Nucleosides, Nucleotides Nucleic Acids* **2004**, *23*, 1815-1824.

[16] Byun, H. G.; Zhang, H. P.; Mochizuki, M.; Adachi, K.; Shizuri, Y.; Lee, W. J.; Kim, S. K. *J. Antibiot.* **2003**, *56*, 102-106.

[17] Asano, N. *Glycobiology* **2003**, *13*, 93R-104R.

[18] Houston, D. R.; Synstad, B.; Eijsink, V. G. H.; Stark, M. J. R.; Eggleston, I. M.; Van Aalten, D. M. F. *J. Med. Chem.* **2004**, *47*, 5713-5720.

[19] Fdhila, F.; Vazquez, V.; Sanchez, J. L.; Riguera, R. *J. Nat. Prod.* **2006**, *69*, 1120-1120.

[20] Kanokmedhakul, S.; Kanokmedhakul, K.; Phonkerd, N.; Soytong, K.; Kongsaeree, P.; Suksamrarn, A. *Planta Med.* **2002**, *68*, 834-836.

[21] Sugie, Y.; Hirai, H.; Inagaki, T.; Ishiguro, M.; Kim, Y. J.; Kojima, Y.; Sakakibara, T.; Sakemi, S.; Sugiura, A.; Suzuki, Y.; Brennan, L.; Duignan, J.; Huang, L. H.; Sutcliffe, J.; Kojima, N. *J. Antibiot.* **2001**, *54*, 911-916.

[22] Abraham, W.-R. *Drug Des. Rev.* **2005**, *2*, 13-33.

[23] De Kievit, T. R.; Iglewski, B. H. *Infect. Immun.* **2000**, *68*.

[24] Kozlovsky, A. G.; Zhelifonova, V. P.; Adanin, V. M.; Antipova, T. V.; Ozerskaya, S. M.; Ivanushkina, N. E.; Grafe, U. *Appl. Biochem. Microbiol.* **2003**, *39*, 393-397.

[25] Kwon, O. S.; Park, S. H.; Yun, B. S.; Pyun, Y. R.; Kim, C. J. *J. Antibiot.* **2000**, *53*, 954-958.

[26] Song, M. K.; Hwang, I. K.; Rosenthal, M. J.; Harris, D. M.; Yamaguchi, D. T.; Yip, I.; Go, V. L. W. *Exp. Biol. Med.* **2003**, *228*, 1338-.

[27] Hwang, I. K.; Harris, D. M.; Yip, I.; Kang, K. W.; Song, M. K. *Diabetes Obes. Metab.* **2003**, *5*, 317-324.

[28] Kilian, G.; Jamie, H.; Brauns, S. C. A.; Dyason, K.; Milne, P. J. *Pharmazie* **2005**, *60*, 305-309.

[29] Imamura, M.; Prasad, C. *Peptides* **2003**, *24*, 445-448.

[30] Lopez-Rodriguez, M. L.; Morcillo, M. J.; Fernandez, E.; Porras, E.; Orensanz, L.; Beneytez, M. E.; Manzanares, J.; Fuentes, J. A. *J. Med. Chem.* **2001**, *44*, 186-197.

[31] Wyatt, P. G.; Allen, M. J.; Borthwick, A. D.; Davies, D. E.; Exall, A. M.; Hatley, R. J. D.; Irving, W. R.; Livermore, D. G.; Miller, N. D.; Nerozzi, F.; Sollis, S. L.; Szardenings, A. K. *Bioorg. Med. Chem. Lett.* **2005**, *15*, 2579-2582.

[32] Fischer, S.; Dunbrack, R. L.; Karplus, M. *J. Am. Chem. Soc.* **1994**, *116*, 11931-11937.

[33] Wei, Y.; Pei, D. *Bioorg. Med. Chem. Lett.* **2000**, *10*, 1073-1076.

[34] Nitecki, D. E.; Halpern, B.; Westley, J. W. *J. Org. Chem.* **1968**, *33*, 864-866.

[35] Hayashi, Y.; Orikasa, S.; Tanaka, K.; Kanoh, K.; Kiso, Y. *J. Org. Chem.* **2000**, *65*, 8402-8405.

[36] Sollis, S. L. *J. Org. Chem.* **2005**, *70*, 4735-4740.

[37] Santagada, V.; Fiorino, F.; Perissutti, E.; Severino, B.; Terracciano, S.; Cirino, G.; Caliendo, G. *Tetrahedron Lett.* **2003**, *44*, 1145-1148.

[38] Jainta, M.; Nieger, M.; Bräse, S. *Eur. J. Org. Chem.* **2008**, 5418-5424.

[39] Ermolat'ev, D. S.; Babaev, E. V. *Molecules* **2003**, *8*, 467-471.

[40] Li, W. R.; Yang, J. H. *J. Comb. Chem.* **2002**, *4*, 106-108.

[41] Wang, D. X.; Liang, M. T.; Tian, G. J.; Lin, H.; Liu, H. Q. *Tetrahedron Lett.* **2002**, *43*, 865-867.

[42] Guo, T.; Adang, A. E. P.; Dong, G.; Fitzpatrick, D.; Geng, P.; Ho, K. K.; Jibilian, C. H.; Kultgen, S. G.; Liu, R. Y.; McDonald, E.; Saionz, K. W.; Valenzano, K. J.; van Straten, N. C. R.; Xie, D.; Webb, M. L. *Bioorg. Med. Chem. Lett.* **2004**, *14*, 1717-1720.

[43] Krattiger, P.; Wennemers, H. *Synlett* **2005**, 706-708.

[44] Wennemers, H.; Nold, M. C.; Conza, M. M.; Kulicke, K. J.; Neuburger, M. *Chem.-Eur. J.* **2003**, *9*, 442-448.

[45] Conza, M.; Wennemers, H. *J. Org. Chem.* **2002**, *67*, 2696-2698.

[46] Wennemers, H.; Conza, M.; Nold, M.; Krattiger, P. *Chem.-Eur. J.* **2001**, *7*, 3342-3347.

[47] Krattiger, P.; Wennemers, H. *Synlett* **2005**, 706-708.

[48] Rodionov, I. L.; Rodionova, L. N.; Baidakova, L. K.; Romashko, A. M.; Balashova, T. A.; Ivanov, V. T. *Tetrahedron* **2002**, *58*, 8515-8523.

[49] Davies, J. S.; Stelmach-Diddams, M.; Fromentin, R.; Howells, A.; Cotton, R. *J. Chem. Soc., Perkin Trans. 1* **2000**, 239-243.

[50] Golebiowski, A.; Klopfenstein, S. R.; Chen, J. J.; Shao, X. *Tetrahedron Lett.* **2000**, *41*, 4841-4844.

[51] Kim, H.-O.; Nakanishi, H.; Lee, M. S.; Kahn, M. *Org. Lett.* **2000**, *2*, 301-302.

[52] Bisang, C.; Weber, C.; Robinson, J. A. *Helv. Chim. Acta* **1996**, *79*, 1825-1842.

[53] Pfeifer, M. E.; Moehle, K.; Linden, A.; Robinson, J. A. *Helv. Chim. Acta* **2000**, *83*, 444-464.

[54] Hintermann, T.; Seebach, D. *Synlett* **1997**, 437-438.

[55] Seebach, D.; Adele, S.; Gademann, K.; Jaun, B. *Angew. Chem., Int. Ed.* **1999**, *38*, 1595-1597.

[56] Chung, Y. J.; Christianson, L. A.; Stanger, H. E.; Powell, D. R.; Gellman, S. H. *J. Am. Chem. Soc.* **1998**, *120*, 10555-10556.

[57] Seebach, D.; Jaun, B.; Sebesta, R.; Mathad, R. I.; Flogel, O.; Limbach, M.; Sellner, H.; Cottens, S. *Helv. Chim. Acta* **2006**, *89*, 1801-1825.

[58] Webster, K. L.; Maude, A. B.; O'Donnell, M. E.; Mehrotra, A. P.; Gani, D. *J. Chem. Soc., Perkin Trans. 1* **2001**, 1673-1695.

[59] Thompson, C. M.; Frick, J. A.; Green, D. L. C. *J. Org. Chem.* **1990**, *55*, 111-116.

[60] Veerman, J. J. N.; Bon, R. S.; Hue, T. B.; Girones, D.; Rutjes, F. P. J. T.; van Maarseveen, J. H.; Hiemstra, H. *J. Org. Chem.* **2003**, *68*, 4486-4494.

[61] McLaughlin, M.; Mohareb, R. M.; Rapoport, H. *J. Org. Chem.* **2003**, *68*, 50-54.

[62] Edwards, A. A.; Sanjayan, G. J.; Hachisu, S.; Soengas, R.; Stewart, A.; Tranter, G. E.; Fleet, G. W. J. *Tetrahedron* **2006**, *62*, 4110-4119.

[63] Equi, A. M.; Brown, A. M.; Cooper, A.; Ner, S. K.; Watson, A. B.; Robins, D. J. *Tetrahedron* **1991**, *47*, 507-518.

[64] Pickersgill, I. F.; Rapoport, H. *J. Org. Chem.* **2000**, *65*, 4048-4057.

[65] Boger, D. L.; Lee, J. K. *J. Org. Chem.* **2000**, *65*, 5996-6000.

[66] Ariza, X.; Urpí, F.; Viladomat, C.; Vilarrasa, J. *Tetrahedron Lett.* **1998**, *39*, 9101-9102.

[67] David, C.; Bischoff, L.; Meudal, H.; Mothé, A.; De Mota, N.; DaNascimento, S.; Llorens-Cortes, C.; Fournié-Zaluski, M.-C.; Roques, B. P. *J. Med. Chem.* **1999**, *42*, 5197-5211.

[68] Carpino, L. A.; El-Faham, A.; Albericio, F. *J. Org. Chem.* **1995**, *60*, 3561-3564.

[69] Belvisi, L.; Gennari, C.; Mielgo, A.; Potenza, D.; Scolastico, C. *Eur. J. Org. Chem.* **1999**, 389-400.

[70] Phillips, S. T.; Blasdel, L. K.; Bartlett, P. A. *J. Org. Chem.* **2005**, *70*, 1865-1871.

[71] Nowick, J. S.; Lam, K. S.; Khasanova, T. V.; Kemnitzer, W. E.; Maitra, S.; Mee, H. T.; Liu, R. W. *J. Am. Chem. Soc.* **2002**, *124*, 4972-4973.

[72] Steffel, L. R.; Cashman, T. J.; Reutershan, M. H.; Linton, B. R. *J. Am. Chem. Soc.* **2007**, *129*, 12956-12957.

[73] Liang, G.-B.; Rito, C. J.; Gellman, S. H. *J. Am. Chem. Soc.* **1992**, *114*, 4440-4442.

[74] Englander, S. W.; Mayne, L. *Annu. Rev. Biophys. Biomol. Struct.* **1992**, *21*, 243-265.

[75] Liang, G.-B.; Desper, J. M.; Gellman, S. H. *J. Am. Chem. Soc.* **1993**, *115*, 925-938.

[76] Stevens, E. S.; Sugawara, N.; Bonora, G. M.; Toniolo, C. *J. Am. Chem. Soc.* **1980**, *102*, 7048-7050.

[77] Rose, G. D.; Gierasch, L. M.; Smith, J. A. *Advances in Protein Chemistry* **1985**, *37*, 1-109.

[78] Jones, I. G.; Jones, W.; North, M. *J. Org. Chem.* **1998**, *63*, 1505-1513.

[79] Chang, G.; Guida, W. C.; Still, W. C. *J. Am. Chem. Soc.* **1989**, *111*, 4379-4386.

[80] Weiner, S. J.; Kollman, P. A.; Nguyem, D. T.; Case, D. A. *J. Comput. Chem.* **1986**, *7*, 6127-6129.

[81] Still, W. C.; Tempczyk, A.; Hawley, R. C.; Hendrickson, T. *J. Am. Chem. Soc.* **1990**, *112*, 6127-6129.

[82] Fox, T.; Kollman, P. A. *J. Phys. Chem. B* **1998**, *102*, 8070-8079.

[83] Duan, Y.; Wu, C.; Chowdhury, S.; Lee, M. C.; M., X. G.; Zhang, W.; Yang, R.; Cieplak, P.; Luo, R.; Lee, T. *J. Comput. Chem.* **2003**, *24*, 1999-2012.

[84] Case, D. A.; Pearlman, D. A.; Caldwell, J. W.; Cheatham III, T. E.; Wang, J.; Ross, W. S.; Simmerling, C. L.; Darden, T. A.; Merz, K. M.; Stanton, R. V.; Cheng, A. L.; Vincent, J. J.; Crowley, M.; Tsui, V.; Gohlke, H.; Radmer, R. J.; Duan, Y.; Pitera, J.; Massova, I.; Seibel, G. L.; Singh, U. C.; Weiner, P. K.; Kollman, P. A.; AMBER 7, University of California, San Francisco, 2002.

[85] Cheng, R. P.; Gellman, S. H.; DeGrado, W. F. *Chem. Rev.* **2001**, *101*, 3219-3232.

[86] Hart, S. A.; Bahadoor, A. B. F.; Matthews, E. E.; Qiu, X. J.; Schepartz, A. *J. Am. Chem. Soc.* **2003**, *125*, 4022-4023.

[87] Ahmed, S.; Beleid, R.; Sprules, T.; Kaur, K. *Org. Lett.* **2007**, *9*, 25-28.

[88] Hynes, R. O. *Cell* **2002**, *110*, 673-687.

[89] Haas, T. A.; Plow, E. F. *Curr. Opin. Cell. Biol.* **1994**, *6*, 656–662.

[90] Plow, E. F.; Haas, T. A.; Zhang, L.; Loftus, J.; Smith, J. W. *J. Biol. Chem.* **2000**, *275*, 21785-21788.

[91] Stupack, D. G. *Cell Death Differ.* **2005**, *12*, 1021–1030.

[92] Xiong, J. P.; Stehle, T.; Diefenbach, B.; Zhang, R.; Dunker, R.; Scott, D. L.; Joachimiak, A.; Goodman, S. L.; Arnaout, M. A. *Science* **2001**, *294*, 339-345.

[93] Xiong, J. P.; Stehle, T.; Zhang, R.; Joachimiak, A.; Frech, M.; Goodman, S. L.; Arnaout, M. A. *Science* **2002**, *296*, 151-155.

[94] Arnaout, M. A.; Goodman, S. L.; Xiong, J.-P. *Curr. Opin. Cell Biol.* **2007**, *19*, 495-507.

[95] Adams, R. H.; Alitalo, K. *Nature Rev. Mol. Cell Biol.* **2007**, *8*, 464–478.

[96] Ferrara, N.; Kerbel, R. S. *Nature* **2005**, *438*, 967-974.

[97] Avraamides, C. J.; Garmy-Susini, B.; Varner, J. A. *Nat. Rev. Cancer* **2008**, *8*, 604-617.

[98] Brooks, P. C.; Clark, R. A.; Cheresh, D. A. *Science* **1994**, *264*, 569-571.

[99] Carmeliet, P. *Nature* **2005**, *42*, 932-936.

[100] Friedlander, M.; Theesfelt, C. L.; Sugita, M.; Fruttiger, M.; Thomas, M. A.; Chang, S.; Cheresh, D. A. *Proc. Natl. Acad. Sci. USA* **1996**, *93*, 9764-9769.

[101] Strömblad, S.; Becker, J. C.; Yebra, M.; Brooks, P. C.; A., C. D. *J. Clin. Invest.* **1996**, *98*, 426-433.

[102] Stupack, D. G.; Puente, X. S.; Boutsaboualoy, S.; Storgard, C. M.; Cheresh, D. A. *J. Cell Biol.* **2001**, *155*, 459-470.

[103] Eliceiri, B. P.; Puente, X. S.; Hood, J. D.; Stupack, D. G.; Schlaepfer, D. D.; Huang, X. Z.; Sheppard, D.; Cheresh, D. A. *J. Cell Biol.* **2002**, *157*, 149-160.

[104] Aumailley, M.; Gurrath, M.; Muller, G.; Calvete, J.; Timpl, R.; Kessler, H. *FEBS Lett.* **1991**, *291*, 50-54.

[105] Pfaff, M.; Tangemann, K.; Muller, B.; Gurrath, M.; Muller, G.; Kessler, H.; Timpl, R.; Engel, J. *J. Biol. Chem.* **1994**, *269*, 20233-20238.

[106] Gurrath, M.; Muller, G.; Kessler, H.; Aumailley, M.; Timpl, R. *Eur. J. Biochem.* **1992**, *210*, 911-921.

[107] Dechantsreiter, M. A.; Planker, E.; Mathä, B.; Lohof, E.; Hölzemann, G.; Jonczyk, A.; Goodman, S. L.; Kessler, H. *J. Med. Chem.* **1999**, *42*, 3033-3040.

[108] Gottschalk, K. E.; Kessler, H. *Angew. Chem., Int. Ed.* **2002**, *41*, 3767-3774.

[109] Wermuth, J.; Goodman, S. L.; Jonczyk, A.; Kessler, H. *J. Am. Chem. Soc.* **1997**, *119*, 1328-1335.

[110] Pitts, W. J.; Wityak, J.; Smallheer, J. M.; Tobin, A. E.; Jetter, J. W.; Buynitsky, J. S.; Harlow, P. P.; Solomon, K. A.; Corjay, M. H.; Mousa, S. A.; Wexler, R. R.; Jadhav, P. K. *J. Med. Chem.* **2000**, *43*, 27-40.

[111] Meissner, R. S.; Perkins, J. J.; T., D. L.; Hartman, G. D.; Hoffman, W. F.; Huff, J. R.; Ihle, N. C.; Leu, C.-T.; Nagy, R. M.; Naylor-Olsen, A.; Rodan, G. A.; Whitman, D. B.; Wesolowski, G. A.; Duggan, M. E. *Bioorg. Med. Chem. Lett.* **2002**, *12*, 25-29.

[112] Duggan, M. E.; Duong, L. T.; Fisher, J. E.; Hamill, T. G.; Hoffman, W. F.; Huff, J. R.; Ihle, N. C.; Leu, C.-T.; Nagy, R. M.; Perkins, J. J.; Rodan, S. B.; Wesolowski, G. A.; Whitman, D. B.; Zartman, A. E.; Rodan, G. A.; Hartman, G. D. *J. Med. Chem.* **2000**, *43*, 3736-3745.

[113] Batt, D. G.; Petraitis, J. J.; Houghton, G. C.; Modi, D. P.; Cain, G. A.; Coryay, M. H.; Mousa, S. A.; Bouchard, P. J.; Forsythe, M. S.; Harlow, P. P.; Barbera, F. A.; Spitz, S. M.; Wexler, R. R.; Jadav, P. K. *J. Med. Chem.* **2000**, *43*, 41-58.

[114] Nicolaou, K. C.; Trujillo, J. T.; Janderleit, B.; Chibale, K.; Rosenfeld, M.; Diefenbach, B.; Cheresh, D. A.; Goodman, S. L. *Bioorg. Med. Chem. Lett.* **1998**, *6*, 1185-1208.

[115] Sulyok, G. A. G.; Gibson, C.; Goodman, S. L.; Hölzemann, G.; Wiesner, M.; Kessler, H. *J. Med. Chem.* **2001**, *44*, 1938-1950.

[116] Gibson, C.; Sulyok, G. A. G.; Hahn, D.; Goodman, S. L.; Hölzemann, G.; Kessler, H. *Angew. Chem., Int. Ed.* **2001**, *40*, 165-169.

[117] Haubner, R.; Schmitt, W.; Holzemann, G.; Goodman, S. L.; Jonczyk, A.; Kessler, H. *J. Am. Chem. Soc.* **1996**, *118*, 7881-7891.

[118] Lohof, E.; Planker, E.; Mang, C.; Burkhart, F.; Dechantsreiter, M. A.; Haubner, R.; Wester, H.-J.; Schwaiger, M.; Hölzemann, G.; Goodman, S. L.; Kessler, H. *Angew. Chem., Int. Ed.* **2000**, *39*, 2761-2764.

[119] Schumann, F.; Müller, A.; Koksch, M.; Müller, G.; Sewald, N. *J. Am. Chem. Soc.* **2000**, *122*, 12009-12010.

[120] Urman, S.; Gaus, K.; Yang, Y.; Strijowski, N. S.; Sewald, N.; De Pol, S.; Reiser, O. *Angew. Chem., Int. Ed.* **2007**, *46*, 3976-3978.

[121] Belvisi, L.; Bernardi, A.; Checchia, A.; Manzoni, L.; Potenza, D.; Scolastico, C.; Castorina, M.; Cupelli, A.; Giannini, G.; Carminati, P.; Pisano, C. *Org. Lett.* **2001**, *3*, 1001-1004.

[122] Belvisi, L.; Bernardi, A.; Manzoni, L.; Potenza, D.; Scolastico, C. *Eur. J. Org. Chem.* **2000**, 2563-2569.

[123] Royo, M.; Van den Nest, W.; del Fresno, M.; Frieden, A.; Yahalom, D.; Rosenblatt, M.; Chorev, M.; Albericio, F. *Tetrahedron Letters* **2001**, *42*, 7387-7391.

[124] Pons, J. F.; Fauchere, J. L.; Lamaty, F.; Molla, A.; Lazaro, R. *European Journal of Organic Chemistry* **1998**, 853-859.

[125] Belvisi, L.; Bernardi, A.; Colombo, M.; Manzoni, L.; Potenza, D.; Scolastico, C.; Giannini, G.; Marcellini, M.; Riccioni, T.; Castorina, M.; P., L.; Pisanoc, C. *Bioorg. Med. Chem.* **2006**, *14*, 169-180.

[126] Boatman, P. D.; Ogbu, C. O.; Eguchi, M.; Kim, H.-O.; Nakanishi, H.; Cao, B.; Shea, J. P.; Kahn, M. *J. Med. Chem.* **1999**, *42*, 1367-1375.

[127] Gibson, F. S.; Bergmeier, S. C.; Rapoport, H. *J. Org. Chem.* **1994**, *59*, 3216-3218.

[128] Tanaka, H.; Sawayama, A. M.; Wandless, T. J. *J. Am. Chem. Soc.* **2003**, *125*, 6864-6865.

[129] Lin, L. S.; Lanza, T.; de Laszlo, S. E.; Truong, Q.; Kamenecka, T.; Hagmann, W. K. *Tetrahedron Lett.* **2000**, *41*, 7013-7016.

[130] Imwinkelried, R.; Schiess, M.; Seebach, D. *Org. Synth.* **1987**, *65*, 230-233.

CHAPTER III:

MOLECULAR TONGS CONTAINING PEPTIDOMIMETIC FRAGMENTS: NEW DIMERIZATION INHIBITORS OF HIV-1 PROTEASE

I. HUMAN IMMUNODEFICIENCY VIRUS (HIV)

Human immunodeficiency virus (HIV) is a lentivirus (a member of the retrovirus family) that can lead to *acquired immunodeficiency syndrome* (AIDS), a condition in humans in which the immune system begins to fail, leading to life-threatening opportunistic infections.

Infection with HIV occurs by the transfer of blood, semen, vaginal fluid, pre-ejaculate, or breast milk. Within these bodily fluids, HIV is present as both free virus particles and virus within infected immune cells. The four major routes of transmission are unprotected sexual intercourse, contaminated needles, breast milk, and transmission from an infected mother to her baby at birth. Screening of blood products for HIV has largely eliminated transmission through blood transfusions or infected blood products in the developed world.

HIV infection in humans is now a pandemic and is considered one of the most destructive ones in recorded history. Every day, approximately 6800 persons acquire the infection and 5700 die from AIDS. The estimated number of people living with HIV in 2007 was 33.2 million, of which 2.1 million are children. The number of new infections in 2007 was 2.5 million and the number of deaths was estimated to 2.1 million.

I.1. HIV-1 REPLICATION CYCLE

HIV-1 infects cells of the human immune system that express its main entry receptor, CD4, on their surface (Figure III.1). The primary targets of HIV-1 are T-lymphocytes and macrophages, but the virus can infect many other cells, such as monocytes, dendritic cells, and microglial cells in the brain. Depletion of $CD4^+$ T-lymphocytes due to HIV-1 infection leads to loss of cellular immunity and is the main cause of AIDS.

HIV life cycle is characterized by the following stages:

BINDING AND ENTRY: HIV can only replicate (make new copies of itself) inside human cells. The process typically begins when a virus particle bumps into a cell that carries on its surface a special protein called CD4. The spikes on the surface of the virus particle stick to the CD4 and allow the viral envelope to fuse with the cell membrane. The contents of the HIV particle are then released into the cell, leaving the envelope behind.

REVERSE TRANSCRIPTION AND INTEGRATION: once inside the cell, the HIV enzyme reverse transcriptase converts the viral RNA into DNA, which is compatible with human genetic material. This DNA is transported to the cell's nucleus, where it is spliced into the human DNA by the HIV enzyme integrase. Once integrated, the HIV DNA is known as provirus.

TRANSCRIPTION AND TRANSLATION: HIV provirus may lie dormant within a cell for a long time, but when the cell becomes activated, it treats HIV genes in much the same way as human genes. First it converts them into messenger RNA (using human enzymes). Then the messenger RNA is transported outside the nucleus, and is used as a blueprint for producing new HIV proteins and enzymes.

ASSEMBLY, BUDDING AND MATURATION: among the strands of messenger RNA produced by the cell are complete copies of HIV genetic material. These gather together with newly made HIV proteins and enzymes to form new viral particles, which are then released from the cell. The enzyme protease plays a vital role at this stage of the HIV life cycle by chopping up long strands of protein into smaller pieces, which are used to construct mature viral cores. The newly matured HIV particles are ready to infect another cell and begin the replication process all over again. In this way the virus quickly spreads through the human body. And once a person is infected, they can pass HIV on to others in their bodily fluids.

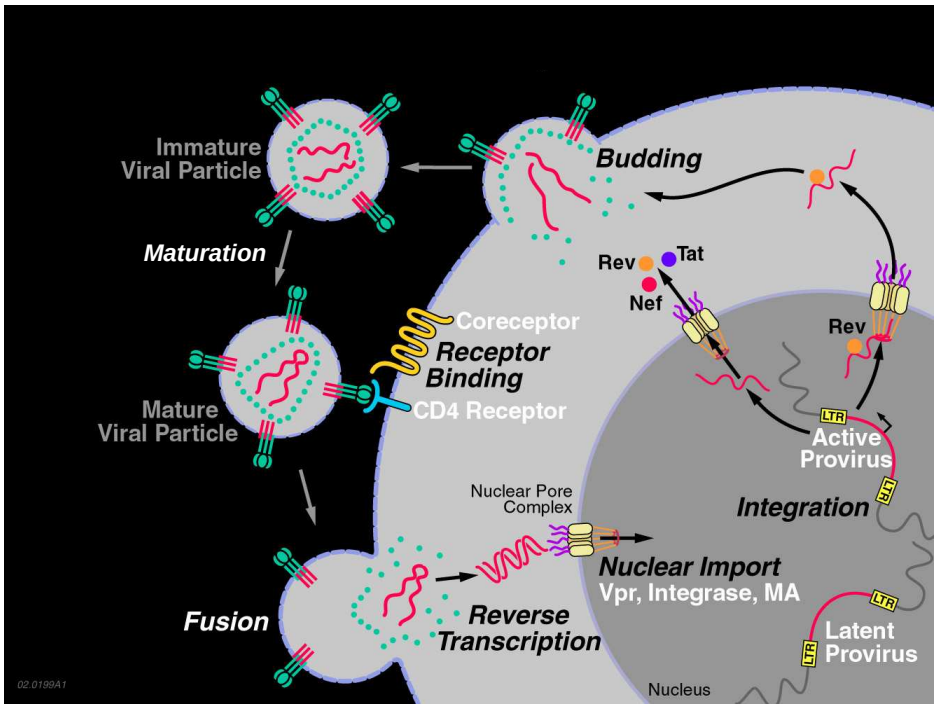

Figure III.1. HIV-1 life cycle.[1]

I.2. THERAPIES

HIV life cycle shows several susceptible points that might be blocked by pharmaceutical agents. Two important characteristics of anti-HIV drugs are that they must be

specific for HIV-1, and interfere minimally with normal cellular processes. Current AIDS treatment involves an approach known as Highly Active Antiretroviral Therapy (HAART), in which antiretroviral drugs, typically three or four, are taken in combination. HAART combination therapy appears to overcome the ability of the virus to rapidly produce mutants that are drug resistant.

There are currently 30 antiretroviral drugs approved by the FDA, which are broadly classified by the layer of the retrovirus life-cycle that the drug inhibits, namely: **i)** Nucleoside and nucleotide reverse transcriptase inhibitors (NRTIs and NtRTIs, respectively), **ii)** Non-nucleoside reverse transcriptase inhibitors (nNRTIs), **iii)** Protease inhibitors (PIs), **iv)** Integrase inhibitors, and **v)** Entry inhibitors (or fusion inhibitors).

I.3. HIV-1 PROTEASE AND PROTEASE INHIBITORS

I.3.1. HIV-1 PROTEASE STRUCTURE

The HIV-1 protease (PR) was structurally characterized by X-ray crystallography for the first time in 1989[2-5] and a large number of different crystal structures are presently available.

HIV-1 protease (Figure III.2) consists of two identical 99-residue monomers assembled into a C_2-symmetric structure, giving rise to a dimer with a molecular weight of 22 kDa. The enzyme is active only in its dimeric form.[6] Each monomer folds into a compact structure of β-strands with a short α-helix near the C-terminal.

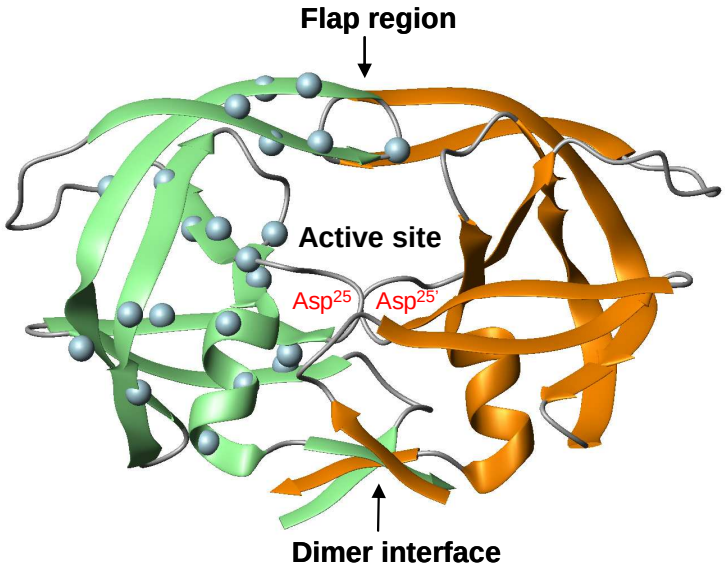

Figure III.2. HIV-1 protease structure. Major mutations that confer resistance to active-site directed drugs are shown in the left monomer (blue spheres).

ACTIVE SITE: Formation of the active protease dimer is a reversible process and high concentrations of monomer are needed for this to occur, this is the case in the newly budded virions. The monomer concentration inside the host cell is too low, preventing the active protease from forming and degradation of cellular proteins is avoided. The C_2-symmetric active site is located at the dimer interface and each subunit contributes with one catalytic aspartic acid residue present in a tripeptide sequence, Asp-Thr-Gly.[7]

FLAP REGION: The active site is flanked by the two flaps, which have to open in order to let the substrate in. The flaps then close for catalysis to take place, after which they open again to release the products. Inhibitors or substrates bind between the two subunits in the dimer through hydrogen bonds and van der Waals interactions with the active site. The flaps fold down over the substrate or inhibitor and act during catalysis both to bind substrate and exclude water molecules from the active site.[7,8]

DIMER INTERFACE: It is structured in a 4-stranded antiparallel β-sheet formed by the interdigitation of N-terminal (residues 1–4) and C-terminal (residues 96–99) β-strands of each monomer.

HIV PR SUBSTRATE SPECIFICITY

Although the native protein is a symmetric dimer, inhibitors bind in an asymmetric manner. The active site contains a number of well-defined subsites where protruding substrate or inhibitor side chains can be accommodated upon binding.[7] According to the Schechter and Berger nomenclature, the amino acid residues of the substrate are termed P1, P2…Pn and P1', P2'…Pn' counted from the bond which is cleaved during hydrolysis, called the 'scissile' bond (Figure III.3). The enzyme subsites occupied by these amino acid residues have the same numbering beginning with the letter: S, S1, S2…Sn and S1', S2'…Sn'. Hydrophobic amino acid residues account for most of the PR subsites, and the S1/S1' pockets are adjacent to S3/S3'. As a consequence of the symmetric nature of the HIV-1 PR the S1 and S1' subsites are identical, as are the S2 and S2' subsites, and so on.

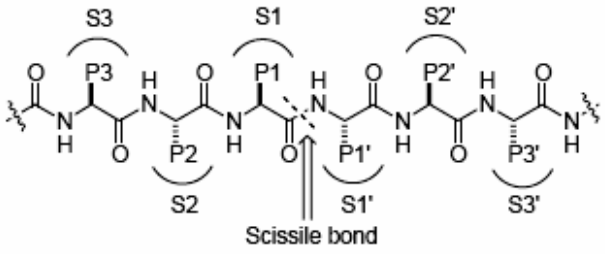

Figure III.3. Standard nomenclature used to denote the substrate amino acid residues and enzyme subsites.

I.3.2. PROTEASE INHIBITORS (PIS)

As it was mentioned before, HIV PR is an aspartic protease that is essential for the life cycle of HIV.[9] HIV PR cleaves newly synthesised polyproteins (gap and gap-pol) at the appropriate places to create the mature protein components of an infectious HIV virion. Without effective HIV PR, HIV virions remain uninfectious.[10,11] Thus, mutation of HIV PR's active site or inhibition of its activity disrupts HIV's ability to replicate and infect additional cells,[12] making HIV PR inhibition the subject of much pharmaceutical research.[13,14]

The protease inhibitors mimic the structure of its regular substrate and compete with its binding, thus blocking protease activity.

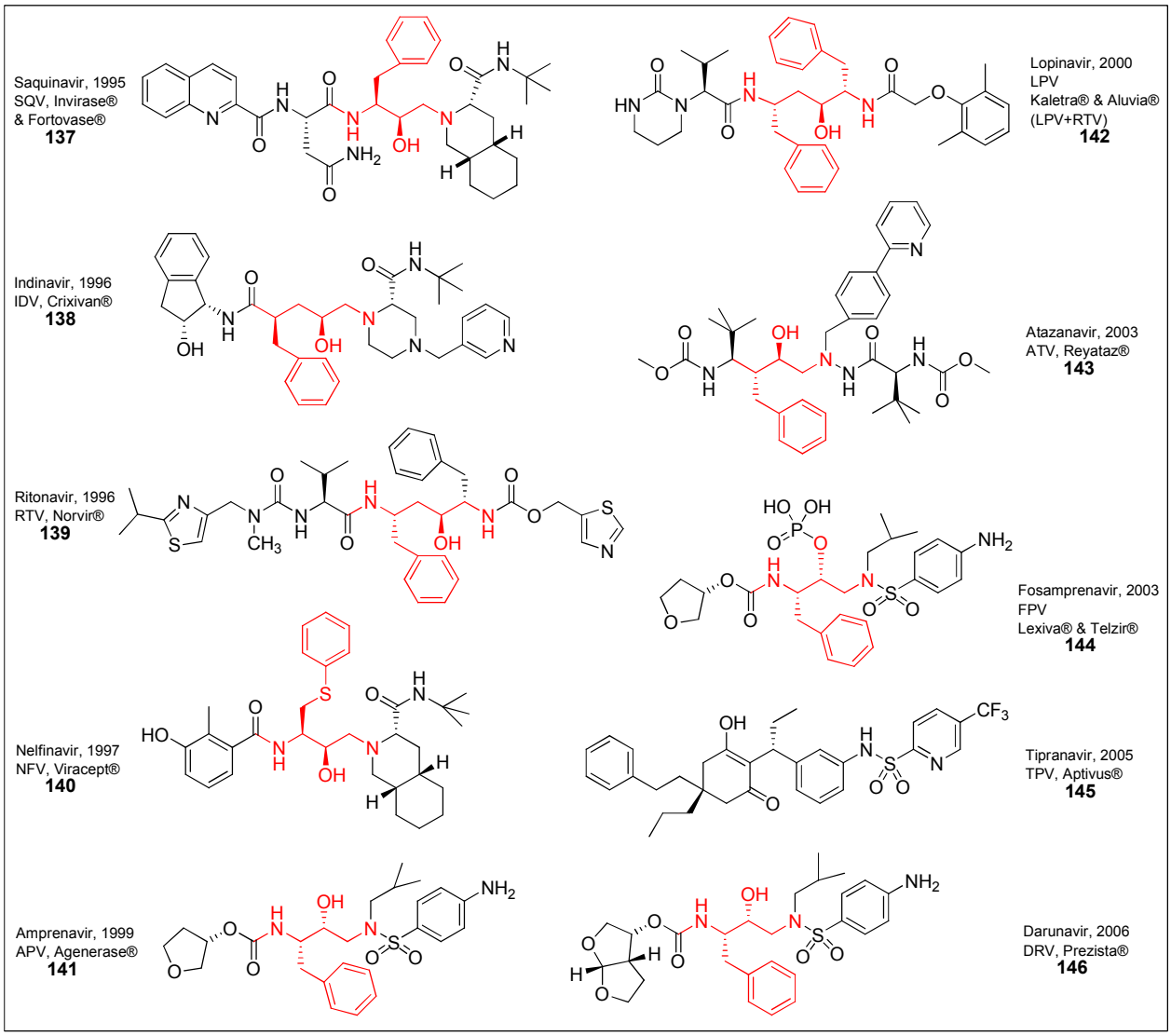

Figure III.4. Structures of currently FDA-approved HIV PR inhibitors. The peptidomimetic core structure found within all PIs (except in Tipranavir) is shown in red.

All of the currently available HIV PR inhibitors (Figure III.4), except for Tipranavir **145**, which is based on the coumarin lactone scaffold, can be considered as peptidomimetics. They are built upon a nonhydrolyzable hydroxyethylene or hydroxyethylamine moiety (instead of the normal peptidic bond), which mimics the peptide linkage (Figure III.3) in the polyprotein precursor gag–pol. Basically, the core (the nonhydrolyzable hydroxyethylene or hydroxyethylamine moiety) is a good isostere replacement at the scissile bond that is believed to mimic the tetrahedral transition state of the proteolytic reaction.[15]

Compared with the substrate analogue, those clinical drugs are smaller and make few interactions with PR. All of these drugs bind to the active site of PR by hydrogen bonds and van der Waals interactions, depending on the nature of the groups at each position.

MULTI-THERAPY AND PIS LIMITATIONS

Shortly after the introduction of the first antiretroviral drug, the limited effects of monotherapy on HIV became clear. However, when the first PIs were launched in the mid 1990s, a new treatment strategy including combination therapy with drugs from different classes of anti-HIV agents was evaluated. Several reports indicated efficient suppression of viral loads and reduced mortality among HIV patients receiving the combination regimen.[16-19] Initially, two NRTIs and one PI were used in this highly active antiretroviral therapy (HAART) and today several different drug associations are available, combining: NRTIs, NtRTIs, PIs and nNRTIs.[20]

Nevertheless, viral resistance to protease inhibitors administrated alone or in combination with reverse transcriptase inhibitors have been described *in vivo*.[21] The mechanism for the development of resistance to PIs is quite complicated, since the locations of PI-resistant mutations vary from substrate/inhibitor binding site, dimer interface, and flap region to surface of protease (Figure III.2).

Besides drug resistance, the adverse metabolic side effects are another major issue involving the PI treatment. The adverse effects that have been reported include peripheral lipodystrophy, visceral adiposity, hyperlipidemia, diabetes mellitus, cardiovascular disease, hypertension and insulin resistance.[22,23] As more and more evidence accumulates, it has been confirmed that PIs do not specifically target HIV PR as designed and they disturb the function of a number of unrelated molecules.

The drug resistance as well as the adverse side-effects suggests that there is a need for structurally diverse antiproteases. Since all protease inhibitors used in HIV-1 therapy interact with the active site it is probably necessary to target other binding locus for HIV-1 PR inhibitors.

II. INHIBITORS OF HIV-1 PROTEASE DIMERIZATION

As mentioned before, the HIV PR is composed of 2 monomers, of 99 amino acids each (Figure III.5) that are self assembling into a homodimeric structure (see also, Figure III.2). The association of these two monomers allows the formation of the active site, meaning that the PR is only active in its dimeric form.

Pro Gln Ile Thr Leu Trp Gln Arg Pro Leu Val Thr Ile	13
Lys Ile Gly Gly Gln Leu Lys Glu Ala Leu Leu **Asp Thr**	26
Gly Ala Asp Asp Ser Ile Val Ala Gly Ile Glu Leu Pro	39
Gly Arg Trp Lys Pro Lys Met Val Gly Gly **Ile** Gly Gly	52
Phe Ile Lys Val Arg Gln Tyr Asp Gln Ile Leu Ile Glu	65
Ile Cys Gly His Lys Ala Ile Gly Thr Val Leu Val Gly	78
Pro Thr Pro Ile Asn Ile Ile Gly Arg Asn Leu Leu Thr	91
Gln Ile Gly Cys **Thr Leu Asn Phe**	99

Figure III.5. Primary structure of the HIV-1 PR monomer.

The HIV protease is characterized among others, by three important areas: **i)** the active site, were Asp25 and Asp25' (in red, Figure III.5) provide important interactions with the substrate or the inhibitor; **ii)** the flap region, where the residues Ile50 and Ile50' (in purple, Figure III.5) also provide important interactions with the substrate or the; and **iii)** the dimerization interface, structured in a 4-stranded β-sheet formed by the residues N-terminal P-Q-I-T ([1-4 and 1'-4'], in green, Figure III.5) and C- terminal T-L-N-F ([96-99 and 96'-99'], in blue, Figure III.5) of each monomer.

In the crystal structures of HIV-1 PR, the polypeptide termini are held at a distance of approximately 10 Å. This four-stranded β-sheet provides a network of hydrogen bonds, by forming an array of 10 and 14 member rings of hydrogen bonds (Figure III.6). It is estimated that this structure contributes close to 75% of the total Gibbs free energy of dimerization.[24]

An important feature of this region of dimerization is that it is found less mutated, even among viruses resistant to antiretroviral treatment,[25] making it an interesting alternative target compared to the classic target, which is the active site. Blocking the assembly of the HIV-1 PR homodimer or disturbing the dimeric interface would be a novel means of inhibiting protease activity.

The development of the PR dimerization inhibitors is based on a thorough knowledge of its structure. In the next sections, the design and synthesis of new dimerization inhibitors of HIV-1 PR will be discussed.

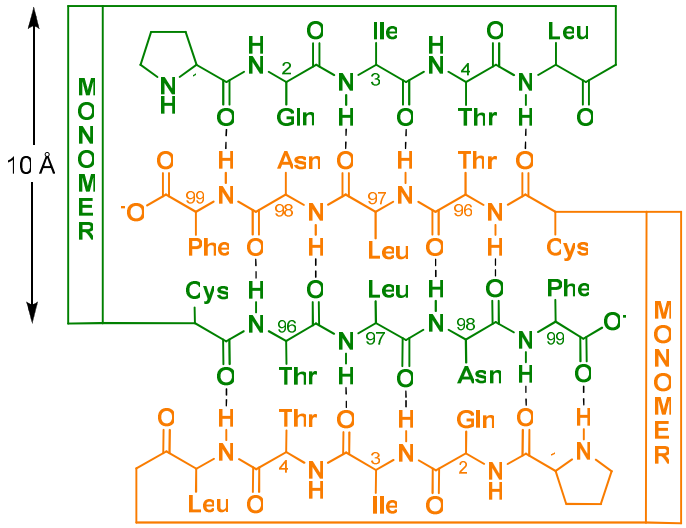

Figure III.6. Antiparallel β-sheet formed by the interdigitation of N-terminal (residues 1-4) and C-terminal (residues 96-99) β-strands of each monomer of the PR. H-bonds represented by dotted lines.

II.1. INHIBITORS IN LITERATURE

The recently approved PIs Tipranavir and Darunavir, which target the HIV-1 PR active site, also disrupt dimer interface.[26,27] Koh *et al* have also reported others non peptidyl small molecules as dimerization inhibitors.[27] The next section describes some short peptides, cross-linked interfacial peptides and non-peptide based inhibitors of PR dimerization.

II.1.1. SHORT PEPTIDES

Short synthetic peptides corresponding to the amino acid sequences of the N- and C-terminal of HIV-1 PR **147**–**157** have been shown to inhibit proteolytic activity by binding to the inactive PR subunits and preventing their association into active dimer.[28-31] However, the concentration of these peptides required to effectively inhibit the PR monomer-dimer equilibrium by 50% (IC_{50}) is relatively high (30-100 μM, Table 3.1).[32] Schramm *et al.* demonstrated that it was possible to significantly improve their inhibitory properties (approximately 50-200 fold) through modification of their amino-acid composition and the addition of a hydrophobic moiety, such aminocaproyl or palmitoyl, to the N-terminus of the peptide.[32,33] The development of these more potent peptide inhibitors firmly established that PR dimerization was a rational target for the development of AIDS therapeutics, and that small-size peptide mimetics could be derived for HIV-1 therapy. In this regard, N-terminally palmitoyl-blocked peptides **155**–**157** consisting of only three residues, one of which is a non-natural amino acid, have been developed and shown to exhibit good inhibitory potency of nanomolar range against PR dimerization.[34-37]

Table III.1. Peptide and small molecule inhibitors of HIV-1 PR dimerization. Kinetic analyses were carried out according to the method described by Zhang *et al*.[28]

STRUCTURE	K_{id} (nM)
PEPTIDES DERIVED FROM THE N- TERMINUS OF HIV-1 PR	
147: H-Leu-Gln-Ile-Thr-Trp-OH[32]	590
148: H-Pro-Gln-Ile-Thr-Leu-Trp-OH[31]	~100000
PEPTIDES DERIVED FROM THE C- TERMINUS OF HIV-1 PR	
149: Ac-Thr-Leu-Asn-Phe-OH[28]	45000
150: H-Ile-Ser-Tyr-Glu-Leu-OH[32]	400
151: H-Ser-Tyr-Glu-Trp-OH[32]	320
152: H-Ser-Tyr-Glu-Leu-OH[32]	1270
153: H-Tyr-Glu-Leu-OH[32]	2400
154: Ac-Ser-Thr-Leu-Asn-Phe-OH[31]	~100000
MODIFIED PEPTIDES DERIVED FROM THE C-TERMINUS OF HIV-1 PR	
155: Palmitoyl-Tyr-Glu-Leu-OH[34]	11
156: Palmitoyl-Thr-Val-Ser-Tyr-Glu-Leu-OH[34]	160
157: 2-aminoPalmitoyl-Tyr-Glu-thyroxine-OH[36]	5

II.1.2. CROSS-LINKED INTERFACIAL PEPTIDES

Cross-linking of the N- and C-terminal peptides to form a mimic of the HIV-1 PR dimerization interface has provided an alternative strategy for the development of more potent PR dimerization inhibitors. The principle of this strategy is illustrated in Figure III.7.[35]

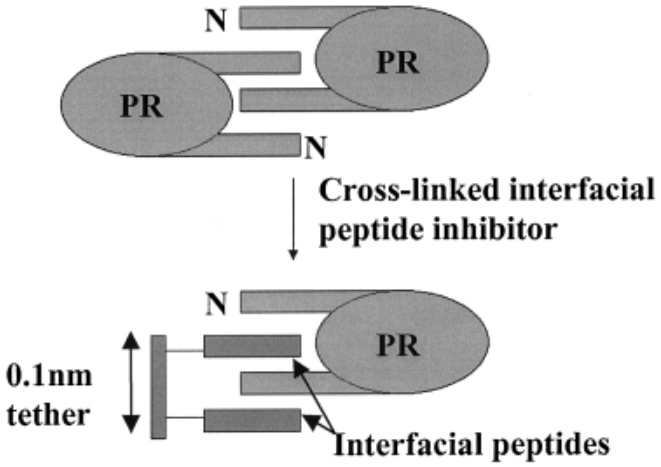

Figure III.7. Schematic representation of the strategy used to inhibit PR dimerization by cross-linked interfacial peptides. The PR N-terminus is indicated (N). The 4-stranded β-sheet formed by amino acid residues at the N- and C-termini of PR is a major binding determinant in the formation of dimeric PR. Cross-linked interfacial

peptides containing a tether region of approximately 10 Å inhibit PR dimerization by permitting the formation of a pseudo antiparallel β-sheet with one of the PR subunits.

II.1.2.1. PEPTIDES WITH FLEXIBLE SPACERS

This approach was initially adopted by Babe *et al.*,[30,38] who cross-linked peptide sequences containing the N- and C-terminal regions of HIV PR with a 3.5 Å tether composed of three glycine residues **158**, (IC_{50} = 40 μM, Figure III.8). However, the resulting compounds were not potent inhibitors of PR dimerization. In the crystal structures of HIV-1 PR, the polypeptide termini are held at a distance of approximately 10 Å (Figure III.7) and this can explain why the N- and C-terminal PR-derived peptides with a 3.5 Å tether are not good inhibitors of PR dimerization.

Accordingly, more potent cross-linked interfacial peptide compounds have been developed using tethers that bridge this gap. For example, Zutshi *et al.* synthesised interfacial peptides cross-linked with alkyl chains in order to reproduce the β-sheet structure with one HIV-1 PR monomer.[39] Their best inhibitor **159** (IC_{50} = 2 μM) was constructed with HN-PQITLW-OH and HN-STLNF-OH polypeptide chains tethered with a C14 alkyl chain (Figure III.8). The major drawback of these cross-linked inhibitors is related to their high conformational freedom which induces an unfavourable entropy term in the interaction energy of the inhibitor-HIV-1 PR monomer complex.

In an effort to simplify the synthesis of HIV-1 PR inhibitor libraries, a new tether, 12-aminododecanoic acid (12-Ado), was developed (Figure III.8). This tether, was crosslink to interfacial peptide, in which the directionality of the southern peptide was changed from N→C to C→N. Furthermore, the terminal amine of the southern peptide can be used to incorporate various functional group (**160**, K_i ≈ 200 nM).[40]

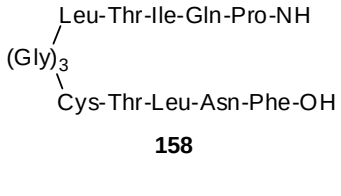

158

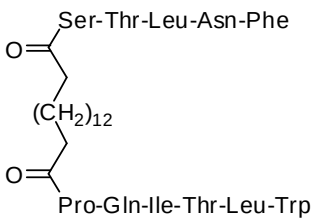

159

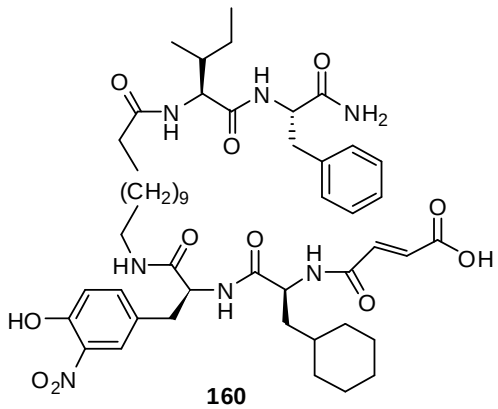

160

Figure III.8. Peptides with flexible spacers.

Designed agents based on cross-linked interfacial peptides of protease showed good potency against HIV-1 protease dimerization and activity, but high molecular complexity.[39] Efforts to identify the minimal structure necessary for activity led to an agent that functioned as a dimerization inhibitor, but with reduced potency.[41] On the basis of a model of the complex of inhibitor **161** (K_i = 3000 nM) and the HIV-1 protease monomer, Chmielewski *et al.* designed a focused library (Figure III.9) of agents, in an effort to regain high potency, by replacing successively the amino acids in positions 1, 2, 3, 4, 5 with unnatural amino acids, bearing side chains like: Thx (thyroxine), Chg (cyclohexylglycine), NaI (naphthylalanine), Cha (cyclohexylalanine), Paf (4-aminophenylalanine) and Hfe (homophenylalanine) (Figure III.9). Concerning the single position modifications, the best result was obtained when the Phe residue at position 1 was replaced with the biphenyl ether moiety of Thx (K_i = 71 nM).[42] An even more powerful inhibitory potency against PR dimerization was obtained when two amino acids of the starting structure **161**. The best results were obtained maintaining the previous modification (Phe1→Thx) and introducing a Paf residue at position 4 or a NaI residue at position 5 (K_i = 29 nM, in both cases).[43]

Irreversible inhibition of PR dimerization has also been achieved by designing a cross-linked interfacial peptide molecule (**162**: K_{inac} = 3.7 μM) that can form a disulfide bond with Cys95 present in the dimerization interface of HIV-1 PR.[44]

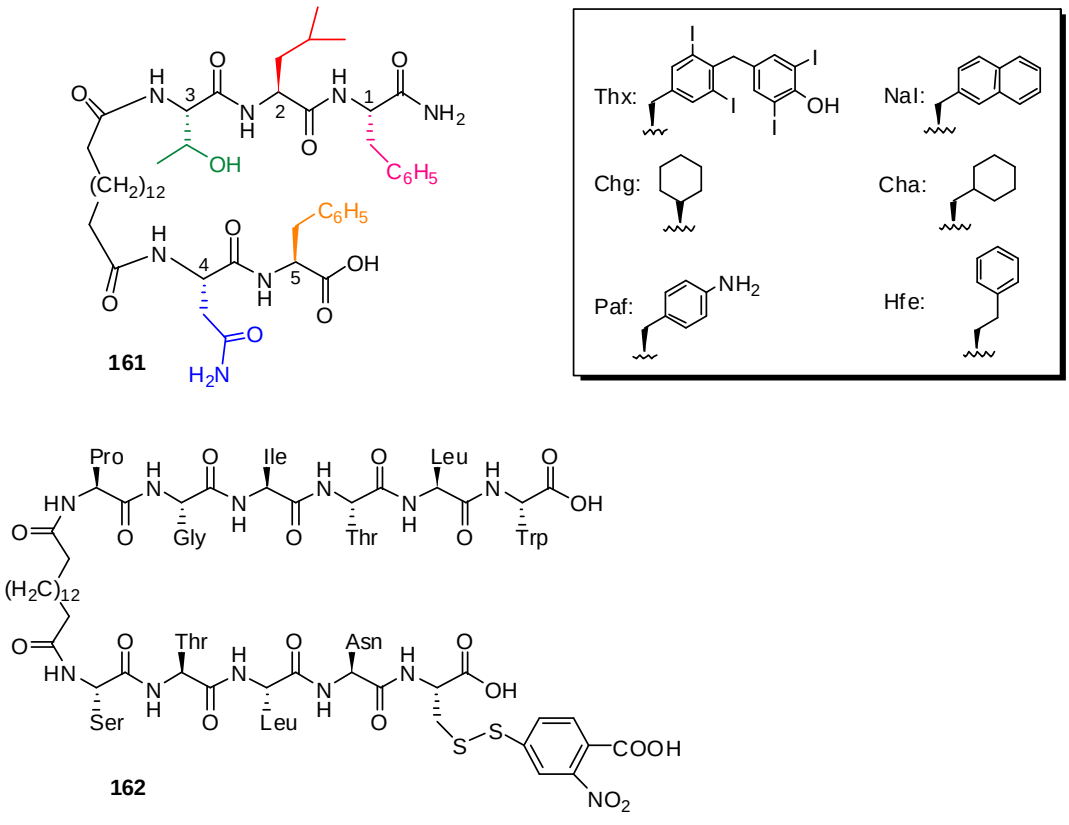

Figure III.9. Peptides with flexible spacers.

II.1.2.2. PEPTIDES WITH UNCHARGED AND CHARGED RIGID SPACERS

Molecular tongs

Sicsic *et al.* introduced in 1999[45] a more rigid scaffold in the tether (to increase conformational constrain), such as resorcinol, 2,6-pyridinediol (**163a** and **163b**, respectively) and 2,7-naphthalenediol **164a** (Figure III.10), leading to compounds (named, "molecular tongs") active in the micro and submicromalor range. In 2004[46] were introduced new molecular tongs based on quinoline and naphthalene scaffolds (**164a** and **164b**, respectively) linked to two peptidic strands of different sequences. In order to increase the resistance to proteolysis of these molecular tongs, in 2006[47] were inserted peptidomimetic motifs into one peptidic strand of the molecular tongs (for more details see Section II.2, page 112).

Guanidinium-based inhibitors

Dimerization inhibitors of HIV-1 PR based on a chiral lipophilic bicyclic guanidinium subunit **165** (Figure III.10) as the central tether between a short peptide mimicking the C-terminal native strand, to interact with both C and N termini of the monomer, and an additional hydrophobic bulky group (TBDPS, Cholesteryl) targeting the dimer interface have also been described.[48] Some of the compounds described inhibited the dimerization of HIV PR in the submicromolar range (K_{id} = 150-400 nM).

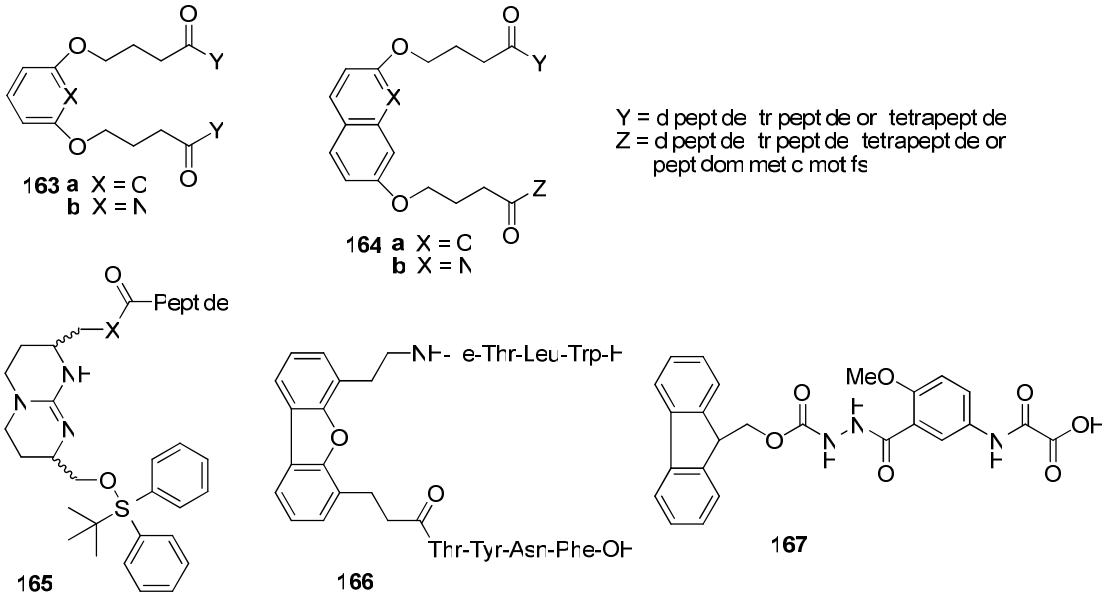

Figure III.10. Peptides with uncharged and charged rigid spacers.

Dibenzofuran-based inhibitors

Song *et al.* have used dibenzofuran-based amino acid **27** (Kelly's "β-sheet nucleator" discussed in Chapter I, page 21) to connect the interfacial N- and C-terminal peptide

fragments from the protease sequence, to obtain inhibitor **166** (K_{id} = 5.4 μM).[49] They have also synthesised compound **166** (K_{id} = 9.1 μM) containing an "unnatural β-strand mimetic" (5-amino-2-methoxybenzoic hydrazide derivative; Nowick's template also discussed in Chapter I, page 27) which interferes with the β-sheet interaction between the two PR monomers and inhibits the enzymatic activity (Figure III.10).[49]

II.1.2.3. NON-PEPTIDE BASED INHIBITORS OF PR DIMERIZATION

To date, two structurally unrelated classes of small-organic molecules which inhibit PR dimerization, have been identified.[50,51] The first class of molecules, which exhibit a polycyclic triterpene structure, were identified following a search of the Cambridge Structural Database (www.ccdc.cam.ac.uk) for pharmacophores that could bridge the 10 Å gap between the termini of a PR subunit.[50] Extensive kinetic analysis of one of these triterpenes, ursolic acid **168** (Figure III.11), demonstrated that these compounds inhibited PR dimerization with relatively high potency (K_i = 3.4 μM). The second class of molecules that inhibited PR dimerization include penta ester derivatives of didemnaketal A **169** (K_i = 2.1 μM, Figure III.11).[51] The identification of these classes of small molecules is significant, as in general many empirical searches for low molecular mass pharmacological inhibitors (<400) of protein–protein interactions have routinely failed.[35,37]

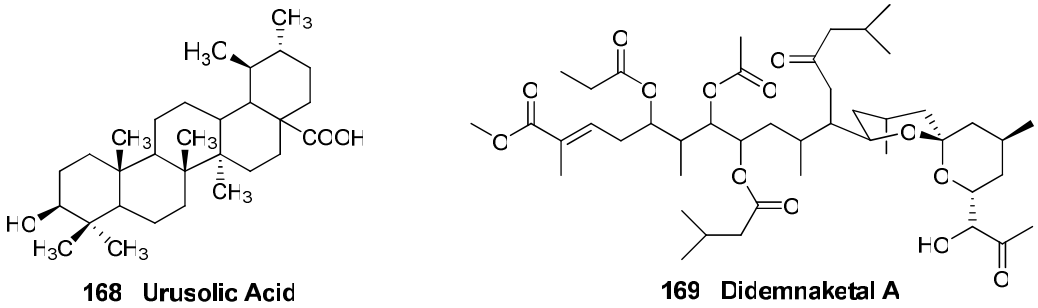

168 Urusolic Acid **169 Didemnaketal A**

Figure III.11. Non-peptide based inhibitors of PR dimerization.

II.2. PREVIOUS WORK IN OUR LABORATORY

Our contribution to the antidimer strategy was the synthesis of the first "molecular tongs" based on a conformationally constrained scaffold attached to two peptidic strands through two carboxypropyl linkers. The advantage of this strategy is that the two peptidic strands could be suitably oriented by the scaffold allowing the putative formation of an

antiparallel β-sheet with the C-terminal and N-terminal of one HIV-1 PR monomer, thus leading to an entropy benefit (Figures 3.12 and 3.13).

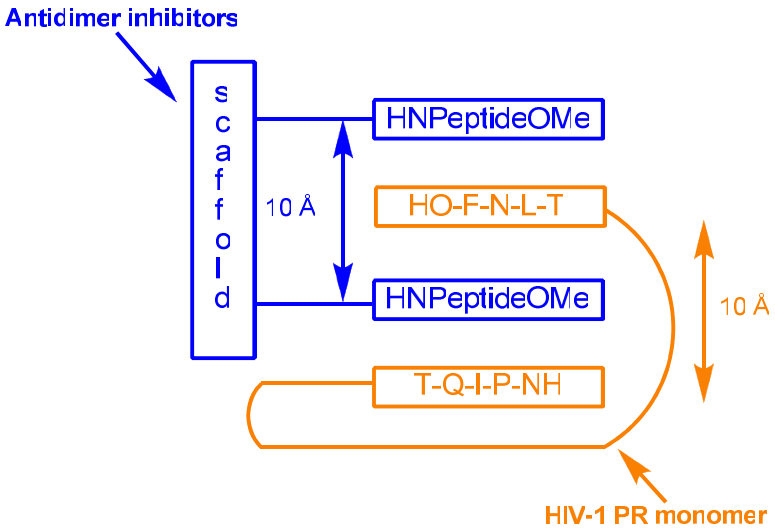

Figure III.12. Strategy of molecular tongs based on conformationally constrained scaffolds.

The amino acids of the molecular tongs that inhibited PR are believed to be involved in hydrogen bond interactions with the N- and C-terminal of one PR monomer, favoring the formation of a β-sheet structure and mimicking the 4-stranded β-sheet structure of the PR dimer (Figure III.13).

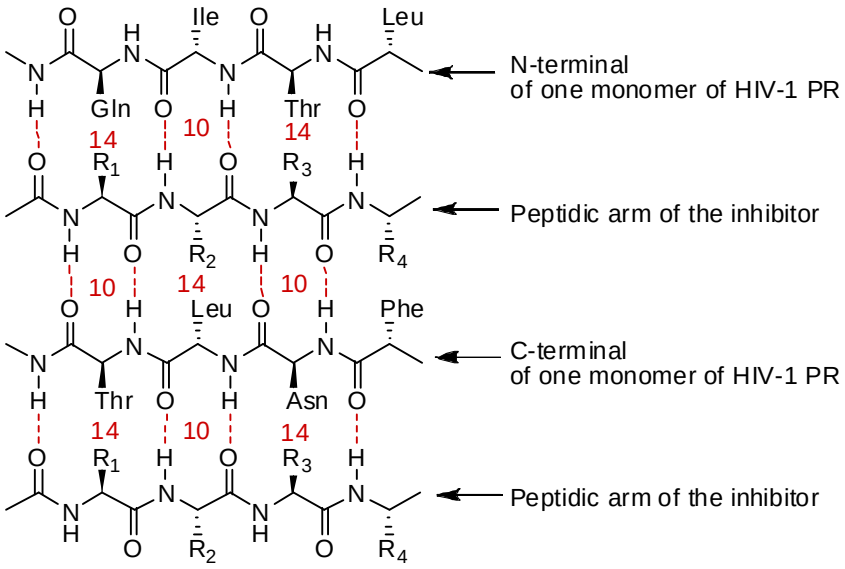

Figure III.13. Illustration of possible interactions (network of 10- and 14-membered H-bond rings) of two peptidic arms of our molecular tong with the N- and C-terminal residues of HIV-1 PR.

For the design of new rigid scaffolds by molecular modeling, crystallographic protease structure 8HVP, downloaded from the Protein Data Bank, was used.[45] One monomer and the TLNF and QITL strands of the other monomer were retained and different rigid scaffolds were bound to the TLNF and QITL strands. The tongs were built on the TLNF and QITL fragments in such a way that the minimization procedure of the obtained complexes converged easily (termination gradient of 0.5 kcal/mol Å). Four constrained scaffolds were designed based on resorcinol, 2,6-pyridinediol, 2,7- naphthalenediol and 2,7- quinolinediol on which carboxypropyl links were bound (Figure III.14).[45] The carboxypropyl links also allowed some flexibility which may be necessary during the complexation process with one monomer of HIV-1 PR.[45]

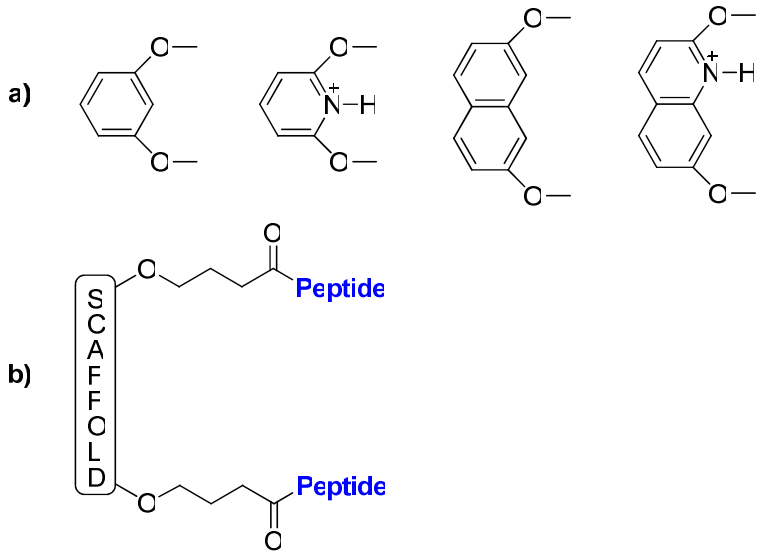

Figure III.14. a) Structures of the designed scaffolds for the molecular tongs and b) structures of the molecular tongs.

II.2.1. PEPTIDIC MOLECULAR TONGS

Two peptidic strands (dipeptide, tripeptide or tetrapeptide) were attached to the scaffold (Figure III.14b).[45] First symmetrical molecular tongs were evaluated,[45] secondly unsymmetrical molecular tongs bearing two different peptidic arms were synthesised and biologically evaluated.[46]

Table III.2 indicates the best results of inhibition of HIV-1 PR by the synthesised molecules within their limit of solubility in test medium (no inhibition was observed for all the resorcinol based tongs).

Table III.2. Biological result of molecular tongs (binding analysis used the Zhang[28] procedure, E* for *tert*-butyl ester of the glutamate).

MOLECULE	SCAFFOLD	PEPTIDE 1	PEPTIDE 2	K_{id} (mM)
170	pyridinediol	T-I-V-OMe	T-I-V-OMe	1.4
171	pyridinediol	T-L-N-F-OMe	T-L-N-F-OMe	10.0
172	pyridinediol	V-L-V-OMe	V-L-V-OMe	3.0
173	pyridinediol	Q-I-T-L-OMe	Q-I-T-L-OMe	ni
174	naphthalenediol	Q-I-T-L-OMe	Q-I-T-L-OMe	ni
175	naphthalenediol	T-L-N-F-OMe	T-L-N-F-OMe	1.0
176	naphthalenediol	V-L-V-OMe	V-L-V-OMe	0.56
177	quinolinediol	V-L-V-OMe	V-L-V-OMe	0.13
178	naphthalenediol	V-L-V-OMe	T-L-OMe	1.4
179	quinolinediol	V-L-V-OMe	T-L-OMe	1.5
180	naphthalenediol	V-L-V-OMe	I-T-NH_2	1.5
181	quinolinediol	V-L-V-OMe	I-T-NH_2	0.25
182	naphthalenediol	V-L-V-OMe	E*-L-NH_2	0.42
183	quinolinediol	V-L-V-OMe	E*-L-NH_2	0.53
184	naphthalenediol	V-L-V-OMe	E-L-NH_2	0.9
185	quinolinediol	V-L-V-OMe	E-L-NH_2	20% at 5.7 µM
186	quinolinediol	V-L-V-OMe	I-T-L- OMe	0.40
187	quinolinediol	V-L-V-OMe	T-L-N-OMe	0.08
188	naphthalenediol	V-L-V-OMe	Y-E*-L-NH_2	0.23
189	quinolinediol	V-L-V-OMe	Y-E*-L-NH_2	0.41

These results may be discussed as follows:

a) for molecular tongs 170-176[45] : the naphthalenediol- and pyridinediol-based scaffolds appear efficient to induce peptidic interface inhibition on PR, while the resorcinol-based scaffold appears inefficient. From a steric point of view, the necessary distance of 10 Å between the two peptidic strands of the tongs could be more easily reached by the naphthalenediol-based tongs than by the two other types of tongs. On the other hand, from an electronic point of view, only the pyridinediol-based tongs could form a favourable ionic interaction between the positively charged pyridine in the medium test and the negatively charged Phe-O^- 99 of the C-end of HIV-1 PR monomer. This argument is supported by the fact that scaffold pyridinediol•HCl had a pKa = 6.15 as measured potentiometrically. The assumption that steric effect and/or electronic effect are favourable for the tongs to induce inhibitory activity could explain why the resorcinol-based tongs were devoid of activity.

The peptidic sequence TLNF-OMe reproducing the internal C-terminal strands of the antiparallel β-sheet of HIV-1 PR led to the active tongs **171** and **175**, while the peptidic sequence QITL-OMe reproducing the external N-terminus β-sheet strand led to the inactive tongs **173** and **174**. These results are consistent with those described in the literature where the best inhibitions were observed with interfacial peptides reproducing the C-terminal strand.[28,32]

Surprisingly, the short peptidic sequence VLV-OMe appeared as the best sequence for inducing inhibitory potency (compounds **172** and **176**), although it did not reproduce the sequences involved in the natural antiparallel β-sheet of HIV-1 PR.[45]

b) for molecular tongs 177-189[46] : to improve the potency of this family of HIV-1 PR dimerization inhibitors, the structure of the scaffold was modified and also nonsymmetric tongs were introduced, consisting of two different peptidic strands attached to each scaffold.

Firstly, a quinoline-based scaffold was introduced, as quinoline contains structural requirements of both naphthalene and pyridine (Figure III.14).

Secondly, in order to easily establish a structure-activity relationship, it was decided to keep unchanged one of the two peptidic strands of these nonsymmetric tongs. According to the first results (molecular tongs **170-176**[45]), the peptidic strand P_1 was fixed as VLV-OMe for all compounds. The other peptidic strand P_2 varied in size (di- or tripeptide) and sequence. In one case P_2 was a part of the C-terminal TLNF strand of monomers of HIV-1 PR (**187**); in other cases it was a part of the N-terminal PQITL strand (**180**, **181** and **186**) of monomers. For compounds **178** and **179**, P_2 was fixed to TL-OMe which is a part of both C-terminal TLNF and N-terminal QITL strands of each monomer. The peptides EL and YEL and their *O*-protected glutamate analogues were introduced in compounds **182**-**185**, **188** and **189** are parts of the powerful dimerization inhibitor lipopeptide Pam-Y-E-L designed by Schramm.[34] Symmetric compounds **177** ($P_1 = P_2$ = VLV-OMe) based on the quinoline scaffold were also synthesised for comparison with symmetric tongs **176** based on the naphthalene scaffold.

FIRST CONCLUSIONS

- quinoline and naphthalene derivatives are valuable scaffolds and are superior to pyridine and resorcinol derivatives (Figure III.15);
- the attached tripeptidic strands induce generally better inhibitions than the dipeptidic and tetrapeptidic ones;
- the best peptidic sequence is Val-Leu-Val-OMe;
- hydrophobicity of the attached peptidic strands is a favourable property to induce inhibition (molecular tongs peptides EL, **184** and **185**, are less active than their *O*-protected glutamate analogues, **188** and **189**, respectively).

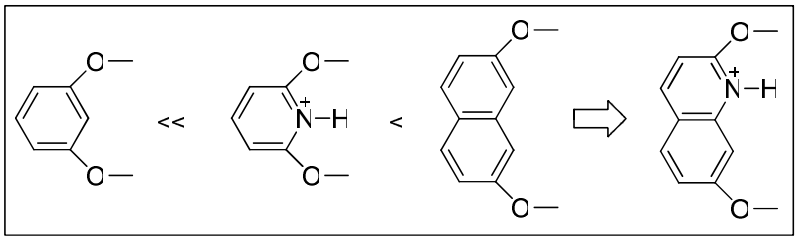

Figure III.15. Comparison of the rigid scaffolds.

II.2.2. MOLECULAR TONGS WITH ONE PEPTIDOMIMETIC ARM

Unsymmetrical molecular tongs containing amino acid mimetic fragments in one strand with the other peptidic strand being VLV-OMe (Figure III.16) were synthesised.[47] These new molecular tongs **190a–195a,b** were designed to have less peptidic character and consequently to be less susceptible to proteases *in vivo*. The peptidic character of a molecule can be decreased by replacing one or more amino acids with groups that mimic their hydrogen-bonding properties. The amino acids of the molecular tongs that inhibited PR are believed to be involved in hydrogen bond interactions with the N- and C-termini of one PR monomer, favouring the formation of a β-sheet structure and mimicking the 4-stranded β-sheet structure of the PR dimer (see Figure III.17). Consequently, the groups replacing amino acids should ideally provide the same array of H-bonding groups as one edge of a peptide β-strand. In literature, Nowick and Sanderson have introduced a 5-amino-2-methoxybenzoic hydrazide derivative[52-57] and a 3-amino-6-methylpyridin-2(1*H*)-one group,[58] respectively, to potentially form hydrogen bonds like those of amino acids. Consequently, our group has designed new molecular tongs with one peptidomimetic strand bearing a 5-amino-2-methoxybenzoic hydrazide derivative (**192a** and **193a,b**), a 5-nitro-2-methoxybenzoic hydrazide derivative (**194a,b**), a Sanderson motif (**190a** and **191a**) or a simplified version of this motif, where the methyl group was omitted (**195a,b**).[47]

Two cases were examined: first, the mimic unit was attached directly to the carboxypropyl link (molecules **190a**, **191a**, and **192a**, Figure III.16); second, it was linked through a Val residue (compounds **193a,b**, **194a,b** and **195a,b**, Figure III.16). The results of building several possible complexes using the Sybyl 7.0 molecular modelling tools indicated that forming the postulated β-sheet structure between the N- and C-terminal of one PR monomer and molecule **193a,b**, **194a,b** or molecule **195a,b** (Figure III.17) is energetically possible, since the correct array of alternating 10- and 14-membered H-bonded rings is still present after minimization. Conversely, no stable β-sheet structure was formed with molecules **190a**, **191a** and **192a**.[47]

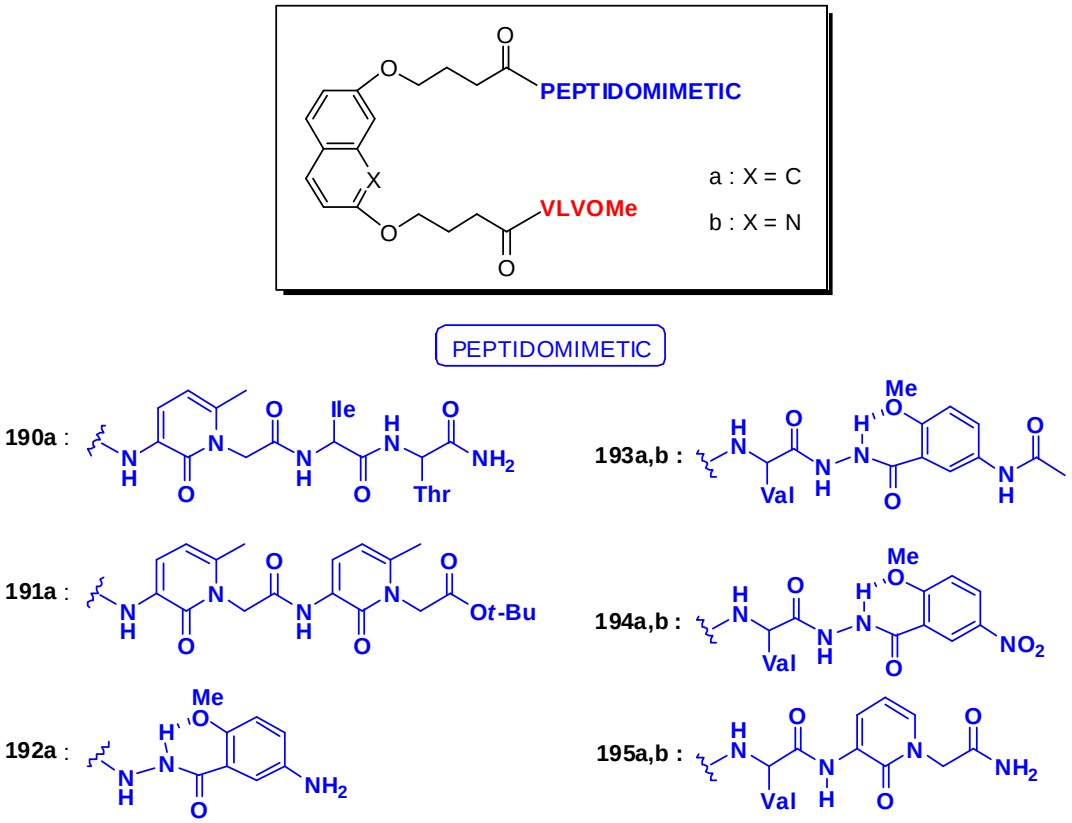

Figure III.16. Molecular tongs with one peptidomimetic arm.

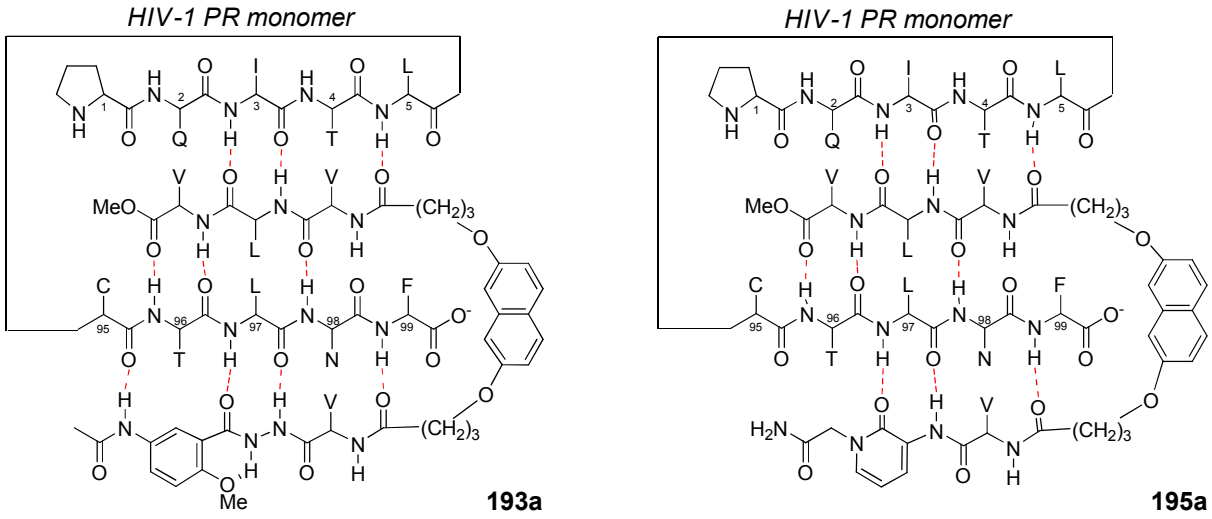

Figure III.17. Putative complexes between HIV-1 PR monomer and molecular tongs **193a** and **195a** based on molecular modeling.[47]

The inhibitory activities of compounds **190a–195a,b** were assayed against recombinant wild-type PR at pH 4.7 and 30 ℃ using a fluorometr ic assay. Compound **195a** was also assayed against six recombinant mutated proteases (Table III.3). The results are in

agreement with molecular modelling and no dimerization inhibition was observed for molecular tongs **190a**, **191a** and **192a**.[47]

Table III.3. Inhibition of wild-type and mutated HIV-1 PR by molecular tongs with one peptidomimetic arm ([a]mutations in the active site showed in bold, [b]competitive active-site inhibition, [c]dimerization inhibition, [d]unpublished results).

COMPOUND	WILD-TYPE (WT) OR MUTATED PROTEASES[a]	K_{ic} (μM)[b]	K_{id} (μM)[c]
190a[47]		9.7	
191a[47]		8.4	
192a[47]		28 % inhibition at 5 μM	
193a[47]	WT		0.2
193b[d]	WT		0.2
194a[d]	WT	30 % inhibition at 1 μM	
194b[d]	WT		0.4
195a[47]	WT		0.4
195a[47]	**D30N**		0.5
195a[47]	**I50V**		0.1
195a[47]	**V82A**		0.24
195a[47]	**G48V**/L90M		0.5
195a[47]	**MDR-HN**		4.8
195a[47]	**ANAM-11**		0.2
195b[d]	WT	30 % inhibition at 2.8 μM	

For the molecular tongs **193a,b**, **194a,b** and **195a,b** the results indicate that replacing the tripeptide VLV (compound **176**) with a peptidomimetic strand composed of a valine residue linked to the Nowick motif (compounds **193a,b** and **194b**) or to the demethylated Sanderson motif (compound **195a**) results in antidimer inhibitors that are still fully active against wild-type PR (K_{id} = 0.2 μM for **193a,b**; K_{id} = 0.4 μM for **194b**; K_{id} = 0.4 μM for **195a**, compared to K_{id} = 0.56 μM for **176**). Thus, the Nowick and demethylated Sanderson peptidomimetic units can be used to replace amino acids in the structures of the previously described molecular tongs. The results are in agreement with molecular modelling, indicating that the antidimer property depends on the position of the mimic unit in the peptidomimetic strand. It was also suggested that the flexibility of valine is required for the formation of the H-bonds in a 4-stranded antiparallel β-sheet, implicating the N- and C-terminal of the PR monomer.[47]

One of these dimerization inhibitors **195a** was also evaluated against proteases with 1, 2, 6, and 11 point mutations; and it was as active (and in some cases more active) on mutated proteases as on wild-type PR. For example, the affinity of ANAM-11 protease for compound **195a** was 2-fold greater (K_{id} = 200 nM) than that of wild-type PR (K_{id} = 400 nM). In contrast, the affinities of this mutated protease for indinavir, nelfinavir, saquinavir, and ritonavir were about 2030, 2840, 4200, and 78 000 times lower than that of wild-type PR.[59] This demonstrates that the peptidomimetic molecular tong **195a** still acts as an efficient inhibitor of the dimerization of mutated proteases.[47] This result confirmed the hypothesis suggesting that inhibitors of dimerization are poorly sensitive to mutations.

Finally, the stability of the peptide (**176**) and peptidomimetic (**193a** and **195a**) molecular tongs in RPMI culture medium containing 20% fetal calf serum was studied. The half-life of compound **176** was about 28 h and that of **195a** about 41 h; no significant degradation of compound **193a** was observed after 33 h of incubation. The results suggest that the metabolic stability has been improved by inserting peptidomimetics into one arm of the molecular tongs.[47]

II.2.3. MOLECULAR TONGS WITH TWO PEPTIDOMIMETIC ARMS

Molecular tongs discussed in this section were synthesised by Anamaria Vidu.[i] In order to establish the superiority or inferiority of the unsymmetrical molecular tongs (**193a** and **195a**) over inhibitors with two identical peptidomimetic strands, we decided to synthesise the symmetric molecular tongs **196** and **197**, containing a valine residue linked to the 5-amino-2-methoxybenzoic hydrazide derivative and the demethylated Sanderson group, respectively (Figure III.18). Evaluation of these molecular tongs against HIV-1 PR showed that they behaved as mixed inhibitors (K_{ic} = 0.2 µM and K_{id} = 0.029 µM for **196**; and K_{ic} = 0.4 µM and K_{id} = 0.15 µM for **197**).

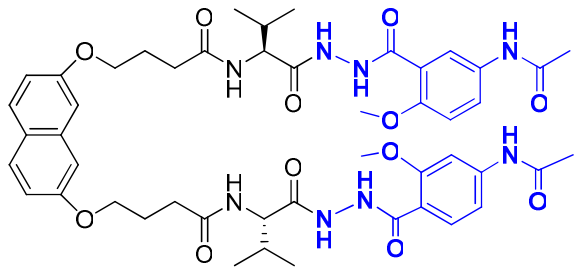

196

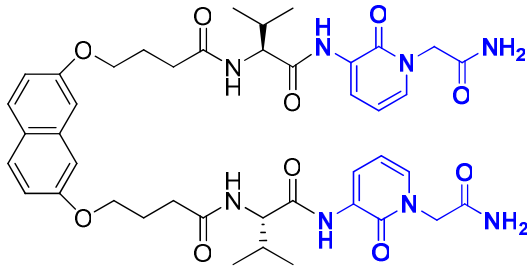

197

Figure III.18. Molecular tongs with two peptidomimetic arms.

[i] Unpublished results.

II.2.3.1. INTRODUCTION OF A POLAR AMINO ACID: LYSINE

In order to increase the solubility of our molecular tongs, specially solubility in mediums compatible with biological evaluation, it was decided to replace the valine residue in the peptidomimetic arms, by a lysine residue.

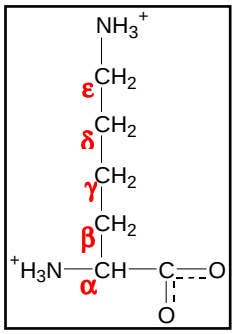

Figure III.19. Chemical structure of lysine.

Lysine was chosen because it has a positively charged ε-amino group in physiological conditions which promotes solubility. However, since the side chain has three methylene groups, even though the terminal amino group will be charged under physiological conditions, the side chain does have significant hydrophobic character.

Lysine has already been used in β-sheet peptidomimetics, in order to increase the solubility without destabilizing the secondary structure.[60]

Two new peptidomimetic arms were then synthesised containing the lysine residue linked to the 5-amino-2-methoxybenzoic hydrazide derivative (**198**) and the 3-amino pyridin-2-one derivative (**201**). After deprotection of the NHα of both peptidomimetic fragments, the new arms were then attached to naphthalene scaffold affording molecular tongs **199** and **202**, respectively. Finally, deprotection of the NHε gave rise to the deprotected molecular tongs **200** and **203**, respectively (Figure III.20).

Evaluation of molecular tongs **199** and **202** against HIV-1 PR showed that they are also mixed inhibitors (K_{ic} = 0.15 μM and K_{id} = 0.053 μM for **199**; and K_{ic} = 0.2 μM and K_{id} = 0.12 μM for **202**). Comparison of the mixed inhibitors **196** *vs* **197** and **199** *vs* **202**, show that the ones containing the 5-amino-2-methoxybenzoic hydrazide derivative (**196** and **199**) are better than the ones containing the 3-amino pyridin-2-one derivative (**197** and **202**).

On the other hand, the deprotected molecular tongs **200** and **203** show much less activity (30% inhibition at 14 μM and 28% inhibition at 12 μM, respectively) than the respective protected analogues **199** and **202**.

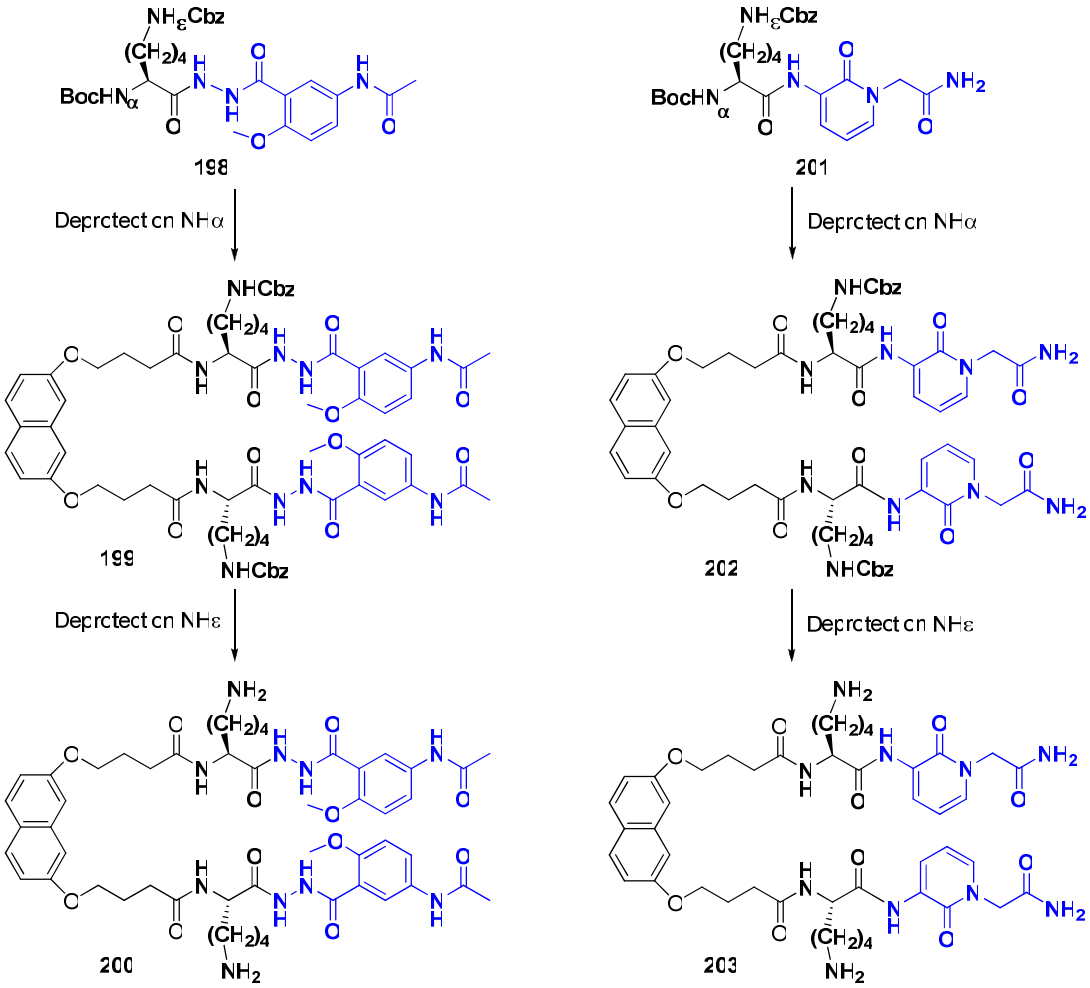

Figure III.20. Symmetrical molecular tongs bearing a lysine residue (I).

II.2.3.2 LOSING TOTALLY THE PEPTIDIC CHARACTER

As was shown before the peptidomimetic fragments are linked to the scaffold through the lysine unit. The presence of the two amino groups of lysine (α-amino group and ε-amino group), gives us the possibility of designing other molecular tongs (Figure III.21).

In fact the peptidic character of the molecular tongs may be totally lost if the linkage to the scaffold is done through the ε-amino group of the lysine residue of peptidomimetic fragment **198** and **201** (Figure III.21), giving rise to molecular tongs **204** and **206**, respectively. Consequently, it is possible to study the influence of the introduction of a totally non-peptidic arm as well as the influence of supplementary flexibility. Finally, deprotection of the NHα gave rise to the deprotected molecular tongs **205** and **207**, respectively (Figure III.21).

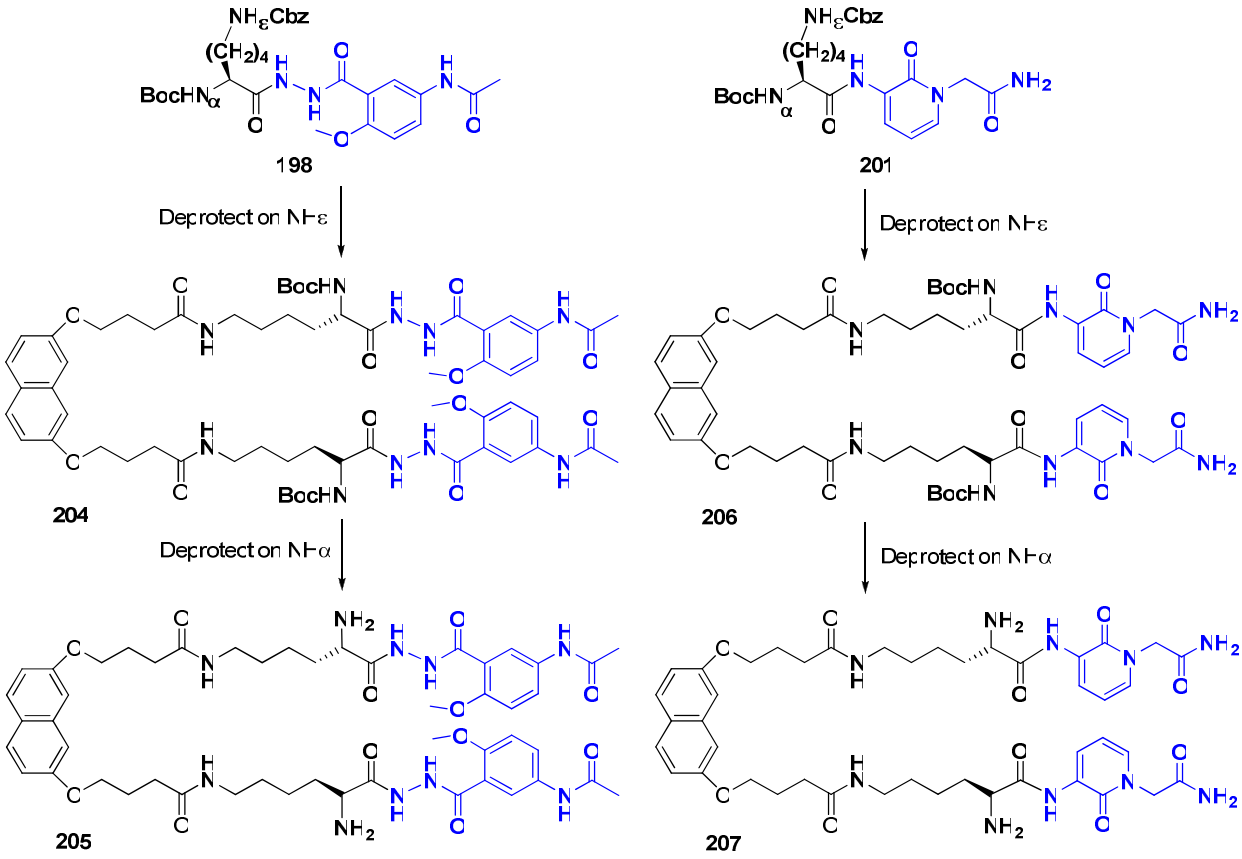

Figure III.21. Symmetrical molecular tongs bearing a lysine residue (II).

Evaluation of the totally peptidomimetic molecular tongs against HIV-1 PR showed that tong **204** is a pure antidimer inhibitor (K_{id} = 0.28 μM), while tong **206**, bearing the 3-amino pyridin-2-one derivative, is only a poor inhibitor of the active site (K_{ic} = 15.5 μM). We could once again note the superiority of the 5-amino-2-methoxybenzoic hydrazide derivative over the demethylated Sanderson motif. The deprotected molecular tongs **205** and **207** show much less activity (30% inhibition at 28 μM, in both cases) than the respective protected analogues **204** and **206**.

The good result obtained with molecular tong **204** demonstrated that is possible to completely suppress the peptidic character without compromising the activity. On the other hand, increasing the polarity of the molecular tong arms has proven to be a much harder task, as by deprotecting the lysine amino group we lose activity without sufficiently improving the molecular tongs solubility.

II.3. CONCEPTION OF OUR MOLECULES

The contribution of our laboratory to the antidimer strategy has been the synthesis of molecular tongs based on a conformationally constrained scaffold, in which peptidic[45,46] or peptidomimetic arms,[47] were attached through a carboxypropyl link.

Despite the good activity demonstrated *in vitro*, all attempts to test the molecular tongs in cell failed due to the lack of solubility in the biological medium.

Consequently, we are now concerned in decreasing the peptidic character of the molecular tongs and increasing their hydrosolubility. For that we have conceived two different strategies: **i)** the introduction of hydrophilic groups in the scaffold and **ii)** the synthesis of new peptidomimetic arms with increased hydrophilicity.

The final aim will be the evaluation of the antiviral efficacy of the new compounds in cell culture assays, as well as, their bioavailability.

CONCERNING THE RIGID SPACER

Previous work in our laboratory showed that both the naphthalenediol and the quinolinediol were suitable rigid spacers, meaning that they were able to impose the distance of 10 Å between the two peptidic or peptidomimetic arms of the molecular tongs.

Since comparable K_{id} values were obtained for both naphthalene- and quinoline-based molecular tongs (Table III.2, page 115 and Table III.3, page 119), we have decided to continue working with the naphthalene scaffold because the synthesis of the corresponding molecular tongs is shorter and easier.

Moreover the naphthalene scaffold is also a suitable candidate for the introduction of hydrophilic groups, affording spacers with increased polarity.

PEPTIDIC ARM

Previous studies have also demonstrated that the peptidic sequence Val-Leu-Val-OMe led to the best dimerization inhibitor, and for that reason we have decided to keep this sequence as the peptidic arm in the synthesis of unsymmetrical molecular tongs.

PEPTIDOMIMETIC ARM

Concerning the peptidomimetic arms, our group demonstrated in previous studies, that it was possible to keep the valine residue and to replace the other two amino acids of the arm by the 5-amino-2-methoxybenzoic hydrazide derivative, which mimics a dipeptide. Later on, it was demonstrated that the valine residue could also be replaced by a amino acid (*e.g.*

lysine), affording a new peptidomimetic arm without peptidic character. We have decided to continue working with these two peptidomimetic arms (Figure III.22).

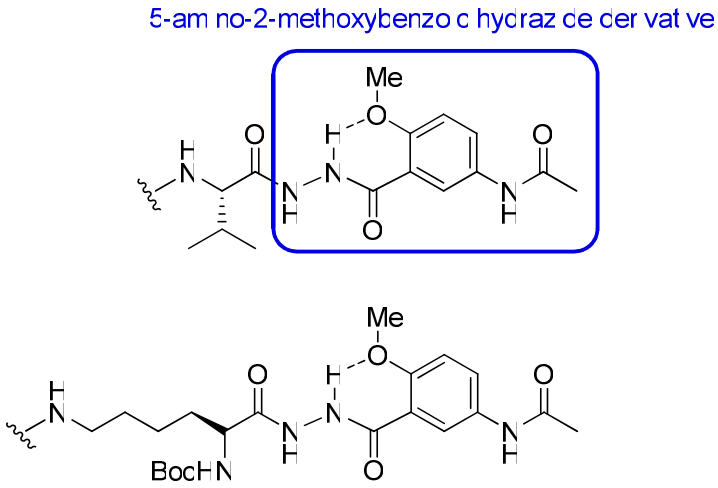

Figure III.22. Peptidomimetic arms bearing the 5-amino-2-methoxybenzoic hydrazide derivative.

II.3.1. INTRODUCTION OF A POLAR FRAGMENT TO THE SCAFFOLD

The first strategy designed to increase the solubility of our molecular tongs is based on the synthesis of new hydrophilic scaffolds. The simplest way to accomplish this purpose relies on the introduction of hydrophilic groups in the naphthalene scaffold. Meaning that it is possible to maintain the steric benefit of this scaffold and to individually study the influence of a hydrophilic group on it.

The hydrophilic group can be introduced through an amination reaction, either using:

1) *"Ullmann-type" Reaction*: involving a copper-catalyzed nucleophilic aromatic substitution between different nucleophiles with aryl halides;

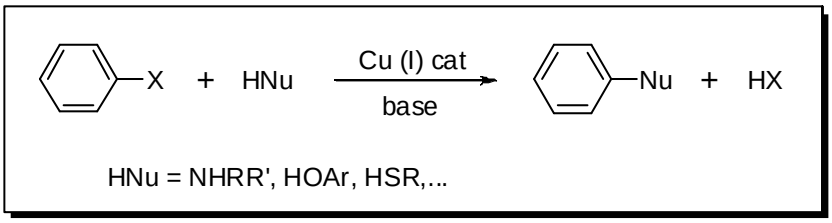

or **2)** *Buchwald-Hartwig Cross Coupling Reaction:* meaning, palladium-catalyzed synthesis of aryl amines. Starting materials are normally aryl halides and primary or secondary amines.

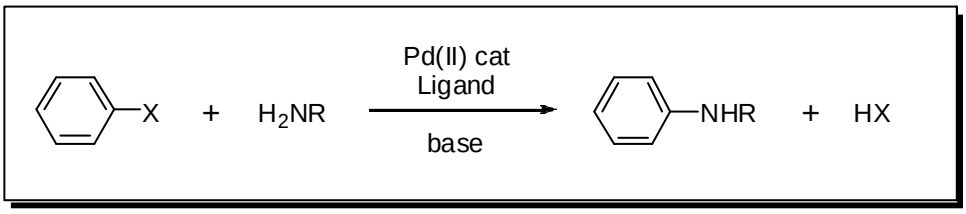

Using one of the two strategies, different polar groups (like: amino propanediol, amino acids, primary amines) will be introduced in the naphthalene scaffold, to afford polar scaffolds of general formula **208**.

In order to establish the superiority or inferiority of the symmetrical molecular tongs containing the naphthalene scaffold (**196** and **204**) over inhibitors with a modified naphthalene scaffold, the new scaffolds will be attached to peptidomimetic arms bearing the 5-amino-2-methoxybenzoic hydrazide derivative (Figure III.22), affording molecular tongs of general formula **209**.

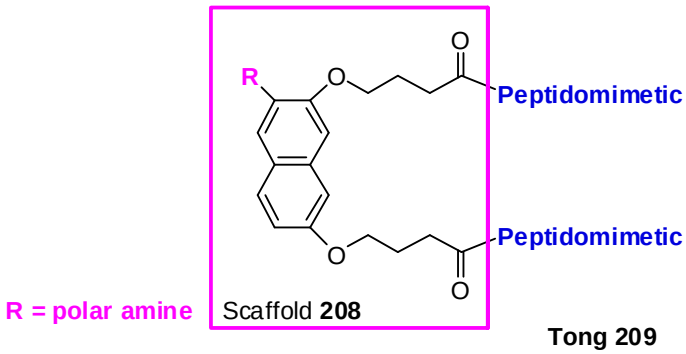

Figure III.23. Molecular tongs with modified naphthalene scaffold.

II.3.2. INTRODUCTION OF A NEW HYDROPHILIC PEPTIDOMIMETIC ARM

The second strategy designed to increase the solubility of our molecular tongs is based on the introduction of new peptidomimetic motifs with increased hydrophilicity.

It was then necessary to search peptidomimetics compatible with our concept of antiparallel β-sheets. Ideally, suitable candidates should have low molecular weight, and should be able to provide the same array of hydrogen-bonding groups, as one edge of a peptidic β-strand.

As was largely discussed in Chapter I (Section III.3, page 17 and Section III.4, page 20) several groups have developed peptidomimetics that were successfully applied in chemical models of β-strands, β-hairpins and β-sheets. These systems, able to mimic the alternating array of hydrogen-bond donors and acceptors of a peptide in a β-strand conformation, inspired Li and co-workers, to design and synthesise a new class of highly stable hydrazide-based heterodimers[61-63] ADDA-DAAD (A = hydrogen-bond acceptor, D = hydrogen-bond donor), that were successful used in the self-assembly of hydrogen bond-mediated supramolecular systems with well-established structures (Figure III.24).

The new type of quadruply hydrogen-bonded heterodimers **210** involved the combination of two different series of hydrazide derivatives (I and II, Figure III.24). The hydrogen-bonding components, meaning the C-O and NH units in both series, were designed to be arranged as closely as possible to reduce the influence of structural flexibility.

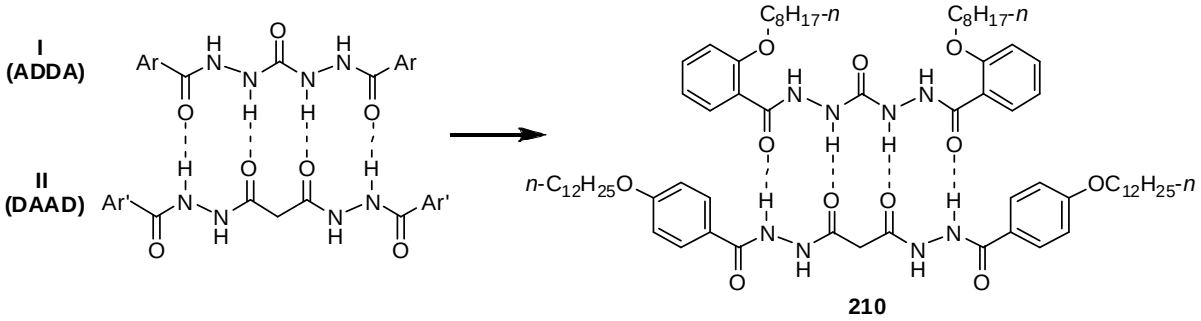

210

Figure III.24. New generation of hydrazide-based quadruply hydrogen-bonded heterodimers.

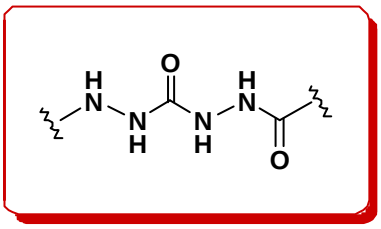

Figure III.25. Hydrazide-based motif to incorporate in new peptidomimetic arms.

With the help of molecular modelling (Figure III.27) we have designed a new peptidomimetic arm **211**, containing the dihydrazide motif of the ADDA monomer (Figure III.25) and a valine residue. This new peptidomimetic arm was then incorporated in the unsymmetrical molecular tong **212** (Figure III.26) and the symmetrical molecular tong **213** (Figure III.26).

This new hydrazide-based motif should increase the hydrophilicity of the molecular tongs, decrease their molecular weight and hopefully stabilize the β-sheet formed between the molecular tong and the homodimer of the HIV-1 PR.

Later on, in order to completely suppress the peptidic character of the new hydrazide-based peptidomimetic arm the valine residue was replace by a β-amino acid and an amine.

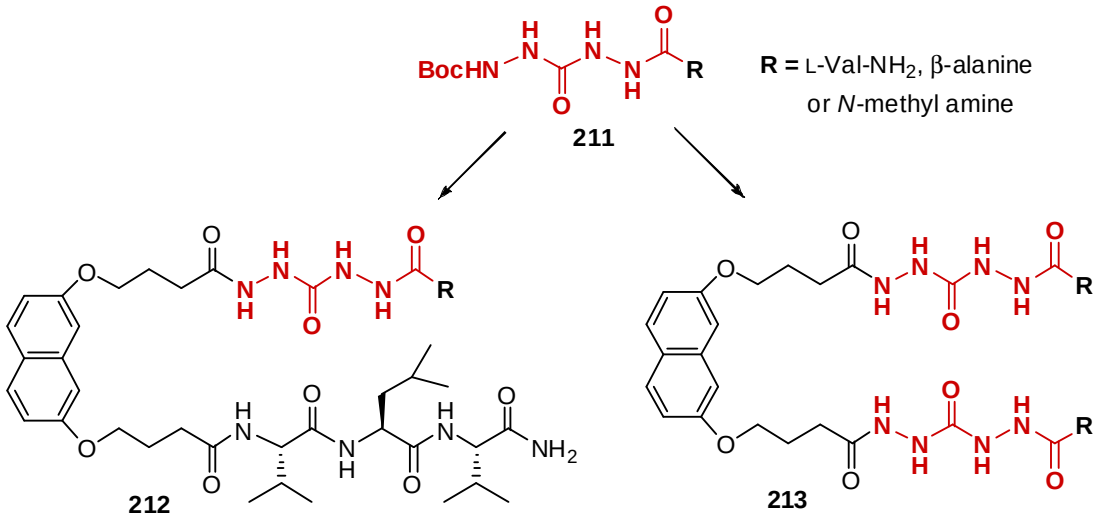

Figure III.26. Unsymmetrical and symmetrical hydrazide-based molecular tongs.

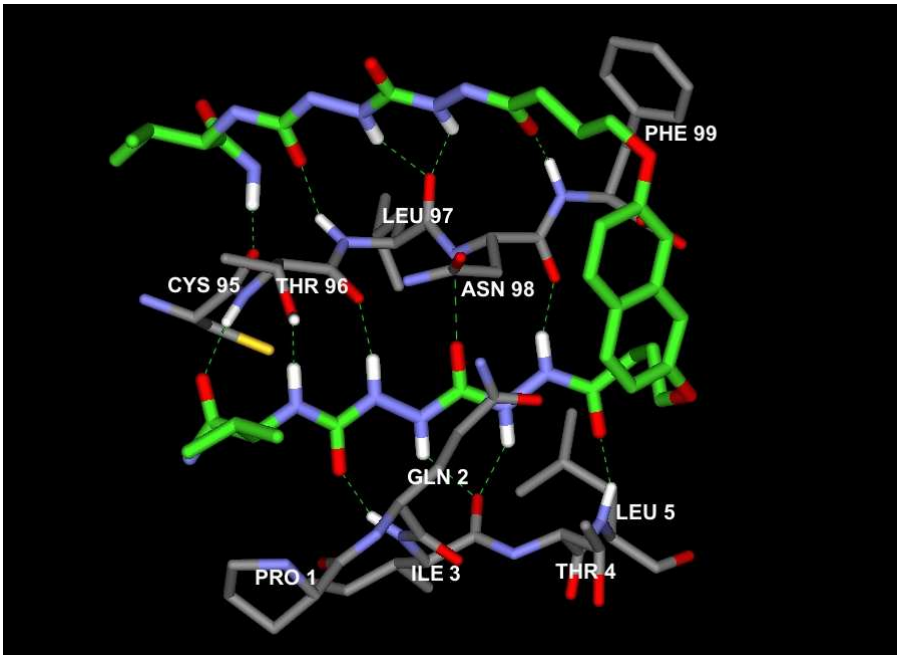

Figure III.27. Overview of interactions between hydrazine-based molecular tong with R = L-Val-NH_2 (showed in green) and the C- and N-terminal of HIV-1 protease monomer (showed in grey). O and N atoms are shown in red and blue, respectively. Hydrogen bonds are indicated with dotted lines.

II.4. SYNTHESIS OF THE TARGET MOLECULES

II.4.1. SYNTHESIS OF THE POLAR SCAFFOLDS

The synthetic procedure designed to obtain the modified naphthalene scaffolds relies on the initial introduction of a halogen (in this case, Br) in position 3 of the 2,7-dihydroxynaphthalene, that could later be substituted by an amine.

Bromination of 2,7-dihydroxynaphthalene gave rise to a mixture of two dibromo derivatives (1,3- and 1,6-isomers), which was initially reduced with β-naphthol and hydrobromic acid in acetic acid.[64] However this procedure led to rather complex crude mixtures and therefore it was complicated, if not impossible, to purify the desired product.

Alternatively, 2,7-dihydroxynaphthalene was brominated as described before giving rise to the mixture of 1,3- and 1,6-dibromo derivatives which, by *in situ* hydrogenolysis of the Br–C(1) bond using Sn powder,[65] afforded the desired 3-bromonaphthalene-2,7-diol **214**, in excellent yield (94%). Compound **214** was then alkylated with benzyl 4-bromobutyrate, to afford the dibenzyl ester **215**, in 89% yield (Scheme III.1).

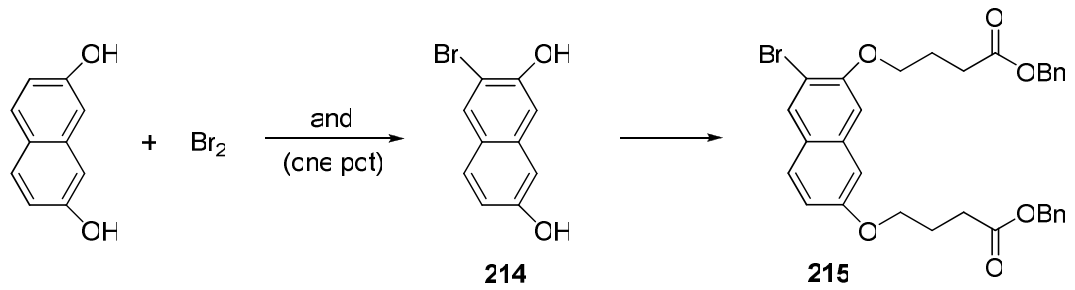

Scheme III.1. i) Br_2, CH_3COOH followed by ii) Sn powder, H_2O: 93%; iii) $Br(CH_2)_3COOBn$, K_2CO_3, DMF: 89%.

Initially, we have decided to couple aryl halide **215** to a primary amine bearing an 2,2-dimethyl-1,3-dioxolane methyl group, which would be the precursor of the polar fragment (respectively, an amino propanediol group).

Nucleophilic aromatic substitution of aryl halide **215** was initially tried using a copper catalyst in presence of base, Ullmann condensation reaction,[66] without (Table III.4, entry 1) or with the presence of a ligand (Table III.4, entries 2-6).

As it is summarised in Table III.4, no substitution is observed without the presence of a ligand (entry 1), however the introduction of L-proline[67,68] as a promoter (entries 2 and 3) was not successful, resulting in complex crude mixtures. Finally, we have decided to use a bidentate ligand[69,70] (entries 4-6), that afforded the desired substituted product but in low

yields. The conditions that afforded the best result are indicated in entry 5: DMEDA (10 equiv), K_2CO_3 (2 equiv) in dioxane at 110 ºC for 24 h, afforded product **216** in 25% yield.

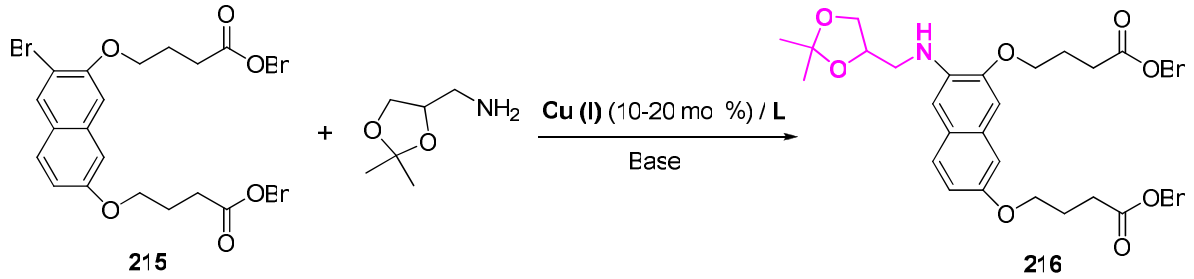

Table III.4. Ullmann-type conditions tried in the amination reaction of **215**.

ENTRY	Cu SOURCE	LIGAND (MOL %)	BASE (EQUIV)	SOLVENT	TEMP.	RX TIME	RESULT
1	CuI	—	K_2CO_3 (3)	DMSO	135 ℃	48 h	SM
2	CuI	Proline (40)	K_2CO_3 (3)	DMSO	135 ℃	48 h	DP
3	CuI	Proline (20)	K_2CO_3 (2)	DMSO	110 ℃	24 h	DP
4	CuI	DMEDA (10)	K_2CO_3 (2)	Dioxane	75 ℃	24 h	SM
5	**CuI**	**DMEDA (10)**	**K_2CO_3 (2)**	**Dioxane**	**110 °C**	**24 h**	**25%[a] (+SM)**
6	CuI	DMEDA (20)	K_2CO_3 (2)	Dioxane	125 ℃	24 h	8% [a] (SM + DP)

[a] Yield of pure isolated compound. Abbreviations used in the table: SM = Starting Material, DP = Degradation products.

As an alternative to the copper-catalyzed reaction, we decided to try the Buchwald-Hartwig reaction,[71,72] in which C(sp^2)-N bond formation is palladium-catalyzed, in presence of a ligand and a base.

Table III.2 summarizes the different conditions tried, always using the bidentate ligand: 9,9-dimethyl-4,5-bis(diphenylphosphino)-xanthene (Xantphos, Figure III.28).[73,74] The best result (entry 4) was obtained using Pd (II) acetate as catalyst and potassium carbonate as base, in dry dioxane. It was observed that the reaction is only complete when a large excess of base is used (20 equiv), the same observation had been already reported by others.[75,76] On the other hand, the use of strong bases (*e.g.*, sodium *tert*-butoxide[71] – entry 6) led mainly to degradation and only traces of the desired substituted product.

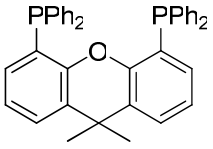

Figure III.28. Xantphos structure.

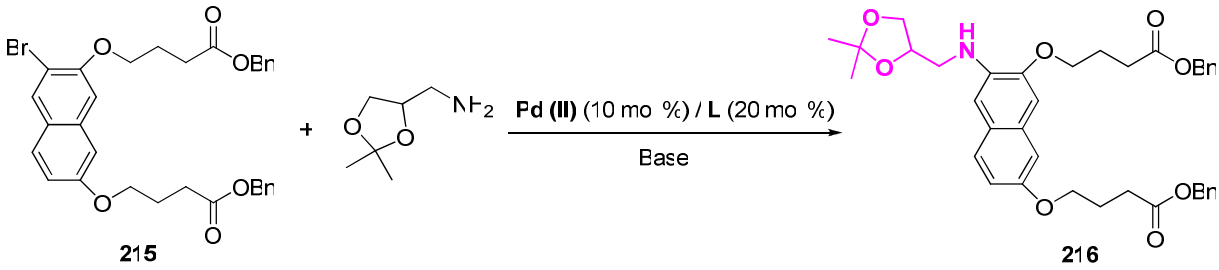

Table III.5. Buchwald-Hartwig conditions tried in the amination reaction of **215**.

ENTRY	Pd SOURCE	LIGAND	BASE (EQUIV)	SOLVENT	TEMP.	RX TIME	RESULT[a]
1	$Pd(OAc)_2$	Xantphos	K_2CO_3 (5)	Dioxane	110 °C	15 h	27%
2	$Pd(OAc)_2$	Xantphos	K_2CO_3 (10)	Dioxane	110 °C	15 h	66%
3	$Pd(OAc)_2$	Xantphos	K_2CO_3 (15)	Dioxane	110 °C	15 h	67%
4	**$Pd(OAc)_2$**	**Xantphos**	**K_2CO_3 (20)**	**Dioxane**	**110 °C**	**15 h**	**70%**
5	$Pd(OAc)_2$	Xantphos	Cs_2CO_3 (20)	Dioxane	110 °C	15 h	51%
6	$Pd(OAc)_2$	Xantphos	NaO*t*-Bu (2)	Dioxane	110 °C	15 h	4%[b]
7	$Pd_2(dba)_3$	Xantphos	K_2CO_3 (20)	Dioxane	110 °C	15 h	50%

[a] Yield of pure isolated compound, [b] the reaction led mainly to degradation products.

Using entry 4 conditions, other amines were coupled to aryl halide **215**. For example, coupling of HCl•H-Gly-OEt afforded compound **217**, bearing an amino ester functionality, precursor of an amino acid group (Scheme III.2).

Arylamine **219** was obtained by initial coupling of benzophenone imine to scaffold **215**, affording intermediate **218** that was subsequently reduced with hydroxylamine in methanol, in presence of sodium acetate,[77] to afford primary amine **219**. Terminal amine in the new scaffold **219** can then be used to incorporate different functional groups (*e.g.* water-soluble groups).[78] All attempts to obtain the *N*-alkylated product **220**, using an excess of bromoacetic acid *tert*-butyl ester in presence of DIPEA,[78] met with no success (Scheme III.2).

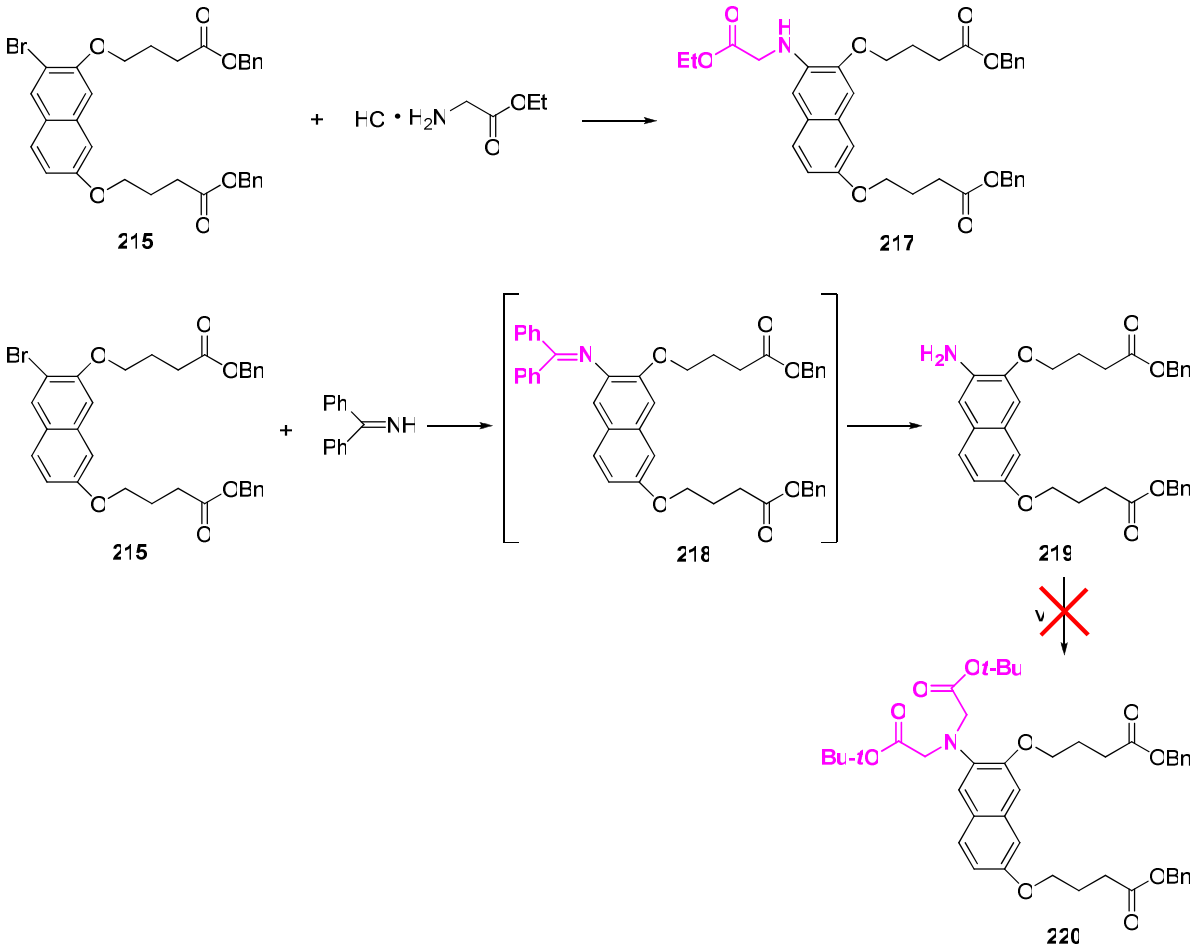

Scheme III.2. i) $Pd(OAc)_2$, Xantphos, K_2CO_3, dioxane: 76%; ii) $Pd(OAc)_2$, Xantphos, K_2CO_3, dioxane, and iii) HCl•NH_2OH, $NaOAc•3H_2O$, MeOH: 62% over two steps; iv) $BrCH_2COO$*t*-Bu, NaI, DIPEA, AcCN.

II.4.2. SYNTHESIS OF THE MOLECULAR TONGS ARMS

II.4.2.1. SYNTHESIS OF THE PEPTIDIC ARM VLV-OME

The peptidic arm VLVOMe was synthesised by solution layer synthesis (Boc strategy) starting from the C-terminus (Scheme III.3).

Boc-L-Leu-OH was condensed with HCl•H-L-Val-OMe using isobutyl chloroformate as condensing agent in CH_2Cl_2, in presence of NMM, to afford the dipeptide **221**. The N-terminus of the dipeptide **221** was deprotected using a solution of HCl in methanol (6 N), and the corresponding hydrochloride salt was then coupled with Cbz-L-Val-OH, using HBTU/HOBt in DMF, in presence of DIPEA, giving rise to the protected tripeptide **222**.

Finally, catalytic hydrogenolysis of the tripeptide **222** in methanol, in presence of HCl (6 N), afforded VLV-OMe **223** as a stable salt. All the yields of coupling and deprotecting reactions were satisfactory (Scheme III.3).

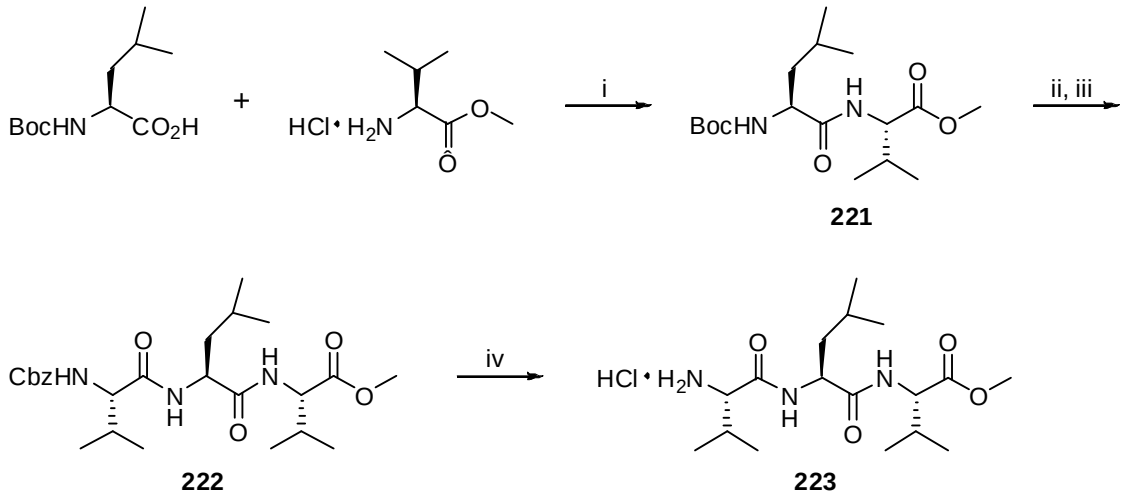

Scheme III.3. Synthesis of peptidic arm VLVOMe: i) $(CH_3)_2CHCH_2OCOCl$, NMM, CH_2Cl_2: 68%; ii) methanolic HCl and iii) Cbz-L-Val-OH, HBTU, HOBt, DIPEA, DMF: 64% over two steps; iv) H_2, Pd/C, methanolic HCl, MeOH: quantitative yield.

II.4.2.2. SYNTHESIS OF 5-AMINO-2-METHOXYBENZOIC HYDRAZIDE DERIVATIVES

The peptidomimetics strands, bearing the 5-amino-2-methoxybenzoic hydrazide derivative, were obtained starting from commercially available 2-methoxybenzoic acid, following procedures described in our laboratory.[47] The 2-methoxybenzoic acid was initially nitrated to give compound **224**, and successively coupled with *tert*-butyl carbazate affording **225**. The nitro group of **225** was then reduced, through catalytic hydrogenation, to afford the Boc-protected 5-amino-2-methoxybenzoic hydrazide **226**, described in the literature by Nowick.[55]

Compound **226** was then acetylated to afford **227**. After Boc deprotection with TFA in CH_2Cl_2 of hydrazide **227**, coupling of either Boc-L-Val-OH or *N*α-Boc-*N*ε-Cbz-L-Lys-OH, afforded protected peptidomimetic arms **228** and **198**, respectively (Scheme III.4).

A final Boc deprotection of **228** afforded the peptidomimetic arm **229** in the form of TFA salt, ready to be coupled to the desired scaffold. On the other hand, cleavage of the Cbz group through catalytic hydrogenolysis, afforded the *N*ε-deprotected peptidomimetic arm **230,** ready to be coupled to the desired scaffold.

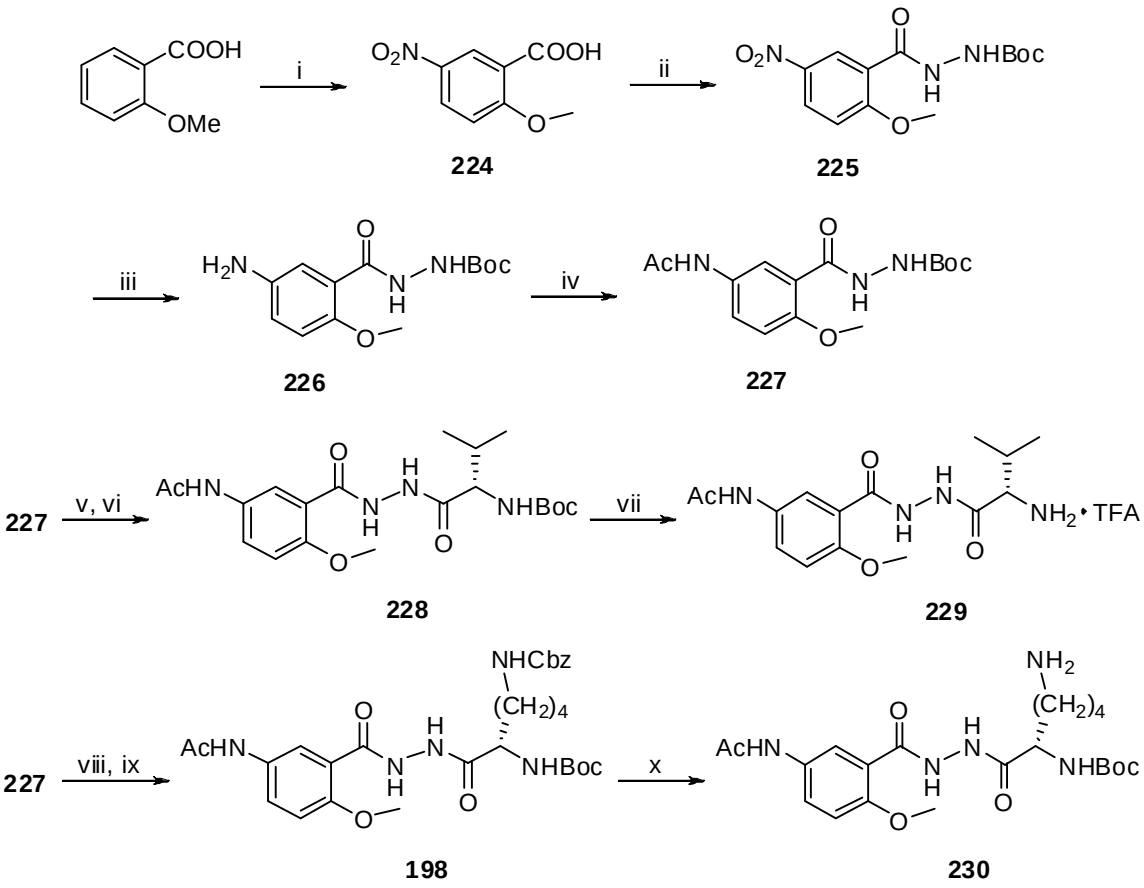

Scheme III.4. Synthesis of peptidomimetic arm containing the 5-amino-2-methoxybenzoic hydrazide derivative: i) NH_4NO_3, H_2SO_4: 80%; ii) $BocNHNH_2$, HOBt, EDC•HCl, CH_2Cl_2: 85%; iii) H_2, Pd/C, MeOH: 95%; iv) Ac_2O, THF: quantitative yield; v) TFA/CH_2Cl_2 (1:1, v/v) and vi) Boc-L-Val-OH, HBTU, HOBt, DIPEA, DMF: 68% over two steps; vii) TFA/CH_2Cl_2 (1:1, v/v): 83%; viii) TFA/CH_2Cl_2 (1:1, v/v) and ix) *N*α-Boc-*N*ε-Cbz-L-Lys-OH, HBTU, HOBt, DIPEA, DMF: 73% over two steps; x) H_2, Pd/C, MeOH: 96%.

II.4.2.3. SYNTHESIS OF HYDRAZIDE-BASED PEPTIDOMIMETIC ARMS

The synthetic procedure designed to obtain the new peptidomimetic arm involves the synthesis of a dihydrazide motif that will be common to all hydrazide-based arms (Scheme III.5). Thus, compound **231** was first prepared from the reaction of commercially available compounds *tert*-butyl carbazate and phenyl chloroformate in dichloromethane, in presence of pyridine.[79] Treatment of **231** with hydrazine hydrate afforded intermediate **232** in 72% yield.[63] Compound **232** was then treated with phenyl chloroformate in THF, in presence of pyridine, to afford the common dihydrazide motif **233**, in good yield (91%).

Initial tries to couple the dihydrazide motif with HCl•H-L-Val-OMe met with no success. Instead of desired linear compound **234**, the major product isolated from the reaction was the cyclic compound **235** (6-membered ring formation).

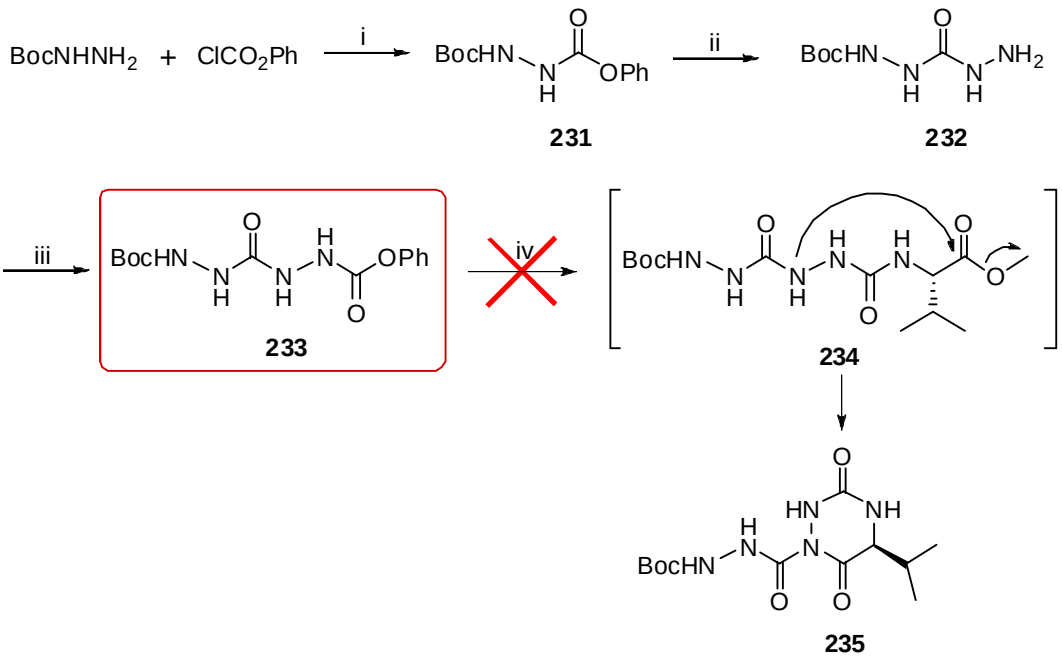

Scheme III.5. i) $ClCO_2Ph$, pyridine, CH_2Cl_2: 97%; ii) $H_2NNH_2 \bullet H_2O$, MeOH: 72%; iii) $ClCO_2Ph$, pyridine, THF: 91%; iv) HCl•H-L-Val-OMe, Et_3N, AcCN: 55%.

In order to avoid intramolecular aminolysis we decided to use a valine residue presenting the carboxylic group protected as an amide (instead of ester). Compound **233** was then coupled with HCl•H-L-Val-NH_2 giving rise to the Boc-protected peptidomimetic arm **236** in good yield (93%). A final Boc deprotection of **236** afforded the new peptidomimetic arm **237** in the form of TFA salt, ready to be coupled to the naphthalene scaffold (Scheme III.6.).

In order to completely suppress the peptidic character of the new polar arms, the valine residue was after substituted by methyl amine and β-alanine methyl ester, to afford Boc-protected peptidomimetic arms **238** and **240**, respectively. In both cases, a final Boc deprotection afforded the new peptidomimetic arms **239** and **241**, respectively, in the form of TFA salt, ready to be coupled to the naphthalene scaffold (Scheme III.6.).

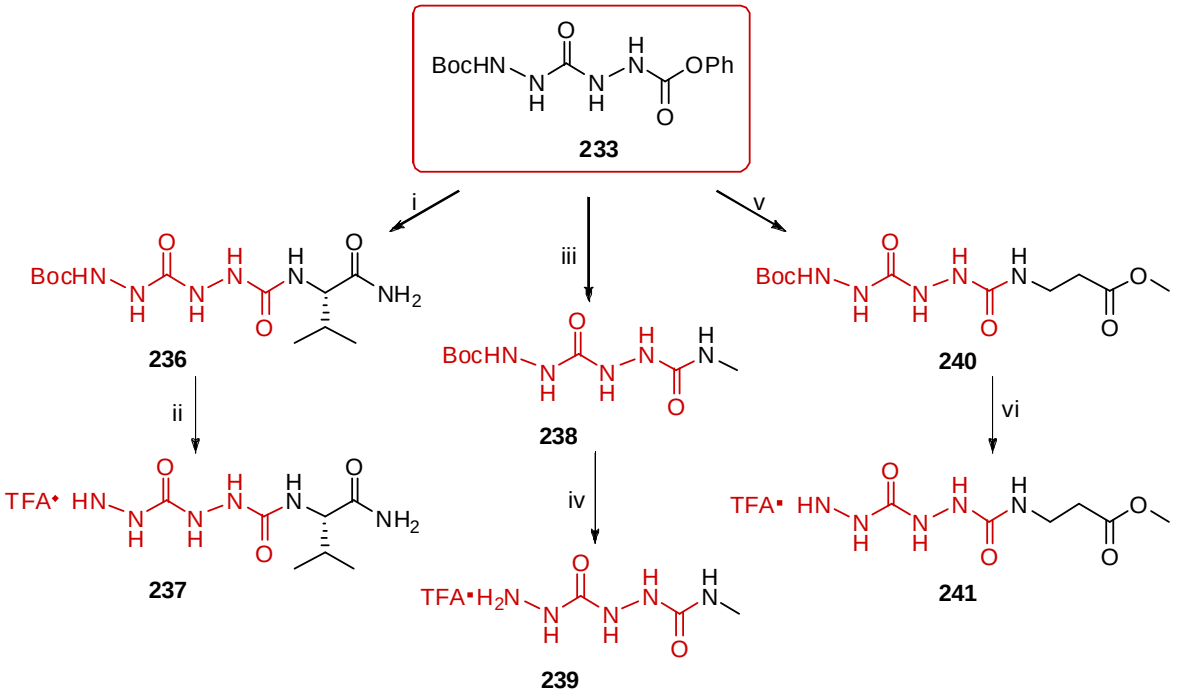

Scheme III.6. i) HCl•H-L-Val-NH_2, Et_3N, AcCN: 93%; ii) TFA/CH_2Cl_2 (1:1, v/v): quantitative yield; iii) HCl•NH_2CH_3, Et_3N, AcCN: 70%; iv) TFA/CH_2Cl_2 (1:1, v/v): quantitative yield; v) HCl•H-β-Ala-OMe, Et_3N, AcCN: 67%; vi) TFA/CH_2Cl_2 (1:1, v/v): quantitative yield.

II.4.3. SYNTHESIS OF MOLECULAR TONGS WITH THE NEW HYDRAZIDE-BASED ARM

II.4.3.1. SYNTHESIS OF UNSYMMETRICAL MOLECULAR TONGS

Unsymmetrical naphthalene-based molecular tongs were synthesised after differential protection of the two OH groups of 2,7-dihydroxynaphthalene, according to a reported procedure of our laboratory.[46] The mono alkylated compound **242** was obtained by etherification of one hydroxyl group of the commercial available 2,7-dihydroxynaphthalene, using 0.9 equiv of the commercial available ethyl 4-bromobutyrate in presence of K_2CO_3, as base, in DMF. Monoester **242** was obtained in 36% yield, along with the diester product and unchanged starting material. Subsequent benzylation of the other OH group gave compound **243**, giving rise to distinguishable OH functions. Compound **243** was then hydrolyzed under basic conditions to afford the desired acid **244**, with 92% yield (Scheme III.7).

Compound **245** was synthesised by coupling the peptidic strand HCl•H-Val-Leu-Val-OMe **223** (synthesis reported in Scheme III.3) to the C-terminus of scaffold **244**, using HBTU/HOBt in DMF, in presence of a tertiary amine (in this case, Et_3N). After a debenzylation step, alcohol **246** was *O*-alkylated with benzyl 4-bromobutyrate, affording the corresponding ester **247** in good yield (81%).

The benzyl protected compound was used in order to selectively generate compound **248** in the subsequent step of deprotection without modifying the terminal ester of the tripeptide strand.

Finally, condensation of **248** with the hydrazide-based peptidomimetic arm **237** (Scheme III.6), using HBTU/HOBt in DMF, in presence of DIPEA, afforded the final unsymmetrical naphthalene-based tong **249** in satisfactory yield (49%).

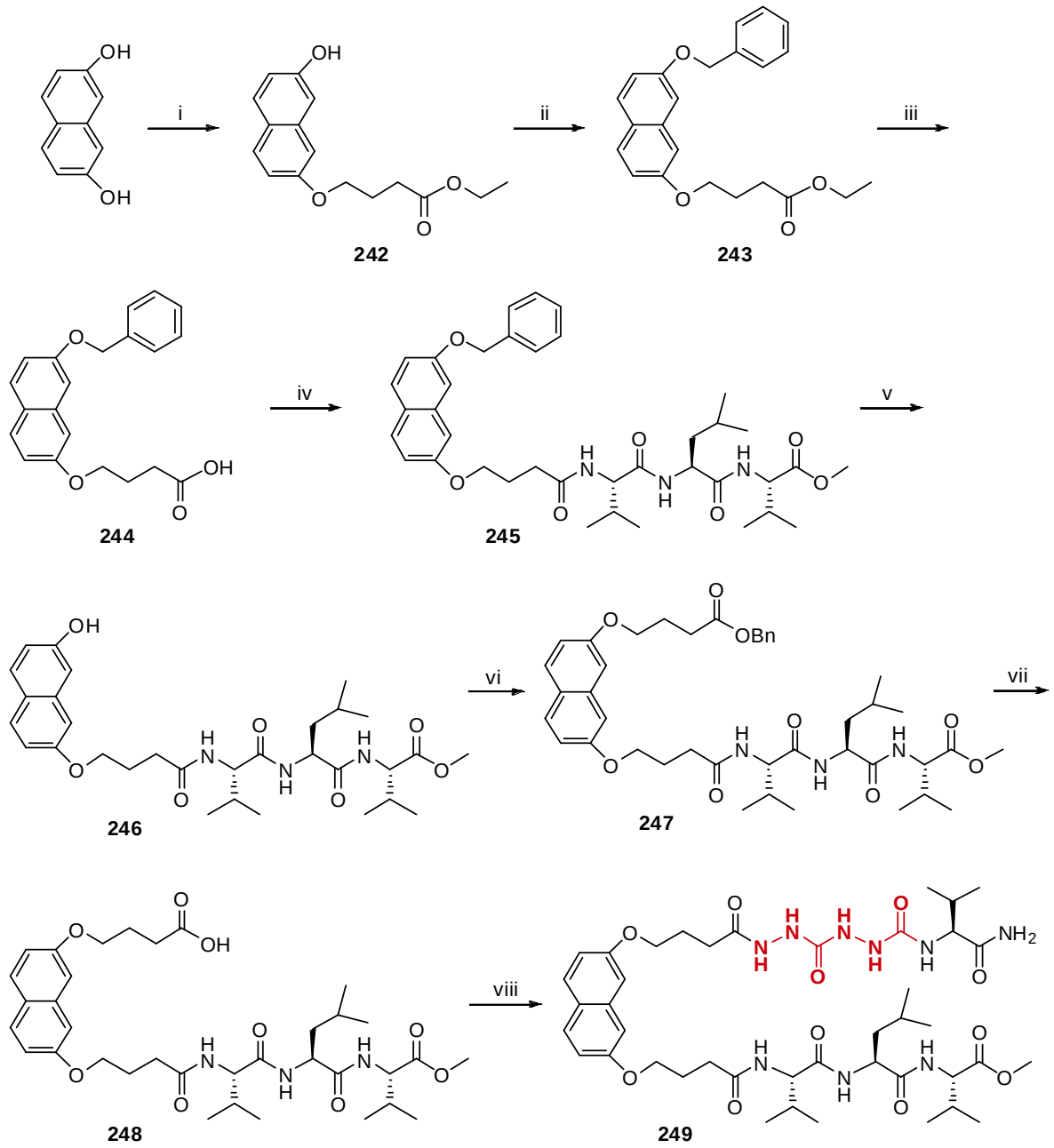

Scheme III.7. Synthesis of the unsymmetrical molecular tong **249**: i) $Br(CH_2)_3COOEt$, K_2CO_3, DMF: 36%; ii) BrBn, K_2CO_3, CH_3CN: 60%; iii) methanolic KOH 10%: 92%; iv) HCl•H-VLV-OMe, Et_3N, HBTU, HOBt, DMF: 90%; v) H_2, Pd/C, MeOH/DMF: quantitative yield; vi) $Br(CH_2)_3COOBn$, K_2CO_3, DMF: 81%; vii) H_2, Pd/C, MeOH/DMF: quantitative yield; viii) peptidomimetic **237**, DIPEA, HBTU, HOBt, DMF: 49%.

II.4.3.2. SYNTHESIS OF SYMMETRICAL MOLECULAR TONGS

Compound **250** was synthesised as previously reported by our laboratory,[45] by alkylation of the two hydroxyl groups of commercially available 2,7-naphthalenediol with ethyl 4-bromobutyrate. Total hydrolysis of **250** with methanolic KOH afforded the diacid **251**, in excellent yield. Finally, symmetrical molecular tongs **252**, **253**, and **254** were obtained by condensation of **251** with peptidomimetic arms **237**, **239**, and **241** (synthesis reported in Scheme III.6), respectively, using HBTU/HOBt in DMF, in presence of DIPEA. The three hydrazide-based symmetrical molecular tongs were obtained in satisfactory yields (56%, 55% and 73%, respectively).

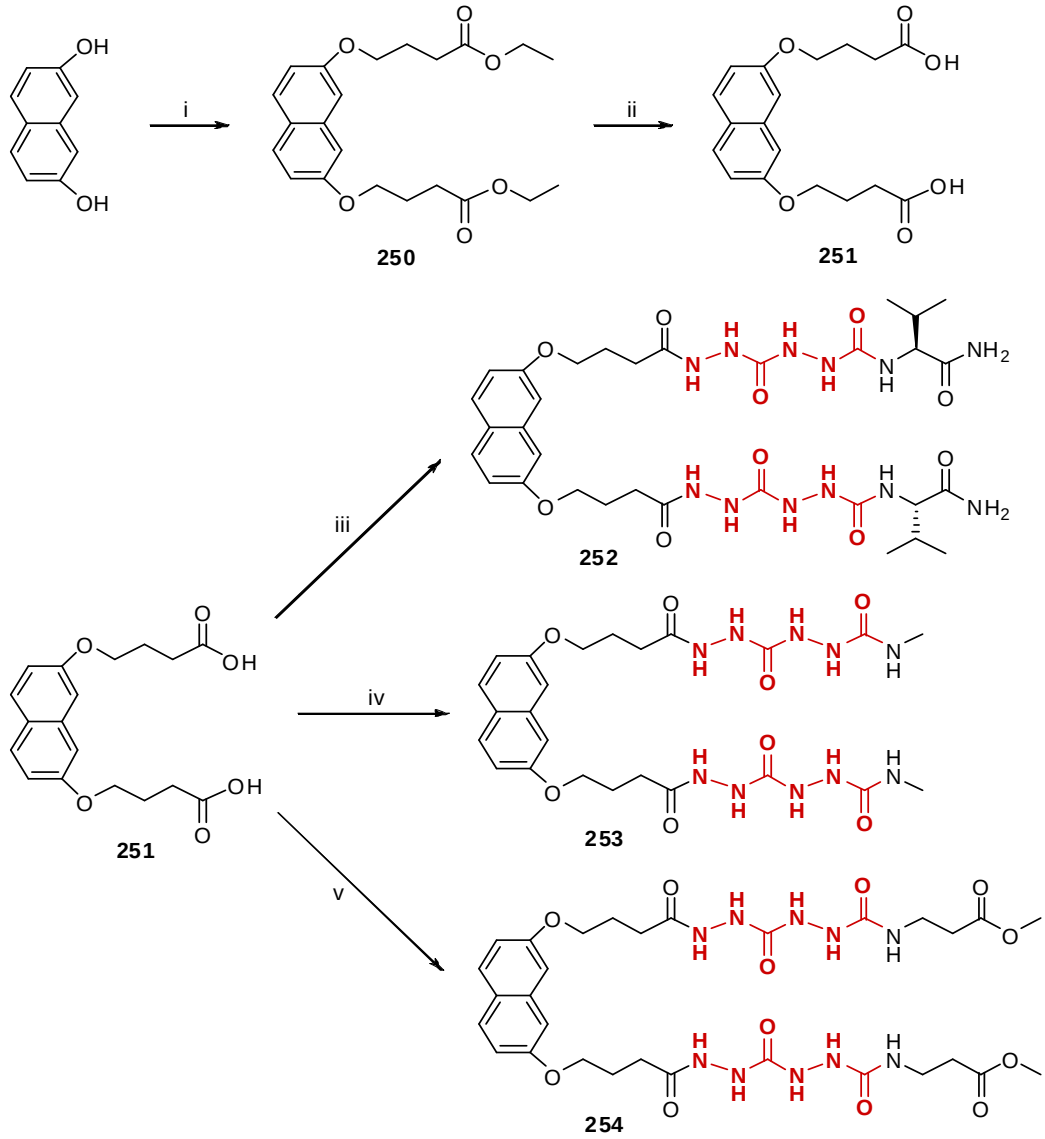

Scheme III.8. Synthesis of hydrazide-based symmetrical molecular tongs: i) $Br(CH_2)_3COOEt$, K_2CO_3, DMF: 87%; ii) methanolic KOH 10%: 97%; iii) peptidomimetic **237**, HBTU, HOBt, DIPEA, DMF: 56%; iv) peptidomimetic **239**, HBTU, HOBt, DIPEA, DMF: 55%; v) peptidomimetic **241**, HBTU, HOBt, DIPEA, DMF: 73%.

II.4.4. SYNTHESIS OF SYMMETRICAL MOLECULAR TONGS WITH A POLAR SCAFFOLD

Scaffold **216** was deprotected by catalytic hydrogenolysis, to afford compound **255** that was then coupled with peptidomimetic arm **229** and **230** (synthesis reported in Scheme III.4) using HBTU/HOBt in DMF, in presence of DIPEA, to afford molecular tongs **256** and **258** (Scheme III.9), respectively, in satisfactory yields (50% and 59%, respectively).

The 2,2-dimethyl-1,3-dioxolane methyl group of compound **256** was finally deprotected with HCl in EtOH/THF,[80] affording molecular tong **257**, in satisfactory yield (60%). In the case of compound **258**, the final deprotection step was performed with *p*-toluene sulfonic acid in methanol[81] due to the presence of acid-labile groups (*N*α-Boc), but even so molecular tong **259** was obtained in low yield (30%). Compound **259** was obtained in a very small amount and therefore was only characterized by mass spectroscopy.

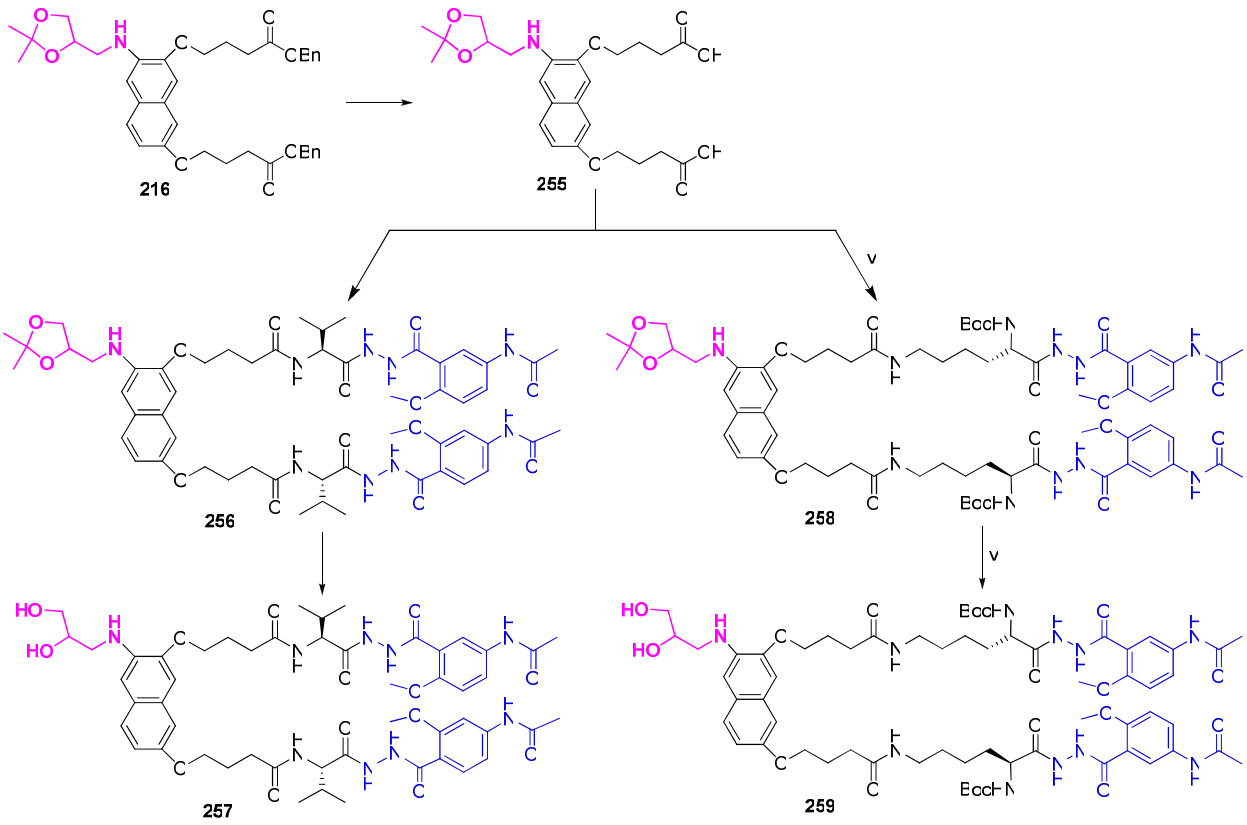

Scheme III.9. Synthesis of symmetrical molecular tongs with polar scaffold **216**: i) H_2, Pd/C, MeOH/EtOAc: quantitative yield; ii) peptidomimetic **229**, HBTU, HOBt, DIPEA, DMF: 50%; iii) 1 M HCl, EtOH/THF: 60% ; iv) peptidomimetic **230**, HBTU, HOBt, DIPEA, DMF: 59%; v) *p*-TsOH, MeOH: 30%.

Scaffold **219** was deprotected by catalytic hydrogenolysis, to afford compound **260** that was then coupled with peptidomimetic arm **229** using HBTU/HOBt in DMF, in presence of DIPEA, to afford molecular tong **261** (Scheme III.10), in satisfactory yields (68%).

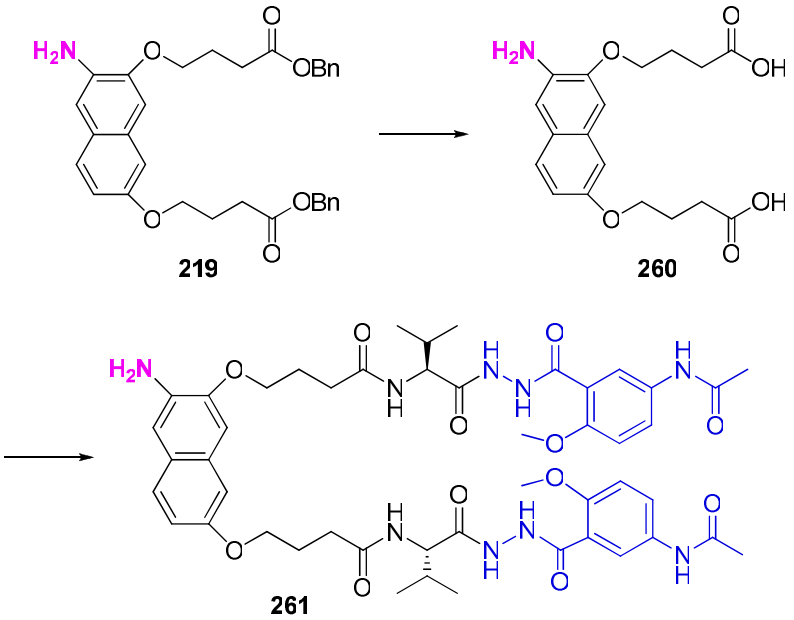

Scheme III.10. Synthesis of symmetrical molecular tongs with polar scaffold **219**: i) H_2, Pd/C, MeOH/EtOAc: quantitative yield; ii) peptidomimetic **229**, HBTU, HOBt, DIPEA, DMF: 68%.

III. BIOLOGICAL RESULTS AND DISCUSSION

In this section we will first present a description of the technique used for biological tests, and the operating conditions of these tests. This is followed by a reminder of the theory of enzyme kinetics. Finally we will present the obtained biological results with a discussion of these results.

III.1. TECHNICAL

III.1.1. USED MATERIAL

PR: was produced in the laboratory of Prof. Reboud-Ravaux (Laboratoire d'Enzymologie Moléculaire, FRE2852, CNRS – Université Paris 6). It is characterized by a molecular weight of 22 kDa and a molar extinction coefficient of 12300 M^{-1} at 280 nm. Two solutions (17 or 34 µM) are stored at -80 °C in buffer MES 50 nM, pH = 6, EDTA 1mM, DTT 1mM, NaCl 0.5 M, 5% glycerol (v/v).

PRODUCTS: to help the solubilisation of molecules in aqueous solutions, DMSO (spectral quality Merck) was used as co-solvent.

The fluorogenic substrate DABCYL-γ-Ser-Gln-Asn-Tyr-Pro-Ile-Val-Gln-EDANS (Bachem) is used for measuring the activity of the PR. To do this, it is solubilised in DMSO at

a concentration of 3 mM and stored at -20 °C. The product EDANS, 5-[(2-aminoethyl)amino]naphthalene-1 sulfonic acid (Sigma) is used as fluorescence standard.

BUFFER: the buffer used is a solution of sodium acetate 100 mM, EDTA 1 mM, 1 M NaCl, pH = 4.7.

III.1.2. KINETIC AND BIOCHEMICAL METHODS OF ANALYSIS

STABILITY, SOLUBILITY AND SPECTRAL PROPERTIES OF COMPOUNDS

Firstly, the solubility of molecular tongs in the co-solvent (DMSO) and buffer was systematically evaluated. The stability and solubility of the inhibitors in buffers used for kinetic analysis, were monitored over a period of 1 h at 30 °C, using spectrofluorometry. Time intervals of 5 minutes were chosen between two consecutive spectra. The lack of change or modification of the absorption spectrum (250 - 450 nm) shows a good solubility and stability under measurement conditions.

DETERMINATION OF ENZYME ACTIVITY

a) Fluorometric activity assay: the fluorometric activity assay of PR, whose protocol was described by Matayoshi *et al.*,[82] has the advantage of using very small amounts of PR and substrate concentrations well below the Michaelis constant K_m (K_m = 103 mM). It is based on the principle of Fluorescence Resonance Energy Transfer (FRET).

The internally quenched fluorogenic substrate DABCYL-γ-Abu-Ser-Gln-Asn-Tyr-Pro-Ile-Val-Gln-EDANS consists of a fluorescent or donor group EDANS connected by a short peptide chain to an extinguisher or acceptor group DABCYL (4-(4-dimethylaminophenylazo) benzoic acid).

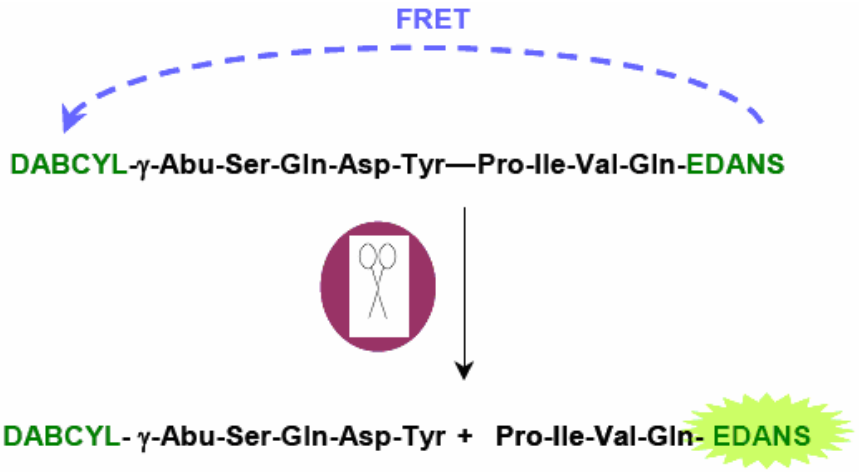

Figure III.29. The principle of fluorometric activity assay of PR, using the fluorogenic substrate DABCYL-γ-Abu-Ser-Gln-Asn-Tyr-Pro-Ile-Val-Gln-EDANS.

The group EDANS absorbs light at 340 nm and fluoresce at 490 nm, while the group DABCYL, absorbs at 490 nm and it is not fluorescent. The peptide chain mimics the cleavage site MA/CA (p17/p24) of the protein gag-pol. When the substrate is not hydrolyzed, the intrinsic fluorescence of EDANS group is insignificant because of the transfer by resonance of its emission energy to the DABCYL group. However, when there is hydrolysis, the separation of these two groups (donor and acceptor) over 100 Å, caused by breaking of the enzymatic cleavage site of PR (at the Tyr-Pro bond) prevents the transfer of energy. The fluorescence emitted by the fragment Pro-Ile-Val-Gln-EDANS at 490 nm is proportional to the amount of hydrolyzed substrate. Proteolysis activity may be followed by recording the increase of fluorescence intensity in function of time.

b) Proteolysis activity: the PR is first diluted in the kinetic buffer containing 1 mg/mL bovine serum albumin to stabilize its enzyme activity throughout a day of experience.

The experimental conditions for kinetic action are: the single substrate or, substrate and inhibitor, prior dissolved in DMSO (final concentration 3% v/v) incubated for 5 min at 30 °C. The PR (7.5 nM) is then added to generate the r eaction. Liberation of substrate hydrolysis product (Pro-Ile-Val-Gln-EDANS) leads to the emergence of fluorescence which is followed for 3 min at 490 nm (λ_{exc} = 340 nm). The initial speeds are evaluated during the first moments of the reaction, when the fluorescence intensity varies linearly with time. There is a standard line involving the intensity of fluorescent concentration ([EDANS] = 0-450 nM). It can express hydrolysis speed in function of the number of moles of substrate hydrolyzed per unit of time. This can correct any fluctuations in the fluorescence intensity due to spectrofluorometer.

Zhang analysis is performed on at least six concentrations of PR (3.5 nM – 31.7 nM). The inhibition of PR is measured at different concentrations of inhibitor (0.56 µM – 17 µM). $[E]_0$ is varying while [S] is fixed.

KINETIC ANALYSIS OF INHIBITION

a) Determination of IC_{50} values: the IC_{50} value corresponds, for a given concentration of substrate, to the concentration of inhibitor leading to a reduction of enzyme activity by 50%. To determine the IC_{50} value of a product, were the inhibitory effect varies from 10 to 80%, we calculate the percentages of inhibition of PR (Eq. 1, where $v_i(I)$ and $v_i(0)$ are, respectively, the inhibition rate in presence and absence of inhibitor and $[I]_0$ is the initial concentration of inhibitor), which are determined in relation to the enzyme activity in the absence of inhibitor (control). This calculation is made for seven to twelve concentrations of the product in question.

$$\% \text{ inhibition} = 100\ (v_i(I)/\ v_i(0)) = 100 \times [I]_0/(IC_{50} + [I]_0) \qquad \text{Eq. 1}$$

For a competitive inhibitor type, the value of the inhibition constant K_{ic} can be estimated from the IC_{50} value using the equation of Cheng & Prusoff (Eq. 2, where $[S]_0$ is the initial concentration of the substrate and K_m, the constant of Michaelis).

$$IC_{50} = K_{ic}\ (1 + [S]_0/K_m) \qquad \text{Eq. 2}$$

b) Determining the mechanism of action of inhibitors and kinetics of inhibition: when a molecule shows a potent inhibitor character, the mechanism of inhibition is obtained by kinetic analysis. For that, different techniques are used to evaluate the inhibition constant characteristics.

First, we begin by determining the reversible and irreversible inhibition. Recall that the reversible inhibition is characterized by the formation of weak links between the enzyme and inhibitor. The activity of the enzyme, in this case is found after removal of inhibitor. However, it is not possible to recover the activity of the enzyme after the action of an irreversible inhibitor because the inhibitor remains bound to the enzyme by a covalent bond. The various states of equilibrium achieved by monomer (M), dimeric enzyme (D), substrate (S), and inhibitor (I) are represented in Figure III.30.

In the case of dimerization inhibition, the only method used to determine the kinetic constants is the Zhang's method[28].

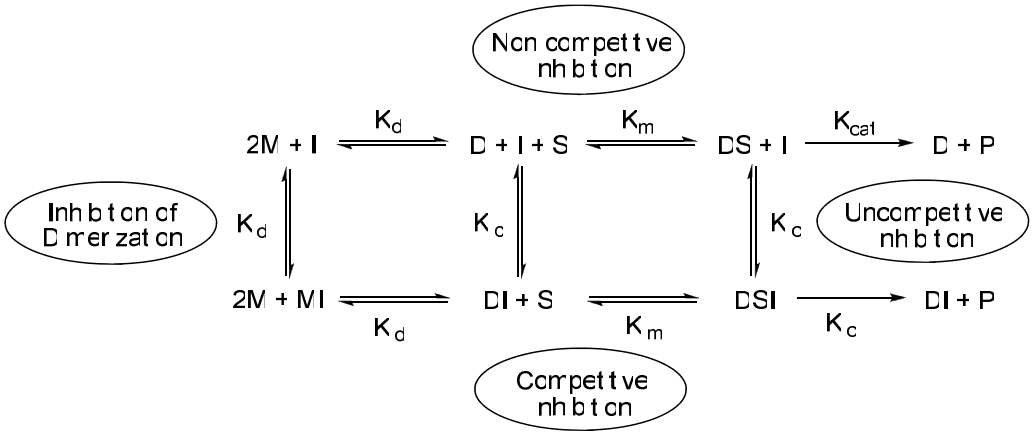

Figure III.30. Equilibrium states between monomer (M), dimer (D), substrate (S), and inhibitor (I).

Competitive inhibition: the inhibitor competes with the substrate for the occupation of the catalytic site and forms a complex enzyme-inhibitor.

Uncompetitive inhibition: the inhibitor cannot bind to the free enzyme. It has an affinity for the complex enzyme-substrate and form a ternary inactive complex.

Noncompetitive inhibition: the inhibitor binds either to the free enzyme or to the complex enzyme-substrate.

Inhibition of dimerization: the conventional Dixon's method is no longer adequate because it does not distinguish an inhibitor of the active site from an inhibitor of dimerization. In both cases, the kinetic analysis using this method may lead only to a competitive inhibition. The only method that allows identifying an inhibitor of dimerization and gives access to the inhibition constant K_{id} (inhibition constant of dimerization) was described by Zhang.[28]

The mechanism of inhibition of PR by other compounds was the assessed using Zhang-Poorman kinetic analysis in which plots of $[E]_0/\sqrt{\nu_i}$ vs $\sqrt{\nu_i}$, with $\sqrt{\nu_i} = K_{exp}[S]_0$, are constructed[28] in order to discriminate between inhibition of dimerization alone (parallel lines), competitive inhibition (altered slopes and unaltered y-axis intercept), and mixed inhibition (altered slopes and altered y-axis intercepts). The respective curves are represented in Figure III.31 and 3.32. The values of constants K_{ic} and K_{id} are calculated respectively from the ordinate values at the origin (Eq. 3 and 4, respectively), where a_i and a_0 represent the slopes of straight lines obtained respectively in the presence and absence of inhibitor and b_i and b_0 represent intercept lines obtained respectively in the presence or in the absence of inhibitor.

$$K_{ic} = a_0 \times [I]/(a_i - a_0) \qquad \text{Eq. 3}$$

$$K_{id} = b_0 \times [I]/(a_i - a_0) \qquad \text{Eq. 4}$$

In practice, two concentrations of inhibitors (situated in both sides of the IC_{50} value) are chosen and tested in the presence of six to ten concentrations of enzyme for a fixed concentration of the substrate.

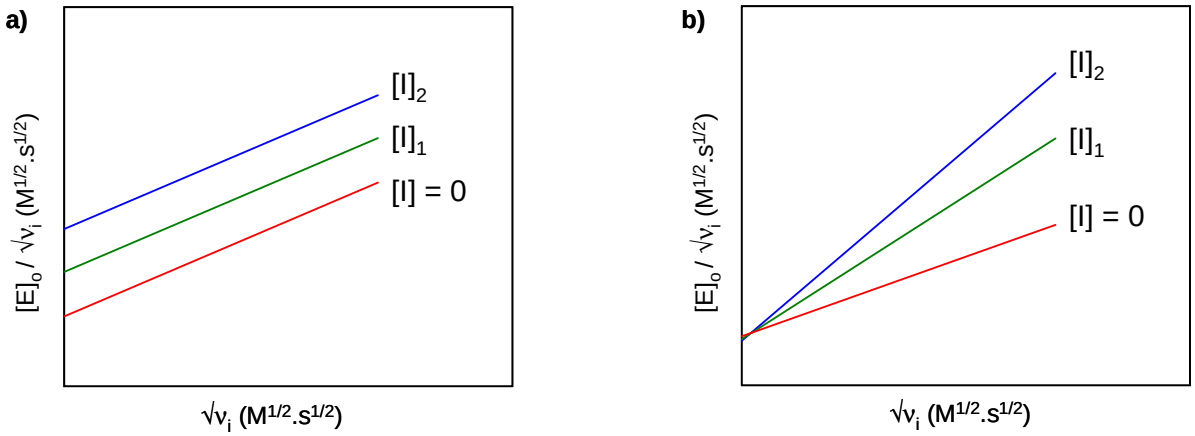

Figure III.31. Zhang plots for: a) dimerization inhibition and b) competitive inhibition.

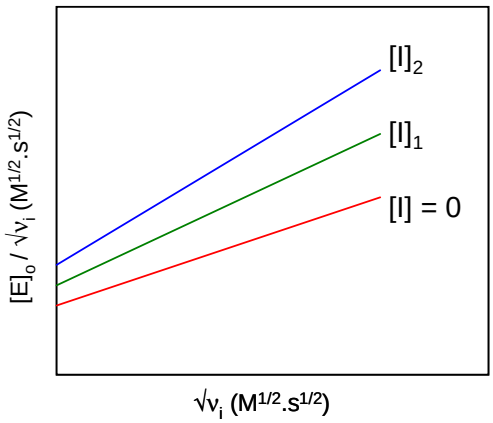

Figure III.32. Zhang plot for mixed inhibition.

III.2. RESULTS AND DISCUSSION

The inhibitory activities of the unsymmetrical and symmetrical hydrazide-based molecular tongs (**249** and **252**-**254**, respectively) and symmetrical molecular tongs bearing a modified naphthalene scaffold **256**-**258** and **261** (Table III.6) were assayed against recombinant wild-type PR at pH 4.7 and 30 ℃ using a fluorometric assay.[45,47] Until now we have not been able to obtain molecular tongs **253** and **257** in a satisfactory degree of purity for biological evaluation.

The mechanism of inhibition of PR by all compounds was assessed using Zhang-Poorman kinetic analysis in which plots of $[E]_0/\sqrt{\nu_i}$ vs $\sqrt{\nu_i}$, with $\sqrt{\nu_i} = K_{exp}[S]_0$, are constructed[28] in order to discriminate between inhibition of dimerization alone (parallel lines), competitive inhibition (altered slopes and unaltered *y*-axis intercept), and mixed inhibition (altered slopes and altered *y*-axis intercepts). In pure dimerization inhibition, the inhibitor binds to the interface region, whereas a competitive inhibitor binds to the active site and a mixed inhibitor may bind to the active site as well as to the interfacial region. The results are summarised in Table III.6.

Parallel lines (Figure III.33) were obtained for all molecular tongs tested (**249**, **252**, **256**, **258** and **261**), except for molecular tong **254**, which is consistent with pure dimerization inhibition. On the other hand, molecular tong **254**, did not show inhibition activity.

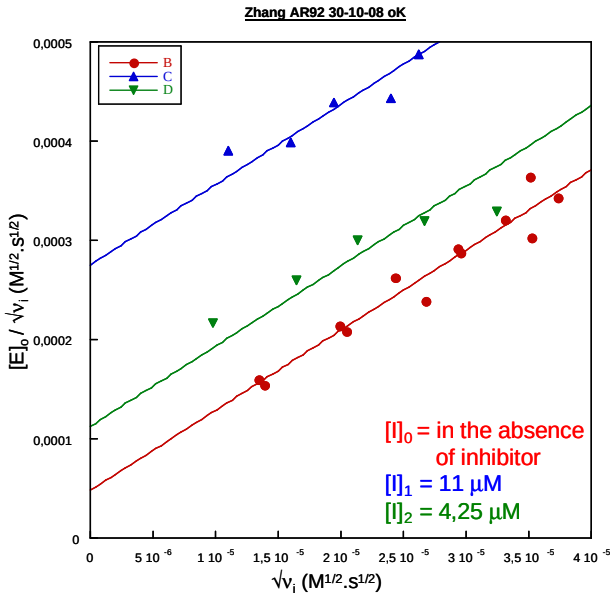

Figure III.33. Plots of $[E]_0/\sqrt{v_i}$ *vs* $\sqrt{v_i}$ for the hydrolysis of the fluorogenic substrate DABCYL-γ-Abu-Ser-Gln-Asn-Tyr-Pro-Ile-Val-Gln-EDANS by HIV-1 PR WT at pH 4.7 and 30 °C, in the absence (■), and presence of 11 µM(▲) and 4.25 µM (▼) for compound **256**.

Table III.6. *In vitro* inhibition of wild-type HIV-1 PR by the new molecular tongs (30 °C and pH 4.7, K_{id} = dimerization inhibition constant).

COMPOUNDS	K_{id} (µM)
HYDRAZIDE-BASED MOLECULAR TONGS	
249 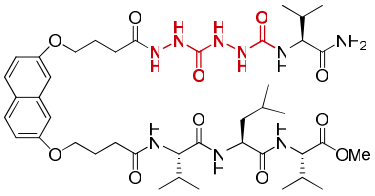	0.15
252 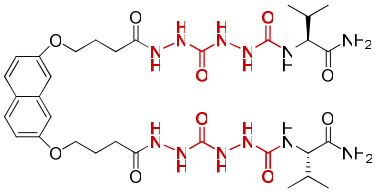	0.7
253 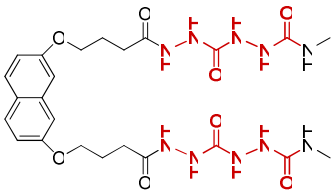	In course
254 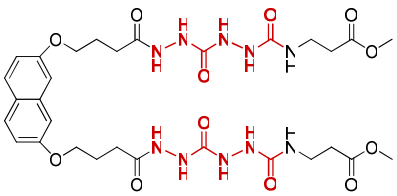	No inhibition

MOLECULAR TONGS WITH A MODIFIED SCAFFOLD

256	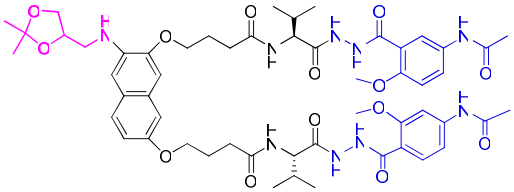	2.7
257	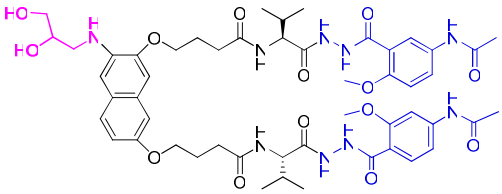	In course
258	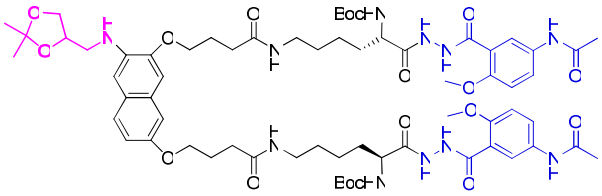	5.9
261	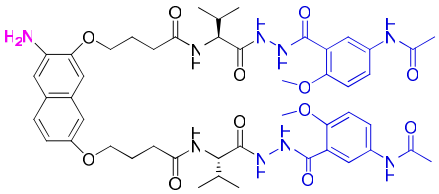	0.4

These results may be discussed as follows:

- All active molecular tongs (**249**, **252**, **256**, **258** and **261**) are pure dimerization inhibitors.
- The best results were obtained with the unsymmetrical and symmetrical hydrazide-based molecular tongs bearing a valine residue (**249** and **252**, respectively). Both molecular tongs are good dimerization inhibitors, however unsymmetrical molecular tong bearing the peptidic arm VLV-OMe (**249**) shows a better activity (K_{id} = 0.15 µM compared with K_{id} = 0.7 µM for **252**).
- On the other hand the totally peptidomimetic hydrazide-based molecular tong (**254**), which is partially water soluble, did not show inhibition activity. Contrary to our expectation, increasing the hydrophilicity of the arms led to a complete loss of activity.
- Considering symmetrical molecular tongs with a modified scaffold (**256**-**258** and **261**), two different aspects can be analysed.

Firstly, we can compare the influence of different peptidomimetic arms when attached to the same scaffold. In this case, molecular tong **256**, with the peptidomimetic arm bearing a valine residue is approximately two times better than molecular tong **258**, with the tottaly peptidomimetic arm bearing a lysine (K_{id} = 2.7 µM *vs* K_{id} = 5.9 µM).

Secondly, using the best peptidomimetic arm (meaning, the one with the valine residue) we can compare the influence of the introduction of different groups in the naphthalene scaffold. In this case, molecular tong **261**, bearing the scaffold with the terminal amine is much better than molecular tong **256**, bearing the scaffold with the 2,2-dimethyl-1,3-dioxolane methyl group (K_{id} = 0.4 μM *vs* K_{id} = 2.7 μM). This may be caused by the larger size and bulkiness of the 2,2-dimethyl-1,3-dioxolane methyl group compared with the amino group.

IV. CONCLUSIONS AND PERSPECTIVES

HIV-1 protease (PR) is an important target for anti-AIDS drugs because its inhibition results in the production of uninfectious virus. Nevertheless, viral resistances to protease inhibitors (inhibitors that interact with the active site preventing the binding of enzyme natural substrates) administered alone or in combination with reverse transcriptase inhibitors have been described *in vivo* suggesting that there is a need for structurally diverse antiproteases.

One possibility is to design inhibitors that prevent the dimerization of PR or favour the dissociation of the dimer, since the protease is only active in its dimeric form. Protein-protein interactions in the dimer include the antiparallel β-sheet formed by interdigitation of the N- (residues 1-4) and C- (residues 96-99) terminal strands of each monomer, which contributes close to 75% of the total Gibbs free energy of dimerization. This antiparallel β-sheet is an attractive target for overcoming resistance to clinical drugs because its amino acid residues are highly conserved in most HIV-1 and HIV-2 isolates. Blocking the formation of the homodimer or disrupting it is an effective way of inhibiting protease activity.

In the present thesis we described the design, synthesis and enzyme inhibitory activity against wild-type HIV-1 PR new unsymmetrical and symmetrical peptidomimetic molecular tongs as inhibitors of HIV-1 PR dimerization.

The main goal of this thesis was to increase hydrosolubility of our molecular tongs. In order to achieve this goal we took two possibilities into consideration: **i)** design of new peptidomimetics motifs with decreased lipophilicity (hydrazide-based motifs); **ii)** design of new hydrophilic scaffolds, by introducing a hydrophilic group on the naphthalene scaffold. The main conclusions are presented below:

1. 3 new hydrazide-based arms were synthesised (**237**, **239** and **241**), two of them completely peptidomimetic (**239** and **241**).

2. 3 new scaffolds with increased hydrophilicity were synthesised: scaffold **216**, **217** and **219**.

3. In total, 9 new molecular tongs were synthesised using the new hydrazide-based arms and the new scaffolds.

a) 4 hydrazide-based molecular tongs were synthesised: two bearing peptidomimetic arm **237** (one unsymmetrical (**249**), with one peptidic arm, and one symmetrical (**252**), with two peptidomimetic arms) and two symmetrical bearing peptidomimetic arms **239** and **241** (**253** and **254**, respectively).

b) 5 symmetrical molecular tongs with modifed scaffolds **216** and **219** were synthesised: three of them bearing in the both strands the amino acid valine and the peptidomimetic 5-amino-2-methoxybenzoic hydrazide derivative (**256**, **257** and **261**) and, the other two, bearing in the both strands the amino acid lysine and the peptidomimetic 5-amino-2-methoxybenzoic hydrazide derivative (**258** and **259**).

4. The inhibitory activities of the new molecular tongs were assayed against recombinant wild-type PR and the results show that:

a) all hydrazide-based molecular tongs, except **254** that does not present inhibitory activity, are pure dimerization inhibitors under micromolar range. The best result was obtained with unsymmetrical molecular tong **249**.

b) all molecular tongs bearing a modified scaffold are also pure dimerization inhibitors, although the introduction of an 2,2-dimethyl-1,3-dioxolane methyl group in the naphthalene scaffold led to a decrease on the inhibitory activity.

In perspective new peptidomimetic arms bearing the dihydrazide motif can be designed, although special attention should be given to the motif that will replace the valine residue. We must wait for the biological evaluation of the deprotected molecular tong **257** to assess if the propanediol group is able to increase hydrosolubility without compromising the PR dimerization inhibition activity.

On the other hand, scaffold **217** can be used to synthesise new molecular tongs and new hydrophilic groups may be introduced on the naphthalene scaffold in order to obtain more hydrophilic scaffolds that will eventually lead to more water-soluble molecular tongs. When this purpose is accomplished, we will be able to evaluate their antiviral efficacy in cell culture assays as well as their bioavailability.

CHAPTER III BIBLIOGRAPHIC REFERENCES:

[1] http://www.hivinsight.com/InSite?page=cfwad05-greene-sl.

[2] Navia, M. A.; Fitzgerald, P. M. D.; McKeever, B. M.; Leu, C.-T.; Heimbach, J. C.; Herber, W. K.; Sigal, I. S.; Darke, P. L.; Springer, J. P. *Nature* **1989**, *337*, 615-620.

[3] Miller, M.; Schneider, J.; Sathyanarayana, B. K.; Toth, M. V.; Marshall, G. R.; Clawson, L.; Selk, L.; Kent, S. B.; Wlodawer, A. *Science* **1989**, *246*, 1149-1152.

[4] Wlodawer, A.; Miller, M.; Jaskolski, M.; Sathyanarayana, B. K.; Baldwin, E.; Weber, I. T.; Selk, L. M.; Clawson, L.; Schneider, J.; Kent, S. B. *Science* **1989**, *245*, 616-621.

[5] Lapatto, R.; Blundell, T.; Hemmings, A.; Overington, J.; Wilderspin, A.; Wood, S.; Merson, J. R.; Whittle, P. J.; Danley, D. E.; Geoghegan, K. F.; Hawrylik, S. J.; Lee, S. E.; Scheld, K. G.; Hobart, P. M. *Nature* **1989**, *342*, 299-302.

[6] Turner, B. G.; Summers, M. F. *J. Mol. Biol.* **1999**, *285*, 1-32.

[7] Wlodawer, A.; Erickson, J. W. *Annu. Rev. Biochem.* **1993**, *62*, 543-585.

[8] Louis, J. M.; Webert, I. T.; Tözsér, J.; Clore, M. G.; Gronenborn, A. M. In *Advances in Pharmacology*; Academic Press: 2000; Vol. 49, p 111-146.

[9] Davies, D. R. *Annu. Rev. Biophys. Biophys. Chem.* **1990**, *19*, 189-215.

[10] Kohl, N. E.; Emini, E. A.; Schleif, W. A.; Davis, L. J.; Heimbach, J. C.; Dixon, R. A. F.; Scolnick, E. M.; Sigal, I. S. *Proc. Natl. Acad. Sci. USA* **1988**, *85*, 4686-4690.

[11] Kräusslich, H.-G.; Ingraham, R. H.; Skoog, M. T.; Wimmer, E.; Pallai, P. V.; Carter, C. A. *Proc. Natl. Acad. Sci. USA* **1989**, *86*, 807-811.

[12] Seelmeier, S.; Schmidt, H.; Turk, V.; von der Helm, K. *Proc. Natl. Acad. Sci. USA* **1988**, *85*, 6612-6616.

[13] McPhee, F.; Good, A. C.; Kuntz, I. D.; Craik, C. S. *Proc. Natl. Acad. Sci. USA* **1996**, *93*, 11477-11481.

[14] Brik, A.; Wong, C. H. *Org. Biomol. Chem.* **2003**, *1*, 5-14.

[15] De Clercq, E. *Nat. Rev. Drug Discovery* **2007**, *6*, 1001-1018.

[16] Hammer, S. M.; Squires, K. E.; Hughes, M. D.; Grimes, J. M.; Demeter, L. M.; Currier, J. S.; Eron, J. J.; Feinberg, J. E.; Balfour, H. H.; Deyton, L. R.; Chodakewitz, J. A.; Fischl, M. A. *N. Engl. J. Med.* **1997**, *337*, 725-733.

[17] Palella, F. J.; Delaney, K. M.; Moorman, A. C.; Loveless, M. O.; Fuhrer, J.; Satten, G. A.; Aschman, D. J.; Holmberg, S. D. *N. Engl. J. Med.* **1998**, *338*, 853-860.

[18] Autran, B.; Carcelain, G.; Li, T. S.; Blanc, C.; Mathez, D.; Tubiana, R.; Katlama, C.; Debre, P.; Leibowitch, J. *Science* **1997**, *277*, 112-116.

[19] Mocroft, A.; Vella, S.; Benfield, T. L.; Chiesi, A.; Miller, V.; Gargalianos, P.; Monforte, A. d. A.; Yust, I.; Bruun, J. N.; Phillips, A. N.; Lundgren, J. D. *Lancet* **1998**, *352*, 1725-1730.

[20] http://www.aidsinfo.nih.gov/ContentFiles/AdultandAdolescentGL.pdf.

[21] Roberts, N. A. *AIDS* **1995**, *9*, 527-532.

[22] Hruz, P. W.; Murata, H.; Mueckler, M. *Am. J. Physiol. Endocrinol. Metab.* **2001**, *280*, E549-553.

[23] Barbaro, G. *Am. J. Ther.* **2006**, *13*, 248-260.

[24] Todd, M. J.; Semo, N.; Freire, E. *J. Mol. Biol.* **1998**, *283*, 475-488.

[25] Miller, V. *JAIDS* **2001**, *26*, S34-S50.

[26] Muzammil, S.; Armstrong, A. A.; Kang, L. W.; Jakalian, A.; Bonneau, P. R.; Schmelmer, V.; Amzel, L. M.; Freire, E. *J. Virol.* **2007**, *81*, 5144-5154.

[27] Koh, Y.; Matsumi, S.; Das, D.; Amano, M.; Davis, D. A.; Li, J.; Leschenko, S.; Baldridge, A.; Shioda, T.; Yarchoan, R.; Ghosh, A. K.; Mitsuya, H. *J. Biol. Chem.* **2007**, *282*, 28709-28720.

[28] Zhang, Z.-Y.; Poorman, R. A.; Maggiora, L. L.; Heinrikson, R. L.; Kezdy, F. J. *J. Biol. Chem.* **1991**, *266*, 15591-15594.

[29] Schramm, H. J.; Nakashima, H.; Schramm, W.; Wakayama, H.; Yamamoto, N. *Biochem. Biophys. Res. Commun.* **1991**, *179*, 847-851.

[30] Babé, L. M.; Rose, J.; Craik, C. S. *Protein Sci.* **1992**, *1*, 1244-1253.

[31] Franciskovich, J.; Houseman, K.; Mueller, R.; Chmielewski, J. *Bioorg. Med. Chem. Lett.* **1993**, *3*, 765-768.

[32] Schramm, H. J.; Boetzel, J.; Büttner, J.; Fritsche, E.; Göhring, W.; Jaeger, E.; König, S.; Thumfart, O.; Wenger, T.; Nagel, N. E.; Schramm, W. *Antiviral Res.* **1996**, *30*, 155-170.

[33] Bannwarth, L.; Reboud-Ravaux, M. *Biochem. Soc. Trans.* **2007**, *035*, 551-554.

[34] Schramm, H. J.; de Rosny, E.; Reboud-Ravaux, M.; Büttner, J.; Dick, A.; Schramm, W. *Biol. Chem.* **1999**, *380*, 593-596.

[35] Sluis-Cremer, N.; Tachedjian, G. *Eur. J. Biochem.* **2002**, *269*, 5103-5111.

[36] Dumond, J.; Boggetto, N.; Schramm, H. J.; Schramm, W.; Takahashi, M.; Reboud-Ravaux, M. *Biochem. Pharmacol.* **2003**, *65*, 1097-1102.

[37] Camarasa, M.-J.; Velázquez, S.; San-Félix, A.; Pérez-Pérez, M.-J.; Gago, F. *Antiviral Res.* **2006**, *71*, 260-267.

[38] Babé, L. M.; Rose, J.; Craik, C. S. *Proc. Natl. Acad. Sci. USA* **1995**, *92*, 10069-10073.

[39] Zutshi, R.; Franciskovich, J.; Shultz, M.; Schweitzer, B.; Bishop, P.; Wilson, M.; Chmielewski, J. *J. Am. Chem. Soc.* **1997**, *119*, 4841-4845.

[40] Hwang, Y. S.; Chmielewski, J. *Bioorg. Med. Chem. Lett.* **2004**, *14*, 4297-4300.

[41] Shultz, M. D.; Bowman, M. J.; Ham, Y.-W.; Zhao, X.; Tora, G.; Chmielewski, J. *Angew. Chem., Int. Ed.* **2000**, *39*, 2710-2713.

[42] Shultz, M. D.; Ham, Y.-W.; Lee, S.-G.; Davis, D. A.; Brown, C.; Chmielewski, J. *J. Am. Chem. Soc.* **2004**, *126*, 9886-9887.

[43] Lee, S.-G.; Chmielewski, J. *Chem. Biol.* **2006**, *13*, 421-426.

[44] Zutshi, R.; Chmielewski, J. *Bioorg. Med. Chem. Lett.* **2000**, *10*, 1901-1903.

[45] Bouras, A.; Boggetto, N.; Benatalah, Z.; de Rosny, E.; Sicsic, S.; Reboud-Ravaux, M. *J. Med. Chem.* **1999**, *42*, 957-962.

[46] Merabet, N.; Dumond, J.; Collinet, B.; VanBaelinghem, L.; Boggetto, N.; Ongeri, S.; Ressad, F.; Reboud-Ravaux, M.; Sicsic, S. *J. Med. Chem.* **2004**, *47*, 6392-6400.

[47] Bannwarth, L.; Kessler, A.; Pethe, S.; Collinet, B.; Merabet, N.; Boggetto, N.; Sicsic, S.; Reboud-Ravaux, M.; Ongeri, S. *J. Med. Chem.* **2006**, *49*, 4657-4664.

[48] Breccia, P.; Boggetto, N.; Perez-Fernandez, R.; VanGool, M.; Takahashi, M.; Rene, L.; Prados, P.; Badet, B.; Reboud-Ravaux, M.; de Mendoza, J. *J. Med. Chem.* **2003**, *46*, 5196-5207.

[49] Song, M.-c.; Rajesh, S.; Hayashi, Y.; Kiso, Y. *Bioorg. Med. Chem. Lett.* **2001**, *11*, 2465-2468.

[50] Quéré, L.; Wenger, T.; Schramm, H. J. *Biochem. Biophys. Res. Commun.* **1996**, *227*, 484-488.

[51] Fan, X.; Flentke, G. R.; Rich, D. H. *J. Am. Chem. Soc.* **1998**, *120*, 8893-8894.

[52] Nowick, J. S.; Cary, J. M.; Tsai, J. H. *J. Am. Chem. Soc.* **2001**, *123*, 5176-5180.

[53] Nowick, J. S.; Chung, D. M.; Maitra, K.; Maitra, S.; Stigers, K. D.; Sun, Y. *J. Am. Chem. Soc.* **2000**, *122*, 7654-7661.

[54] Nowick, J. S.; Holmes, D. L.; Mackin, G.; Noronha, G.; Shaka, A. J.; Smith, E. M. *J. Am. Chem. Soc.* **1996**, *118*, 2764-2765.

[55] Nowick, J. S.; Pairish, M.; Lee, I. Q.; Holmes, D. L.; Ziller, J. W. *J. Am. Chem. Soc.* **1997**, *119*, 5413-5424.

[56] Nowick, J. S.; Smith, E. M.; Ziller, J. W.; Shaka, A. J. *Tetrahedron* **2002**, *58*, 727-739.

[57] Tsai, J. H.; Waldman, A. S.; Nowick, J. S. *Bioorg. Med. Chem.* **1999**, *7*, 29-38.

[58] Sanderson, P. E. J.; Lyle, T. A.; Cutrona, K. J.; Dyer, D. L.; Dorsey, B. D.; McDonough, C. M.; Naylor-Olsen, A. M.; Chen, I. W.; Chen, Z.; Cook, J. J.; Cooper, C. M.; Gardell, S. J.; Hare, T. R.; Krueger, J. A.; Lewis, S. D.; Lin, J. H.; Lucas, B. J.; Lyle, E. A.; Lynch, J. J.; Stranieri, M. T.; Vastag, K.; Yan, Y.; Shafer, J. A.; Vacca, J. P. *J. Med. Chem.* **1998**, *41*, 4466-4474.

[59] Muzammil, S.; Ross, P.; Freire, E. A. *Biochemistry* **2003**, *42*, 631-638.

[60] Nesloney, C. L.; Kelly, J. W. *J. Am. Chem. Soc.* **1996**, *118*, 5836-5845.

[61] Zhao, X.; Wang, X.-Z.; Jiang, X.-L.; Chen, Y.-Q.; Li, Z.-T.; Chen, G.-J. *J. Am. Chem. Soc.* **2003**, *125*, 15128-15139.

[62] Hou, J.-L.; Shao, X.-B.; Chen, G.-J.; Zhou, Y.-X.; Jiang, X.-K.; Li, Z.-T. *J. Am. Chem. Soc.* **2004**, *126*, 12386-12394.

[63] Feng, D.-J.; Wang, P.; Li, X.-Q.; Li, Z.-T. *Chin. J. Chem.* **2006**, *24*, 1200-1208.

[64] Cooke, R. G.; Johnson, R. L.; Owen, W. R. *Aust. J. Chem.* **1960**, *13*, 256-260.

[65] Martinborough, E.; Denti, T. M.; Castro, P. P.; Wyman, T. B.; Knobler, C. B.; Diederich, F. *Helv. Chim. Acta* **1995**, *78*, 1037-1066.

[66] Ullmann, F. *Ber. Dtsch. Chem. Ges.* **1903**, *36*, 2382-2384.

[67] Ma, D.; Cai, Q.; Zhang, H. *Org. Lett.* **2003**, *5*, 2453-2455.

[68] Zhang, H.; Cai, Q.; Ma, D. *J. Org. Chem.* **2005**, *70*, 5164-5173.

[69] Klapars, A.; Antilla, J. C.; Huang, X.; Buchwald, S. L. *J. Am. Chem. Soc.* **2001**, *123*, 7727-7729.

[70] Liu, Y.; Bai, Y.; Zhang, J.; Li, Y.; Jiao, J.; Qi, X. *Eur. J. Org. Chem.* **2007**, 6084-6088.

[71] Louie, J.; Hartwig, J. F. *Tetrahedron Lett.* **1995**, *36*, 3609-3612.

[72] Guram, A. S.; Rennels, R. A.; Buchwald, S. L. *Angew. Chem. Int. Ed.* **1995**, *34*, 1348-1350.

[73] Yin, J.; Zhao, M. M.; Huffman, M. A.; McNamara, J. M. *Org. Lett.* **2002**, *4*, 3481-3484.

[74] Garnier, E.; Audoux, J.; Pasquinet, E.; Suzenet, F.; Poullain, D.; Lebret, B.; Guillaumet, G. *J. Org. Chem.* **2004**, *69*, 7809-7815.

[75] Jonckers, T. H. M.; Maes, B. U. W.; Lemière, G. L. F.; Dommisse, R. *Tetrahedron* **2001**, *57*, 7027-7034.

[76] Košmrlj, J.; Maes, B. U. W.; Lemière, G. L. F.; Haemers, A. *Synlett* **2000**, 1581-1584.

[77] Gelmi, M. L.; Pocar, D.; Pontremoli, G.; Pellegrino, S.; Bombardelli, E.; Fontana, G.; Riva, A.; Balduini, W.; Carloni, S.; Cimino, M.; Johnson, F. *J. Med. Chem.* **2006**, *49*, 5571-5577.

[78] Noguchi, M.; Skwarczynski, M.; Prakash, H.; Hirota, S.; Kimura, T.; Hayashia, Y.; Kisoa, Y. *Bioorg. Med. Chem.* **2008**, *16*, 5389-5397.

[79] Gray, C. J.; Ireson, J. C.; Parker, R. C. *Tetrahedron* **1977**, *33*, 739-743.

[80] Ojida, A.; Matsunaga, N.; Kaku, T.; Tasaka, A. *Tetrahedron: Asymmetry* **2004**, *15*, 1555-1559.

[81] Chakraborty, T. K.; Hussain, A. K.; Joshi, S. P. *Chem. Lett.* **1992**, 2385-2388.

[82] Matayoshi, E. D.; Wang, G. T.; Krafft, G. A.; Erickson, J. *Science* **1990**, *247*, 954-958.

CHAPTER IV:

EXPERIMENTAL PART

I. CHAPTER II EXPERIMENTAL PART

MATERIALS AND METHODS: All manipulations requiring anhydrous conditions were carried out in flame-dried glassware, with magnetic stirring and under a nitrogen atmosphere. All commercially available reagents were used as received. Anhydrous solvents were purchased from commercial sources and withdrawn from the container by syringe, under a slight positive pressure of nitrogen. (2*S*)-aspartic acid β-allyl ester hydrochloride,[1] *N*-(*tert*-butoxycarbonyl)-(2*S*)-aspartic acid β-allyl ester,[1] (*S*)-serine methyl ester hydrochloride,[2] (*S*)-*N*-benzylserine methyl ester[3] and Boc-(*S*)-Ala-NH-CH_2-Ph[4] were prepared according to literature procedures and their analytical data were in agreement with those already published. Reactions were monitored by analytical thin layer chromatography using 0.25 mm pre-coated silica gel glass plates (DURASIL-25 UV_{254}) and compounds visualized using UV fluorescence, aqueous potassium permanganate or ninhydrin. Flash column chromatography was performed according to the method of Still and co-workers[5] using Chromagel 60 ACC (40-63 µm) silica gel.

Melting points were obtained in an open capillary apparatus and are uncorrected. Proton NMR spectra were recorded on a spectrometer operating at 400.16 MHz. Proton chemical shifts are reported in ppm (δ) with the solvent reference relative to tetramethylsilane (TMS) employed as the internal standard. The following abbreviations are used to describe spin multiplicity: s = singlet, d = doublet, t = triplet, q = quartet, m = multiplet, br = broad signal, dd = doublet of doublet. Carbon NMR spectra were recorded on a spectrometer operating at 100.63 MHz, with complete proton decoupling. Carbon chemical shifts are reported in ppm (δ) relative to TMS with the respective solvent resonance as the internal standard. Infrared spectra were recorded on a standard FT-IR and peaks are reported in cm^{-1}. Optical rotation values were measured on an automatic polarimeter with a 1 dm cell at the sodium D line and are given in units of 10^{-1} deg.cm^2.g^{-1}. Elemental analyses were performed using a Perkin Elmer 2400 Series II CHNS/O Analyzer. High resolution mass spectra (HRMS) were performed on a hybrid quadrupole time of flight mass spectrometer equipped with an ESI ion source. A Reserpine solution 100 pg/µl (about 100 count/s), 0.1% HCOOH/CH_3CN 1:1 was used as reference compound (Lock Mass). FAB mass spectra were recorded using a glycerol matrix.

COMPUTATIONAL METHODS: Monte Carlo/Energy Minimization (MC/EM) conformational searches on the compounds **93** and **96**, were performed within the framework of Macromodel[6] version 8.5, using the MacroModel implementation of the Amber all-atom Force field.[7] Duplicate conformations and those with an energy greater than 6.00 kcal/mol above

the global minimum were discarded. For each search, at least 1000 starting structures for each variable torsion angle were generated and minimized until the gradient was less than 0.05 kJ/Å mol using the truncated Newton-Raphson method[8] implemented in MacroModel.
For compound **96**, simulated annealing protocol in explicit DMSO solvent[9] was performed using the ff03 force field[10] and the SANDER module of the AMBER7 package.[11] According to the NOE data, two distance NOE restraints were imposed between the protons $C_\alpha H$ of the Val1 and $C_\alpha H$ of the Ala2 residues (upper bound of 3.0 Å and force constant of 20 kcal/mol Å) and between the proton $C_\alpha H$ of the Ala2 residue and NH2 amide (upper bound of 4.0 Å and force constant of 20 kcal/mol Å). A 9 Å cutoff and the Ewald sums were used for non-bonded interactions. The SHAKE algorithm[12] was used to keep the hydrogen atoms fixed together with a 1 fs time step. The **96b** conformation was solvated in a cubic box by 643 DMSO molecules and gradually heated at 900 K. The density of the system was first equilibrated at 300 K for 140 ps, then was kept constant for the next of the simulated annealing steps. After 1 ns of equilibration at 900 K, the system was cooled up to 0 K during 1 ns. Structures for analysis were saved every 10 ps.

SOLID-LAYER RECEPTOR-BINDING ASSAY: Purified $\alpha_v\beta_3$ and $\alpha_v\beta_5$ receptors (Chemicon International, Inc., Temecula, CA) were diluted to 0.5 μg/mL in coating buffer containing 20 mmol/L Tris-HCl (pH 7.4), 150 mmol/L NaCl, 1 mmol/L $MnCl_2$, 2 mmol/L $CaCl_2$ and 1 mmol/L $MgCl_2$. An aliquot of diluted receptors (100 μL/well) was added to 96-well microtiter plates (NUNC MW 96F MEDISORP STRAIGHT) and incubated overnight at 4 ℃. The plates were then incubated with blocking solution (coating buffer plus 1% bovine serum albumin) for additional 2 hours at room temperature to block nonspecific binding followed by 3-hour incubation at room temperature with various concentrations (10^{-10}–10^{-5} M) of test compounds in the presence of 1 μg/mL vitronectine biotinylated using EZ-Link Sulfo-NHS-Biotynilation kit (Pierce, Rockford, IL). After washing, the plates were incubated for 1 hour at room temperature with streptavidin-biotinylated peroxidase complex (Amersham Biosciences, Uppsala, Sweden) followed by 30-minutes incubation with 100 μL Substrate Reagent Solution (R&D Systems, Minneapolis, MN) before stopping the reaction by addition of 50 μL of 1 N H_2SO_4. Absorbance at 415 nm was read in a Synergy™ HT Multi-Detection Microplate Reader (BioTek Instruments, Inc.). Each data point is the result of the average of triplicate wells and was analysed by nonlinear regression analysis with Prism GraphPad program.

SOLUTION LAYER SYNTHESIS OF PEPTIDOMIMETICS: GENERAL PROCEDURES

GENERAL PROCEDURE A FOR DEPROTECTION REACTIONS: To a solution of the *N*-Boc-protected amino acid or peptide in CH_2Cl_2 (0.13 M) was added an equal volume of TFA and the reaction was stirred at r.t. for 3 h. The solvent was evaporated, methanol (3×) was added followed by evaporation, and then ether was added and evaporated to afford the corresponding TFA salt.

GENERAL PROCEDURE B FOR COUPLING REACTIONS: The TFA salt of the amino acid or peptide derivative was dissolved in DMF (0.1 M), and the *N*-protected amino or peptide acid (1.05 equiv) was added followed by HOBt (1.1 equiv) and DIPEA (2 equiv). The solution was cooled in an ice bath and treated with EDC (1.1 equiv). The reaction was stirred at 0 ºC for 1 h and at r.t. overnight. The mixture was diluted with EtOAc and consecutively extracted with 1 M $KHSO_4$ (2×), aqueous $NaHCO_3$ (2×) and brine (2×), dried over Na_2SO_4 and the solvent evaporated under reduced pressure to afford the crude product.

GENERAL PROCEDURE C FOR COUPLING REACTIONS: To a solution of the *N*-protected amino acid in CH_2Cl_2, under nitrogen atmosphere and at 0 ºC, was added HATU (1.1 equiv) and DIPEA (2 equiv). After 30 min, a solution of the TFA salt of the peptide in CH_2Cl_2 and DIPEA (1 equiv), was added and the reaction mixture was stirred at 0 ºC for 1 h and at r.t. overnight. The mixture was diluted with EtOAc and consecutively extracted with 1 M $KHSO_4$ (2×), aqueous $NaHCO_3$ (2×) and brine (2×), dried over Na_2SO_4 and the solvent evaporated under reduced pressure to afford the crude product.

GENERAL PROCEDURE D FOR COUPLING REACTIONS: To a solution of the *N*-protected amino acid (or *N*-protected DKP) in DMF, under nitrogen atmosphere and at 0 ºC, was added HBTU (1.2 equiv), HOBt (1.2 equiv) and DIPEA (3 equiv). After 30 min, a solution of the TFA salt of the peptide in DMF and DIPEA (1 equiv), was added and the reaction mixture was stirred at 0 ºC for 1 h and at r.t. overnight. The mixture was diluted with EtOAc and consecutively extracted with 1 M $KHSO_4$ (2×), aqueous $NaHCO_3$ (2×) and brine (2×), dried over Na_2SO_4 and the solvent evaporated under reduced pressure to afford the crude product.

GENERAL PROCEDURE E FOR COUPLING REACTIONS: To a solution of the *N*-protected amino acid in DMF, under nitrogen atmosphere and at 0 ºC, was added HATU (1.5 equiv), HOAt (1.5 equiv) and DIPEA (3 equiv). After 30 min, a solution of the TFA salt of the peptide in DMF and DIPEA (1 equiv), was added and the reaction mixture was stirred at 0 ºC for 1 h

and at r.t. overnight. The mixture was diluted with EtOAc and consecutively extracted with 1 M $KHSO_4$ (2×), aqueous $NaHCO_3$ (2×) and brine (2×), dried over Na_2SO_4 and the solvent evaporated under reduced pressure to afford the crude product.

(2*S*)-Aspartic acid β-allyl ester hydrochloride (98)

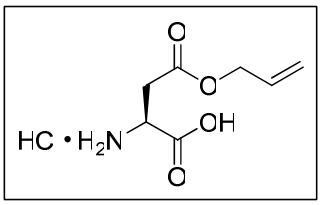

Acetyl chloride (10.4 mL, 0.15 mol, 4 equiv) was added dropwise to ice-cold allylic alcohol (45 mL). The resulting solution was stirred at 0 ºC for 15 min and then at r.t. for 1 h. (*S*)-aspartic acid (5.00 g, 38 mmol) was added in a single portion and the suspension was stirred at r.t. for 18 h and then poured into ice-cold Et_2O. After stirring at 0 ºC for 1 h the precipitate was collected by filtration and washed on the pad with Et_2O, to afford hydrochloride **98** as a white solid (7.09 g, 90%).

Mp: 181-183 ℃ (Lit. 185-186 ℃) [13]

$[\alpha]^{20}_D$ = +22.7 (*c* 1.0, CH_3OH)

^{1}H NMR (400 MHz, D_2O) δ: 5.86-5.96 (m, 1H), 5.23-5.33 (m, 2H), 4.64 (d, 2H, *J*=5.7 Hz), 4.34-4.37 (m, 1H), 3.11 (dd, 2H, J_1=18.4 Hz, J_2=4.8 Hz).

^{13}C NMR (100 MHz, D_2O) δ: 171.5, 171.2, 131.8, 119.3, 67.1, 49.7, 34.4.

IR (KBr) ν_{max}: 3437, 2913, 1742, 1726, 1505, 1227, 1206.

***N*-(*tert*-Butoxycarbonyl)-(2*S*)-aspartic acid β-allyl ester (99)**

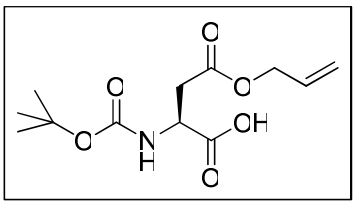

Triethylamine (11.8 mL, 84 mmol, 3 equiv) was added dropwise to a stirred solution of Boc_2O (7.37 g, 34 mmol, 1.2 equiv) and compound **98** (5.90 g, 28 mmol) in H_2O/dioxane (50 mL, 1:1 v/v). After 18 h the solution was extracted with petroleum ether (2 × 50 mL) and the aqueous layer was cooled on ice and carefully acidified to pH 3 by slow addition of 1 M $KHSO_4$ solution. The urethane was then extracted into EtOAc (3 × 50 mL) and the combined organic

layers were washed with brine (2 × 25 mL), dried over Na_2SO_4, filtered and concentrated under reduced pressure to give product **99** as a viscous transparent oil (7.38 g, 96%).

$[\alpha]^{20}_D$ = +33.3 (*c* 1.0, $CHCl_3$)

^{1}H NMR (400 MHz, $CDCl_3$) δ: 9,90 (br s, 1H), 5.86-5.94 (m, 1H), 5.57 (d, 1H, *J*=8.4 Hz), 5.19-5.32 (m, 2H), 4.52-4.60 (m, 3H), 3.07 (dd, 1H, J_1=17.2 Hz, J_2=4.2 Hz), 2.89 (dd, 1H, J_1=17.1 Hz, J_2=4.8 Hz), 1.46 (s, 9H).

^{13}C NMR (100 MHz, $CDCl_3$) δ: 176.2, 171.2, 156.0, 132.0, 119.1, 80.9, 66.2, 50.2, 36.9, 28.7.

IR (Nujol) ν_{max}: 3331, 2980, 1732, 1504, 1385, 1163.

(*S*)-Serine methyl ester hydrochloride (100)

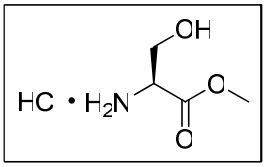

Acetyl chloride (16.2 mL, 0.23 mol, 4 equiv) was added dropwise to ice-cold methanol (45 mL). The resulting solution was stirred at 0 ºC for 15 min and (*S*)-serine (6.00 g, 57 mmol) was added in a single portion and the reaction mixture was brought to reflux. After refluxing for 2.5 h, the mixture was cooled to r.t. and then poured into ice-cold Et_2O (200 mL). The resulting precipitate was collected by filtration and washed on the pad with Et_2O, to afford hydrochloride **100** as a white powder (7.27 g, 82%).

Mp: 162-164 ℃ (Lit. 160-165 ℃)

$[\alpha]^{20}_D$ = +3.98 (*c* 1.0, CH_3OH)

^{1}H NMR (400 MHz, D_2O) δ: 4.25 (t, 1H, *J*=3.8 Hz), 4.08 (dd, 1H, J_1=12.6 Hz, J_2=4.3 Hz), 3.98 (dd, 1H, J_1=12.6 Hz, J_2=3.4 Hz), 3.83 (s, 3H).

^{13}C NMR (100 MHz, D_2O) δ: 169.3, 59.6, 55.1, 54.1.

IR (KBr) ν_{max}: 3358, 2928, 1750, 1595, 1510, 1260, 1095, 1040.

(*S*)-*N*-Benzylserine methyl ester (101)

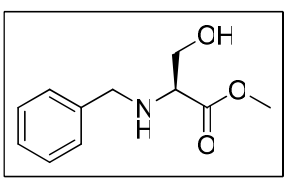

Compound **100** (1.20 g, 7.7 mmol) was dissolved in methanol (18 mL) and cooled to 0 ºC. Triethylamine (1.5 mL, 11 mmol, 1.4 equiv) was added, the reaction was then stirred for 10 min, and freshly distilled benzaldehyde (0.79 mL, 7.7 mmol, 1 equiv) was successively added. The reaction mixture was stirred for 2 h, at which time $NaBH_4$ (584 mg, 15.4 mmol, 2 equiv) was added portionwise to the reaction mixture over a period of 30 min. The solution was partitioned between 4 M HCl (12 mL) and Et_2O (30 mL). The organic layer was extracted with 4 M HCl (2 × 7 mL) and the combined aqueous layers were washed with Et_2O (2 × 15 mL). All organic layers were discarded. The aqueous layers were carefully neutralized with sat. aqueous $NaHCO_3$, until a pH 8 was reached. The aqueous layer was then extracted with Et_2O (4 × 15 mL) and the combined organic layers dried over Na_2SO_4. Evaporation of volatiles under reduced pressure afforded product **101** as a transparent oil (1.39 g, 86 %).

$[\alpha]^{20}_D$ = -39.4 (*c* 1.0, $CHCl_3$)

^{1}H NMR (400 MHz, $CDCl_3$) δ: 7.26-7.38 (m, 5H), 3.91 (d, 1H, *J*=13.0 Hz), 3.82 (dd, 1H, J_1=10.9 Hz, J_2=4.4 Hz), 3.75-3.79 (m, 4H), 3.66 (dd, 1H, J_1=10.8 Hz, J_2=6.2 Hz), 3.46 (dd, 1H, J_1=6.1 Hz, J_2=4.5 Hz), 2.78 (s, 1H).

^{13}C NMR (100 MHz, $CDCl_3$) δ: 173.6, 139.3, 129.0, 128.8, 127.8, 62.8, 62.2, 52.6, 52.4.

IR (Nujol) ν_{max}: 3320, 2951, 1736, 1454, 1202, 1142, 1057.

(*S*)-*N*-Benzyl-3-*tert*-butoxycarbonylamino-*N*-[(*S*)-2-hydroxy-1-methoxycarbonyl-ethyl]-succinamic acid allyl ester (97)

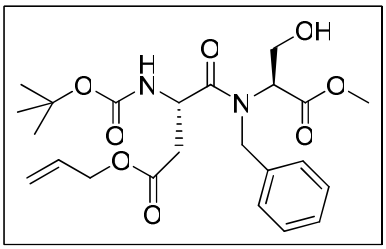

To a solution of **99** (329 mg, 1.2 mmol) in CH_2Cl_2 (8 mL), under a nitrogen atmosphere and at 0 ºC, was added HATU (510 mg, 1.3 mmol, 1.1 equiv) and DIPEA (417 µL, 2.4 mmol, 2 equiv). After 30 min, a solution of **101** (251 mg, 1.2 mmol, 1 equiv) in CH_2Cl_2 (1.6 mL) was added and the reaction was stirred at 0 ºC for 1 h and at r.t. for 24 h. The mixture was then diluted with EtOAc (100 mL) and the organic layer was washed in order with: 1 M $KHSO_4$ (2 × 20 mL), aqueous $NaHCO_3$ (2 × 20 mL) and brine (2 × 20 mL), dried over Na_2SO_4 and volatiles were removed under reduced pressure. The residue was purified by flash chromatography on silica gel (petroleum ether/EtOAc, 75/25) to afford product **97** as a yellow oil (401 mg, 72%).

$[\alpha]^{21}_D$ = -2.65 (*c* 1.0, $CHCl_3$)

^{1}H NMR (400 MHz, $CDCl_3$) δ: 7.24-7.34 (m, 5H), 5.83-5.93 (m, 1H), 5.48 (d, 1H, *J*=8.2 Hz), 5.30 (d, 1H, *J*=17.2 Hz), 5.23 (d, 1H, *J*=10.4 Hz), 4.51-4.61 (m, 3H), 4.32-4.48 (m, 2H), 3.88 (d, 1H, *J*=13.1 Hz), 3.75 (s, 3H), 3.73 (d, 1H, *J*=13.1 Hz), 3.55 (t, 1H, *J*=4.7 Hz), 2.99 (dd, 1H, J_1=17.0 Hz, J_2=4.3 Hz), 2.85 (dd, 1H, J_1=17.0 Hz, J_2=4.7 Hz), 2.21 (br s, 1H), 1.45 (s, 9H).

Two set of signals were observed in the ^{13}C spectrum due to the presence of two rotational isomers A:B (20:1 ratio): **^{13}C NMR (100 MHz, $CDCl_3$) δ**: 172.8 (A), 172.1 (B), 171.0 (A), 170.3 (B), 155.7 (A), 155.0 (B), 139.6 (A), 138.9 (B), 132.1 (A), 131.4 (B), 128.9 (A), 128.7 (A), 128.1 (B), 127.9 (B), 127.6 (A), 126.9 (B), 119.1 (A), 118.4 (B), 80.6 (A), 79.9 (B), 66.2 (A), 66.1 (A), 65.5 (B), 65.4 (B), 59.5 (A), 58.8 (B), 52.7 (A), 52.2 (A), 51.9 (B), 51.4 (B), 50.3 (A), 49.6 (B), 37.1 (A), 36.4 (B), 28.7 (A), 27.9 (B).

IR ($CHCl_3$) ν_{max}: 3438, 3338, 3026, 2983, 2953, 2857, 1739, 1500, 1453, 1378, 1341, 1279, 1247, 1176.

HRMS (ESI) *m/z* calcd for $[C_{23}H_{33}N_2O_8]^+$: 465.22314 $[M+H]^+$; found: 465.22326.

Anal. Calcd for $C_{23}H_{32}N_2O_8$: C 59.47, H 6.94, N 6.03; found C 59.07, H 7.01, N 5.91.

[(2*S*,5*S*)-4-Benzyl-5-hydroxymethyl-3,6-dioxo-piperazin-2-yl]-acetic acid allyl ester (102)

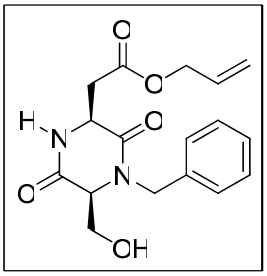

Dipeptide **97** (1.95 g, 4.2 mmol) was deprotected according to general procedure A. The corresponding trifluoroacetate salt was dissolved in a mixture of saturated aqueous $NaHCO_3$/EtOAc (0.1 M, 1:1 v/v) and stirred at r.t. for 24-48 h. Subsequently, the layers were separated and the aqueous layer was extracted with EtOAc (4×). The combined organic layers were washed with brine, dried over Na_2SO_4 and volatiles were removed under reduced pressure. The residue was purified by flash chromatography on silica gel (CH_2Cl_2/CH_3OH, 97/3) to afford product **102** as a white solid (1.13 g, 81%).

Mp: 119-120 ºC

$[\alpha]^{25}_D$ = -72.1 (*c* 1.0, $CHCl_3$)

^{1}H NMR (400 MHz, $CDCl_3$) δ: 7.25-7.37 (m, 5H), 7.05 (br s, 1H), 5.84-5.94 (m, 1H), 5.25-5.34 (m, 3H), 4.55-4.66 (m, 2H), 4.49-4.51 (m, 1H), 4.07 (d, 1H, *J*=15.0 Hz), 3.98 (d, 1H, *J*=11.1 Hz), 3.85-3.89 (m, 2H), 3.21 (dd, 1H, J_1=17.5 Hz, J_2=2.8 Hz), 3.16 (br s, 1H); 3.13 (dd, 1H, J_1=17.5 Hz, J_2=10.4 Hz).

^{13}C NMR (100 MHz, $CDCl_3$) δ: 171.9, 167.0, 166.3, 135.6, 131.9, 129.5, 128.6, 119.5, 66.4, 61.3, 60.5, 52.8, 47.6, 40.7.

IR ($CHCl_3$) ν_{max}: 3388, 3275, 3031, 3017, 2945, 1728, 1680, 1452, 1379, 1336, 1276, 1183, 1124.

MS (FAB$^+$) *m/z* 333 ([M+1]$^+$, 80%), 275 (11%), 154 (57%), 136 (48%), 91 (100%).

Anal. Calcd for $C_{17}H_{20}N_2O_5$: C 61.44, H 6.07, N 8.43; found C 61.23, H 5.97, N 8.24.

X-ray crystallographic data of 102. Crystal data: $C_{17}H_{20}N_2O_5$; MW = 332.35 g mol^{-1}; T = 293 K; λ(Mo, Kα) = 0.71073 Å, monoclinic, space group $P2_1$, a = 7.394(4) Å, b = 10.764(19) Å, c = 10.800(5) Å, β = 99.71(4)°, V = 847(2) Å^3, ρ_{calc} = 1.303 g cm^{-3}, Z = 2; μ(Mo, Kα) = 1.0 cm^{-1}. R and wR2 0.086 and 0.155, respectively, for 1230 unique data collected in the 3-25.3° 2θ range.

[(2*S*,5*S*)-5-Azidomethyl-4-benzyl-3,6-dioxo-piperazin-2-yl]-acetic acid allyl ester (105)

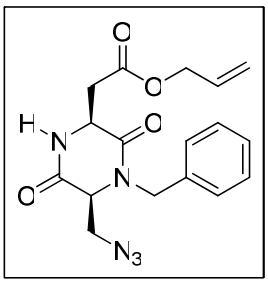

To a solution of **102** (565 mg, 1.7 mmol) in CH_2Cl_2/toluene (6.6 mL/12.2 mL), under nitrogen atmosphere and at -20 ºC, was added PPh_3 (530 mg, 2.0 mmol, 1.2 equiv) and the mixture was stirred until a solution was obtained. Hydrazoic acid (0.45 M in toluene,[14] 7.6 mL, 3.4 mmol, 2 equiv) was added followed by a dropwise addition of DIAD (0.41 mL, 2.0 mmol, 1.2 equiv) and the reaction was stirred at -20 ºC for 3.5 h. After evaporation of the solvent under reduced pressure, a quick chromatographic purification (petroleum ether/EtOAc, 6/4) was performed to remove the hydrazo-derivative and the resulting crude residue was then purified by flash chromatography on silica gel (CH_2Cl_2/CH_3OH, 99/1) to afford product **105** as a colorless oil (291 mg, 48%).

$[\alpha]^{23}_D$ = -72.7 (*c* 1.9, $CHCl_3$)

^{1}H NMR (400 MHz, $CDCl_3$) δ: 7.26-7.39 (m, 5H), 6.91 (br s, 1H), 5.89-5.99 (m, 1H), 5.36 (d, 1H, *J*=17.2 Hz), 5.30 (d, 1H, *J*=10.4 Hz), 5.18 (d, 1H, *J*=15.0 Hz), 4.62-4.71 (m, 2H), 4.51-4.54 (m, 1H), 4.20 (d, 1H, *J*=15.0 Hz), 3.95 (br s, 1H), 3.89 (dd, 1H, J_1=12.7 Hz, J_2=1.7 Hz), 3.68 (dd, 1H, J_1=12.7 Hz, J_2=3.4 Hz), 3.31 (dd, 1H, J_1=17.7 Hz, J_2=2.2 Hz), 3.08 (dd, 1H, J_1=17.7 Hz, J_2=11.2 Hz).

^{13}C NMR (100 MHz, $CDCl_3$) δ: 171.6, 165.7, 165.1, 135.3, 131.8, 129.6, 128.8, 128.6, 119.6, 66.5, 58.8, 52.6, 51.1, 48.0, 40.7.

IR (thin film) ν_{max}: 2984, 2929, 2853, 2119, 1734, 1686, 1667, 1451, 1336, 1274, 1181.

MS (FAB$^+$) *m/z* 358 ([M+1]$^+$, 12%), 330 (2%), 149 (16%), 109 (27%), 91 (100%).

Anal. Calcd for $C_{17}H_{19}N_5O_4$: C 57.14, H 5.36, N 19.60; found C 57.39, H 5.28, N 19.25.

[(2*S*,5*S*)-4-Benzyl-5-(*tert*-butoxycarbonylamino-methyl)-3,6-dioxo-piperazin-2-yl]-acetic acid allyl ester (108)

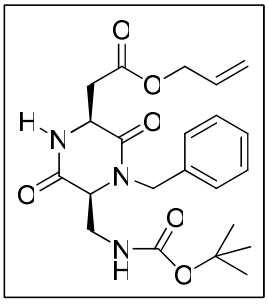

To a solution of azide **105** (268 mg, 0.75 mmol) in THF (2.5 mL), under nitrogen atmosphere and at -20 ºC, was added Me_3P (830 µL of 1 M solution in THF, 0.83 mmol, 1.1 equiv) and 2-(*t*-butoxycarbonyloxyimino)-2-phenylacetonitrile (Boc-ON, 206 mg, 0.83 mmol, 1.1 equiv). After stirring for 5 h at r.t., CH_2Cl_2 (60 mL) was added and the solution was washed with H_2O (3 × 30 mL) and brine. The organic layer was dried over Na_2SO_4 and volatiles were removed under reduced pressure. The residue was purified by flash chromatography on silica gel (CH_2Cl_2/CH_3OH, 99/1) to afford product **108** as a white solid (253 mg, 78%).

Mp: 57-58 ºC

[α]$^{28}_D$ = -123.7 (*c* 1.0, $CHCl_3$)

^{1}H NMR (400 MHz, $CDCl_3$) δ: 7.28-7.36 (m, 5H), 7.06 (br s, 1H), 5.86-5.96 (m, 1H), 5.56 (d, 1H, *J*=15.1 Hz), 5.25-5.36 (m, 3H), 4.60-4.69 (m, 2H), 4.48-4.51 (m, 1H), 4.09 (d, 1H, *J*=15.1 Hz), 3.80-3.86 (m, 2H), 3.45-3.49 (m, 1H), 3.27 (dd, 1H, J_1=17.6 Hz, J_2=1.7 Hz), 2.85 (dd, 1H, J_1=17.6 Hz, J_2=11.1 Hz), 1.46 (s, 9H).

^{13}C NMR (100 MHz, $CDCl_3$) δ: 171.5, 166.7, 164.9, 156.2, 135.6, 131.8, 129.4, 128.9, 128.5, 119.3, 80.8, 66.4, 59.2, 52.4, 47.2, 40.8, 40.6, 28.7.

IR (Nujol) v_{max}: 3323, 3308, 1716, 1684, 1658, 1339, 1272, 1167, 1127.

MS (FAB$^+$) *m/z* 432 ([M+1]$^+$, 12%), 376 (49%), 332 (41%), 302 (16%), 91 (100%).

Anal. Calcd for $C_{22}H_{29}N_3O_6$: C 61.24, H 6.77, N 9.74; found C 61.47, H 6.93, N 9.56.

[(2*S*,5*S*)-4-Benzyl-5-(*tert*-butoxycarbonylamino-methyl)-3,6-dioxo-piperazin-2-yl]-acetic acid, DKP-90 (90)

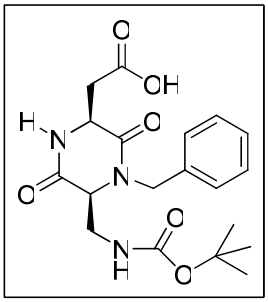

To a solution of **108** (242 mg, 0.56 mmol) in CH_2Cl_2 (3.0 mL), under nitrogen atmosphere and at 0 ºC, was added pyrrolidine (56 µL, 0.67 mmol, 1.2 equiv), PPh_3 (26 mg, 0.10 mmol, 0.18 equiv) and then [$Pd(PPh_3)_4$] (24 mg, 0.02 mmol, 0.04 equiv). After stirring for 1 h at 0 ºC, EtOAc (25 mL) was added and the solution was extracted with aqueous $NaHCO_3$ (4 × 10 mL). The combined aqueous layers were acidified to pH 2 with a 1 M $KHSO_4$ solution and then extracted with CH_2Cl_2. The resulting organic layer was dried over Na_2SO_4 and the solvent evaporated to afford product **90** as a fluffy white solid (209 mg, 95%).

Mp: 85-86 ºC

[α]$^{26}_D$ = -69.9 (*c* 1.0, $CHCl_3$)

^{1}H NMR (400 MHz, $CDCl_3$, 50ºC) δ: 10.02 (br s, 1H), 8.05 (br s, 1H), 7.25-7.37 (m, 5H), 5.59 (d, 1H, *J*=14.2 Hz), 5.36 (br s, 1H), 4.52 (d, 1H, *J*=11.4 Hz), 4.03 (br s, 1H), 3.88 (s, 1H), 3.79-3.85 (m, 1H), 3.49-3.54 (m, 1H), 3.28 (dd, 1H, J_1=17.7 Hz, J_2=2.3 Hz), 2.74 (dd, 1H, J_1=17.7 Hz, J_2=11.4 Hz), 1.50 (s, 9H).

^{13}C NMR (100 MHz, $CDCl_3$, 50ºC) δ: 175.1, 168.1, 164.9, 157.0, 135.4, 129.4, 128.8, 128.6, 81.4, 59.5, 52.4, 47.3, 40.9, 40.6, 28.7.

IR (Nujol) v_{max}: 3382, 3325, 3227, 1715, 1659, 1647, 1272, 1162, 1125.

HRMS (ESI) *m/z* calcd for [$C_{19}H_{25}N_3NaO_6$]$^+$: 414.16356 [M+Na]$^+$; found: 414.16367.

Boc-(*S,S*)-DKP-90-NH-CH_2-Ph (109)

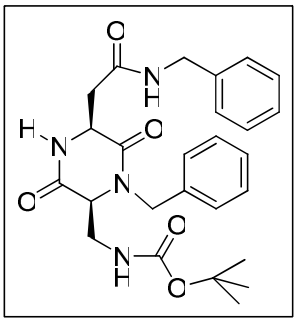

According to general procedure B (without DIPEA, because no TFA salt of the amino acid was present), coupling of benzylamine (26 mL, 0.24 mmol) with DKP-**90** (98 mg, 0.25 mmol, 1.05 equiv), afforded product **109** (103 mg, 90%) as a white solid after purification by flash chromatography on silica gel (CH_2Cl_2/CH_3OH, 95/5).

Mp: 88-90 ºC

$[\alpha]^{23}_D$ = -100.7 (*c* 0.29, $CHCl_3$)

^{1}H NMR (400 MHz, DMSO-d_6, 50 ºC) δ: 8.33 (br s, 1H), 7.93 (br s, 1H), 7.26-7.36 (m, 10H), 6.85 (br s, 1H), 5.17 (d, 1H, *J*=15.3 Hz), 4.31-4.41 (m, 3H), 4.13 (d, 1H, *J*=15.3 Hz), 3.78 (t, 1H, *J*=4.2 Hz), 3.55 (dt, 1H, J_1=14.1 Hz, J_2=5.6 Hz), 3.44 (dt, 1H, J_1=14.1 Hz, J_2=4.2 Hz), 2.83 (dd, 1H, J_1=15.3 Hz, J_2=3.8 Hz), 2.74 (dd, 1H, J_1=15.3 Hz, J_2=7.9 Hz), 1.38 (s, 9H).

^{13}C NMR (100 MHz, DMSO-d_6) δ: 170.2, 166.6, 165.9, 156.5, 139.9, 137.5, 129.4, 129.2, 128.6, 128.3, 128.2, 127.7, 78.9, 59.5, 52.9, 47.6, 43.1, 41.9, 41.3, 29.0.

IR (Nujol) ν_{max}: 3301, 3198, 3168, 1711, 1658, 1643, 1276, 1167, 1126.

MS (FAB$^+$) *m/z* 481 ($[M+1]^+$, 14%), 425 (21%), 381 (32%), 245 (15%), 154 (33%), 136 (30%), 91 (100%).

Anal. Calcd for $C_{26}H_{32}N_4O_5$: C 64.98, H 6.71, N 11.66; found C 64.63, H 6.83, N 11.48.

Ac-(*S,S*)-DKP-90-NH-CH_2-Ph (91)

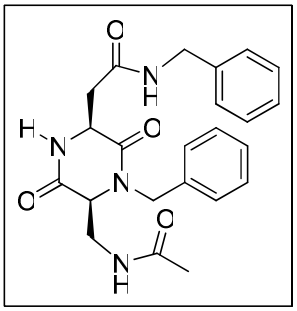

Compound **109** (48 mg, 0.10 mmol) was deprotected according to general procedure A. To a solution of the corresponding trifluoroacetate salt in CH_2Cl_2 (2.0 mL) and DIPEA (52 μL, 0.30 mmol, 3 equiv), was added the acetic anhydride (28 μL, 0.30 mmol, 3 equiv) and the solution was stirred at r.t. during 18 h. The mixture was concentrated *in vacuo* and the residue was recrystallized from methanol to afford **91** as a white solid (35 mg, 80%).

Mp: 136-138 ºC

$[\alpha]^{27}_D$ = -84.9 (*c* 1.0, $CHCl_3$)

^{1}H NMR (400 MHz, $CDCl_3$) δ: 8.29 (br s, 1H), 7.63 (br s, 1H), 7.39 (br s, 1H), 7.18-7.35 (m, 10H), 5.35 (d, 1H, *J*=15.2 Hz), 4.25-4.41 (m, 3H), 4.18 (d, 1H, *J*=15.2 Hz), 3.88 (m, 1H), 3.72 (m, 2H), 3.05 (dd, 1H, J_1=15.7 Hz, J_2=3.1 Hz), 2.96 (dd, 1H, J_1=15.7 Hz, J_2=8.8 Hz), 1.80 (s, 3H).

^{13}C NMR (100 MHz, $CDCl_3$) δ: 171.9, 170.4, 166.3, 166.2, 138.0, 135.7, 129.4, 129.0, 128.6, 128.5, 127.9, 58.3, 52.9, 47.4, 43.9, 40.2, 39.5, 23.0.

IR (Nujol) ν_{max}: 3264, 3224, 3199, 1645, 1551, 1302.

HRMS (ESI) *m/z* calcd for $[C_{23}H_{26}N_4NaO_4]^+$: 445.18463 $[M+Na]^+$; found: 445.18364.

Boc-(*S,S*)-DKP-90-(*S*)-Ala-NH-CH_2-Ph (111)

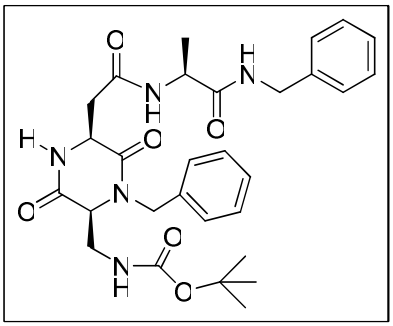

Boc-(*S*)-Ala-NH-CH_2-Ph (67 mg, 0.24 mmol) was deprotected according to general procedure A. Coupling of the corresponding trifluoroacetate salt with DKP-**90** (98 mg, 0.25 mmol, 1.05 equiv), according to general procedure B, afforded **111** (122 mg, 92%) as a white solid after purification by flash chromatography on silica gel (CH_2Cl_2/CH_3OH, 95/5).

Mp: 112-113 ºC

$[\alpha]^{28}_D$ = -98.4 (*c* 0.50, $CHCl_3$)

^{1}H NMR (400 MHz, $CDCl_3$, 40 ºC) δ: 7.48 (br s, 1H), 7.18-7.34 (m, 12H), 5.83 (br s, 1H), 5.41 (d, 1H, *J*=15.0 Hz), 4.51-4.59 (m, 1H), 4.35-4.44 (m, 3H), 3.99 (d, 1H, *J*=15.0 Hz), 3.78 (br s, 1H), 3.61-3.72 (m, 1H), 3.49-3.59 (m, 1H), 3.05 (dd, 1H, J_1=15.1 Hz, J_2=3.9 Hz), 2.74 (dd, 1H, J_1=15.1 Hz, J_2=8.8 Hz), 1.42 (s, 9H), 1.36 (d, 3H, *J*=6.9 Hz).

^{13}C NMR (100 MHz, $CDCl_3$, 40 ºC) δ: 172.5, 170.4, 166.4, 166.1, 156.4, 138.6, 135.6, 129.3, 128.9, 128.8, 128.5, 128.0, 127.7, 80.6, 59.2, 53.2, 49.6, 47.5, 43.9, 41.7, 41.4, 28.8, 18.5.
IR (Nujol) v_{max}: 3354, 3320, 3240, 1717, 1658, 1639, 1552, 1532, 1249, 1173, 1076.
MS (FAB$^+$) *m/z* 552 ([M+1]$^+$, 4%), 452 (18%), 369 (6%), 147 (31%), 109 (54%), 91 (100%).
Anal. Calcd for $C_{29}H_{37}N_5O_6$: C 63.14, H 6.76, N 12.70; found C 62.84, H 6.75, N 12.53.

Boc-(*S*)-Ala-(*S,S*)-DKP-90-(*S*)-Ala-NH-CH_2-Ph (92)

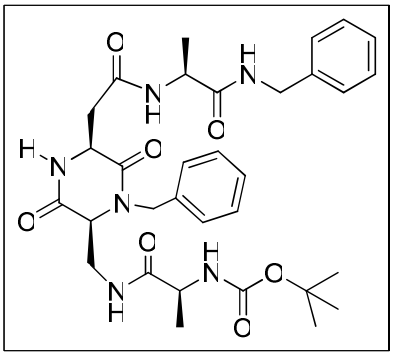

Compound **111** (61 mg, 0.11 mmol) was deprotected according to general procedure A. Coupling of the corresponding trifluoroacetate salt with Boc-(*S*)-Ala-OH (21 mg, 0.11 mmol, 1 equiv), according to general procedure C, afforded **92** (54 mg, 82%) as a white solid, after purification by flash chromatography on silica gel (CH_2Cl_2/CH_3OH, 95/5).
Mp: 127-128 ºC
$[\alpha]^{25}_D$ = -42.5 (*c* 0.41, CH_3OH)
^{1}H NMR (400 MHz, $CDCl_3$) δ: 8.20 (br s, 1H), 8.06 (br s, 1H), 7.75 (d, 1H, *J*=6.9 Hz), 7.55 (br s, 1H), 7.26-7.35 (m, 7H), 7.15-7.21 (m, 3H), 5.52 (d, 1H, *J*=7.5 Hz), 5.39 (d, 1H, *J*=15.0 Hz), 4.67 (t, 1H, *J*=6.0 Hz), 4.47 (t, 1H, *J*=6.7 Hz), 4.41 (br s, 2H), 4.08 (br s, 1H), 3.99 (br s, 1H), 3.96 (d, 1H, *J*=15.0 Hz), 3.75-3.82 (m, 2H), 3.16 (d, 1H, *J*=15.2 Hz), 2.80 (d, 1H, *J*=15.2 Hz), 1.42 (d, 3H, *J*=6.0 Hz), 1.29 (br s, 12H).
^{13}C NMR (100 MHz, $CDCl_3$) δ: 173.9, 173.7, 170.3, 166.1, 165.7, 155.9, 138.4, 135.5, 129.4, 129.0, 128.7, 128.5, 127.6, 127.2, 80.1, 57.1, 52.4, 49.8, 46.9, 43.6, 39.5, 38.3, 28.7, 20.8, 19.4.
IR ($CHCl_3$) v_{max}: 3429, 3395, 3330, 3295, 2930, 1689, 1657, 1556, 1506, 1449, 1368, 1332, 1255, 1166.
HRMS (ESI) *m/z* calcd for $[C_{32}H_{42}N_6NaO_7]^+$: 645.30072 [M+Na]$^+$; found: 645.29916.
Anal. Calcd for $C_{32}H_{42}N_6O_7$: C 61.72, H 6.80, N 13.50; found C 61.42, H 6.78, N 13.35.

Ac-(*S*)-Ala-(*S,S*)-DKP-90-(*S*)-Ala-NH-CH_2-Ph (93)

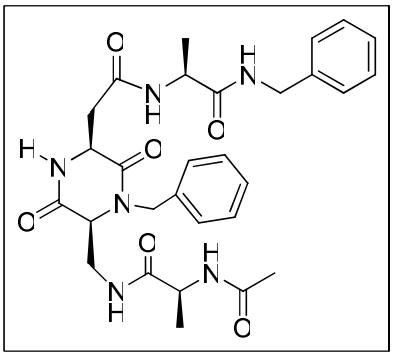

Compound **111** (72 mg, 0.13 mmol) was deprotected according to general procedure A. Coupling of the corresponding trifluoroacetate salt with Ac-(*S*)-Ala-OH (17 mg, 0.13 mmol, 1 equiv), according to general procedure C, afforded **93** (54 mg, 76%) as a white solid after purification by flash chromatography on silica gel (CH_2Cl_2/CH_3OH, 94/6).

Mp: 178-179 ºC

$[\alpha]^{27}_D$ = -22.8 (*c* 0.20, CH_3OH)

^{1}H NMR (400 MHz, $CDCl_3$) δ: 8.31 (br s, 1H), 8.27 (br s, 1H), 7.53 (br s, 1H), 7.22-7.37 (m, 11H), 6.55 (br s, 1H), 5.36 (d, 1H, *J*=14.9 Hz), 4.71-4.78 (m, 2H), 4.51 (dd, 1H, J_1=15.1 Hz, J_2=6.0 Hz), 4.28 (dd, 1H, J_1=15.1 Hz, J_2=4.3 Hz), 4.18 (br, 1H), 4.07 (d, 1H, *J*=14.9 Hz), 4.05 (br, 1H), 3.86-3.93 (m, 1H), 3.66-3.75 (m, 1H), 3.28-3.35 (m, 1H), 2.78-2.88 (m, 1H), 1.71 (s, 3H), 1.43 (d, 3H, *J*=6.8 Hz), 1.28 (d, 3H, *J*=7.0 Hz).

^{13}C NMR (100 MHz, $CDCl_3$) δ: 173.4, 170.4, 169.8, 166.1, 165.4, 138.2, 135.6, 129.4, 129.1, 128.6, 128.5, 127.8, 57.3, 52.3, 49.6, 48.8, 47.1, 43.9, 39.6, 38.2, 23.4, 20.3, 19.7.

IR ($CHCl_3$) ν_{max}: 3413, 3290, 2931, 1687, 1652, 1556, 1518, 1448, 1372, 1330, 1281.

HRMS (ESI) *m/z* calcd for $[C_{29}H_{36}N_6NaO_6]^+$: 587.25885 $[M+Na]^+$; found: 587.25770.

Boc-(*S*)-Ala-NH-*n*Bu (112)

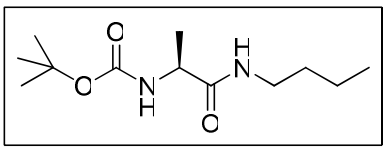

According to general procedure B (without DIPEA, because no TFA salt of the amino acid was present), coupling of butylamine (200 µL, 2.0 mmol) with Boc-(*S*)-Ala-OH (405 mg, 2.1 mmol, 1.05 equiv), afforded **112** (467 mg, 95%) as a white solid.

Mp: 75-76 ºC

$[\alpha]^{27}_D$ = -33.9 (*c* 1.0, $CHCl_3$)

^{1}H NMR (400 MHz, $CDCl_3$) δ: 6.36 (br s, 1H), 5.14 (br s, 1H), 4.14 (br, 1H), 3.22-3.27 (m, 2H), 1.44-1.50 (m, 2H), 1.44 (s, 9H), 1.34 (d, 3H, *J*=7.0 Hz), 1.28-1.39 (m, 2H), 0.91 (t, 3H, *J*=7.3 Hz).

^{13}C NMR (100 MHz, $CDCl_3$) δ: 173.2, 155.9, 80.1, 50.4, 39.4, 31.9, 28.7, 20.3, 19.1, 14.1.

IR (Nujol) ν_{max}: 3328, 3280, 1683, 1652, 1554, 1529, 1322, 1248, 1170, 1071, 1023.

MS (FAB$^+$) *m/z* 245 ([M+1]$^+$, 28%), 189 (100%), 145 (95%).

Anal. Calcd for $C_{12}H_{24}N_2O_3$: C 58.99, H 9.90, N 11.47; found C 59.35, H 10.25, N 11.22.

Boc-(*S*)-Val-(*S*)-Ala-NH-*n*Bu (113)

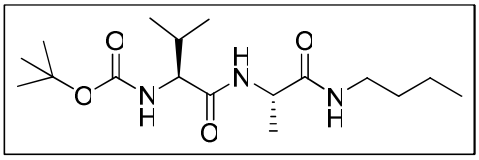

Compound **112** (244 mg, 1.0 mmol) was deprotected according to general procedure A. Coupling of the corresponding trifluoroacetate salt with Boc-(*S*)-Val-OH (228 mg, 1.05 mmol, 1.05 equiv), according to general procedure B, afforded **113** (338 mg, 96%) as a white solid.

Mp: 147-149 ºC

$[\alpha]^{26}_D$ = -45.5 (*c* 0.53, $CHCl_3$)

^{1}H NMR (400 MHz, $CDCl_3$) δ: 6.67 (d, 1H, *J*=6.2 Hz), 6.45 (br s, 1H), 5.07 (d, 1H, *J*=7.3 Hz), 4.44-4.52 (m, 1H), 3.95 (br, 1H), 3.17-3.32 (m, 2H), 2.12-2.20 (m, 1H), 1.44-1.53 (m, 2H), 1.46 (s, 9H), 1.39 (d, 3H, *J*=7.0 Hz), 1.30-1.39 (m, 2H), 0.98 (d, 3H, *J*=6.8 Hz), 0.90-0.94 (m, 6H).

^{13}C NMR (100 MHz, $CDCl_3$) δ: 172.3, 172.0, 156.4, 80.4, 60.3, 49.3, 39.6, 31.9, 31.4, 28.7, 20.4, 19.6, 18.7, 18.1, 14.1

IR (Nujol) ν_{max}: 3333, 3290, 1689, 1647, 1554, 1529, 1304, 1248, 1173, 1047, 1021.

MS (FAB$^+$) *m/z* 344 ([M+1]$^+$, 36%), 288 (75%), 244 (15%), 145 (100%), 116 (41%).

Anal. Calcd for $C_{17}H_{33}N_3O_4$: C 59.45, H 9.68, N 12.23; found C 59.72, H 9.89, N 12.04.

Boc-(*S,S*)-DKP-90-(*S*)-Val-(*S*)-Ala-NH-*n*Bu (114)

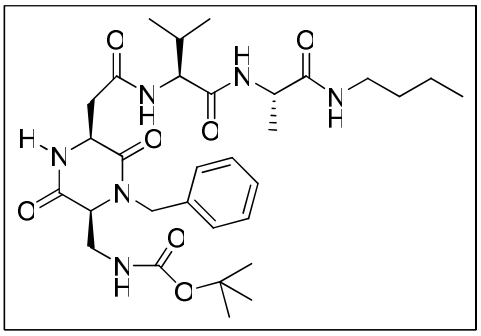

Compound **113** (113 mg, 0.33 mmol) was deprotected according to general procedure A. Coupling of the corresponding trifluoroacetate salt with DKP-**90** (137 mg, 0.35 mmol, 1.05 equiv), according to general procedure B, afforded **114** (161 mg, 80%) as a white solid after purification by flash chromatography on silica gel (CH_2Cl_2/CH_3OH, 94/6).

Mp: 117-119 ºC

$[\alpha]^{20}_D$ = -102.8 (*c* 0.50, $CHCl_3$)

^{1}H NMR (400 MHz, $CDCl_3$, 45 ºC) δ: 7.25-7.37 (m, 6H), 7.14 (br s, 1H), 6.98 (br s, 1H), 6.52 (br s, 1H), 5.49 (d, 1H, *J*=15.0 Hz), 5.42 (br s, 1H), 4.47-4.56 (m, 2H), 4.33 (t, 1H, *J*=7.3 Hz), 4.08 (d, 1H, *J*=15.0 Hz), 3.84-3.86 (m, 1H), 3.72-3.78 (m, 1H), 3.57-3.62 (m, 1H), 3.17-3.31 (m, 3H), 2.75 (dd, 1H, J_1=15.4 Hz, J_2=8.9 Hz), 2.11-2.21 (m, 1H), 1.45-1.52 (m, 11H), 1.38 (d, 3H, *J*=7.0 Hz), 1.30-1.36 (m, 2H), 0.99 (d, 3H, *J*=4.0 Hz), 0.97 (d, 3H, *J*=4.0 Hz), 0.91 (t, 3H, *J*=7.2 Hz).

^{13}C NMR (100 MHz, $CDCl_3$) δ: 172.5, 171.2, 171.1, 166.1, 156.5, 135.3, 129.5, 128.8, 80.4, 59.1, 58.9, 53.2, 49.2, 47.4, 41.0, 39.6, 31.9, 31.7, 28.8, 20.4, 19.6, 18.8, 14.1.

IR ($CHCl_3$) ν_{max}: 3439, 3363, 3344, 3309, 2972, 2935, 2875, 1682, 1653, 1526, 1509, 1453, 1393, 1369, 1335, 1165.

MS (FAB$^+$) *m/z* 617 ([M+1]$^+$, 23%), 517 (100%), 487 (11%), 318 (18%), 245 (16%), 154 (40%), 136 (32%), 91 (79%).

Anal. Calcd for $C_{31}H_{48}N_6O_7$: C 60.37, H 7.84, N 13.63; found C 60.16, H 8.01, N 13.36.

Boc-(*S*)-Ala-(*S,S*)-DKP-90-(*S*)-Val-(*S*)-Ala-NH-*n*Bu (94)

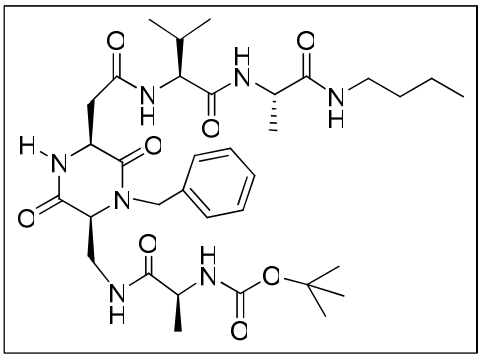

Compound **114** (148 mg, 0.24 mmol) was deprotected according to general procedure A. Coupling of the corresponding trifluoroacetate salt with Boc-(*S*)-Ala-OH (46 mg, 0.24 mmol, 1 equiv), according to general procedure C, afforded **94** (142 mg, 85%) as a white solid after purification by flash chromatography on silica gel (CH_2Cl_2/CH_3OH, 95/5).

Mp: 129-131 ºC

$[\alpha]^{22}_D$ = -31.0 (*c* 0.23, CH_3OH)

^{1}H NMR (400 MHz, $CDCl_3$, 45 ºC) δ: 7.68 (br s, 1H), 7.54 (d, 1H, *J*=6.1 Hz), 7.47 (br s, 1H), 7.27-7.36 (m, 5H), 7.21 (br s, 1H), 6.48 (br s, 1H), 5.43 (d, 1H, *J*=15.0 Hz), 5.35 (br s, 1H), 4.41-4.48 (m, 3H), 4.37 (t, 1H, *J*=7.3 Hz), 4.05 (d, 1H, *J*=15.0 Hz), 3.99 (br s, 1H), 3.86-3.92 (m, 1H), 3.73-3.79 (m, 1H), 3.15-3.30 (m, 2H), 3.10 (dd, 1H, J_1=15.5 Hz, J_2=4.7 Hz), 2.98 (dd, 1H, J_1=15.5 Hz, J_2=5.6 Hz), 2.12-2.20 (m, 1H), 1.44-1.51 (m, 11H), 1.37 (d, 6H, *J*=7.0 Hz), 1.29-1.36 (m, 2H), 1.02 (d, 3H, *J*=4.6 Hz), 1.00 (d, 3H, *J*=4.6 Hz), 0.92 (t, 3H, *J*=7.3 Hz).

^{13}C NMR (100 MHz, $CDCl_3$) δ: 174.3, 172.9, 171.9, 170.9, 166.3, 166.1, 156.1, 135.4, 129.4, 128.8, 128.6, 80.5, 59.8, 57.4, 52.8, 50.2, 47.1, 39.7, 31.9, 31.3, 28.8, 20.4, 20.3, 19.4, 18.7, 17.9, 14.1.

IR (Nujol) ν_{max}: 3504, 3389, 3314, 3288, 3198, 1680, 1660, 1629, 1540, 1528, 1248, 1166.

HRMS (ESI) *m/z* calcd for $[C_{34}H_{53}N_7NaO_8]^+$: 710.38478 $[M+Na]^+$; found: 710.38410.

Anal. Calcd for $C_{34}H_{53}N_7O_8$: C 59.37, H 7.77, N 14.25; found C 59.04, H 7.78, N 13.98.

Boc-(*S*)-Val-(*S*)-Ala-(*S,S*)-DKP-90-(*S*)-Val-(*S*)-Ala-NH-*n*Bu (95)

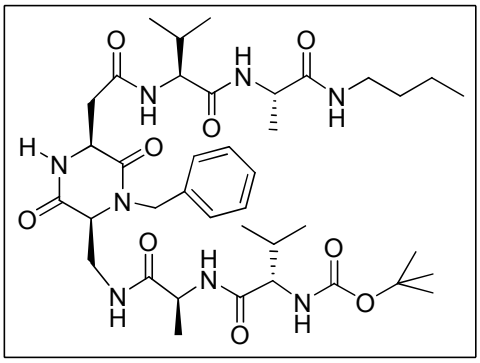

Compound **94** (76 mg, 0.11 mmol) was deprotected according to general procedure A. The corresponding trifluoroacetate salt was then coupled to Boc-(*S*)-Val-OH (21 mg, 0.11 mmol, 1 equiv), a slightly modified general procedure C (no aqueous quenching and immediate purification of the reaction mixture by flash chromatography on silica gel, CH_2Cl_2/CH_3OH, 96/4), which afforded **95** (61 mg, 70%) as a white solid.

Mp: 235-236 ºC

$[\alpha]^{22}_D$ = -26.0 (*c* 0.39, CH_3OH)

^{1}H NMR (400 MHz, DMSO-d_6) δ: 8.31 (br s, 1H), 8.27 (d, 1H, *J*=8.1 Hz), 8.26 (s, 1H), 8.12 (d, 1H, *J*=7.4 Hz), 8.02 (d, 1H, *J*=7.8 Hz), 7.72 (t, 1H, *J*=5.6 Hz), 7.23-7.33 (m, 5H), 6.87 (d, 1H, *J*=9.1 Hz), 4.86 (d, 1H, *J*=14.8 Hz), 4.53 (t, 1H, *J*=7.4 Hz), 4.25-4.38 (m, 4H), 3.85-3.94 (m, 2H), 3.48-3.62 (m, 2H), 3.01-3.10 (m, 2H), 2.77-2.90 (m, 2H), 1.91-2.02 (m 2H), 1.37 (s, 9H), 1.34-1.41 (m, 2H), 1.23-1.30 (m, 2H), 1.20 (d, 3H, *J*=7.1 Hz), 1.12 (d, 3H, *J*=6.9 Hz), 0.78-0.91 (m, 15H).

^{13}C NMR (100 MHz, DMSO-d_6) δ: 173.1, 172.5, 171.9, 170.9, 170.6, 167.3, 165.6, 156.3, 137.7, 129.3, 128.5, 128.1, 78.9, 60.3, 59.3, 58.8, 52.4, 49.1, 48.6, 48.0, 40.9, 39.5, 38.9, 32.0, 31.9, 31.5, 29.0, 20.2, 20.1, 19.9, 19.6, 19.1, 19.1, 18.8, 14.5.

IR (Nujol) ν_{max}: 3310, 3278, 3273, 3247, 3231, 3174, 1685, 1668, 1633, 1532, 1172.

HRMS (ESI) *m/z* calcd for $[C_{39}H_{62}N_8NaO_9]^+$: 809.45320 $[M+Na]^+$; found: 809.45219.

Anal. Calcd for $C_{39}H_{62}N_8O_9$: C 59.52, H 7.94, N 14.24; found C 59.22, H 7.87, N 13.98.

Ac-(*S*)-Val-(*S*)-Ala-(*S,S*)-DKP-90-(*S*)-Val-(*S*)-Ala-NH-*n*Bu (96)

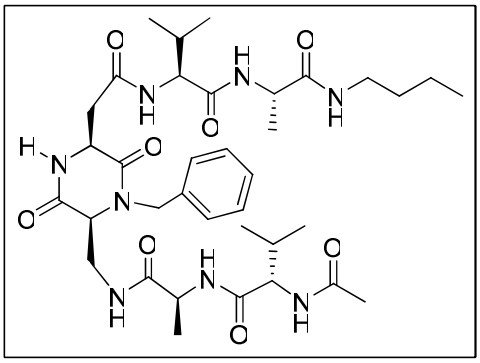

Compound **94** (83 mg, 0.12 mmol) was deprotected according to general procedure A. The corresponding trifluoroacetate salt was then coupled to Ac-(*S*)-Val-OH (19 mg, 0.12 mmol, 1 equiv), according to a slightly modified general procedure C (no aqueous quenching and immediate purification of the reaction mixture by flash chromatography on silica gel, CH_2Cl_2/CH_3OH, 90/10), which afforded **96** (50 mg, 60%) as a white solid.

Mp: 257-258 ºC

$[\alpha]^{22}_D$ = +15.7 (*c* 0.23, CH_3OH)

^{1}H NMR (400 MHz, DMSO-d_6) δ: 8.29 (d, 1H, *J*=7.2 Hz), 8.28 (br s, 1H), 8.25 (t, 1H, *J*=5.3 Hz), 8.19 (d, 1H, *J*=7.8 Hz), 8.18 (d, 1H, *J*=7.9 Hz), 7.96 (d, 1H, *J*=8.9 Hz), 7.83 (t, 1H, *J*=5.6 Hz), 7.24-7.32 (m, 5H), 4.92 (d, 1H, *J*=15.6 Hz), 4.51 (t, 1H, *J*=7.3 Hz), 4.38 (t, 1H, *J*=7.3 Hz), 4.32 (t, 1H, *J*=7.5 Hz), 4.22-4.29 (m, 3H), 3.89-3.91 (m, 1H), 3.49-3.62 (m, 2H), 3.05 (q, 2H, *J*=6.5 Hz), 2.78-2.89 (m, 2H), 1.89 (s, 3H), 1.86-1.99 (m, 2H), 1.34-1.41 (m, 2H), 1.23-1.30 (m, 2H), 1.20 (d, 3H, *J*=7.0 Hz), 1.13 (d, 3H, *J*=7.0 Hz), 0.89 (d, 3H, *J*=3.9 Hz), 0.87 (d, 3H, *J*=3.9 Hz), 0.80-0.85 (m, 9H).

^{13}C NMR (100 MHz, DMSO-d_6) δ: 173.2, 172.7, 171.8, 170.9, 170.6, 170.1, 167.2, 165.6, 137.6, 129.3, 128.6, 128.1, 59.1, 58.8, 58.3, 52.4, 48.9, 48.6, 47.9, 39.6, 38.9, 31.9, 31.9, 31.7 , 23.3, 20.2, 20.1, 19.9, 19.4, 19.3, 19.1, 19.0, 14.5.

IR (Nujol) ν_{max}: 3521, 3418, 3276, 3243, 1685, 1649, 1629, 1539, 1224, 1156, 1075.

HRMS (ESI) *m/z* calcd for $[C_{36}H_{56}N_8NaO_8]^+$: 751.41133 $[M+Na]^+$; found: 751.41109.

Cbz-Arg(Mtr)-Gly-OMe (130)

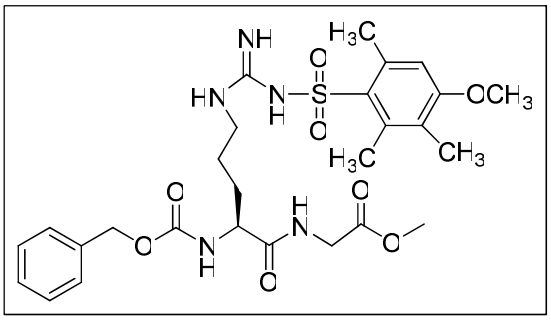

Cbz-Arg(Mtr)-OH•CHA (1.76 g, 3.4 mmol, 1.05 eq) was dissolved in EtOAc (200 mL) and washed with 1 M $KHSO_4$ (2 × 50 mL). The organic layer was dried over Na_2SO_4, filtered and concentrated under reduced pressure. Coupling of the corresponding free acid Cbz-Arg(Mtr)-OH with HCl•H-Gly-OMe (404 mg, 3.22 mmol, 1 equiv), according to general procedure D, afforded **130** (1.56 g, 78%) as a white solid after purification by flash chromatography on silica gel (EtOAc/CH_3OH, 97/3).

Mp: 69-70 °C

$[\alpha]^{26}_D$ = +16.9 (*c* 1.0, $CHCl_3$)

^{1}H NMR (400 MHz, $CDCl_3$) δ: 7.61 (t, 1H, *J*=5.2 Hz), 7.29-7.34 (m, 5H), 6.53 (s, 1H), 6.33 (s, 2H), 6.12 (br s, 1H), 6.01 (d, 1H, *J*=7.9 Hz), 5.07 (s, 2H), 4.35-4.39 (m, 1H), 4.02 (dd, 1H, J_1=17.8 Hz, J_2=5.5 Hz), 3.89 (dd, 1H, J_1=17.8 Hz, J_2=5.5 Hz), 3.83 (s, 3H), 3.67 (s, 3H), 3.36-3.13 (m, 2H), 2.67 (s, 3H), 2.61 (s, 3H), 2.13 (s, 3H), 1.86-1.92 (m, 1H), 1.70-1.62 (m, 3H).

^{13}C NMR (100 MHz, $CDCl_3$) δ: 173.3, 171.1, 159.0, 157.0, 156.9, 138.9, 137.0, 136.6, 133.7, 128.9, 128.5, 128.3, 125.3, 112.2, 67.4, 55.8, 54.5, 52.7, 41.5, 40.6, 30.4, 25.6, 24.5, 18.7, 12.4.

IR (KBr) ν_{max}: 3343, 2944, 1719, 1671, 1622, 1551, 1250, 1175.

HRMS (ESI) *m/z* calcd for $[C_{27}H_{37}N_5O_8SNa]^+$: 614.22550 $[M+Na]^+$; found: 614.22460.

H_2N-Arg(Mtr)-Gly-OMe (131)

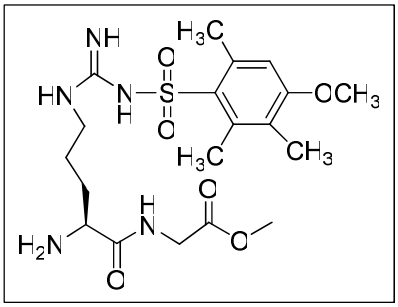

Compound **130** (450 mg, 0.76 mmol) was dissolved in methanol (20 mL) and $Pd(OH)_2/C$ (45 mg, 10% weight) was added. The reaction flask was purged three times with hydrogen, and stirring was maintained under hydrogen atmosphere at r.t. overnight. The mixture was filtered trough Celite, and the cake was washed thoroughly with methanol. The filtrate was concentrated and dried, under vacuum, to give product **131** (345 mg, 99 %) as a white foam, that was used without further purification.

^{1}H NMR (400 MHz, $CDCl_3$) δ: 7.95 (t, 1H, *J*=5.6 Hz), 6.53 (s, 1H), 6.41 (br, 3H), 4.00 (d, 2H, *J*=5.7 Hz), 3.83 (s, 3H), 3.72 (s, 3H), 3.44-3.52 (m, 1H), 3.18-3.26 (m, 2H), 2.67 (d, 3H, *J*=7.3 Hz), 2.60 (d, 3H, *J*=7.4 Hz), 2.13 (d, 3H, *J*=3.8 Hz), 2.05 (br s, 2H), 1. 77-1.92 (m, 1H), 1. 56-1.72 (m, 3H).

^{13}C NMR (100 MHz, $CDCl_3$) δ: 175.8, 171.0, 158.9, 157.0, 138.8, 136.9, 133.8, 125.2, 112.2, 55.8, 54.6, 52.7, 41.3, 41.0, 32.1, 25.6, 24.5, 18.7, 12.4.

IR (KBr) ν_{max}: 3436, 3343, 2942, 1751, 1690, 1624, 1555, 1119.

MeO-Gly-Arg(Mtr)-DKP-90-NHBoc (132)

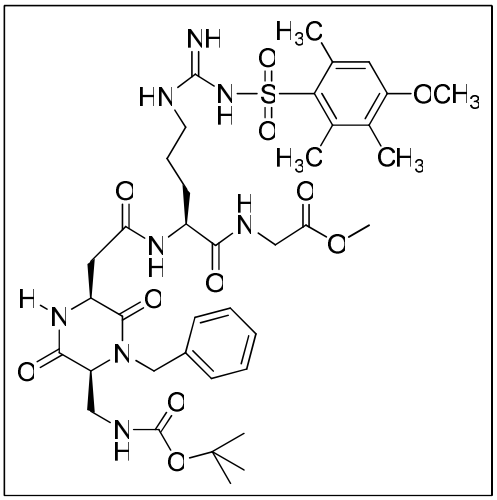

According to general procedure D, coupling of **131** (119 mg, 0.26 mmol) with DKP-**90** (100 mg, 0.26 mmol, 1 equiv), afforded **132** (156 mg, 72%) as a white solid after purification by flash chromatography on silica gel (CH_2Cl_2/CH_3OH, 93/7).

Mp: 121-122 ℃

$[\alpha]^{24}_D$ = -48.9 (*c* 0.94, $CHCl_3$)

^{1}H NMR (400 MHz, $CDCl_3$) δ: 7.96 (s, 1H), 7.50-7.77 (m, 2H), 7.25-7.30 (m, 5H), 6.52 (s, 1H), 6.41 (br s, 3H), 6.09 (br s, 1H), 5.44 (d, 1H, *J* = 14.5 Hz), 4.57 (br s, 1H), 3.99-4.10 (m, 3H), 3.77-3.83 (m, 4H), 3.63-3.76 (m, 5H), 3.38-3.55 (m, 1H), 3.10-3.33 (m, 3H), 2.78-2.96

(m, 1H), 2.66 (s, 3H), 2.59 (s, 3H), 2.12 (s, 3H), 1.83-1.98 (m, 1H), 1.54-1.80 (m, 2H), 1.41 (s, 9H).

^{13}C NMR (100 MHz, $CDCl_3$) δ: 173.0, 171.1, 166.9, 166.3, 158.9, 156.9, 156.6, 138.9, 136.9, 135.7, 133.8, 129.4, 128.8, 128.5, 125.3, 112.2, 80.4, 59.1, 55.8, 53.4, 53.0, 52.8, 47.6, 41.5, 41.0, 30.1, 28.8, 25.5, 24.5, 18.7, 12.4.

IR (KBr) ν_{max}: 3337, 1655, 1551, 1453, 1254, 1167, 1119.

HRMS (ESI) *m/z* calcd for $[C_{38}H_{54}N_8O_{11}SNa]^+$: 853.35250 $[M+Na]^+$; found: 853.35043.

MeO-Gly-Arg(Mtr)-DKP-90-Asp(O*t*Bu)-Cbz (133)

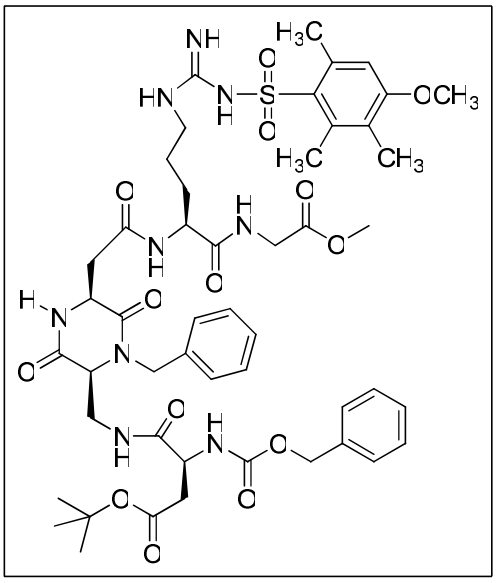

Compound **132** (290 mg, 0.34 mmol) was deprotected according to general procedure A. The corresponding trifluoroacetate salt was then coupled to Cbz-L-Asp(O*t*Bu)-OH (167 mg, 0.52 mmol, 1.5 equiv), according to general procedure E, afforded **133** (298 mg, 84%) as a white solid after purification by flash chromatography on silica gel (CH_2Cl_2/CH_3OH, 93/7).

Mp: 122-123 °C

$[\alpha]^{24}_D$ = -30.6 (*c* 1.0, $CHCl_3$)

^{1}H NMR (400 MHz, $CDCl_3$) δ: 7.97 (m, 3H), 7.0 (br s, 1H), 7.29 (m, 10H), 6.52 (s, 1H), 6.31 (s, 3H), 6.11 (br s, 1H), 5.39 (d, 1H, *J*=13.9 Hz), 5.09 (d, 1H, *J*=12.0 Hz), 5.00 (d, 1H, *J*=12.0 Hz), 4.67-4.71 (m, 2H), 4.41 (br s, 1H), 3.88-4.01 (m, 4H), 3.82 (s, 3H), 3.68-3.72 (m, 2H), 3.64 (s, 3H), 2.95-3.21 (m, 4H), 2.60-2.68 (m, 8H), 2.12 (s, 3H), 1.81-1.96 (m, 1H), 1.65-1.75 (s, 3H), 1.39 (s, 9H).

^{13}C NMR (100 MHz, $CDCl_3$) δ: 173.4, 171.7, 171.0, 170.9, 170.7, 166.4, 166.0, 158.9, 156.8, 156.6, 139.0, 137.1, 136.5, 135.5, 129.4, 128.9, 128.7, 128.6, 128.5, 128.2, 125.3, 112.2,

82.2, 67.2, 57.5, 55.8, 53.5, 52.7, 52.5, 51.9, 47.1, 41.6, 40.9, 39.9, 39.4, 30.1, 28.4, 25.5, 24.5, 18.7, 12.4.

IR (KBr) ν_{max}: 3443, 2928, 1655, 1547, 1453, 1385, 1262, 1117.

HRMS (ESI) *m/z* calcd for $[C_{49}H_{65}N_9O_{14}SNa]^+$: 1058.42639 $[M+Na]^+$; found: 1058.42503.

BnO-Gly-Arg(Mtr)-DKP-90-Asp(O*t*Bu)-Cbz (134)

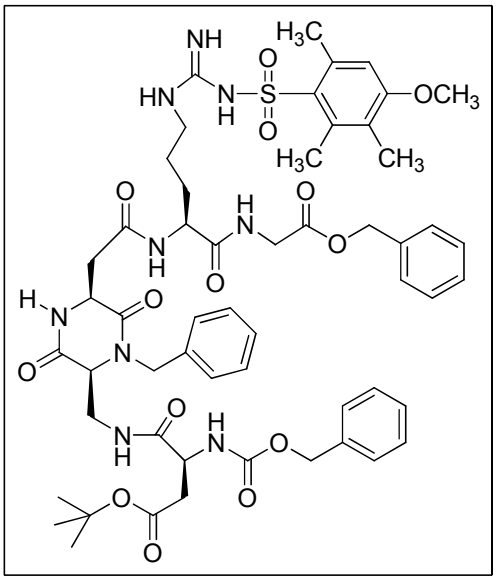

To a solution of **133** (153 mg, 0.15 mmol) in dry THF (5 mL), under nitrogen atmosphere, freshly distilled benzyl alcohol (1.52 mL, 14.4 mmol, 100 equiv), and molecular sieves 4 Å (300 mg), and $Ti(O\textit{i}Pr)_4$, (50 μL, 0.16 mmol, 1.05 equiv) were added. The suspension was stirred at 90 ºC for 20 h, then filtered through a pad of celite and washed with THF. The solvent was evaporated under reduced pressure and the crude residue was purified by flash chromatography on silica gel (CH_2Cl_2/ CH_3OH, 93/7) to afford **134** as a white solid (159 mg, 97%).

Mp: 135-137 ℃

$[\alpha]^{24}_D$ = -23.8 (*c* 0.73, $CHCl_3$)

^{1}H NMR (400 MHz, $CDCl_3$) δ: 7.96 (m, 2H), 7.66 (br s, 1H), 7.27-7.38 (m, 16H), 6.52 (s, 1H), 6.27 (s, 3H), 6.10 (d, 1H, *J*=8.6 Hz), 5.39 (d, 1H, *J*=15.6 Hz), 5.05-5.11 (m, 1H), 4.95 (d, 1H, *J*=12.4 Hz), 4.58-4.77 (m, 4H), 4.37 (br s, 1H), 3.93-4.06 (m, 4H), 3.82 (s, 3H), 3.69 (m, 1H), 3.07-3.20 (m, 3H), 2.94 (d, 1H, *J*=16.1 Hz), 2.60-2.68 (m, 8H), 2.12 (s, 3H), 1.55-1.97 (m, 3H), 1.39 (s, 9H).

^{13}C NMR (100 MHz, $CDCl_3$) δ: 173.3, 171.7, 170.9, 170.5, 170.1, 166.3, 166.0, 158.9, 156.9, 156.6, 138.9, 137.0, 136.4, 135.6, 135.8, 129.4, 129.0, 128.9, 128.8, 128.7, 128.6, 128.5,

128.2, 125.2, 112.1, 82.1, 67.5, 65.8, 57.5, 55.8, 53.5, 52.5, 51.9, 47.1, 41.7, 40.9, 39.9, 39.5, 39.4, 29.9, 28.4, 25.5, 24.5, 18.7, 12.4.

IR (KBr) ν_{max}: 3339, 2940, 1655, 1547, 1259, 1119.

HRMS (ESI) *m/z* calcd for $[C_{55}H_{69}N_9O_{14}SNa]^+$: 1134.45769 $[M+Na]^+$; found: 1134.45891.

HO-Gly-Arg(Mtr)-DKP-90-Asp(O*t*Bu)-NH_2 (135)

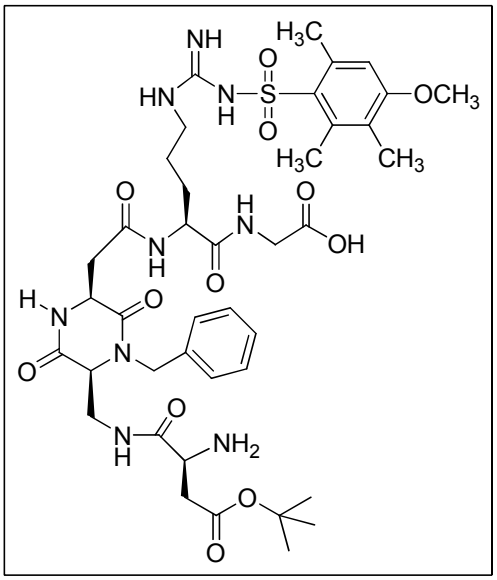

Compound **134** (160 mg, 0.14 mmol) was dissolved in methanol (10 mL) and Pd/C (32 mg, 20% weight) was added. The reaction flask was purged three times with hydrogen, and stirring was maintained under hydrogen atmosphere at r.t. overnight. The mixture was filtered trough Celite, and the cake was washed thoroughly with methanol. The filtrate was concentrated and dried to give the desired product **135** (124 mg, 100 %) as a white foam, that was used without further purification.

Mp: 180-182 ℃

^{1}H NMR (400 MHz, CD_3OD) δ: 7.29-7.39 (m, 5H), 6.67 (s, 1H), 5.23 (d, 1H, *J*=15.5 Hz), 5.04 (d, 1H, *J*=14.8 Hz), 4.45-4.53 (m, 2H), 4.30 (d, 1H, *J*=15.2 Hz), 4.15 (s, 1H), 3.67-4.08 (m, 9H), 3.36 (s, 2H), 3.21 (br s, 2H), 2.94 (m, 2H), 2.59-2.69 (m, 8H), 2.13 (s, 3H), 1.82-1.94 (m, 1H), 1.56-1.75 (m, 3H), 1.45 (s, 9H).

^{13}C NMR (100 MHz, CD_3OD) δ: 173.4, 173.0, 171.0, 170.0, 168.5, 167.5, 166.1, 158.9, 138.9, 138.5, 136.9, 133.8, 128.9, 128.3, 127.9, 124.7, 111.8, 83.1, 65.9, 58.7, 55.0, 53.3, 52.1, 49.8, 42.3, 40.6, 38.0, 36.4, 31.7, 29.5, 27.4, 26.0, 23.3, 22.7, 17.8, 11.1.

IR (KBr) ν_{max}: 3447, 2935, 1657, 1552, 1253, 1157.

***Cyclo*[Arg(Mtr)-Gly-Asp(O*t*Bu)-DKP-90] (136)**

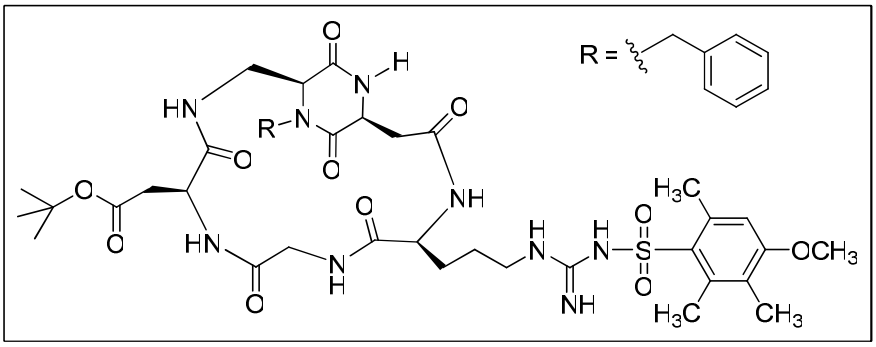

To a solution of crude **135** (120 mg, 0.135 mmol) in DMF (7.4 mL), under nitrogen atmosphere and at 0 ºC, HATU (103 mg, 0.27 mmol, 2 equiv), HOAt (0.54 mL, 0.27 mmol, 2 equiv) and 2,4,6-collidine (54 μL, 0.4 mmol, 3 equiv) were added. The reaction was stirred at 0 ºC for 1 h and at r.t. overnight. The mixture was then diluted with EtOAc (100 mL) and the organic layer was washed in order with: 1 M $KHSO_4$ (2 × 30 mL), aqueous $NaHCO_3$ (2 × 30 mL) and brine (2 × 20 mL), dried over Na_2SO_4 and volatiles were removed under reduced pressure. The residue was purified by flash chromatography on silica gel (CH_2Cl_2/CH_3OH, 90/10) to afford **136** as a white solid (71 mg, 61%).

Mp: 215-225 ℃

$[\alpha]^{24}_D$ = +36.75 (*c* 0.59, CH_3OH)

^{1}H NMR (400 MHz, CD_3OH) δ: 8.72 (t, 1H, *J*=6.0 Hz), 8.48 (d, 1H, *J*=3.5 Hz), 8.25 (br s, 1H), 7.97 (d, 1H, *J*=8.9 Hz), 7.76 (t, 1H, *J*=5.2 Hz), 7.27-7.38 (m, 5H), 6.68 (s, 1H), 6.52 (br s, 1H), 5.11 (d, 1H, *J*=15.3 Hz), 4.64-4.70 (m, 1H), 4.44 (t, 1H, *J*=3.6 Hz), 4.30 (d, 2H, *J*=15.3 Hz), 4.09-4.15 (m, 2H), 3.95-4.04 (m, 2H), 3.84 (s, 3H), 3.67 (dt, 1H, J_1=14.3 Hz, J_2=4.1 Hz), 3.49 (dd, 1H, J_1=16.5 Hz, J_2=5.1 Hz), 3.14-3.24 (m, 3H), 2.77-2.82 (m, 2H), 2.68 (s, 3H), 2.62 (s, 3H), 2.54 (d, 1H, *J*=9.1 Hz), 2.13 (s, 3H), 1.68-1.83 (m, 2H), 1.53-1.68 (m, 2H), 1.45 (s, 9H).

^{13}C NMR (100 MHz, CD_3OH) δ: 174.0, 172.2, 172.0, 170.8, 170.0, 167.2, 165.7, 158.9, 157.4, 138.4, 136.9, 136.1, 133.8, 128.9, 128.0, 127.9, 124.7, 111.8, 81.4, 58.5, 55.4, 55.0, 52.1, 52.0, 43.7, 47.5, 40.4, 39.3, 38.4, 37.2, 27.7, 27.3, 26.0, 23.3, 17.8, 11.1.

IR (KBr) ν_{max}: 3429, 2937, 1655, 1545, 1450, 1258, 1120.

II. CHAPTER III EXPERIMENTAL PART

MATERIALS AND METHODS: Usual solvents were purchased from commercial sources. Dimethylformamide (DMF) was distilled from $CaSO_4$, tetrahydrofurane (THF) was distilled from sodium/benzophenone, acetonitrile was distilled from $CaCl_2$, CH_2Cl_2 was distilled from calcium hydride. TLC was performed on silica gel, 60F-254 (0.26 mm thickness) plates. The plates were visualized with UV light (254 nm) or with a solution of vanillin in ethanol or with a solution of ninhydrin in ethanol. Liquid chromatography was performed on Merck 60 silica gel (230-400 mesh). Melting points were determined on a Kofler melting point apparatus. NMR spectra were performed on a Bruker AMX 200 (^{1}H, 200 MHz; ^{13}C, 50 MHz), Bruker Advance 300 (^{1}H, 300 MHz; ^{13}C, 75 MHz) or a Bruker AVANCE 400 (^{1}H, 400 MHz; ^{13}C, 100 MHz). Proton chemical shifts are reported in ppm (δ) with the solvent reference relative to tetramethylsilane (TMS) employed as the internal standard. The following abbreviations are used to describe spin multiplicity: s = singlet, d = doublet, t = triplet, q = quartet, qt = quintuplet, m = multiplet, br = broad signal, dd = doublet of doublet. Carbon chemical shifts are reported in ppm (δ) relative to TMS with the respective solvent resonance as the internal standard. Infrared spectra were recorded on a Bruker Vector 22 FT-IR spectrometer and peaks are reported in cm^{-1}. Mass spectra were obtained using a Bruker Esquire electrospray ionization apparatus. Element analyses (C, H, N) were performed on a Perkin-Elmer CHN Analyser 2400, by the microanalyses Service of the Faculty of Pharmacy at Châtenay-Malabry (France) or by microanalyses Service at I.C.S.N-C.N.R.S. 91198 Gif sur Yvette Cedex.

GENERAL PROCEDURES:

GENERAL PROCEDURE A FOR DEPROTECTION REACTIONS: To a solution of the *N*-Boc-protected amino acid or dipeptide in methanol was added a solution of HCl/CH_3OH 6N (30 equiv). The solution was stirred at r.t. overnight. The solvent was evaporated to afford the corresponding hydrochloride salt.

GENERAL PROCEDURE B FOR DEPROTECTION REACTIONS: To a solution of the *N*-Boc-protected amino acid or peptidomimetic in CH_2Cl_2 (0.13 M) was added an equal volume of TFA and the reaction was stirred at r.t. for 3 h. The solvent was evaporated, methanol (3×) was added followed by evaporation, and then ether was added and evaporated to afford the corresponding trifluoroacetate salt.

SYNTHESIS OF THE POLAR SCAFFOLDS:

3-Bromonaphthalene-2,7-diol (214)

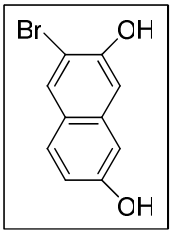

To a solution of 2,7-dihydroxylnaphthalene (500 mg, 3.0 mmol) in AcOH (7 mL) at 10–15 ºC, Br_2 (312 µL, 6.1 mmol, 2 equiv) in AcOH (2.5 mL) was added dropwise at r.t. over 40 min. After the addition was complete, the mixture was refluxed during 15 min and after cooled to r.t.. Then, H_2O (2 mL) and Sn powder (740 mg, 6.3 mmol) were added, and the reaction was stirred at 80 ºC for 24 h. The mixture was cooled to r.t., diluted with ice-cold distilled H_2O (18 mL), and extracted with EtOAc (3 × 25 mL). The combined organic layers were dried over Na_2SO_4, filtered and concentrated under reduced pressure. The crude residue was purified by flash chromatography on silica gel (cyclohexane/EtOAc, 85/15) to afford product **214** as a light pink solid (677 mg, 94%).

Mp: 184-186 ºC (Lit. 190-191 ºC)[15]

^{1}H NMR (300 MHz, DMSO-d_6) δ: 10.33 (s, 1H), 9.68 (s, 1H), 7.98 (s, 1H), 7.60 (d, 1H, *J*=8.7 Hz), 7.05 (s, 1H), 6.85-6.88 (m, 2H).

^{13}C NMR (75 MHz, DMSO-d_6) δ: 155.9, 151.8, 135.2, 131.4, 128.3, 123.4, 116.3, 108.5, 108.4, 106.9.

IR ν_{max}: 3430, 1172.

MS (APCI Negative) *m/z* 238 $[M-1]^+$

Anal. Calcd for $C_{10}H_7BrO_2$: C 50.24, H 2.95; found C 49.89, H 2.82.

4-[7-(3-Benzyloxycarbonyl-propoxy)-3-bromo-naphthalen-2-yloxy]-butyric acid benzyl ester (215)

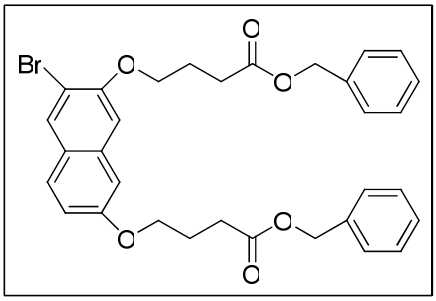

To a solution of **214** (676 mg, 2.8 mmol) and potassium carbonate (977 mg, 7.1 mmol, 2.5 equiv) in DMF (25 mL) was added slowly benzyl 4-bromobutyrate (2.18 g, 8.5 mmol, 3 equiv), and the reaction was stirred, under argon atmosphere, at r.t. overnight. The solvent was evaporated under reduced pressure and the residue was dissolved in EtOAc (70 mL). The organic layer was washed with H_2O (50 mL), 1 N HCl (40 mL), H_2O (50 mL), and brine. The organic layer was dried over Na_2SO_4, filtered and concentrated under reduced pressure. The crude residue was purified by flash chromatography on silica gel (cyclohexane/EtOAc, 90/10) to afford product **215** as a white solid (1.49 g, 89%).

Mp: 60-62 ºC

^{1}H NMR (400 MHz, $CDCl_3$) δ: 7.94 (s, 1H), 7.56 (d, 1H, *J*=9.5 Hz), 7.31-7.34 (m, 10H), 6.97-7.01 (m, 3H), 5.15 (s, 4H), 4.16 (t, 2H, *J*=6.2 Hz), 4.10 (t, 2H, *J*=6.0 Hz), 2.71 (t, 2H, *J*=7.3 Hz), 2.63 (t, 2H, *J*=7.3 Hz), 2.25 (qt, 2H, *J*=6.5 Hz), 2.20 (qt, 2H, *J*=6.5 Hz).

^{13}C NMR (100 MHz, $CDCl_3$) δ: 173.0, 157.5, 153.2, 135.9, 134.8, 131.9, 128.5, 128.2, 124.9, 117.2, 110.8, 106.9, 105.9, 67.6, 66.7, 66.3, 30.8, 30.7, 24.6, 24.4.

IR ν_{max}: 1720, 1159.

MS (ESI Positive) *m/z* 614 $[M+23]^+$

Anal. Calcd for $C_{32}H_{31}BrO_6$: C 64.98, H 5.28; found C 64.86, H 5.38.

4-(7-(3-Benzyloxycarbonyl-propoxy)-3-[(2,2-dimethyl-[1,3]dioxolan-4-ylmethyl)-amino]-naphthalen-2-yloxy)-butyric acid benzyl ester (216)

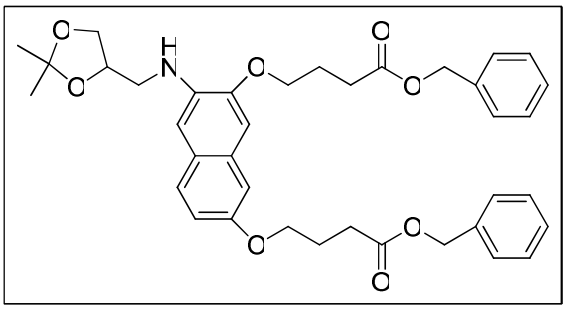

A flame-dried schlenk tube was charged with **215** (100 mg, 0.17 mmol), palladium acetate (4 mg, 17 μmol, 10 mol %), xantphos (20 mg, 34 μmol, 20 mol %), and potassium carbonate (467 mg, 3.4 mmol, 20 equiv). The schlenk tube was flushed with argon, and dry dioxane (2.3 mL) was added followed by the amine (34 μL, 0.25 mmol, 1.5 equiv). The reaction mixture was then stirred, under argon atmosphere, for 15 h at 110 ºC. The mixture was cooled to r.t., diluted with EtOAc (30 mL), filtered through a small pad of silica, that was thoroughly washed with EtOAc (3 × 20 mL). The filtrate was evaporated under reduced

pressure and the residue was purified by flash chromatography on silica gel (CH_2Cl_2, 100% to CH_2Cl_2/EtOAc, 95/5) to afford the product **216** as a yellow oil (76 mg, 70%).

^{1}H NMR (400 MHz, $CDCl_3$) δ: 7.49 (d, 1H, *J*=8.6 Hz), 7.32-7.35 (m, 10H), 6.90-6.96 (m, 3H), 6.76 (s, 1H), 5.15 (s, 4H), 4.70 (br s, 1H), 4.47 (qt, 1H, *J*=5.5 Hz), 4.06-4.17 (m, 5H), 3.84-3.88 (m, 1H), 3.39 (dd, 1H, J_1=12.7 Hz, J_2=4.8 Hz), 3.33 (dd, 1H, J_1=12.7 Hz, J_2=5.3 Hz), 2.63 (t, 4H, *J*=6.8 Hz), 2.25 (qt, 2H, *J*=6.5 Hz), 2.18 (qt, 2H, *J*=6.5 Hz), 1.47 (s, 3H), 1.38 (s, 3H).

^{13}C NMR (100 MHz, $CDCl_3$) δ: 173.1, 172.9, 154.6, 147.9, 136.6, 136.0, 135.8, 128.5, 128.2, 126.8, 125.3, 116.1, 109.4, 106.8, 104.9, 104.2, 74.3, 67.3, 67.1, 66.7, 66.4, 66.3, 46.2, 31.0, 30.9, 26.8, 25.3, 24.8, 24.6.

IR ν_{max}: 3423, 1731, 1153.

MS (ESI Positive) *m/z* 643 $[M+1]^+$

Anal. Calcd for $C_{38}H_{43}NO_8$: C 71.12, H 6.75, N 2.18; found C 71.05, H 6.79, N 2.14.

Benzyl 4,4'-(3-(2-ethoxy-2-oxoethylamino)naphthalene-2,7-diyl)bis(oxy)dibutanoate (217)

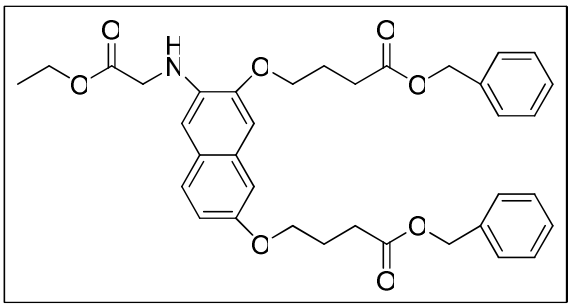

A flame-dried schlenk tube was charged with **215** (300 mg, 0.51 mmol), palladium acetate (12 mg, 51 μmol, 10 mol %), xantphos (60 mg, 0.10 mmol, 20 mol %), potassium carbonate (1.40 g, 10 mmol, 20 equiv), and HCl•H-Gly-OEt (106 mg, 0.76 mmol). The schlenk tube was flushed with argon, and dry dioxane (7 mL) was added. The reaction mixture was then stirred, under argon atmosphere, for 15 h at 110 ºC. The mixture was cooled to r.t., diluted with EtOAc (30 mL), filtered through a small pad of silica, that was thoroughly washed with EtOAc (3 × 20 mL). The filtrate was evaporated under reduced pressure and the residue was purified by flash chromatography on silica gel (cyclohexane/EtOAc, 75/25) to afford product **217** as a orange oil (235 mg, 76%).

^{1}H NMR (300 MHz, $CDCl_3$) δ: 7.40 (d, 1H, *J*=8.7 Hz), 7.26 (br s, 10H), 6.86-6.88 (m, 2H), 6.83 (s, 1H), 6.55 (s, 1H), 5.07 (s, 4H), 4.18 (q, 2H, *J*=6.9 Hz), 4.09 (t, 2H, *J*=6.0 Hz), 3.99 (t, 2H, *J*=6.0 Hz), 3.91 (s, 2H), 2.51-2.59 (m, 4H), 2.07-2.20 (m, 4H), 1.22 (t, 3H, *J*=6.9 Hz).

^{13}C NMR (75 MHz, $CDCl_3$) δ: 173.1, 173.0, 171.0, 154.8, 147.8, 135.9, 135.8, 128.5, 128.2, 127.0, 125.2, 116.1, 106.9, 105.1, 104.5, 67.1, 66.8, 66.4, 66.3, 61.2, 45.8, 31.0, 29.7, 24.8, 24.6, 14.2.

IR ν_{max}: 2942, 1731, 1160.

MS (ESI Positive) *m/z* 636 $[M+23]^+$, 652 $[M+39]^+$

4-[3-Amino-7-(3-benzyloxycarbonyl-propoxy)-naphthalen-2-yloxy]-butyric acid benzyl ester (219)

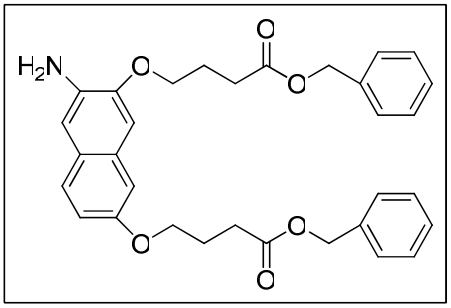

A flame-dried schlenk tube was charged with **215** (100 mg, 0.17 mmol), palladium acetate (4 mg, 17 μmol, 10 mol %), xantphos (20 mg, 34 μmol, 20 mol %), and potassium carbonate (467 mg, 3.4 mmol, 20 equiv). The schlenk tube was flushed with argon, and dry dioxane (2.3 mL) was added followed by benzophenone imine (44 μL, 0.25 mmol, 1.5 equiv). The reaction mixture was then stirred, under argon atmosphere, for 15 h at 110 ºC. The mixture was cooled to r.t., diluted with EtOAc (30 mL), filtered through a small pad of silica, that was thoroughly washed with EtOAc (3 × 20 mL). The filtrate was evaporated under reduced pressure and the resulting crude residue containing the imine adduct **218** was dissolved in dioxane (1.5 mL). To the reaction mixture was added a solution of $NaOAc•3H_2O$ (96 mg, 0.71 mmol, 4.2 equiv) in methanol (7 mL) followed by $NH_2OH•HCl$ (38 mg, 0.53 mmol, 3.1 equiv). After stirring for 5 h at r.t., the solvent was evaporated under reduced pressure, and the crude residue was purified by flash chromatography on silica gel (cyclohexane/EtOAc, 80/20) to afford product **219** as a light pink solid (55 mg, 62%).

Mp: 87-89 ºC

^{1}H NMR (300 MHz, $CDCl_3$) δ: 7.37 (d, 1H, *J*=8.7 Hz), 7.26 (br, 10H), 6.91 (s, 1H), 6.83-6.87 (m, 3H), 5.07 (s, 4H), 4.08 (t, 2H, *J*=6.0 Hz), 3.99 (t, 2H, *J*=6.0 Hz), 2.58-2.52 (m, 4H), 2.17 (qt, 2H, *J*=7.2 Hz), 2.10 (qt, 2H, *J*=7.2 Hz).

^{13}C NMR (75 MHz, $CDCl_3$) δ: 173.2, 173.1, 154.9, 148.2, 136.0, 135.9, 134.9, 129.2, 128.6, 128.3, 128.2, 126.8, 125.1, 116.3, 109.3, 106.7, 105.4, 67.1, 66.7, 66.5, 66.3, 31.2, 31.0, 24.8, 24.6.

IR ν_{max}: 3367, 1725, 1160.

MS (APCI Positive) *m/z* 528 $[M+1]^+$

Anal. Calcd for $C_{32}H_{33}NO_6 \cdot 0.15\ H_2O$: C 72.47, H 6.34, N 2.60; found C 72.15, H 6.14, N 2.60.

SYNTHESIS OF THE MOLECULAR TONGS ARMS:

2-(2-*tert*-Butoxycarbonylamino-4-methyl-pentanoylamino)-3-methyl-butyric acid methyl ester (221)

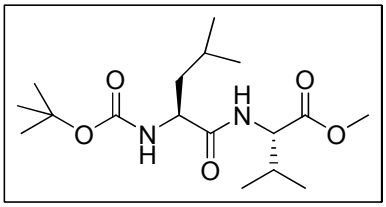

To a solution of Boc-L-Leu-OH (4.14 g, 18 mmol) in CH_2Cl_2 was added NMM (2.4 mL, 21 mmol, 1.2 equiv) and the mixture was stirred at -10 ℃ for 30 min. Isobutyl chloroformate (2.6 mL, 20 mmol, 1.1 equiv) was then added, dropwise, and the resulting mixture was stirred at -10 ℃ for 40 min. Finally, a solution of H-L-Val-OMe and NMM (2.4 mL, 22 mmol, 1.2 equiv) in CH_2Cl_2 was added, dropwise, and the reaction mixture was stirred ar r.t. for 24 h. The solvent was evaporated and the resulting residue was dissolved in EtOAc (200 mL), washed sucessively with: 10% aqueous citric acid (50 mL), H_2O (50 mL) and 10% aqueous K_2CO_3 (50 mL). The organic layer was dried over Na_2SO_4, filtered and concentrated under reduced pressure. The crude residue was purified by chromatography on silica gel (cyclohexane/EtOAc, 70/30) to afford product **221** as a white solid (4.21 g, 68%).

^{1}H NMR (300 MHz, $CDCl_3$) δ: 6.53 (d, 1H, *J*=8.0 Hz), 4.83 (d, 1H, *J*=7.4 Hz), 4.47 (dd, 1H, J_1=8.9 Hz, J_2=4.9 Hz), 4.05 (m, 1H), 3.67 (s, 3H), 2.10-2.20 (m, 1H), 1.49-1.74 (m, 3H), 1.37 (s, 9H), 0.80-0.92 (m, 12H).

^{13}C NMR (75 MHz, $CDCl_3$) δ: 174.7, 157.7, 70.6, 61.8, 54.7, 50.4, 41.7, 28.7, 27.4, 22.4, 21.7, 16.6.

IR ν_{max}: 3312, 1746, 1690, 1654, 1171.

3-Methyl-2-[4-methyl-2-(3-methyl-2-phenoxycarbonylamino-butyrylamino)-pentanoyl amino]-butyric acid methyl ester (222)

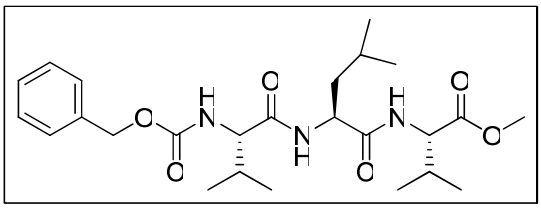

Compound **221** (4.52 g, 13 mmol) was deprotected according to general method A. To a solution of the corresponding hydrochloride salt in dry CH_2Cl_2 (70 mL), was added Z-L-Val-OH (3.95 g, 16 mmol, 1.2 equiv), DIPEA (11.4 mL; 66 mmol, 5 equiv), EDCI (3.77 g; 20 mmol, 1.5 equiv) and HOBt (2.13 g; 16 mmol, 1.2 equiv). The reaction mixture was stirred, under argon, overnight. The solvent was evaporated under reduced pressure and the residue was dissolved in EtOAc (200 mL). The organic layer was washed sucessively with: 10% aqueous citric acid (50 mL), H_2O (100 mL), 10% aqueous K_2CO_3 (50 mL), and brine (25 mL), dried over Na_2SO_4, filtered and concentrated under reduced pressure. The resulting crude residue was purified by flash chromatography on silica gel (cyclohexane /EtOAc, 75/25). Product **222** was obtained as a white powder (3.90 g, 64%).

^{1}H NMR (300 MHz, $CDCl_3$) δ: 7.26-7.32 (m, 5H), 6.62 (d, 1H, *J*=8.7 Hz), 6.37 (d, 1H, *J*=7.6 Hz), 5.41 (d, 1H, *J*=8.7 Hz), 5.08 (s, 2H), 4.34-4.58 (m, 2H), 3.99 (m, 1H), 3.70 (s, 3H), 1.85 - 2.35 (m, 2H), 1.37 -1.75 (m, 3H), 0.87-1.09 (m, 18H).

^{13}C NMR (75 MHz, $CDCl_3$) δ: 172.2, 171.7, 171.5, 156.5, 136.3, 128.5-128.0, 67.0, 60.4, 57.2, 52.1, 51.9, 41.0, 31.2, 24.7, 22.7, 22.3, 19.2, 18.9, 18.0, 17.8.

IR ν_{max}: 3282, 1736, 1692, 1641, 1537, 1247.

2-[2-(2-Amino-3-methyl-butyrylamino)-4-methyl-pentanoylamino]-3-methyl-butyric acid methyl ester (223)

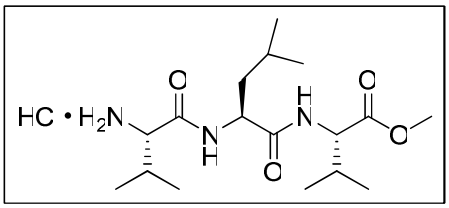

To a solution of **222** (382 mg, 0.83 mmol) in methanol (15 mL) and HCl/CH_3OH 6N (1 mL) was added Pd/C (50 mg, 13% weight). The reaction flask was purged three times with hydrogen, and stirring was maintained under hydrogen atmosphere at r.t. for 12 h. The mixture was filtered through celite, and the cake was washed with methanol (200 mL). The

filtrate was concentrated and dried to give the crude product **223** as a white powder (314 mg, 100%). The crude product was used without further purification in the course of the synthesis.

^{1}H NMR (300 MHz, DMSO-d_6) δ: 8.61 (d, 1H, *J*=8.0 Hz), 8.34 (d, 1H, *J*=8.1 Hz), 8.24 (s, 3H), 4.48 (q, 1H, *J*=6.9 Hz), 4.14 (dd, 1H, J_1=8.4 Hz, J_2=1.8 Hz), 3.61-3.64 (m, 4H), 2.05 (m, 2H), 1.65 (m, 1H), 1.46 (m, 2H), 0.66-1.05 (m, 18H).

^{13}C NMR (75 MHz, DMSO-d_6) δ: 172.4, 172.2, 167.9, 57.8, 57.4, 52.1, 51.5, 41.3, 30.3, 30.2, 24.4, 23.4, 22.3, 19.4, 18.6, 18.2.

IR ν_{max}: 2962, 1746, 1687, 1637, 1530, 1205.

2-Methoxy-5-nitrobenzoic acid (224)

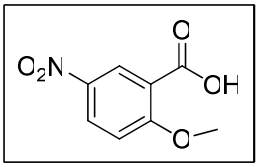

To an ice-cold suspension of 2-methoxybenzoic acid (3.00 g, 20 mmol) in concentrated aqueous H_2SO_4 (36 mL) was added portionwise NH_4NO_3 (1.74 g, 22 mmol, 1.1 equiv). The reaction mixture was stirred at 0℃ for 30 min and at r.t. for 3h. H_2O (150 mL) was then added and the resulting precipitate was filtered. The solid was finally washed with H_2O (200 mL) and dried under vacumn (over P_2O_5 in a desiccator) to give **224** as a white solid (3.10 g, 80%).

Mp: 149-150 ℃ (Lit. 161-162 ℃) [17]

^{1}H NMR (200 MHz, CD_3OD) δ: 8.64 (d, 1H, *J*=2.9 Hz), 8.40 (dd, 1H, J_1=9.3 Hz, J_2=2.9 Hz), 7.31 (d, 1H, *J*=9.3 Hz), 4.02 (s, 3H).

^{13}C NMR (50 MHz, CD_3OD) δ: 165.9, 163.6, 140.3, 129.4, 126.7, 122.8, 112.4, 55.9.

IR ν_{max}: 3258, 1725, 1611, 1514, 1342, 1177.

***N*'-(2-Methoxy-5-nitrobenzoyl) hydrazinecarboxylic acid *tert*-butyl ester (225)**

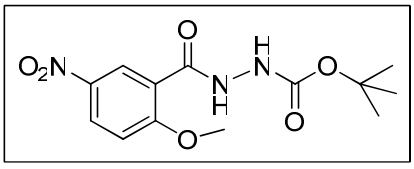

To a solution of **224** (3.05 g, 15 mmol) in dry CH_2Cl_2 (70 mL), was added *tert*-butyl carbazate (2.25 g, 17 mmol, 1.1 equiv), DIPEA (8.1 mL; 46 mmol, 3 equiv), EDCI (3.26 g; 17 mmol, 1.1 equiv) and HOBt (2.30 g; 17 mmol, 1.1 equiv). The reaction mixture was stirred, under argon atmosphere, overnight. The solvent was evaporated under reduced pressure and the residue was dissolved in EtOAc (200 mL) and the organic layer was washed with: 10% aqueous citric acid (50 mL), H_2O (100 mL), 10% aqueous K_2CO_3 (50 mL), and brine (25 mL). The organic layer was dried over Na_2SO_4, filtered and concentrated under reduced pressure. The resulting crude residue was purified by flash chromatography on silica gel (EtOAc/cyclohexane, 60/40) to afford compound **225** as a white solid (4.10 g, 85%).

Mp: 113-115 ℃

^{1}H NMR (200 MHz, $CDCl_3$) δ: 9.40 (br s, 1H), 9.07 (d, 1H, *J*=3.0 Hz), 8.35 (dd, 1H, J_1=9.2 Hz, J_2=3.0 Hz), 7.10 (d, 1H, *J*=9.2 Hz), 6.99 (br s, 1H), 4.12 (s, 3H), 1.51 (s, 9H).

^{13}C NMR (50 MHz, $CDCl_3$) δ: 162.0, 161.7, 155.1, 141.9, 128.7, 128.5, 120.3, 111.9, 82.0, 57.2, 28.7.

IR ν_{max}: 3410, 1741, 1678.

***N*'-(5-Amino-2-methoxybenzoyl) hydrazinecarboxylic acid *tert*-butyl ester (226)**

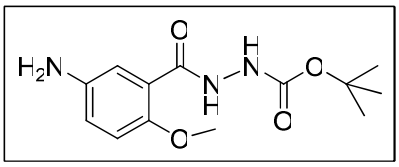

To a solution of **225** (2.30 g, 7.4 mmol) in methanol (100 mL) was added Pd/C (460 mg, 20% weight). The reaction flask was purged three times with hydrogen, and stirring was maintained under hydrogen atmosphere at r.t. for 12 h. The mixture was filtered through celite, and the cake was washed with methanol (200 mL). The filtrate was concentrated to give **226** as a beige foam (1.97 g, 95%).

^{1}H NMR (300 MHz, CD_3OD) δ: 7.35 (s, 1H), 6.87-6.99 (m, 2H), 3.88 (s, 3H), 1.49 (s, 9H).

^{13}C NMR (75 MHz, CD_3OD) δ: 168.2, 157.8, 152.2, 142.7, 122.5, 122.2, 119.5, 114.7, 81.9, 57.1, 29.1.

IR ν_{max}: 3290, 1734, 1657, 1614, 1511, 1342, 1274, 1236, 1156.

_N_'-(5-Acetylamino-2-methoxybenzoyl) hydrazinecarboxylic acid _tert_-butyl ester (227)

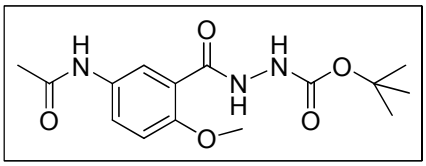

A solution of **226** (1.74 g, 6.2 mmol) in dry THF (20 mL) was heated at 60℃ and acetic anhydride (2.9 mL, 31 mmol, 5 equiv) was then added dropwise. The reaction mixture was stirred for 40 min at 60℃. THF was evaporated under reduced pressure and the crude product was dried under vacuum to yield a white powder (1.97 g, 99%). The crude product **227** was used without any further purification in the course of the synthesis.

Mp: 209-211 ℃ (Lit. 211-213 ºC) [17]

^{1}H NMR (300 MHz, DMSO-d_6) δ: 9.93 (s, 1H), 9.62 (s, 1H), 8.92 (s, 1H), 7.89 (s, 1H), 7.75 (d, 1H, *J*=8.9 Hz), 7.07 (d, 1H, *J*=8.9 Hz), 3.83 (s, 3H), 2.01 (s, 3H), 1.42 (s, 9H).

^{13}C NMR (75 MHz, DMSO-d_6) δ: 167.9, 164.9, 155.1, 152.6, 132.4, 123.1, 121.2, 112.2, 79.0, 55.9, 28.0, 23.7.

IR ν_{max}: 3275, 1712, 1665, 1596, 1491, 1245, 1163.

Anal. Calcd for $C_{15}H_{21}N_3O_5$: C 55.72, H 6.55, N 13.00; found C 55.53, H 6.46, N 12.89.

(1-[_N_'-(5-Acetylamino-2-methoxybenzoyl)hydrazinocarbonyl]-2-methyl-propyl)carbamic acid _tert_-butyl ester (228)

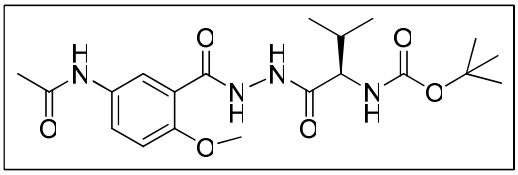

Compound **227** (297 mg, 0.92 mmol) was deprotected according to general procedure B. The corresponding trifluoroacetate salt and Boc-L-Val-OH (200 mg, 0.92 mmol, 1 equiv) were dissolved in DMF (15 mL). DIPEA (2.0 mL, 12 mmol, 12.5 equiv), HBTU (417 mg, 1.1 mmol, 1.2 equiv) and HOBt (135 mg, 1.0 mmol, 1.1 equiv) were successively added and the reaction mixture was stirred, under argon atmosphere, for 48 h at r.t.. The solvent was evaporated under reduced pressure and the resulting residue was dissolved in EtOAc (200 mL) and the organic layer was washed sucessively with: 10% aqueous citric acid (50 mL), 10% aqueous K_2CO_3 (50 mL), H_2O (100 mL), dried over Na_2SO_4, filtered and concentrated under reduced pressure. The crude product was purified by flash chromatography on silica

gel (EtOAc/cyclohexane, 80/20). The solid obtained was recristallyzed from EtOAc/petroleum ether to afford product **228** as a white solid (265 mg, 68 %).

^{1}H NMR (400 MHz, $CDCl_3$) δ: 12.15 (d, 1H, *J*=7.0 Hz), 11.42 (d, 1H, *J*=7.0 Hz), 8.82 (s, 1H), 8.47 (d, 1H, *J*=7.0 Hz), 8.11 (s, 1H), 7.02 (d, 1H, *J*=7.0 Hz), 5.60 (d, 1H, *J*=8.7 Hz), 4.79 (m, 1H), 4.08 (s, 3H), 2.19 (s, 3H), 2.02 (m, 1H), 1.48 (s, 9H), 0.88 (m, 6H).

^{13}C NMR (100 MHz, $CDCl_3$) δ: 169.0, 165.8, 158.2, 156.0, 153.6, 133.2, 125.9, 122.8, 117.8, 112.0, 79.6, 57.1, 56.6, 33.4, 28.5, 24.7, 17.9.

IR ν_{max}: 3314, 2969, 1712, 1658, 1492, 1245, 1168.

MS (ESI Positive) *m/z* 445 $[M+23]^+$

(6-[*N*'-(5-Acetylamino-2-methoxybenzoyl)hydrazino]-5-benzyloxycarbonyl amino-6-oxo -hexyl)-carbamic acid *tert*-butyl ester (198)

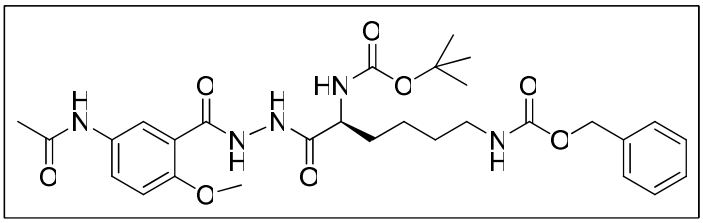

Compound **227** (479 mg, 1.5 mmol) was deprotected according to general procedure B. The corresponding trifluoroacetate salt and *N*α-Boc-*N*ε-Z-L-Lys-OH (563 mg, 1.5 mmol, 1 equiv) were dissolved in DMF (15 mL). DIPEA (2.6 mL, 15 mmol, 10 equiv), HBTU (618 mg, 1.6 mmol, 1.1 equiv) and HOBt (220 mg, 1.6 mmol, 1.1 equiv) were successively added to the reaction mixture. The reaction mixture was stirred, under argon atmosphere, for 24 h at r.t.. The solvent was evaporated under reduced pressure and the resulting residue was dissolved in EtOAc (200 mL). The organic layer was washed sucessively with: 10% aqueous citric acid (50 mL), 10% aqueous K_2CO_3 (50 mL), H_2O (100 mL), dried over Na_2SO_4, filtered and concentrated under reduced pressure. The crude product was purified by flash chromatography on silica (EtOAc, 100%). The solid obtained was recristallyzed from EtOAc/petroleum ether to afford product **198** as a white solid (635 mg, 73 %).

Mp: 136-138 ℃

^{1}H NMR (400 MHz, $CDCl_3$) δ: 11.9 (s, 1H), 11.3 (d, 1H, *J*=7.0 Hz), 8.78 (s, 1H), 8.44 (d, 1H, *J*=9.0 Hz), 7.9 (s, 1H), 7.28 (m, 5H), 6.97 (d, 1H, *J*=9.0 Hz), 5.64 (d, 1H, *J*=7.5 Hz), 5.01 (s, 2H), 4.92 (m, 1H), 4.76 (s, 1H), 4.02 (s, 3H), 3.04 (m, 2H), 2.20 (s, 3H), 1.81 (m, 1H), 1.74 (m, 1H), 1.46 (s, 9H), 1.35-1.46 (m, 4H).

^{13}C NMR (100 MHz, $CDCl_3$) δ: 169.0, 166.3, 158.6, 156.3, 155.6, 153.6, 136.6, 133.1, 128.4, 128.0, 126.1, 122.5, 117.8, 112.4, 79.8, 66.5, 56.5, 52.0, 40.7, 34.0, 29.5, 28.6, 24.6, 21.9.
IR v_{max}: 3312, 1663, 1627, 1530, 1494, 1246, 1168, 1015.
MS (ESI Positive) *m/z* 608 $[M+Na]^+$
HRMS (ESI) *m/z* calcd for $[C_{29}H_{39}N_5O_8Na]^+$: 608.2696 $[M+Na]^+$; found: 608.2697.
Anal. Calcd for $C_{29}H_{39}N_5O_8$: C 59.47, H 6.71, N 11.96; found C 59.33, H 6.75, N 11.74.

(6-[*N*'-(5-Acetylamino-2-methoxybenzoyl)hydrazino]5-amino-6-oxohexyl) carbamic acid *tert*-butyl ester (230)

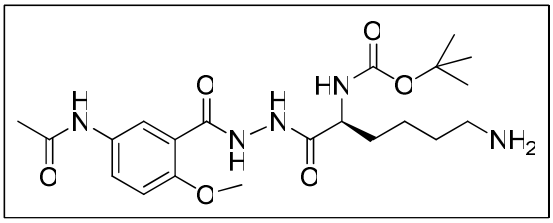

To a solution of **198** (150 mg, 0.26 mmol) in methanol (15 mL) was added Pd/C (23 mg, 20% weight). The reaction flask was purged three times with hydrogen, and stirring was maintained under hydrogen atmosphere at r.t. for 12 h. The mixture was filtered through celite, and the cake was washed with methanol (200 mL). The filtrate was concentrated and dried to give the crude product **230** as a white powder (111 mg, 96%). The crude product was used without further purification in the course of the synthesis.
^{1}H NMR (300 MHz, $CDCl_3$) δ: 9.29 (s, 1H), 8.91 (s, 1H), 8.29 (s, 2H), 7.87 (m, 1H), 6.94 (m, 1H), 5.65 (m, 1H), 4.67 (m, 2H), 3.94-4.13 (m, 4H), 2.19-2.27 (m, 5H), 1.78 (br, 2H), 1.33-1.51 (m, 13H).
^{13}C NMR (75 MHz, $CDCl_3$) δ: 169.2, 169.1, 158.5, 155.6, 153.7, 132.9, 125.9, 122.7, 118.2, 112.0, 79.9, 56.4, 52.3, 52.2, 50.2, 27.0, 28., 24.4, 22.2.
IR v_{max}: 1651, 1512, 1170.
MS (ESI Positive) *m/z* 452 $[M+1]^+$

1-*tert*-Butyl 2-phenyl hydrazine-1,2-dicarboxylate (231)

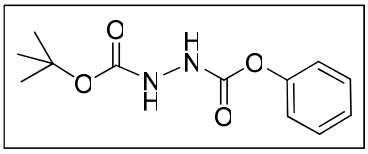

To a solution of *tert*-butyl carbazate (2.55 g, 18 mmol) in CH_2Cl_2 (20 mL), under argon atmosphere and at 0 ºC, was added pyridine (3.4 mL, 42 mmol, 2.2 equiv). After 10 min, a solution of phenyl chloroformate (2.6 mL, 21 mmol, 1.1 equiv) in CH_2Cl_2 (20 mL) was added dropwise and the reaction was stirred at 0 ºC for 40 min and at r.t. overnight. After evaporation of the solvent and volatiles under reduced pressure, the resulting residue was triturated with *n*-hexane affording product **231** as a white solid (4.65 g, 97%).

Mp: 134-136 ºC

^{1}H NMR (300 MHz, $CDCl_3$) δ: 7.14-7.39 (m, 5H), 6.99 (br s, 1H), 6.50 (br s, 1H), 1.49 (s, 9H).

^{13}C NMR (75 MHz, $CDCl_3$) δ: 155.6, 155.1, 150.6, 129.4, 125.8, 121.4, 82.2, 28.2.

IR ν_{max}: 3273, 3221, 1756, 1691, 1523, 1486, 1218, 1150.

MS (ESI Positive) *m/z* 275 $[M+23]^+$

Anal. Calcd for $C_{12}H_{16}N_2O_4$: C 57.13, H 6.39, N 11.10; found C 57.03, H 6.14, N 10.92.

***tert*-Butyl 2-(hydrazinecarbonyl)hydrazinecarboxylate (232)**

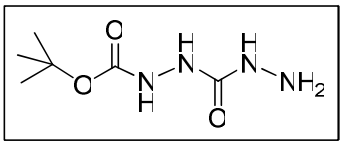

To a solution of **231** (2.50 g, 9.9 mmol) in methanol (40 mL) was added hydrazine monohydrate (3.3 g, 64 mmol, 6.5 equiv) and the mixture was stirred at 60 ºC for 1.5 h. After evaporation of the solvent, the resulting residue was triturated with petroleum ether. The resulting precipitate was recrystallized from EtOAc/petroleum ether, to afford product **232** as a white solid (1.35 g, 72%).

Mp: 138-140 ºC

^{1}H NMR (300 MHz, DMSO-d_6) δ: 8.41 (s, 1H), 7.80 (s, 1H), 7.30 (s, 1H), 4.04 (br s, 2H), 1.38 (s, 9H).

^{13}C NMR (75 MHz, DMSO-d_6) δ: 159.9, 155.9, 78.7, 28.1.

IR ν_{max}: 3254, 3254, 3046, 1729, 1649, 1508, 1150.

MS (ESI Positive) *m/z* 213 $[M+23]^+$

Anal. Calcd for $C_6H_{14}N_4O_3$: C 37.89, H 7.42, N 29.46; found C 38.03, H 7.39, N 29.53.

tert-Butyl 2-(2-(phenoxycarbonyl)hydrazinecarbonyl)hydrazinecarboxylate (233)

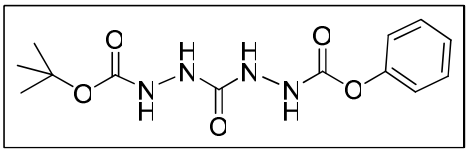

To a solution of **232** (625 mg, 3.3 mmol) in THF (50 mL) was added pyridine (678 μL, 8.2 mmol, 2.5 equiv) and the mixture was stirred until a homogeneous solution was obtained. The solution was then cooled to 0 ºC and phenyl chloroformate (458 μL, 3.6 mmol, 1.1 equiv) was added. After stirring for 15 min at r.t., the solvent was evaporated under reduced pressure and the residue was dissolved in EtOAc (50 mL). The organic layer was washed sucessively with: H_2O (2 × 25 mL), 5% aqueous citric acid (2 × 20 mL), 10% aqueous K_2CO_3 (2 × 20 mL), dried over Na_2SO_4, filtered and concentrated under reduced pressure. The residue was purified by flash chromatography on silica gel (EtOAc/cyclohexane, 80/20) to afford product **233** as a white solid (923 mg, 91%).

Mp: 173-174 ºC

^{1}H NMR (300 MHz, $CDCl_3$) δ: 7.81 (br s, 2H), 7.68 (br s, 1H), 7.09-7.31 (m, 5H), 6.99 (br s, 1H), 1.43 (s, 9H).

^{13}C NMR (75 MHz, $CDCl_3$) δ: 158.7, 156.7, 155.8, 150.6, 129.3, 125.7, 121.4, 82.1, 28.1.

IR ν_{max}: 3262, 3238, 1712, 1682, 1519, 1489, 1226, 1154.

MS (ESI Positive) *m/z* 333 $[M+23]^+$

Anal. Calcd for $C_{13}H_{18}N_4O_5$: C 50.32, H 5.85, N 18.06; found C 50.29, H 5.52, N 17.87.

(*S*)-*tert*-Butyl 2-(2-(1-amino-3-methyl-1-oxobutan-2-ylcarbamoyl)hydrazinecarbonyl) hydrazinecarboxylate (236)

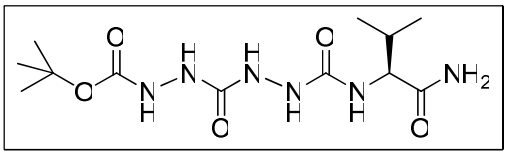

Coumpond **233** (273 mg, 0.88 mmol) and HCl•H-L-Val-NH_2 (151 mg, 0.97 mmol, 1.1 equiv) were dissolved in acetonitrile (17 mL), and triethylamine (741 μL, 5.3 mmol, 6 equiv) was successively added to the reaction mixture. The reaction was stirred, under argon atmosphere, for 3 days at r.t.. The solvent was evaporated under reduced pressure and the resulting residue was purified by flash chromatography on silica gel (EtOAc/CH_3OH, 90/10) to afford product **236** as a white solid (272 mg, 93%).

Mp: 154-156 ºC

^{1}H NMR (300 MHz, DMSO-d_6) δ: 8.61 (br s, 1H), 8.13 (s, 2H), 7.77 (s, 1H), 7.37 (br s, 1H), 7.08 (s, 1H), 6.05 (d, 1H, *J*=8.4 Hz), 4.00 (dd, 1H, J_1=8.4 Hz, J_2=5.1 Hz), 1.95-2.02 (m, 1H), 1.41 (s, 9H), 0.87 (d, 3H, *J*=6.6 Hz), 0.82 (d, 3H, *J*=6.6 Hz).

^{13}C NMR (75 MHz, DMSO-d_6) δ: 173.5, 158.6, 158.1, 155.9, 79.0, 57.5, 30.6, 28.1, 19.3, 17.4.

IR v_{max}: 3259, 2969, 1658, 1529, 1241, 1158.

MS (ESI Positive) *m/z* 355 $[M+23]^+$

Anal. Calcd for $C_{12}H_{24}N_6O_5$•0.2 EtOAc: C 43.37, H 7.29, N 23.71; found C 43.19, H 7.37, N 23.38.

***tert*-Butyl 2-(2-(methylcarbamoyl)hydrazinecarbonyl)hydrazinecarboxylate (238)**

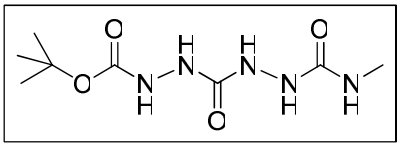

Coumpond **233** (150 mg, 0.48 mmol) and HCl•NH_2CH_3 (37 mg, 0.53 mmol, 1.1 equiv) were dissolved in acetonitrile (9 mL), and triethylamine (475 μL, 3.4 mmol, 6 equiv) was successively added to the reaction mixture. The reaction was stirred, under argon atmosphere, for 3 days at r.t.. The resulting precipitate was filtered and washed successively with EtOAc, methanol, and ether, to give product **248** as a white solid (84 mg, 70%).

Mp: 232-234 ºC

^{1}H NMR (300 MHz, DMSO-d_6) δ: 8.54 (br s, 1H), 8.05 (br s, 2H), 7.61 (s, 1H), 6.07 (br s, 1H), 2.56 (d, 3H, *J*=4.5 Hz), 1.40 (s, 9H).

^{13}C NMR (75 MHz, DMSO-d_6) δ: 159.1, 158.4, 155.9, 79.0, 28.1, 26.1.

IR v_{max}: 3272, 3106, 2936, 1665, 1474, 1159.

MS (ESI Positive) *m/z* 270 $[M+23]^+$

Anal. Calcd for $C_8H_{17}N_5O_4$: C 38.86, H 6.93, N 28.32; found C 38.89, H 6.76, N 27.97.

***tert*-Butyl 2-(2-(3-methoxy-3-oxopropylcarbamoyl)hydrazinecarbonyl) hydrazinecarboxylate (240)**

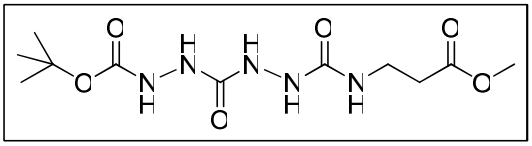

Compound **233** (400 mg, 1.3 mmol) and HCl•H-β-Ala-OCH_3 (198 mg, 1.4 mmol, 1.1 equiv) were dissolved in acetonitrile (25 mL), and triethylamine (1.1 mL, 7.7 mmol, 6 equiv) was successively added to the reaction mixture. The reaction was stirred, under argon atmosphere, for 3 days at r.t.. The solvent was evaporated under reduced pressure and the resulting crude residue was triturated with EtOAc. The solid was filtered and washed successively with EtOAc, methanol, and ether, to afford product **240** as a white solid (274 mg, 67%).

Mp: 122-124 ºC

^{1}H NMR (300 MHz, DMSO-d_6) δ: 8.54 (s, 1H), 8.05 (br s, 2H), 7.68 (s, 1H), 6.20 (br, 1H), 3.61 (s, 3H), 3.25 (dt, 2H, J_1=11.7 Hz, J_2=5.7 Hz), 2.45 (t, 2H, J=5.7 Hz), 1.40 (s, 9H).

^{13}C NMR (75 MHz, DMSO-d_6) δ: 172.0, 158.4, 155.9, 79.0, 51.3, 35.2, 34.3, 28.1.

IR ν_{max}: 3270, 3106, 2936, 1666, 1542, 1161.

MS (ESI Positive) *m/z* 342 $[M+23]^+$

Anal. Calcd for $C_{11}H_{21}N_5O_6$•0.15 H_2O: C 41.03, H 6.68, N 21.75; found C 41.10, H 6.31, N 21.40.

SYNTHESIS OF THE MOLECULAR TONGS:

4-(7-Hydroxy-naphthalen-2-yloxy)butyric acid ethyl ester (242)

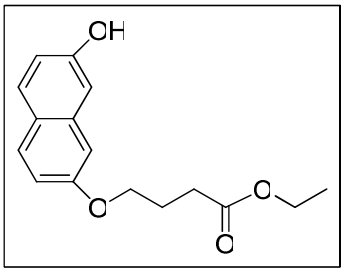

To a solution of 2,7-dihydroxynaphthalene (5.00 g, 30 mmol) and K_2CO_3 (6.50 g, 47 mmol, 1.5 equiv) in dry DMF (50 mL) was added, dropwise, ethyl 4-bromobutyrate (4 mL, 27 mmol, 0.9 equiv) and the reaction mixture was stirred for 24 h at r.t.. The solvent was evaporated under reduced pressure and the resulting residue was dissolved in CH_2Cl_2. The organic layer was washed with H_2O (5 × 30 mL), dried over Na_2SO_4, and concentrated in vacuo. The resulting crude residue was purified by chromathography on silica gel (petroleum ether/EtOAc, 4/1) to afford **242** as white needles (2.80 g, 36%).

Mp: 91-93 ℃ (Lit. 91-93 ℃) [18]

^{1}H NMR (200 MHz, $CDCl_3$) δ: 7.6 (d, 2H, J=8.8 Hz, 2H), 6.9-7.0 (m, 4H), 5.5 (br s, 1H), 4.0-4.2 (m, 4H), 2.5 (t, 2H, *J*=7.0 Hz), 2.1 (m, 2H), 1.2 (t, 3H, *J*=7.1 Hz).

^{13}C NMR (50 MHz, $CDCl_3$) δ: 174.4, 157.2, 136.3, 129.3, 123.4, 116.2, 115.5, 108.4, 105.8, 66.7, 60.2, 30.5, 24.6, 14.4.

IR v_{max}: 3292, 1699.

4-(7-Benzyloxy-naphthalen-2-yloxy)butyric acid ethyl ester (243)

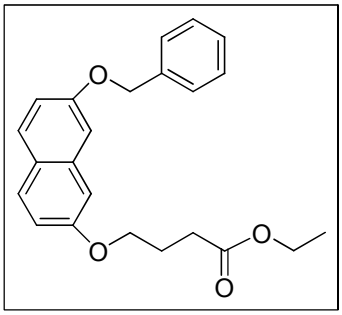

To a solution of **242** (6.5 g, 24 mmol) and K_2CO_3 (4.1 g, 29 mmol) in dry CH_3CN (70 mL) was added benzyl bromide (3.5 mL, 29 mmol, 1 equiv) and the reaction mixture was stirred for 3 h at reflux and for 24 h at r.t.. The resulting suspension was filtered and the filtrate was concentrated under reduced pressure. The resulting residue was dissolved in CH_2Cl_2 (70 mL), and the organic layer was washed with H_2O (3 × 10 mL), dried over Na_2SO_4, filtered, and concentrated under reduced pressure. The crude product was purified by chromatography on silica gel (petroleum ether/EtOAc, 9/1) to give **243** as white crystals (4.98 g, 60%).

Mp: 84-85 ℃ (Lit. 84-85 ºC) [18]

^{1}H NMR (200 MHz, $CDCl_3$) δ: 69-7.7 (m, 11H), 5.1 (s, 2H), 4.0-4.2 (m, 4H), 2.5 (t, 2H, *J*=7.2 Hz), 2.1 (m, 2H), 1.3 (t, 3H, *J*=7.0 Hz).

^{13}C NMR (50 MHz, $CDCl_3$) δ: 174.4, 157.2, 136.3, 129.3, 128.0, 123.4, 116.2, 115.5, 108.4, 105.8, 69.5, 66.7, 60.2, 30.5, 24.6, 14.4.

IR v_{max}: 1732, 1623, 1383, 1180.

4-(7-Benzyloxy-naphthalen-2-yloxy)butyric acid (244)

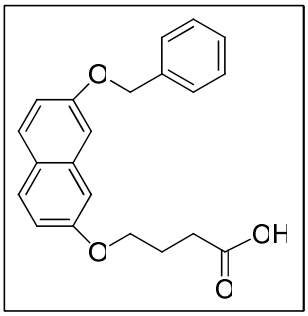

A suspension of **243** (0.9 g, 2.5 mmol) in a 10% KOH methanolic solution (25 mL) was stirred at reflux for 4 h. The solvent was evaporated and the resulting residue was suspended in H_2O (10 mL) and the aqueous layer was acidified with HCl 1 N, extracted with CH_2Cl_2 (2×) and the organic layers were dried over $MgSO_4$ and concentrated undewr reduced pressure. The crude product was then recrystallized from EtOAc/petroleum ether (85/15) to give **244** as white crystals (0.76 g, 92%).

Mp: 132-134 ℃ (Lit. 132-134 ºC) [18]

^{1}H NMR (300 MHz, DMSO-d_6) δ: 12.19 (s, 1H), 7.73 (dd, 2H, J_1=8.9 Hz, J_2=3.6 Hz), 7.27-7.56(m, 6H), 7.20 (d, 1H, J=2.2 Hz), 7.02 (ddd, J_1=8.9 Hz, J_2=2.4 Hz), 5.2 (s, 2H), 4.08 (t, 2H, J=6.4 Hz), 2.43 (t, 2H, J=7.3 Hz), 2.01 (qt, 2H, J= 6.8 Hz).

^{13}C NMR (75 MHz, DMSO-d_6) δ: 174.6, 157.4, 157.2, 137.5, 136.1, 129.5, 128.9, 128.2, 124.3, 116.5, 107.2, 106.7, 69.9, 67.0, 30.6, 24.7.

IR ν_{max}: 1732, 1625, 1384, 1208.

4-(7-Benzyloxy-naphthalen-2-yloxy)butyryl-Val-Leu-Val-OMe (245)

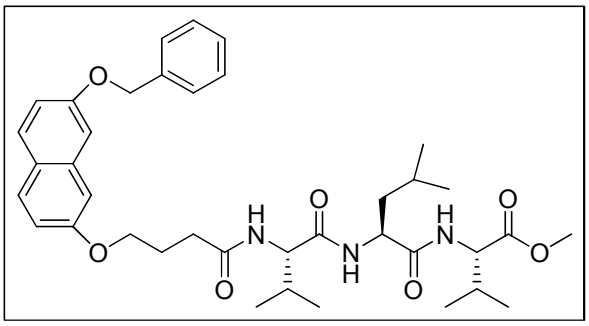

To a solution of **244** (1.24 g, 3.7 mmol), HBTU (1.53 g, 4.0 mmol, 1.1 equiv), and triethylamine (0.6 mL, 4.0 mmol, 1.1 equiv) in dry DMF (25 mL) was added H-VLV-OMe (1.26 g, 3.7 mmol, 1 equiv) and 0.5 mL of triethylamine and the mixture was stirred for 24 h at r.t.. DMF was evaporated under reduced pressure and the resulting residue was dissolved

in CH_2Cl_2, and the organic layer was washed sucessively with: HCl 1 N (30 mL), NaOH 1 N (30 mL), and H_2O, dried over $MgSO_4$ and evaporated under reduced pressure. The crude product was finally recrystallized from EtOAc/MeOH, to afford **245** as a white powder (2.7 g, 90%).

Mp: 215-217 ºC

^{1}H NMR (300 MHz, DMSO-d_6) δ: 7.95 (m, 3H), 7.73 (dd, 2H, J_1=8.9 Hz, J_2=4.0 Hz), 7.32-7.54 (m, 5H), 7.30 (d, 1H, J=2.4 Hz), 7.17 (d, 1H, J=2.3 Hz), 7.05 (dd, 1H, J_1=8.9 Hz, J_1=2.5 Hz), 6.98 (dd, 1H, J_1=8.9 Hz, J_1=2.5 Hz), 5.20 (s, 2H), 4.35-4.43 (q, 1H, J=7.8 Hz), 4.11-4.23 (m, 2H), 4.06 (t, 2H, J=6.6 Hz), 3.60 (s, 3H), 2.37 (t, 2H, J=6.9 Hz), 1.92-1.99 (m, 4H), 1.52-1.69 (m, 1H), 1.45 (t, 2H, J=7.3 Hz), 0.71-0.97 (m, 18).

^{13}C NMR (75 MHz, DMSO-d_6) δ: 172.7, 172.2, 171.4, 157.5, 157.2, 137.5, 136.1, 129.5, 129.4, 128.9, 128.3, 128.2, 124.3, 116.6, 116.4, 107.2, 106.6, 69.7, 67.4, 58.3, 57.7, 52.1, 51.3, 41.2, 32.0, 30.7, 30.3, 25.5, 24.5, 23.4, 22.1, 19.6, 19.3, 18.7, 18.6.

4-(7-Hydroxy-naphthalen-2-yloxy) butyryl-Val-Leu-Val-OMe (246)

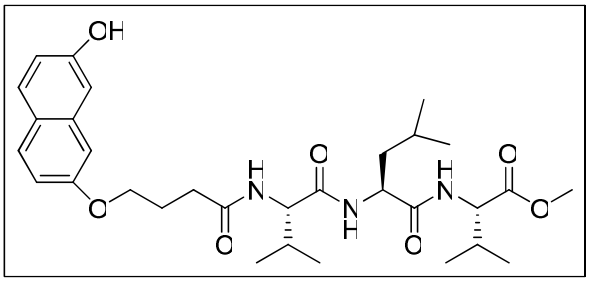

To a solution of **245** (535 mg, 0.81 mmol) in methanol/DMF (30 mL/40 mL) was added Pd/C (80 mg, 20% weight). The reaction flask was flushed three times with hydrogen, and the reaction was stirred, under hydrogen atmosphere, for 24 h at r.t.. The mixture was filtered through a pad of celite, and the cake was thoroughly washed with methanol (200 mL). The filtrate was evaporated under reduced pressure to afford product **246** as a white solid (462 mg, 100%). The product was used without any further purification in the course of the synthesis.

^{1}H NMR (300 MHz, DMSO-d_6) δ: 9.61 (s, 1H), 7.96 (m, 3H), 7.64 (dd, 2H, J_1=8.9 Hz, J_2=2.7 Hz), 7.02 (dd, 2H, J_1=12.7 Hz, J_2=2.1 Hz), 6.88 (dd, 2H, J_1=8.8 Hz, J_2=2.3 Hz), 4.39 (m, 1H), 4.16 (m, 2H), 4.03 (t, 2H, J=6.4 Hz), 3.61 (s, 3H), 2.36 (m, 2H), 2.00 (m, 4H), 1.60 (s, 1H), 1.44 (t, 2H, J=7.1 Hz), 0.7-0.8 (m, 18H).

^{13}C NMR (75 MHz, DMSO-d_6) δ: 172.7, 172.2, 171.4, 157.3, 156.2, 136.5, 129.4, 123.4, 116.3, 115.7, 108.5, 105.7, 67.3, 58.2, 57.7, 52.1, 51.3, 41.2, 32.0, 30.7, 30.3, 25.51 (C_{12}), 24.5, 23.4, 22.1, 19.6, 19.3, 18.7, 18.6.

IR v_{max}: 3279, 2957, 1740, 1634, 1542, 1207.

4-Bromo-butyric acid benzyl ester

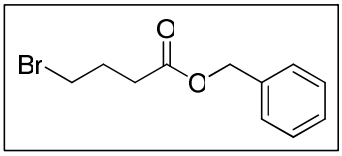

To a solution of 4-bromo butyric acid (5.0 g, 30 mmol, 1 equiv) in dry THF (35 mL) was added, dropwise, oxalyl chloride and dry DMF (6 drops). The reaction mixture was stirred at 0 ℃ for 2 h. The solvent was evaporated and a solu tion of benzyl alcohol (4.6 mL, 45 mmol, 1.5 equiv) and triethylamine (8.5 mL, 60 mmol, 2 equiv) in CH_2Cl_2 (45 mL) was added. The resulting mixture was then stirred at 0 ℃ for 8 h. The solution color was changed from yellow to orange. The mixture was washed with H_2O (2 × 300 mL) and brine (2 x 50 mL), dried over $MgSO_4$, filtered and concentrated under reduced pressure. The resulting residue was purified by chromatography on silica gel (CH_2Cl_2/cyclohexane, 70/30), to give the desired compound as a colorless oil (6 g, 78%).

^{1}H NMR (200 MHz, $CDCl_3$) δ: 7.26-7.36 (m, 5H), 5.2 (s, 2H), 3.46 (t, 2H, *J*=6.4 Hz), 2.6 (t, 2H, *J*=7.1 Hz), 2.2 (m, 2H).

^{13}C NMR (50 MHz, $CDCl_3$) δ: 172.2, 135.8, 128.1, 128.5, 66.2, 32.4-32.5, 27.6.

IR v_{max}: 1735.

4-[7-(3-Benzyloxycarbonyl-propoxy)naphthalen-2-yloxy]butyryl-Val-Leu-Val-OMe (247)

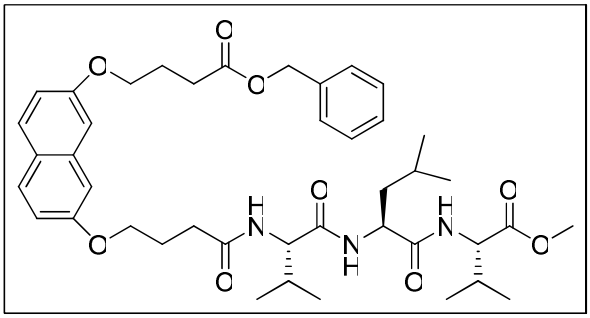

A solution of **246** (900 mg, 1.6 mmol), K_2CO_3 (391 mg, 2.8 mmol, 1.8 equiv) and benzyl 4-bromobutyrate (645 mg, 2.5 mmol, 1.6 equiv) in anhydrous DMF (100 mL) was stirred for 24 h at 50 ℃. The solvent was evaporated under reduce d pressure and the resulting residue was dissolved in EtOAc (200 mL). The organic layer was washed with H_2O (100 mL), HCl 2 M (70 mL), H_2O (50 mL), brine (50 mL), dried over $MgSO_4$, filtered, and concentrated under reduced pressure. The crude product was purified by chromatography on silica gel (EtOAc/cyclohexane, 6/4) to yield compound **247** as a white solid (950 mg, 81%).

Mp: 153-154 ℃

^{1}H NMR (300 MHz, DMSO-d_6) δ: 7.96 (m, 3H), 7.70 (d, 2H, *J*=8.5 Hz), 7.34 (m, 5H), 7.17 (br s, 2H), 6.93-6.99 (m, 2H), 5.12 (s, 2H), 4.36-4.42 (m, 1H), 4.05-4.20 (m, 6H), 3.60 (s, 3H), 2.58 (t, 2H, *J*=7.3 Hz), 2.37 (t, 2H, *J*=7.3 Hz), 1.94-2.01 (m, 6H), 1.60 (m, 1H), 1.43 (m, 2H), 0.84 (m, 18H).

^{13}C NMR (75 MHz, DMSO-d_6) δ: 172.9, 172.7, 172.2, 171.4, 157.4, 157.3, 136.6, 136.7, 129.4, 128.9, 128.4, 124.2, 116.4, 116.3, 106.6, 67.4, 66.9, 66.0, 58.2, 57.7, 52.1, 51.3, 41.2, 32.0, 30.7, 30.3, 25.5, 24.7, 24.5, 23.4, 22.1, 19.7, 19.3, 18.7, 18.6.

IR ν_{max}: 3281, 2955, 1744, 1633, 1541, 1209.

4-[7-(3-Carboxy-propoxy)naphthalen-2-yloxy]butyryl-Val-Leu-Val-OMe (248)

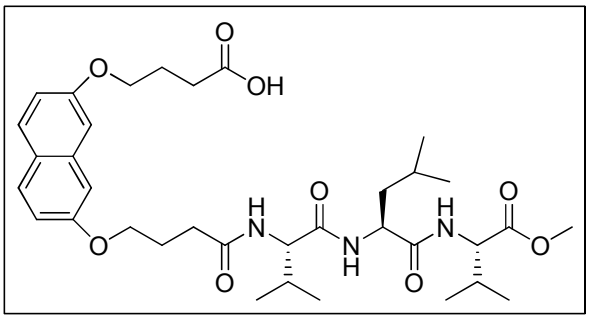

To a solution of **247** (929 mg, 1.2 mmol) in DMF (50 mL) was added Pd/C (140 mg, 15% weight). The reaction flask was flushed three times with hydrogen, and the reaction was stirred, under hydrogen atmosphere, for 24 h at r.t.. The mixture was filtered through a pad of Celite, and the cake was thoroughly washed with methanol (200 mL). The filtrate was evaporated under reduced pressure to afford product **248** as a white solid (462 mg, quantitative yield), which was used without any further purification in the course of the synthesis.

Mp: 192-194℃

^{1}H NMR (300 MHz, DMSO-d_6) δ: 8.02 (m, 3H), 7.72 (d, 2H, *J*=8.8 Hz), 7.20 (br s, 2H), 6.98 (d, 2H, *J*=8.9 Hz), 4.36-4.42 (m, 1H), 4.01-4.24 (m, 6H), 3.62 (s, 3H), 2.30-2.47 (m, 4H), 1.88-2.12 (m, 6H), 1.62 (m, 1H), 1.46 (m, 2H), 0.86 (m, 18H).

^{13}C NMR (75 MHz, DMSO-d_6) δ: 172.9, 172.7, 172.2, 171.4, 157.4, 157.3, 136.6, 136.2, 129.4, 128.9, 128.4, 128.2, 124.2, 116.4, 116.3, 106.6, 67.4, 66.9, 58.2, 57.7, 52.1, 51.3, 41.2, 32.0, 30.7, 30.3, 25.5, 24.7, 24.5, 23.4, 22.1, 19.7, 19.3, 18.7, 18.6.

(*S*)-Methyl 2-((*S*)-2-((*S*)-2-(4-(7-(4-(2-(2-((*S*)-1-amino-3-methyl-1-oxobutan-2-yl-carbamoyl)hydrazinecarbonyl)hydrazinyl)-4-oxobutoxy)naphthalen-2-yloxy) butanamido)-3-methylbutanamido)-4-methylpentanamido)-3-methylbutanoate (249)

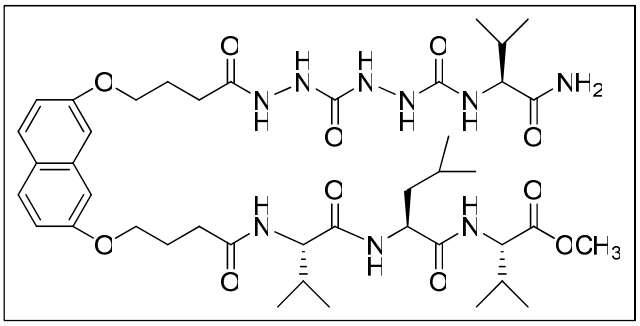

Compound **236** (128 mg, 0.38 mmol) was deprotected according to general procedure B. The corresponding trifluoroacetate salt **237** and compound **248** (230 mg, 0.35 mmol) were dissolved in DMF. DIPEA (207 µL, 1.2 mmol, 3.5 equiv), HBTU (159 mg, 0.42 mmol, 1.2 equiv), and HOBt (52 mg, 0.38 mmol, 1.1 equiv) were successively added to the reaction mixture that was then stirred, under argon atmosphere, for 24 h at r.t.. The solvent was evaporated under reduced pressure to afford a beige oil. Trituration in EtOAc yielded a beige solid that was filtered and washed successively with EtOAc, CH_2Cl_2, distilled H_2O, CH_3OH, and ether. Product **249** was obtained as a white powder (150 mg, 49%).

Mp: 218-220 ºC

^{1}H NMR (400 MHz, DMSO-d_6) δ: 9.63 (s, 1H), 8.20 (br s, 2H), 7.92-7.97 (m, 3H), 7.78 (s, 1H), 7.71 (d, 2H, *J*=9.3 Hz), 7.32 (br s, 1H), 7.17 (s, 2H), 7.05 (s, 1H), 6.98 (br s, 2H), 6.09 (d, 1H, *J*=7.2 Hz), 4.36-4.40 (m, 1H), 3.99-4.17 (m, 7H), 3.60 (s, 3H), 2.33-2.37 (m, 4H), 1.98-2.03 (m, 7H), 1.60 (br, 1H), 1.44 (br, 2H), 0.81-0.85 (m, 24H).

^{13}C NMR (100 MHz, DMSO-d_6) δ: 173.5, 172.2, 171.7, 170.9, 158.3, 158.1, 157.0, 135.7, 129.0, 123.7, 115.9, 106.2, 66.9, 66.8, 57.8, 57.6, 57.3, 51.6, 50.8, 40.8, 31.6, 30.7, 30.3, 29.9, 29.7, 25.1, 24.4, 24.1, 23.0, 21.6, 19.3, 19.2, 18.8, 18.2, 18.1, 17.4.

IR ν_{max}: 3278, 2963, 1632, 1545, 1210.

MS (ESI Positive) ***m/z*** 895 $[M+23]^+$, 911 $[M+39]^+$

Anal. Calcd for $C_{42}H_{65}N_9O_{11}$•1.5 H_2O: C 56.11, H 7.64, N 14.02; found C 56.18, H 7.27, N 13.72.

Ethyl 4-((7-(4-ethoxy-4-oxobutoxy)-2-naphthyl)oxy)butanoate (250)

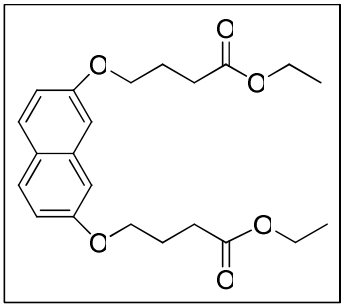

To a solution of 2,7-dihydroxynaphthalene (1.5 g, 9.37 mmol) and potassium carbonate (3.24 g, 23 mmol, 2.5 equiv) in DMF (60 mL) was slowly added ethyl 4-bromobutyrate (4.0 mL, 28 mmol, 3 equiv), and the reaction mixture was stirred for 12 h at r.t.. The solvent and volatiles were evaporated and the resulting residue was dissolved in CH_2Cl_2 (100 mL). The organic layer was washed with H_2O (2×50 mL), dried over $MgSO_4$, and the solvent was evaporated. The crude product was purified by chromatography on silica gel (cyclohexane/EtOAc, 70/30) giving rise to **250** as a white oil (3.15 g, 87%).

^{1}H NMR (300 MHz, $CDCl_3$) δ: 7.66 (d, 2H, *J*=8.8 Hz), 6.88-7.11 (m, 4H), 3.98-4.32 (m, 8H), 2.58 (t, 4H, *J*=7.3 Hz), 2.10-2.29 (m, 4H), 1.25-1.30 (dt, 6H, *J*=7.1 Hz).

^{13}C NMR (75 MHz, $CDCl_3$) δ: 173.6, 157.3, 135.8, 129.0, 124.3, 116.1, 106.0, 66.6, 60.4, 51.6, 30.8, 24.6.

IR ν_{max}: 2965, 1729, 1627, 1177.

4-((7-(3-Carboxypropoxy)-2-naphthyl)oxy)butanoic acid (251)

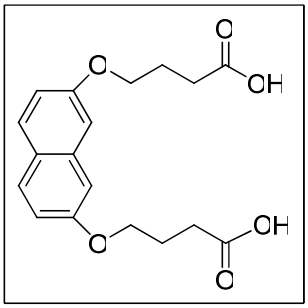

A solution of ethanol (50 mL) containing **250** (2.76 g, 7.1 mmol) and 10% aqueous KOH (50 mL) was stirred at reflux for 4 h. The solution was then poured in ice and extracted with CH_2Cl_2 (2 × 50 mL). The aqueous layer was acidified with 10% aqueous HCl and the resulting precipitate was filtered and washed with H_2O to afford product **251** as a white solid (2.29 g, 97%).

Mp: 158-159℃ (Lit. 144 ℃) [16]

^{1}H NMR (300 MHz, $CDCl_3$) δ: 7.75 (d, 2H, *J*=7.0 Hz), 7.25 (d, 2H, *J*=1.3 Hz), 7.00 (dd, 2H, J_1=7.0 Hz, J_2=7.0 Hz), 4.10 (t, 4H, *J*=7.0 Hz), 2.50 (t, 4H, *J*=7.0 Hz), 2.00 (m, 4H).

^{13}C NMR (75 MHz, $CDCl_3$) δ: 174.1, 157.0 1, 136.0, 129.0, 123.8, 116.1, 106.2, 66.4, 30.2, 24.2.

IR ν_{max}: 3209, 1712, 1629, 1209.

Molecular tong (252)

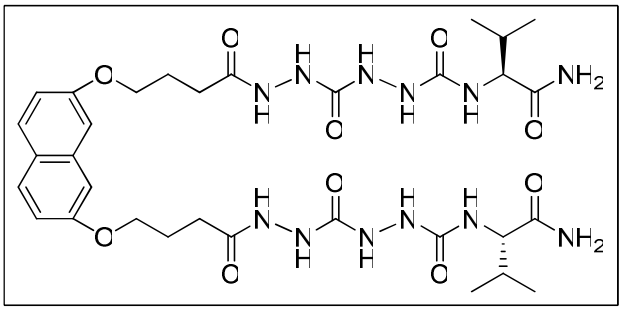

Compound **236** (301 mg, 0.91 mmol) was deprotected according to general procedure A. The corresponding trifluoroacetate salt **237** and compound **251** (137 mg, 0.41 mmol) were dissolved in DMF. DIPEA (486 µL, 2.9 mmol, 7 equiv), HBTU (391 mg, 1.0 mmol, 2.5 equiv), and HOBt (123 mg, 0.91 mmol, 2.2 equiv) were successively added to the reaction mixture that was then stirred, under argon atmosphere, for 48 h at r.t.. The solvent was evaporated under reduced pressure to afford a beige oil. Trituration in EtOAc yielded a beige solid that was filtered and washed successively with EtOAc, CH_2Cl_2, H_2O, CH_3OH, and ether. Product **252** was obtained as a white powder (174 mg, 56%).

Mp: 181-185 ºC

^{1}H NMR (400 MHz, DMSO-d_6) δ: 9.63 (s, 2H), 8.20 (br s, 4H), 7.77 (s, 2H), 7.71 (d, 2H, *J*=8.8 Hz), 7.32 (br s, 2H), 7.18 (s, 2H), 7.05 (s, 2H), 6.97 (d, 2H, *J*=7.6 Hz), 6.08 (d, 2H, *J*=8.4 Hz), 3.97-4.08 (m, 6H), 2.31-2.34 (m, 4H), 1.91-2.03 (m, 6H), 0.85 (d, 6H, *J*=6.7 Hz), 0.82 (d, 6H, *J*=6.7 Hz).

^{13}C NMR (100 MHz, DMSO-d_6) δ: 173.5, 171.8, 158.3, 158.1, 157.0, 135.7, 129.0, 123.7, 115.9, 106.2, 66.7, 57.6, 30.7, 29.6, 24.4, 19.3, 17.4.

IR v_{max}: 3252, 2967, 1657, 1516, 1211.

MS (ESI Positive) *m/z* 783 $[M+23]^+$, 799 $[M+39]^+$

Anal. Calcd for $C_{32}H_{48}N_{12}O_{10}$•1.5 H_2O: C 48.78, H 6.54, N 21.34; found C 48.61, H 6.37, N 21.03.

Molecular tong (253)

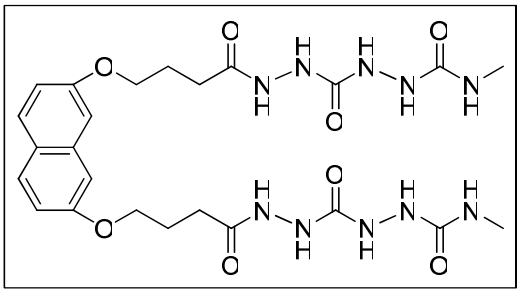

Compound **238** (157 mg, 0.64 mmol) was deprotected according to general procedure A. The corresponding trifluoroacetate salt **239** and compound **251** (101 mg, 0.30 mmol) were dissolved in DMF. DIPEA (358 μL, 2.1 mmol, 7 equiv), HBTU (287 mg, 0.76 mmol, 2.5 equiv), and HOBt (90 mg, 0.67 mmol, 2.2 equiv) were successively added to the reaction mixture that was then stirred, under argon atmosphere, for 48 h at r.t.. The solvent was evaporated under reduced pressure to afford a pale-pink oil. Trituration in EtOAc yielded a white solid that was filtered and washed successively with EtOAc, CH_2Cl_2, distilled H_2O, CH_3CN, acetone, CH_3OH, and ether. Product **253** was obtained as a white powder (98 mg, 55%).

Mp: 206-210 ºC

^{1}H NMR (400 MHz, DMSO-d_6) δ: 9.59 (s, 2H), 8.14 (br s, 4H), 7.63-7.72 (m, 4H), 7.19 (s, 2H), 6.96 (s, 2H), 6.09 (br, 2H), 4.08 (br, 4H), 2.57 (s, 6H), 2.33-2.42 (m, 4H), 2.01 (br, 4H).

^{13}C NMR (100 MHz DMSO-d_6) δ: 174.1, 159.2, 158.1, 156.9, 135.7, 128.9, 123.7, 115.9, 106.1, 66.6, 29.7, 26.2, 24.2.

IR v_{max}: 3280, 2947, 1664, 1515, 1210.

MS (ESI Positive) *m/z* 613 $[M+23]^+$

Molecular tong (254)

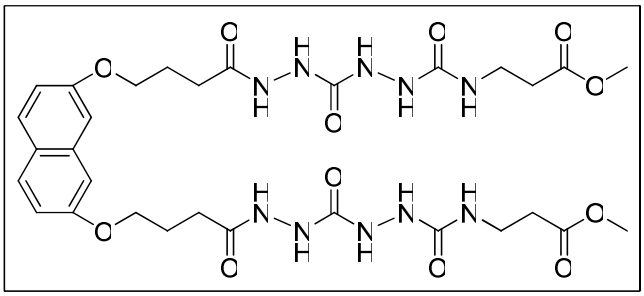

Compound **240** (218 mg, 0.68 mmol) was deprotected according to general procedure A. The corresponding trifluoroacetate salt **241** and compound **251** (101 mg, 0.30 mmol) were dissolved in DMF. DIPEA (384 μL, 2.3 mmol, 7 equiv), HBTU (308 mg, 0.81 mmol, 2.5 equiv), and HOBt (97 mg, 0.72 mmol, 2.2 equiv) were successively added to the reaction mixture that was then stirred, under argon atmosphere, for 48 h at r.t.. The solvent was evaporated under reduced pressure to afford a pale-yellow oil. Trituration in EtOAc yielded a pale-grey solid that was filtered and washed successively with EtOAc, CH_2Cl_2, distilled H_2O, CH_3CN, acetone, CH_3OH, and ether. Product **254** was obtained as a pale-grey powder (174 mg, 73%).

Mp: 177-187 ºC

^{1}H NMR (400 MHz, DMSO-d_6) δ: 9.60 (s, 2H), 8.14 (br s, 4H), 7.70-7.72 (m, 4H), 7.19 (s, 2H), 6.97 (d, 2H, *J*=8.4 Hz), 6.23 (br, 2H), 4.08 (br, 4H), 2.59 (s, 6H), 3.22-3.28 (m, 4H), 2.43-2.47 (m, 4H), 2.32 (t, 4H, *J*=7.1 Hz), 2.02 (br, 4H).

^{13}C NMR (100 MHz, DMSO-d_6) δ: 171.9, 158.5, 158.1, 157.0, 135.7, 129.0, 123.7, 115.9, 106.2, 66.8, 51.3, 35.3, 34.3, 29.7, 24.5.

IR ν_{max}: 3304, 2947, 1663, 1552, 1208.

MS (ESI Positive) *m/z* 757 $[M+23]^+$

Anal. Calcd for $C_{30}H_{42}N_{10}O_{12}$•2 H_2O: C 46.75, H 6.03, N 18.18; found C 46.90, H 5.62, N 17.35.

4-(7-(3-Carboxy-propoxy)-3-[(2,2-dimethyl-[1,3]dioxolan-4-ylmethyl)-amino]-naphthalen-2-yloxy)-butyric acid (255)

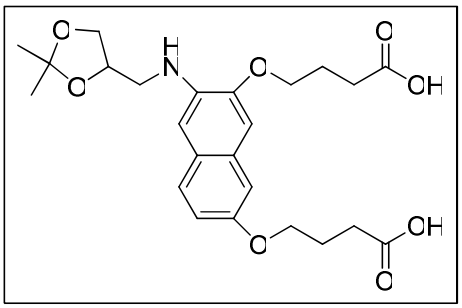

To a solution of **216** (282 mg, 0.44 mmol) in CH_3OH/EtOAc (20 mL/20 mL) was added Pd/C (56 mg, 20% weight). The reaction flask was flushed three times with hydrogen, and the reaction was stirred, under hydrogen atmosphere, for 24 h at r.t.. The mixture was filtered through a pad of celite, and the cake was thoroughly washed with methanol (200 mL). The filtrate was evaporated under reduced pressure to afford product **255** as a beige solid (201 mg, 99%).

Mp: 90-92 ºC

^{1}H NMR (300 MHz, CD_3OD) δ: 7.46 (d, 1H, *J*=9.0 Hz), 7.03 (d, 1H, *J*=2.1 Hz), 7.02 (s, 1H), 6.89 (dd, 1H, J_1=8.7 Hz, J_2=2.4 Hz), 6.79 (s, 1H), 4.45 (qt, 1H, *J*=5.4 Hz), 4.03-4.17 (m, 5H), 3.84 (dd, 1H, J_1=12.7 Hz, J_2=6.2 H), 3.23-3.36 (m, 2H), 2.48-2.53 (m, 4H), 2.16 (qt, 2H, *J*=6.6 Hz), 2.08 (qt, 2H, *J*=6.6 Hz), 1.46 (s, 3H), 1.36 (s, 3H).

^{13}C NMR (75 MHz, CD_3OD) δ: 175.8, 154.4, 147.8, 136.5, 128.3, 126.3, 125.2, 115.4, 109.0, 106.4, 104.5, 103.8, 74.2, 66.9, 66.7, 66.5, 45.5, 30.3, 25.7, 24.5, 24.3, 24.0.

IR v_{max}: 2918, 1703, 1248.

MS (APCI Positive) *m/z* 462 $[M+1]^+$

Anal. Calcd for $C_{24}H_{31}NO_8$: C 62.46, H 6.77, N 3.04; found C 62.13, H 6.63, N 2.90.

4,4'-(3-((2,2-Dimethyl-1,3-dioxolan-4-yl)methylamino)naphthalene-2,7-diyl)bis(oxy)bis (*N*-((*S*)-1-(2-(5-acetamido-2-methoxybenzoyl)hydrazinyl)-3-methyl-1-oxobutan-2-yl) butanamide) (256)

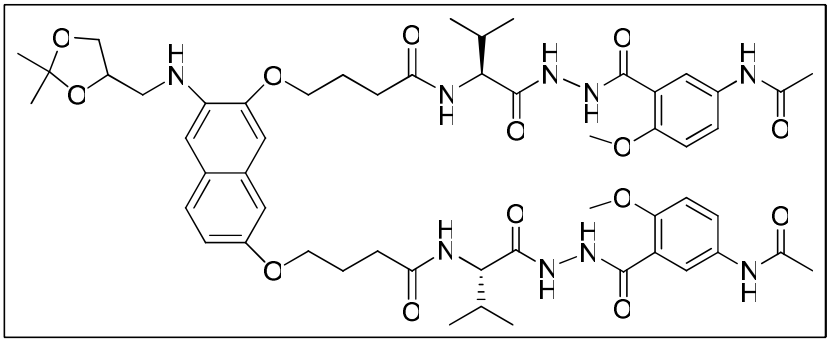

Compound **228** (312 mg, 0.72 mmol) was deprotected according to general procedure A. The corresponding trifluoroacetate salt **229** and **255** (150 mg, 0.33 mmol) were dissolved in DMF. DIPEA (384 μL, 2.3 mmol, 7 equiv), HBTU (308 mg, 0.81 mmol, 2.5 equiv), and HOBt (97 mg, 0.72 mmol, 2.2 equiv) were successively added to the reaction mixture that was then stirred, under argon atmosphere, for 48 h at r.t.. The solvent was evaporated under reduced pressure to afford an orange oil. Trituration in EtOAc yielded a orange solid that was filtered and washed successively with EtOAc, CH_2Cl_2, CH_3OH, and ether. Product **256** was obtained as a orange powder (174 mg, 50%).

Mp: 188-194 ºC

^{1}H NMR (400 MHz, DMSO-d_6) δ: 10.33 (s, 1H), 10.32 (s, 1H), 9.93 (s, 4H), 7.94-8.00 (m, 4H), 7.75 (d, 2H, *J*=8.7 Hz), 7.48 (d, 1H, *J*=9.0 Hz), 7.09 (d, 2H, *J*=9.0 Hz), 7.06 (s, 2H), 6.88 (dd, 1H, J_1=8.8 Hz, J_2=1.7 Hz), 6.77 (s, 1H), 5.03 (t, 1H, *J*=5.0 Hz), 4.31-4.41 (m, 3H), 3.97-4.08 (m, 5H), 3.84 (s, 6H), 3.75-3.79 (m, 1H), 3.28 (br, 2H), 2.33-2.44 (m, 4H), 2.02 (s, 6H), 1.97 (br, 6H), 1.39 (s, 3H), 1.29 (s, 3H), 0.95 (d, 6H, *J*=6.4 Hz), 0.90 (d, 6H, *J*=6.4 Hz).

^{13}C NMR (100 MHz, DMSO-d_6) δ: 171.6, 169.5, 168.0, 163.3, 153.9, 152.7, 147.6, 136.6, 132.6, 127.7, 126.5, 124.9, 123.3, 121.3, 121.1, 115.6, 112.4, 106.8, 104.9, 103.1, 73.7, 67.4, 66.9, 66.8, 56.1, 56.0, 45.6, 31.6, 30.7, 26.7, 25.2, 25.0, 23.8, 19.2, 18.3.

IR v_{max}: 3260, 2953, 1604, 1490, 1250.

MS (ESI Positive) *m/z* 1093 $[M+23]^+$

Anal. Calcd for $C_{54}H_{71}N_9O_{14}$•1 H_2O: C 59.60, H 6.78, N 11.59; found C 59.24, H 6.35, N 11.36.

4,4'-(3-(2,3-Dihydroxypropylamino)naphthalene-2,7-diyl)bis(oxy)bis(N-((S)-1-(2-(5-acetamido-2-methoxybenzoyl)hydrazinyl)-3-methyl-1-oxobutan-2-yl)butanamide) (257)

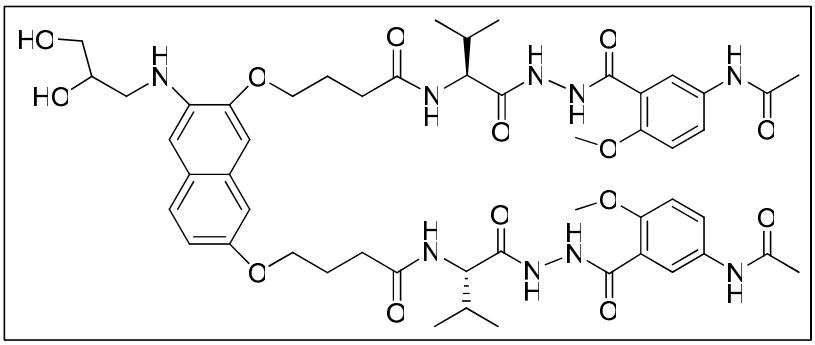

Compound **256** (51 mg, 48 μmol) was dissolved in a mixture of 1 M HCl/THF/EtOH (1:1:2, v/v/v) that was then stirred for 1 h at 55 ºC. The solvent was evaporated under reduced pressure, and the resulting residue was triturated with ether, filtered and washed successively with: saturated aqueous $NaHCO_3$, distilled H_2O, EtOH, EtOAc, cyclohexane and ether. Product **257** was obtained as a orange powder (30 mg, 60%).

^{1}H NMR (300 MHz,DMSO-d_6) δ: 10.33 (s, 2H), 9.94 (s, 4H), 7.93-8.02 (m, 4H), 7.73-7.77 (m, 2H), 7.47 (d, 1H, *J*=9.0 Hz), 7.05-7.11 (m, 4H), 6.88-6.92 (m, 1H), 6.73 (s, 1H), 4.31-4.35 (m, 3H), 3.99-4.09 (m, 5H), 3.84 (s, 6H), 3.81-3.84 (m, 1H), 3.28 (br, 2H), 1.91-2.06 (m, 12H), 0.95 (d, 6H, *J*=6.6 Hz), 0.90 (d, 6H, *J*=6.6 Hz).

^{13}C NMR (75 MHz, DMSO-d_6) δ: 171.7, 169.5, 168.0, 167.9, 163.3, 152.7, 149.1, 137.0, 135.0, 132.6, 131.6, 128.9, 128.0, 124.8, 123.3, 121.3, 121.2, 114.6, 112.4, 106.8, 103.9, 103.2, 69.5, 67.3, 66.5, 64.3, 56.1, 53.7, 31.5, 30.7, 30.4, 25.0, 23.8, 19.2, 18.3.

IR v_{max}: 3271, 2936, 1641, 1490, 1249.

MS (ESI Positive) *m/z* 1053 $[M+23]^+$, 1069 $[M+39]^+$

Anal. Calcd for $C_{51}H_{67}N_9O_{14}$•2 H_2O: C 57.45, H 6.73, N 11.83; found C 57.66, H 6.57, N 10.97.

Molecular tong (258)

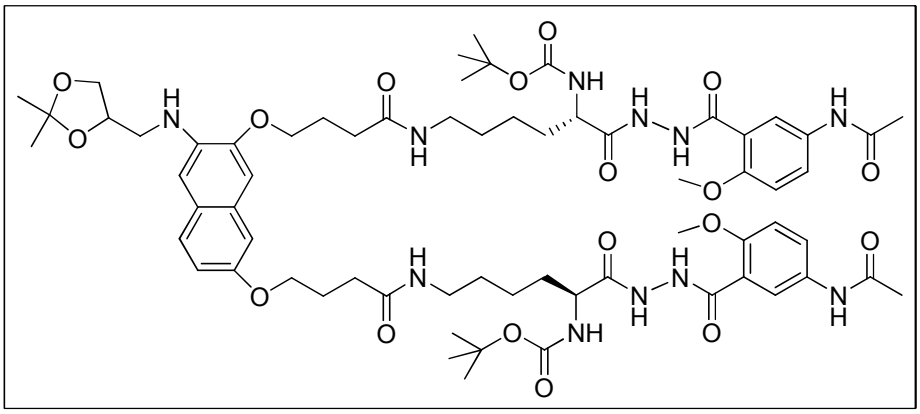

Compound **255** (71 mg, 0.15 mmol) and **230** (152 mg, 0.34 mmol, 2.2 equiv) were dissolved in DMF. DIPEA (129 μL, 0.77 mmol, 5 equiv), HBTU (145 mg, 0.38 mmol, 2.5 equiv), and HOBt (46 mg, 0.34 mmol, 2.2 equiv) were successively added to the reaction mixture that was then stirred, under argon atmosphere, for 48 h at r.t.. The solvent was evaporated under reduced pressure and the residue was dissolved in EtOAc (200 mL). The organic layer was washed with H_2O (100 mL), 10% aqueous citric acid (50 mL), 10% aqueous K_2CO_3 (50 mL), H_2O (100 mL), dried over Na_2SO_4 and concentrated under reduced pressure. The crude residue was then purified by flash chromatography on silica gel (CH_2Cl_2/CH_3OH, 90/10) to afford product **258** as a light pink powder (119 mg, 59%).

Mp: 160-170 ºC

^{1}H NMR (400 MHz, $CDCl_3$) δ: 11.99 (br s, 2H), 11.34 (s, 2H), 8.93 (s, 2H), 8.43 (s, 2H), 7.97 (s, 1H), 7.95 (s, 1H), 7.42 (d, 1H, *J*=8.3 Hz), 6.82-7.00 (m, 5H), 6.70 (s, 1H), 5.89 (br s, 1H), 5.63-5.70 (m, 3H), 4.92 (br, 2H), 4.45 (br, 1H), 3.81-4.13 (m, 12H), 3.28-3.48 (m, 3H), 3.03-3.10 (m, 4H), 2.04-2.28 (m, 14H), 1.62-1.79 (m, 4H), 1.19-1.46 (m, 32H).

^{13}C NMR (100 MHz, $CDCl_3$) δ: 172.1, 172.0, 169.2, 169.1, 166.3, 155.6, 154.6, 153.6, 148.0, 136.3, 133.2, 128.4, 126.9, 126.2, 126.1, 125.1, 122.6, 117.8, 116.0, 112.1, 109.5, 107.0, 105.4, 104.4, 79.8, 74.2, 74.1, 67.2, 67.1, 66.7, 56.6, 52.1, 46.5, 39.3, 34.2, 32.8, 32.6, 29.7, 29.3, 28.4, 26.9, 25.2, 25.1, 24.9, 24.6, 22.2.

IR ν_{max}: 3309, 2926, 1643, 1492, 1248.

MS (ESI Positive) *m/z* 1351 $[M+23]^+$

Anal. Calcd for $C_{66}H_{93}N_{11}O_{18}$•2 H_2O: C 58.09, H 7.18, N 11.29; found C 57.86, H 7.29, N 11.08.

Molecular tong (259)

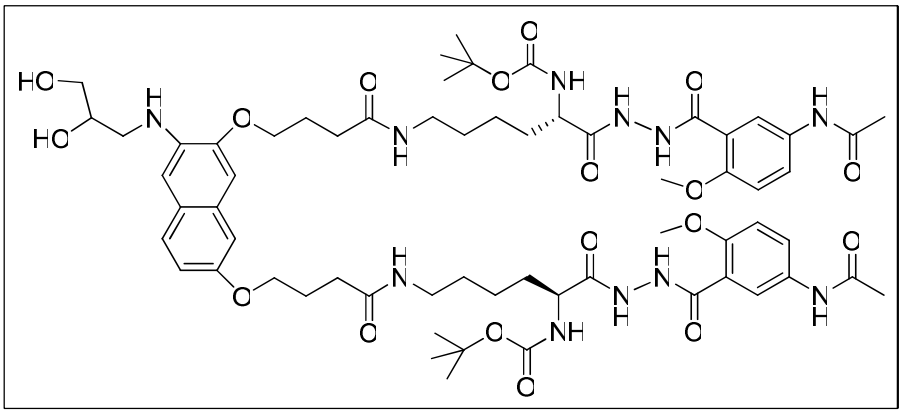

Compound **258** (23 mg, 17 μmol) was dissolved in methanol (1.5 mL) and *p*-TsOH•H_2O (5.5 mg, 29 μmol, 1.7 equiv) was added. The mixture was then stirred for 3 h at 50 ºC. The solvent was evaporated under reduced pressure, and the resulting crude residue was purified by flash chromatography on silica gel (CH_2Cl_2/CH_3OH, 80/20) to afford product **259** as a light pink powder (6 mg, 30%).

MS (ESI Positive) *m/z* 1289 $[M+1]^+$

4,4'-(3-Aminonaphthalene-2,7-diyl)bis(oxy)dibutanoic acid (260)

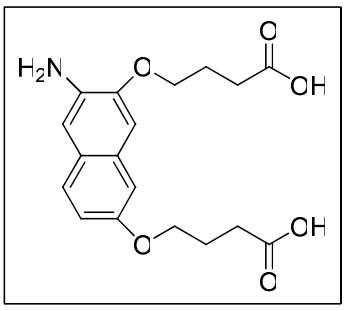

To a solution of **219** (156 mg, 0.30 mmol) in CH_3OH/EtOAc (5 mL/5 mL) was added Pd/C (31 mg, 20% weight). The reaction flask was flushed three times with hydrogen, and the reaction was stirred, under hydrogen atmosphere, for 24 h at r.t.. The mixture was filtered through a pad of celite, and the cake was thoroughly washed with methanol (200 mL). The filtrate was evaporated under reduced pressure to afford product **260** as a light-pink solid (102 mg, 99%).

Mp: 144-146 ºC

^{1}H NMR (300 MHz, CD_3OD) δ: 7.40 (d, 1H, *J*=9.0 Hz), 7.04 (s, 2H), 7.00 (s, 1H), 6.88 (dd, 1H, J_1=8.7 Hz, J_2=2.1 Hz), 4.03-4.17 (m, 5H), 2.48-2.57 (m, 4H), 2.17 (qt, 2H, *J*=6.6 Hz), 2.08 (qt, 2H, *J*=6.5 Hz), 1.23 (br s, 2H).

^{13}C NMR (75 MHz, CD_3OD) δ: 177.3, 177.2, 156.4, 150.1, 136.1, 131.2, 127.8, 126.6, 117.2, 111.3, 107.8, 106.6, 68.5, 68.1, 31.9, 31.6, 26.0, 25.9.

IR ν_{max}: 2923, 1714, 1253.

MS (APCI Positive) *m/z* 348 $[M+1]^+$

4,4'-(3-Aminonaphthalene-2,7-diyl)bis(oxy)bis(N-((S)-1-(2-(5-acetamido-2-methoxy benzoyl)hydrazinyl)-3-methyl-1-oxobutan-2-yl)butanamide) (261)

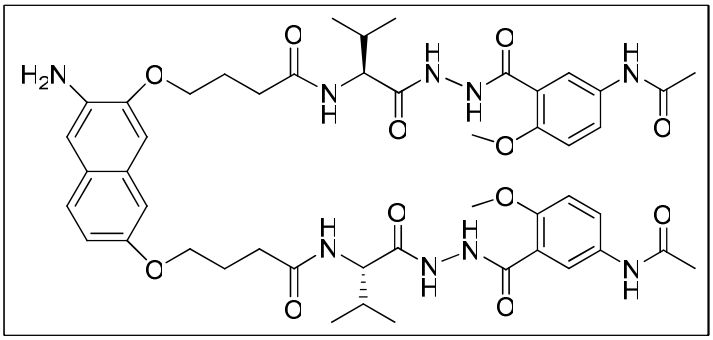

Compound **228** (275 mg, 0.65 mmol) was deprotected according to general procedure A. The corresponding trifluoroacetate salt **229** and compound **260** (103 mg, 0.30 mmol) were dissolved in DMF. DIPEA (394 μL, 2.1 mmol, 7 equiv), HBTU (281 mg, 0.74 mmol, 2.5 equiv), and HOBt (88 mg, 0.65 mmol, 2.2 equiv) were successively added to the reaction mixture that was then stirred, under argon atmosphere, for 48 h at r.t.. The solvent was evaporated under reduced pressure to afford an orange oil. Trituration in EtOAc yielded a orange solid that was filtered and washed successively with EtOAc, CH_2Cl_2, CH_3OH, and ether. Product **261** was obtained as a brick colour powder (192 mg, 68%).

Mp: 208-214 ºC

^{1}H NMR (400 MHz, DMSO-d_6) δ: 10.31 (s, 2H), 9.92 (s, 4H), 7.92-8.01 (m, 4H), 7.75 (d, 2H, *J*=7.2 Hz), 7.38 (d, 1H, *J*=8.3 Hz), 7.09 (d, 2H, *J*=8.1 Hz), 7.03 (s, 2H), 6.86 (s, 2H), 4.94 (br s, 2H), 4.33 (d, 2H, *J*=6.7 Hz), 3.96-4.08 (m, 4H), 3.84 (s, 6H), 2.37-2.42 (m, 4H), 2.01 (br, 12H), 0.95 (s, 6H), 0.90 (s, 6H).

^{13}C NMR (100 MHz, DMSO-d_6) δ: 171.8, 171.7, 169.5, 168.0, 163.3, 157.3, 152.6, 148.0, 136.3, 132.6, 128.0, 126.0, 124.8, 123.3, 121.3, 121.1, 115.6, 112.4, 107.0, 106.7, 105.1, 67.1, 66.9, 56.1, 56.0, 31.7, 31.6, 30.8, 30.7, 25.1, 23.8, 19.2, 18.3.

IR ν_{max}: 3258, 1607, 1491, 1250.

MS (ESI Positive) *m/z* 979 $[M+23]^+$

Anal. Calcd for $C_{48}H_{61}N_9O_{12}$•2.5 H_2O: C 57.58, H 6.66, N 12.60; found C 57.94, H 6.32, N 12.26.

CHAPTER IV BIBLIOGRAPHIC REFERENCES:

[1] Webster, K. L.; Maude, A. B.; O'Donnell, M. E.; Mehrotra, A. P.; Gani, D. *J. Chem. Soc., Perkin Trans. 1* **2001**, 1673-1695.

[2] Huang, Y.; Dalton, D. R.; Carroll, P. J. *J. Org. Chem.* **1997**, *62*, 372-376.

[3] Thompson, C. M.; Frick, J. A.; Green, D. L. C. *J. Org. Chem.* **1990**, *55*, 111-116.

[4] Maki, T.; Ishihara, K.; Yamamoto, H. *Org. Lett.* **2006**, *8*, 1431-1434.

[5] Still, W. C.; Kahn, M.; Mitra, A. *J. Org. Chem.* **1978**, *43*, 2923-2925.

[6] Mohamadi, F.; Richards, N. G. J.; Guida, W. C.; Liskamp, R.; Lipton, M.; Caufield, C.; Chang, G.; Hendrickson, T.; Still, W. C. *Comp. Chem.* **1990**, *11*, 440-467.

[7] Weiner, S. J.; Kollman, P. A.; Nguyem, D. T.; Case, D. A. *J. Comput. Chem.* **1986**, *7*, 6127-6129.

[8] Ponder, J. W.; Richards, F. M. *J. Comput. Chem.* **1987**, *8*, 1016-1024.

[9] Fox, T.; Kollman, P. A. *J. Phys. Chem. B* **1998**, *102*, 8070-8079.

[10] Duan, Y.; Wu, C.; Chowdhury, S.; Lee, M. C.; M., X. G.; Zhang, W.; Yang, R.; Cieplak, P.; Luo, R.; Lee, T. *J. Comput. Chem.* **2003**, *24*, 1999-2012.

[11] Case, D. A.; Pearlman, D. A.; Caldwell, J. W.; Cheatham III, T. E.; Wang, J.; Ross, W. S.; Simmerling, C. L.; Darden, T. A.; Merz, K. M.; Stanton, R. V.; Cheng, A. L.; Vincent, J. J.; Crowley, M.; Tsui, V.; Gohlke, H.; Radmer, R. J.; Duan, Y.; Pitera, J.; Massova, I.; Seibel, G. L.; Singh, U. C.; Weiner, P. K.; Kollman, P. A.; AMBER 7, University of California, San Francisco, 2002.

[12] Allen, P.; Tildesley, D. J. *Computer Simulation of Liquids*; Clarendon Press: Oxford, 1987.

[13] Baldwin, J. E.; Moloney, M. G.; North, M. *Tetrahedron* **1989**, *45*, 6319-6330.

[14] Equi, A. M.; Brown, A. M.; Cooper, A.; Ner, S. K.; Watson, A. B.; Robins, D. J. *Tetrahedron* **1991**, *47*, 507-518.

[15] Martinborough, E.; Denti, T. M.; Castro, P. P.; Wyman, T. B.; Knobler, C. B.; Diederich, F. *Helv. Chim. Acta* **1995**, *78*, 1037-1066.

[16] Bouras, A.; Boggetto, N.; Benatalah, Z.; de Rosny, E.; Sicsic, S.; Reboud-Ravaux, M. *J. Med. Chem.* **1999**, *42*, 957-962.

[17] Bannwarth, L.; Kessler, A.; Pethe, S.; Collinet, B.; Merabet, N.; Boggetto, N.; Sicsic, S.; Reboud-Ravaux, M.; Ongeri, S. *J. Med. Chem.* **2006**, *49*, 4657-4664.

[18] Merabet, N.; Dumond, J.; Collinet, B.; VanBaelinghem, L.; Boggetto, N.; Ongeri, S.; Ressad, F.; Reboud-Ravaux, M.; Sicsic, S. *J. Med. Chem.* **2004**, *47*, 6392-6400.

SUPPORTING INFORMATION OF CHAPTER II

I. CONFORMATIONAL STUDIES OF COMPOUND 92:

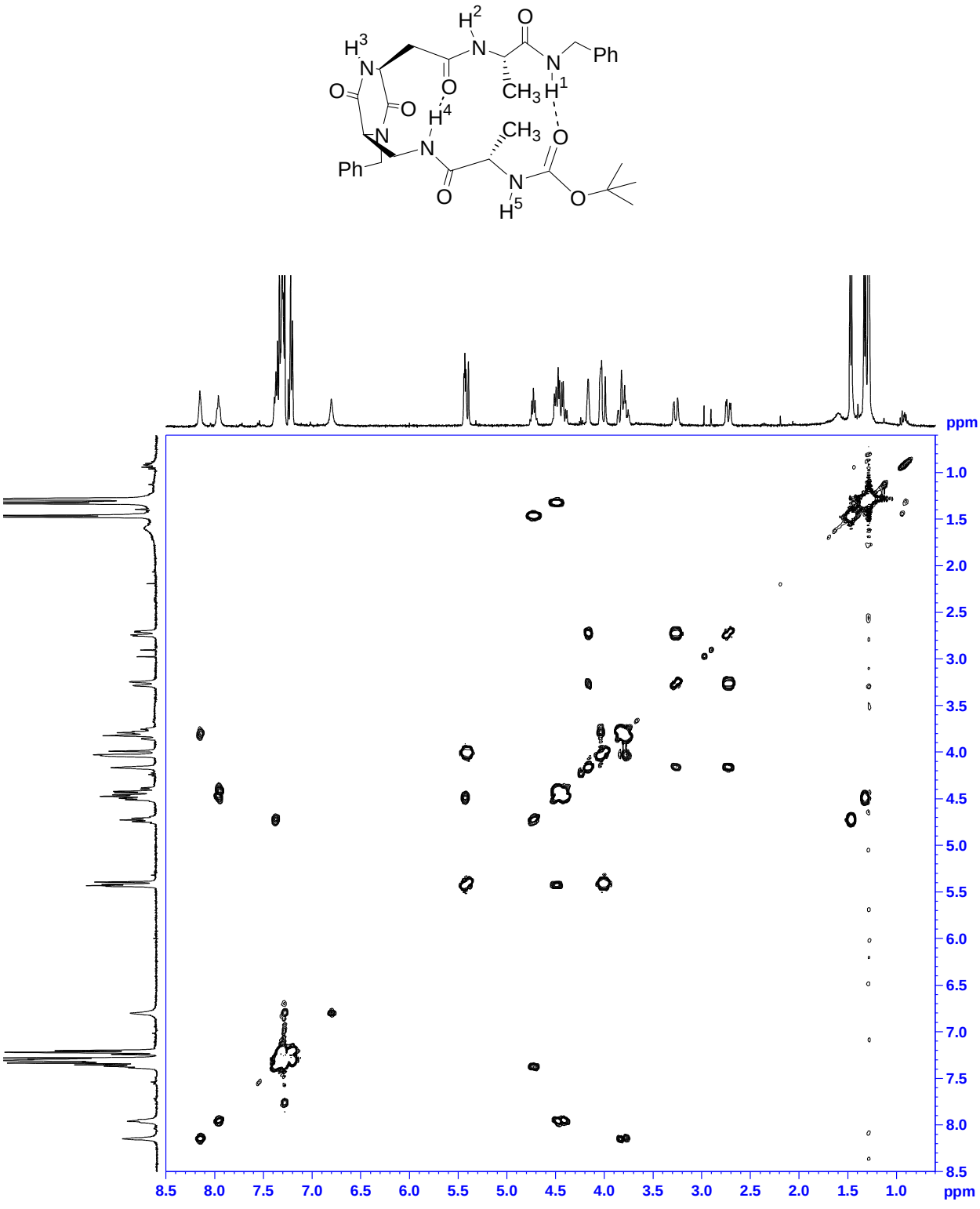

Figure I. COSY spectra of compound **92** (concentration 5 mM) in $CDCl_3$ at 25 ℃.

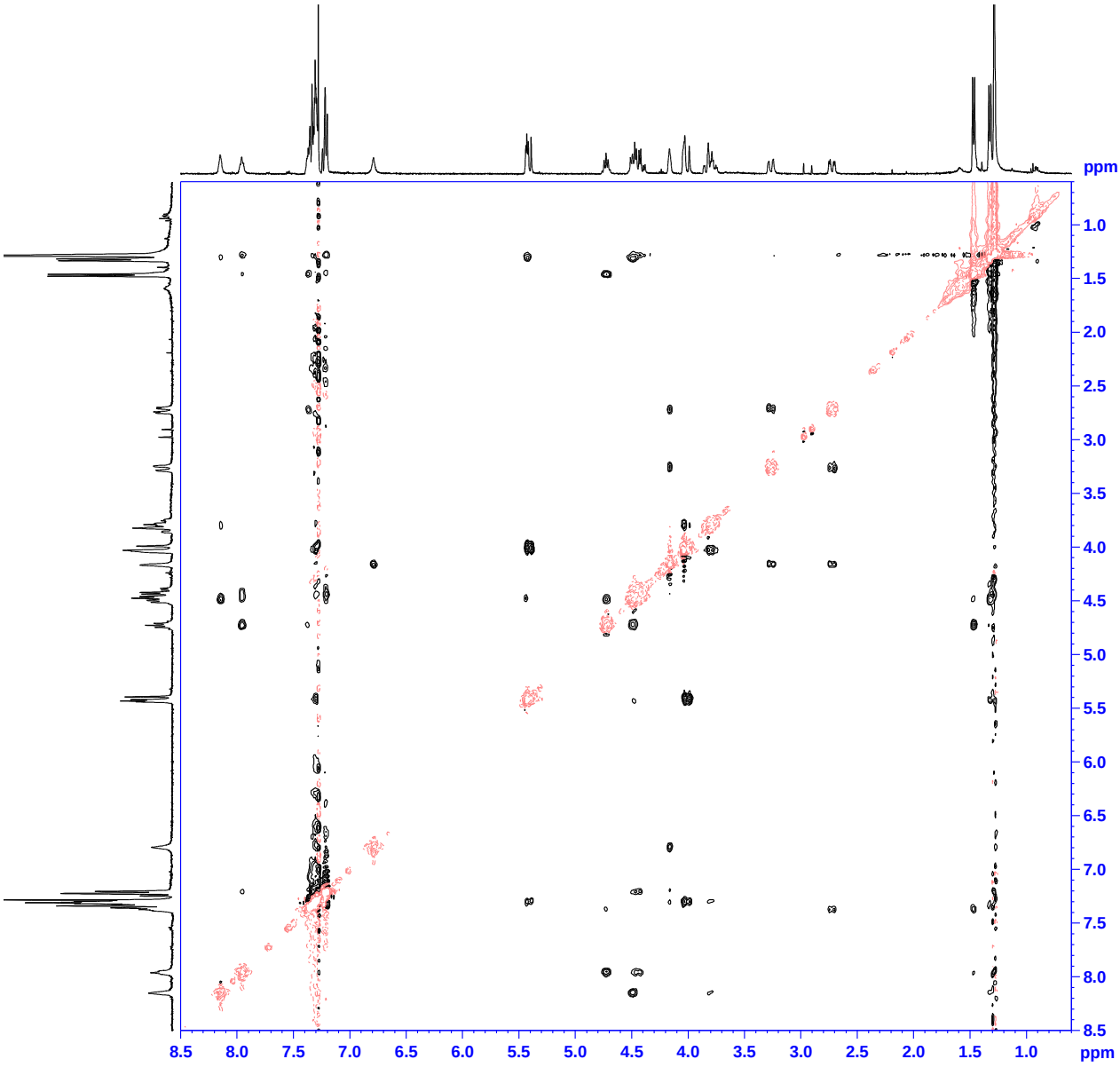

Figure II. NOESY spectra of compound **92** (concentration 5 mM) in $CDCl_3$ at 25 ℃, d8 = 800 ms. NOESY data collected with a noesytp pulse program with 1024 data points in F2 and 256 data points in F2.

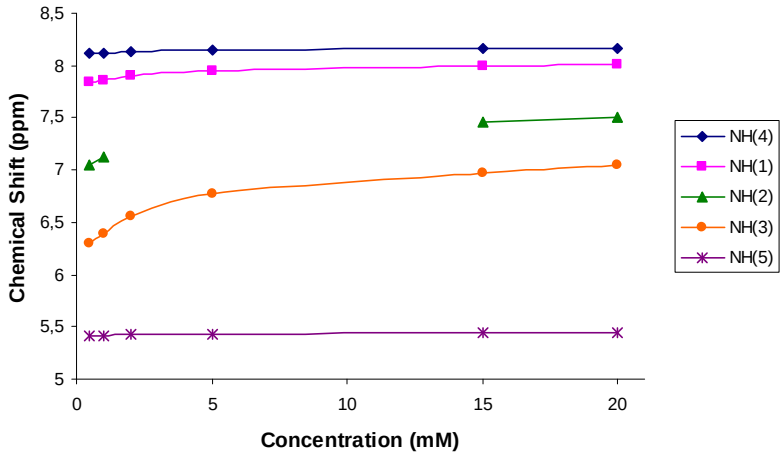

Figure III. Concentration dependence of NH chemical shifts of compound **92** in $CDCl_3$ at 25 ℃.

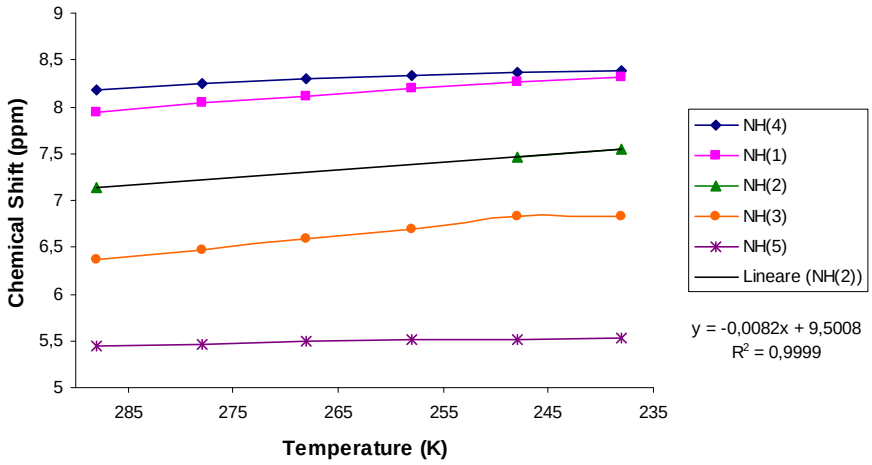

Figure IV. Temperature dependence of NH chemical shifts of compound **92** (concentration 0.5 mM) in $CDCl_3$.

II. CONFORMATIONAL STUDIES OF COMPOUND 93:

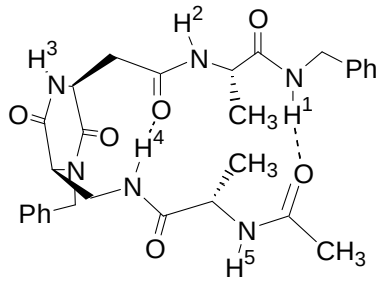

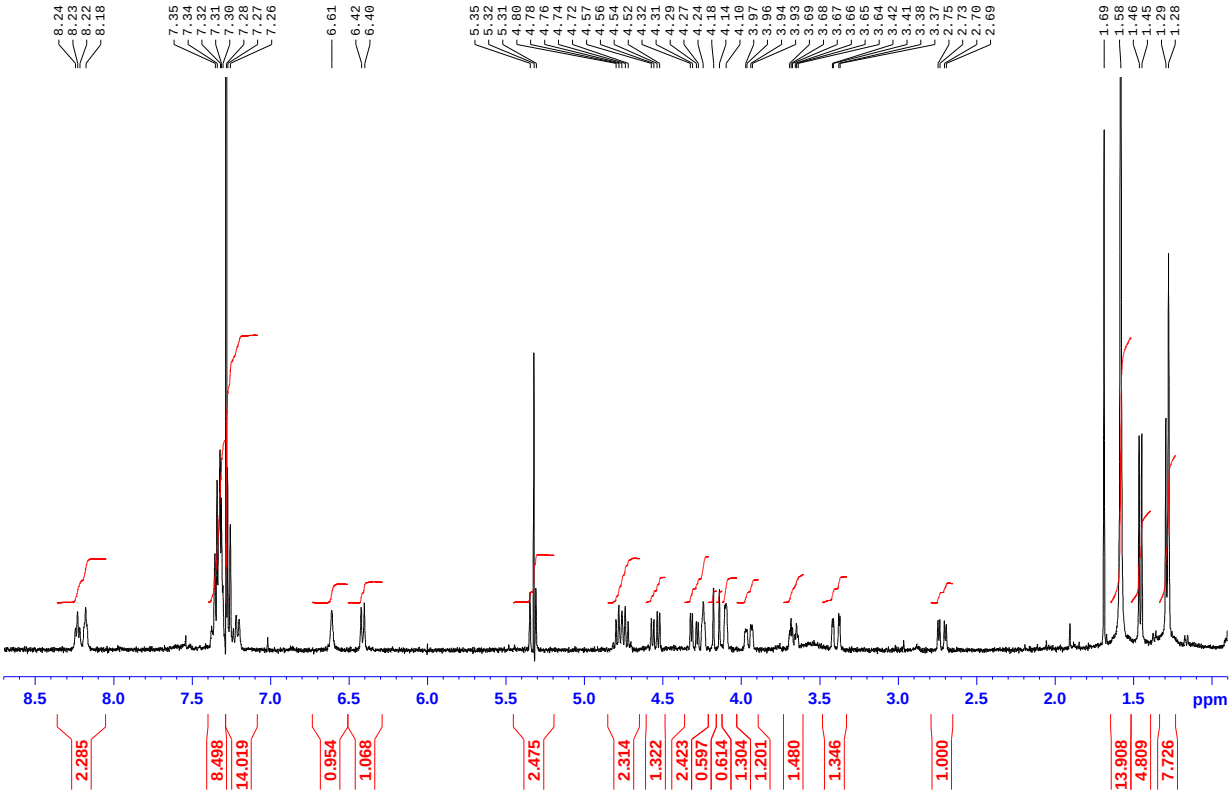

Figure V. ^{1}H-NMR spectra of compound **93** (concentration 2 mM) in $CDCl_3$ at 25 ℃.

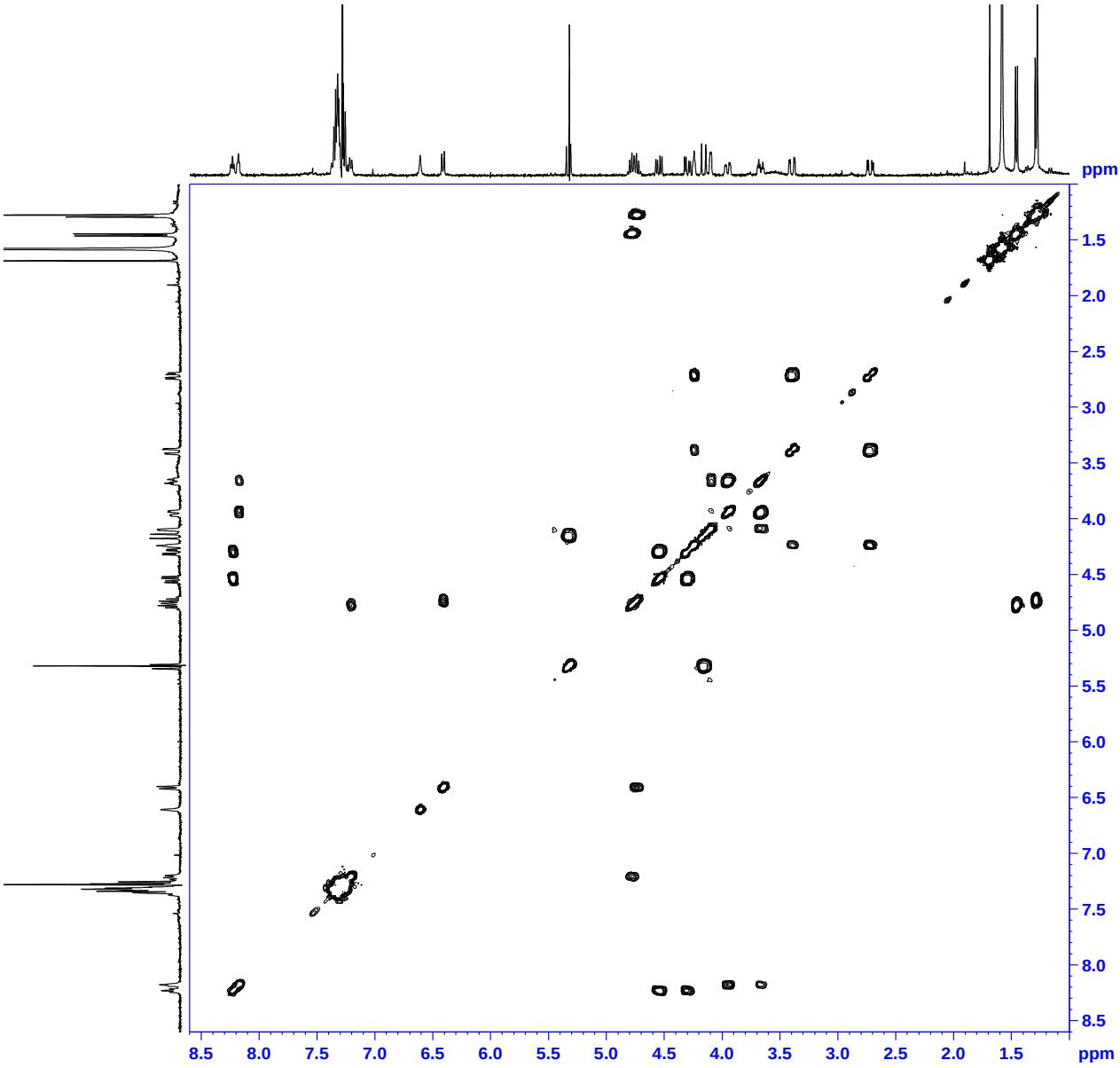

Figure VI. COSY spectra of compound **93** (concentration 2 mM) in $CDCl_3$ at 25 ℃.

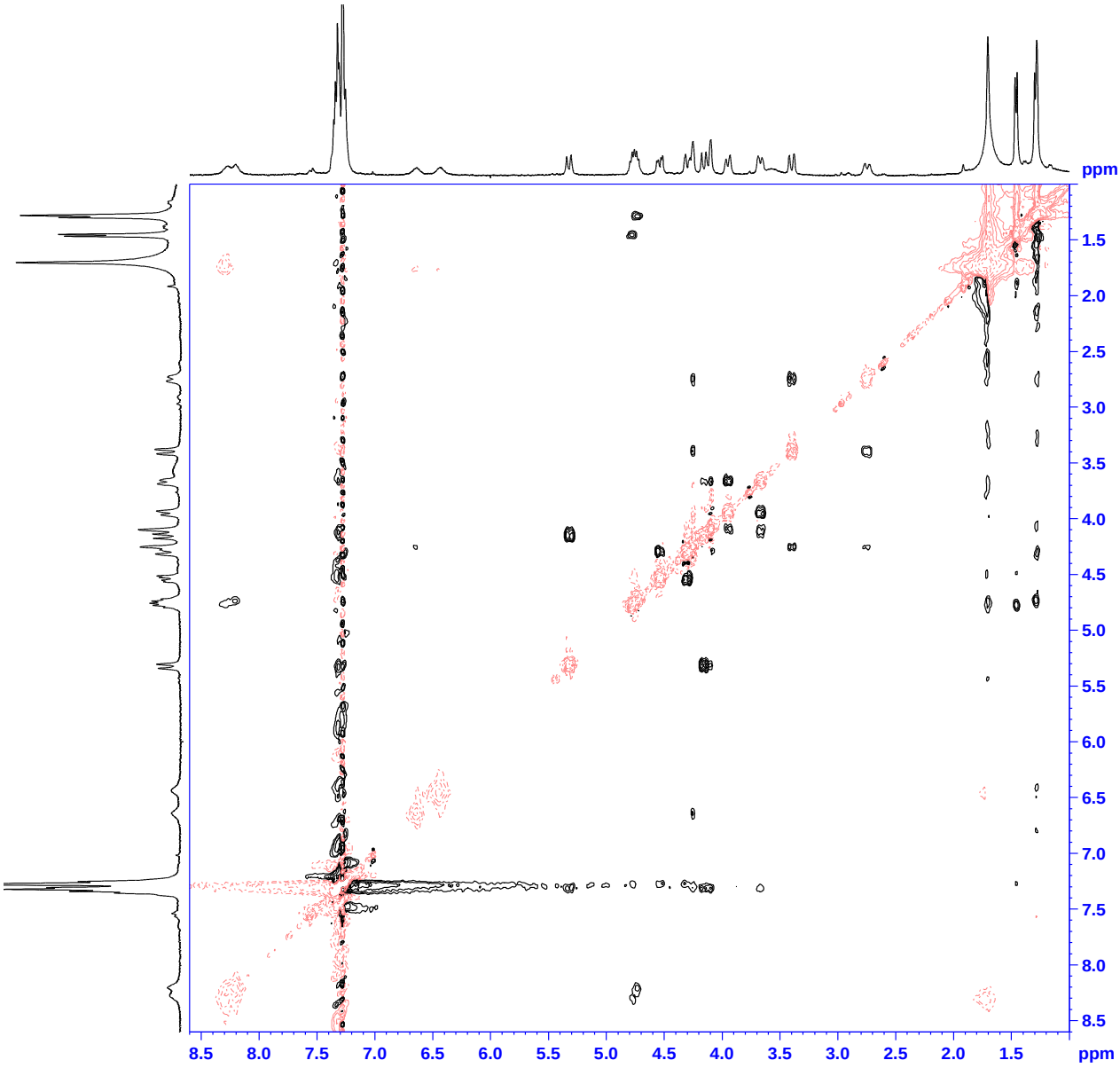

Figure VII. NOESY spectra of compound **93** (concentration 2 mM) in $CDCl_3$ at 25 ℃, d8 = 800 ms. NOESY data collected with a noesytp pulse program with 1024 data points in F2 and 256 data points in F2.

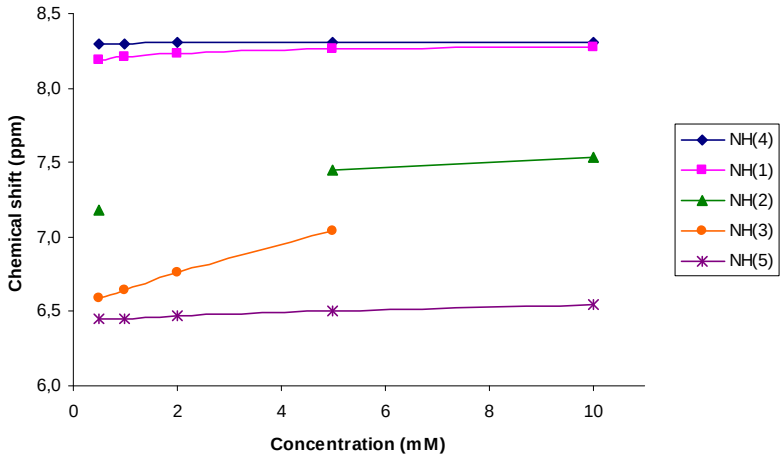

Figure VIII. Concentration dependence of NH chemical shifts of compound **93** in $CDCl_3$ at 25 ℃.

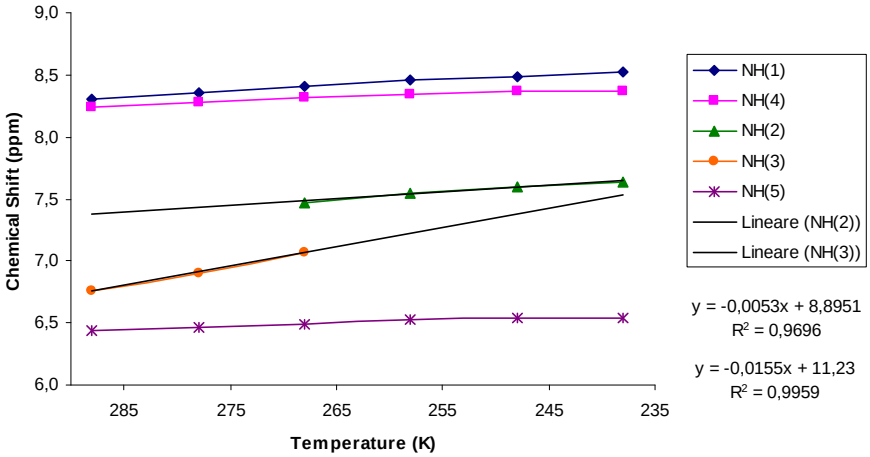

Figure IX. Temperature dependence of NH chemical shifts of compound **93** (concentration 2 mM) in $CDCl_3$.

Table I. ^{1}H-NMR data for the amide protons in compounds **92** and **93**.

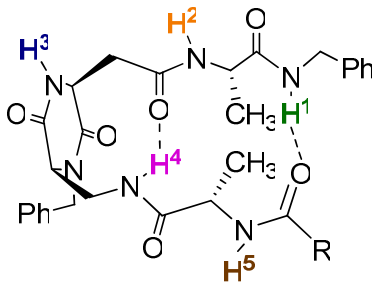

92: R = O-*t*Bu
93: R = CH_3

	92		**93**			
	$\delta^{a,c}$ (ppm)	$\Delta\delta/\Delta T^{a,d}$ (ppb/K)	$\delta^{b,c}$ (ppm)	$\Delta\delta/\Delta T^{b,d}$ (ppb/K)	$\Delta\delta^{b,e}$ (added CH_3OH)	NH/ND exchange^{b,f} (min)
NH^1	**7.81**	**-7.6**	**8.21**	**-4.6**	**-0.07**	**300**
NH^2	7.03	-8.2	7.21	-5.3	0.53	160
NH^3	6.28	-9.1	6.61	-15.5	1.25	< 10
NH^4	**8.10**	**-4.1**	**8.18**	**-2.7**	**0.03**	**960**
NH^5	5.41	-1.8	6.40	-2.3	≥ 0.7	-^{g}

a) Concentration 0.5 mM in $CDCl_3$; b) Concentration 2.0 mM in $CDCl_3$; c) at 298 K; d) determined between 238 and 288 K; e) measured in $CDCl_3/CH_3OH$ 4/1; f) measured in $CDCl_3/CD_3OD$ 4/1; g) not determined due to overlap with other resonances.

III. CONFORMATIONAL STUDIES OF COMPOUND 94:

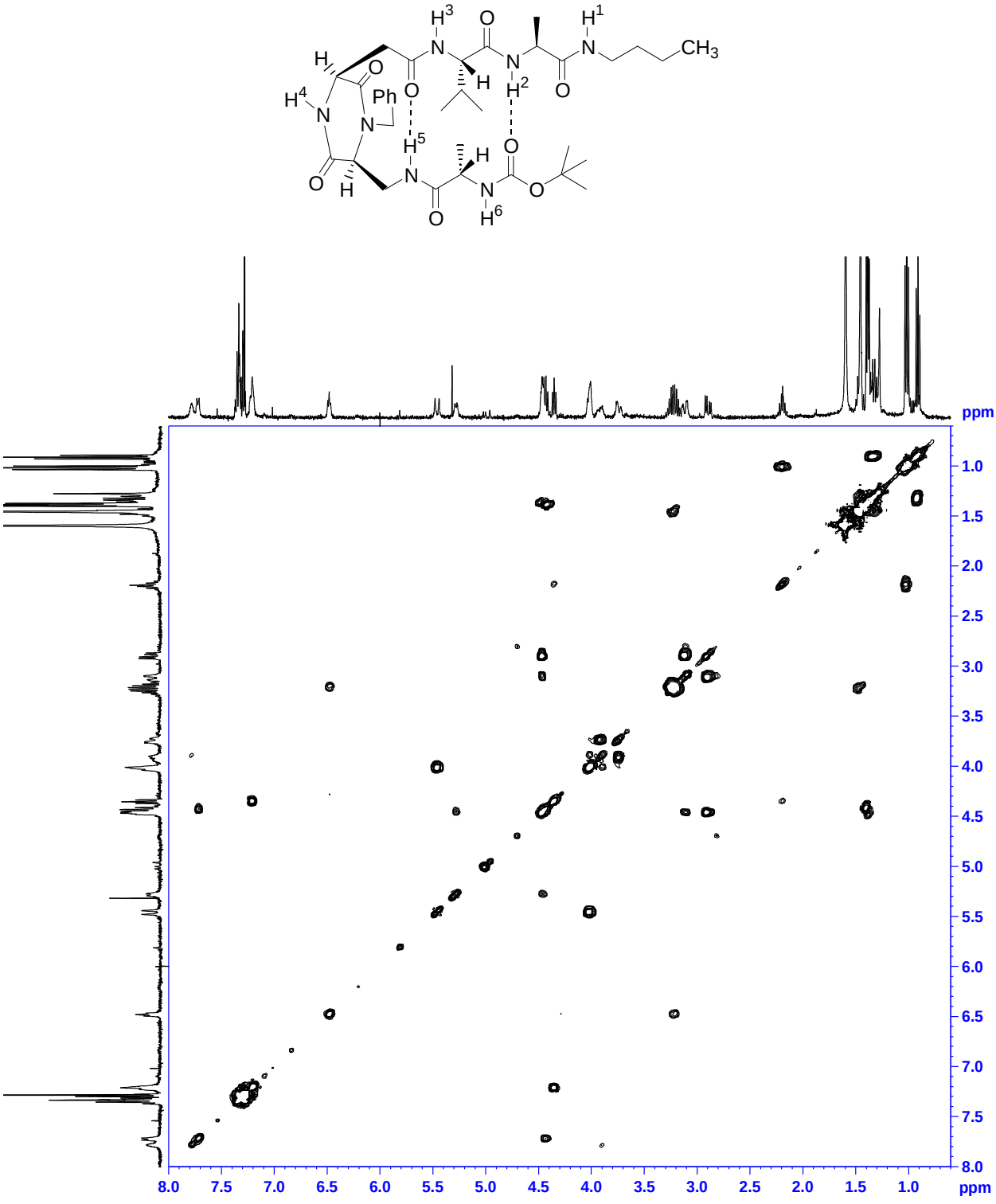

Figure X. COSY spectra of compound **94** (concentration 2 mM) in $CDCl_3$ at 25 ℃.

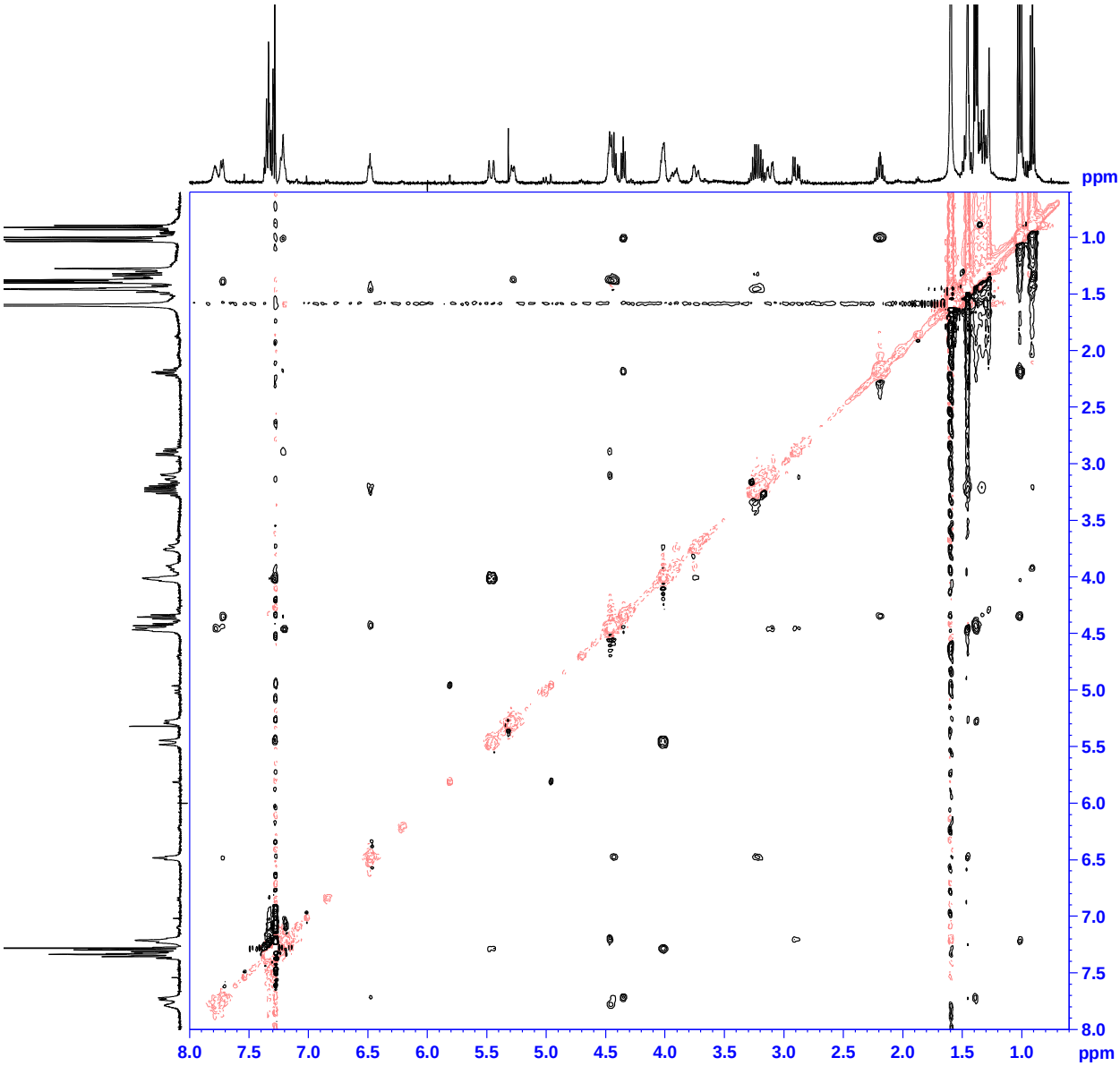

Figure XI. NOESY spectra of compound **94** (concentration 2 mM) in $CDCl_3$ at 25 ℃, d8 = 800 ms. NOESY data collected with a noesytp pulse program with 1024 data points in F2 and 256 data points in F2.

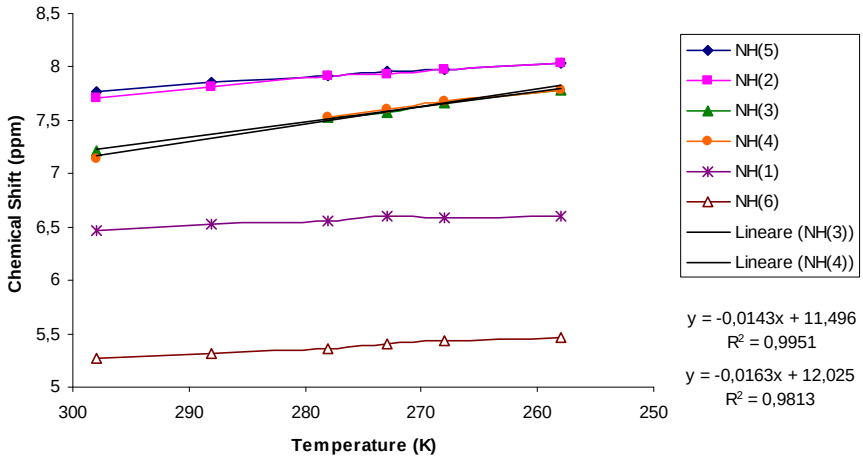

Figure XII. Temperature dependence of NH chemical shifts of compound **94** (concentration 2 mM) in $CDCl_3$.

Table II. ^{1}H-NMR data for the amide protons in compound **94**.

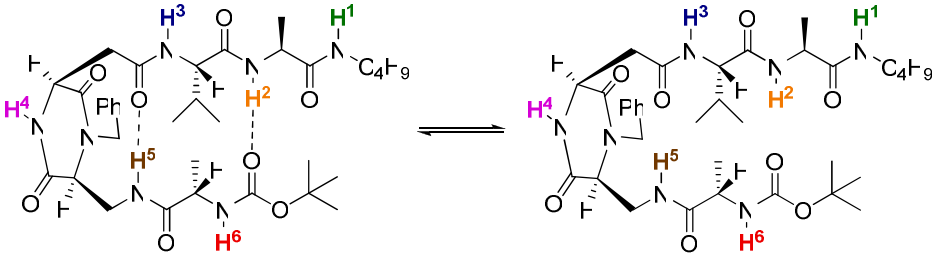

	94	
	$\delta^{a,b}$ (ppm)	$\Delta\delta/\Delta T$ ^{a,c} (ppb/K)
NH^1	6.47	-2.5
NH^2	7.71	-8.3
NH^3	7.21	-14.3
NH^4	7.14	-16.0
NH^5	7.77	-6.8
NH^6	5.27	-4.8

a) Concentration 2.0 mM in $CDCl_3$; b) at 298 K; c) determined between 258 and 298 K.

IV. CONFORMATIONAL STUDIES OF COMPOUND 95:

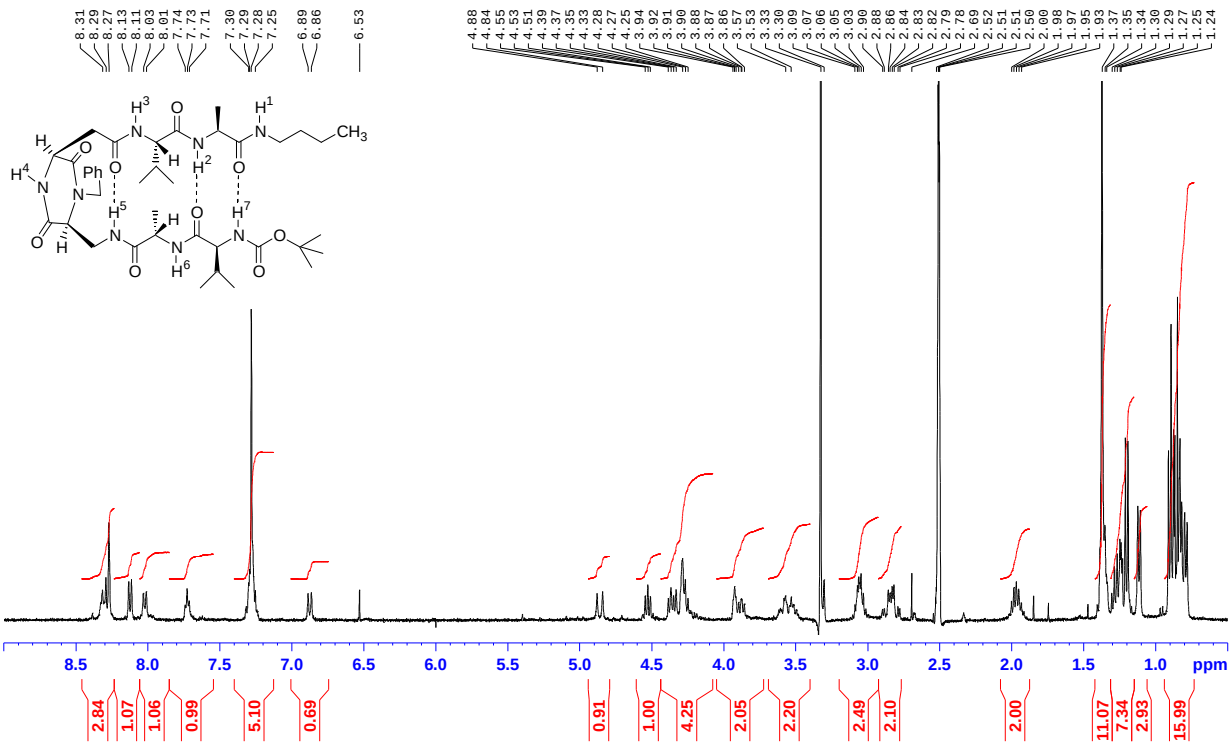

Figure XIII. ^{1}H-NMR spectra of compound **95** (concentration 2 mM) in DMSO-d_6 at 25 ℃.

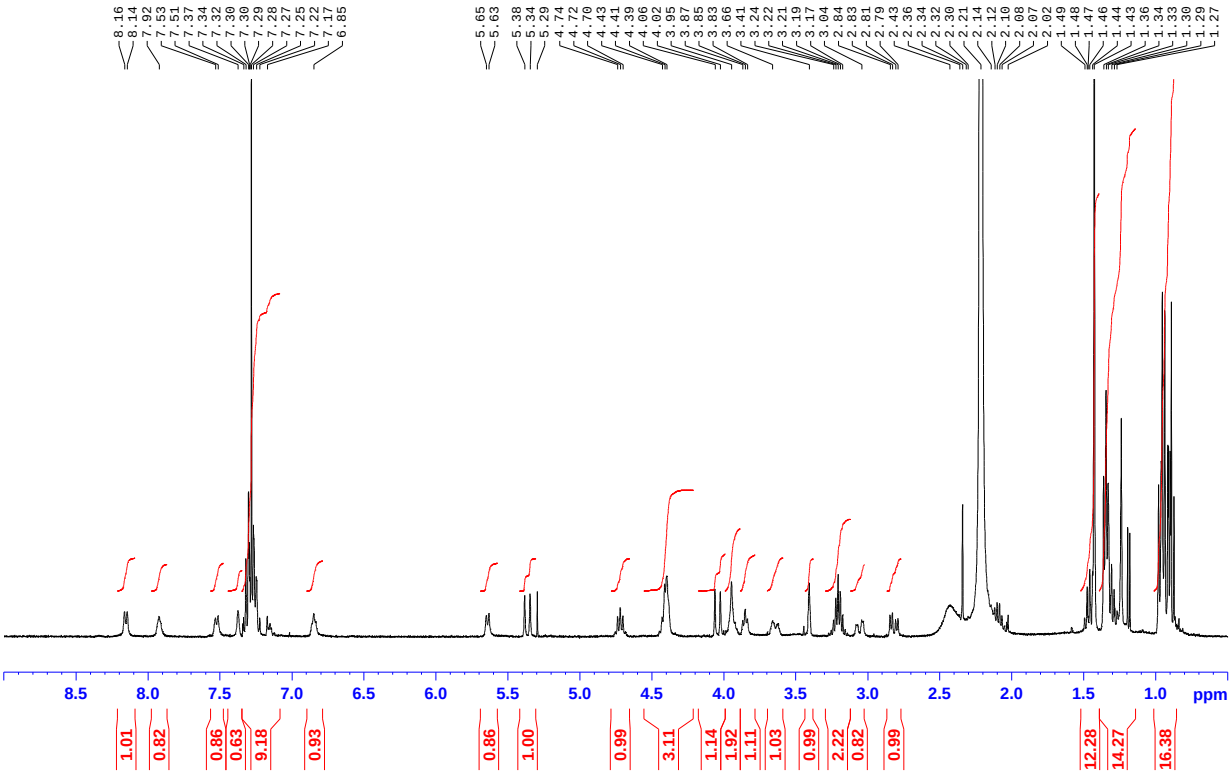

Figure XIV. ^{1}H-NMR spectra of compound **95** (concentration 2 mM) in 5% CD_3OH-$CDCl_3$ at 25 ℃.

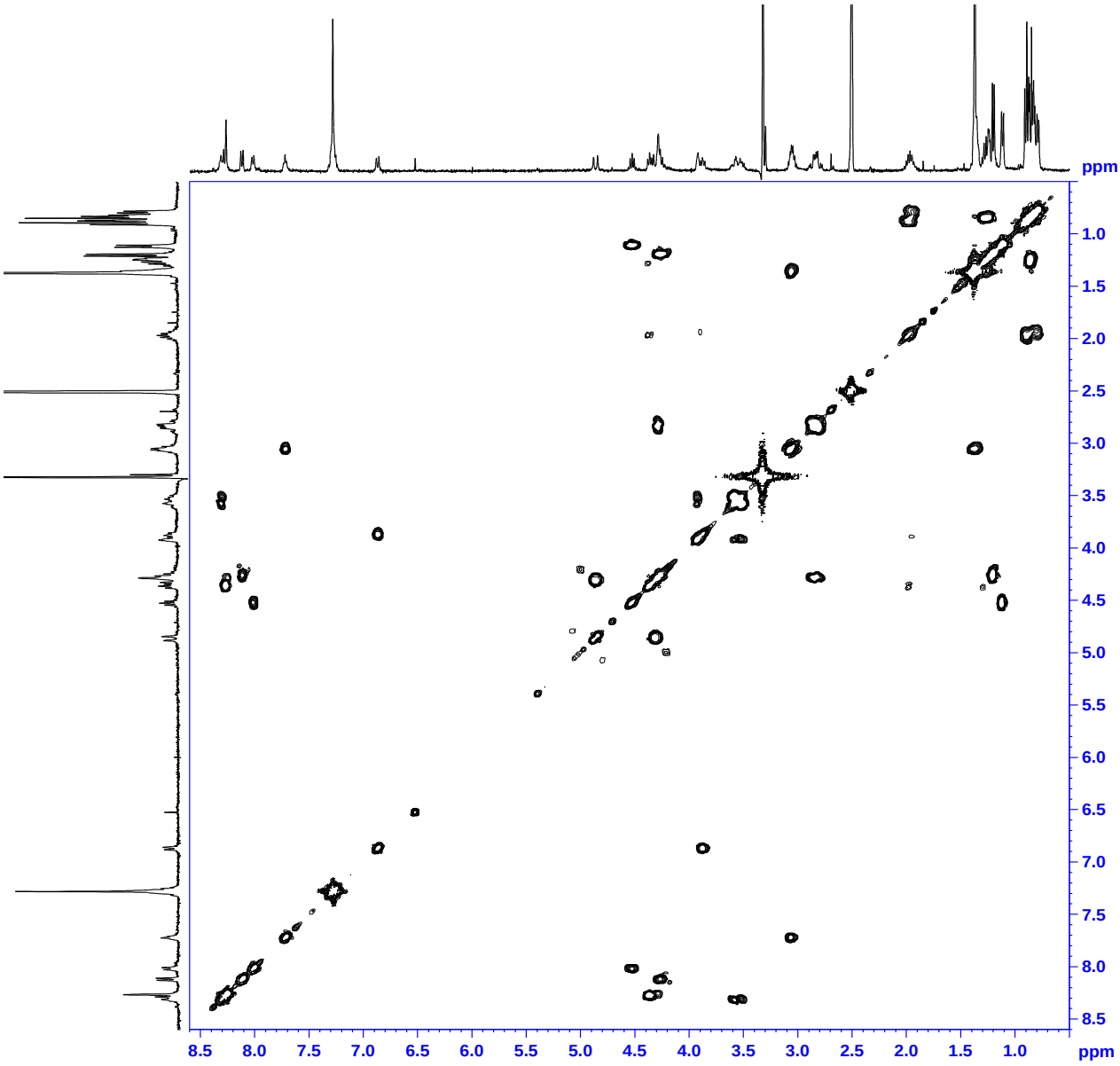

Figure XV. COSY spectra of compound **95** (concentration 2 mM) in DMSO-d_6 at 25 ℃.

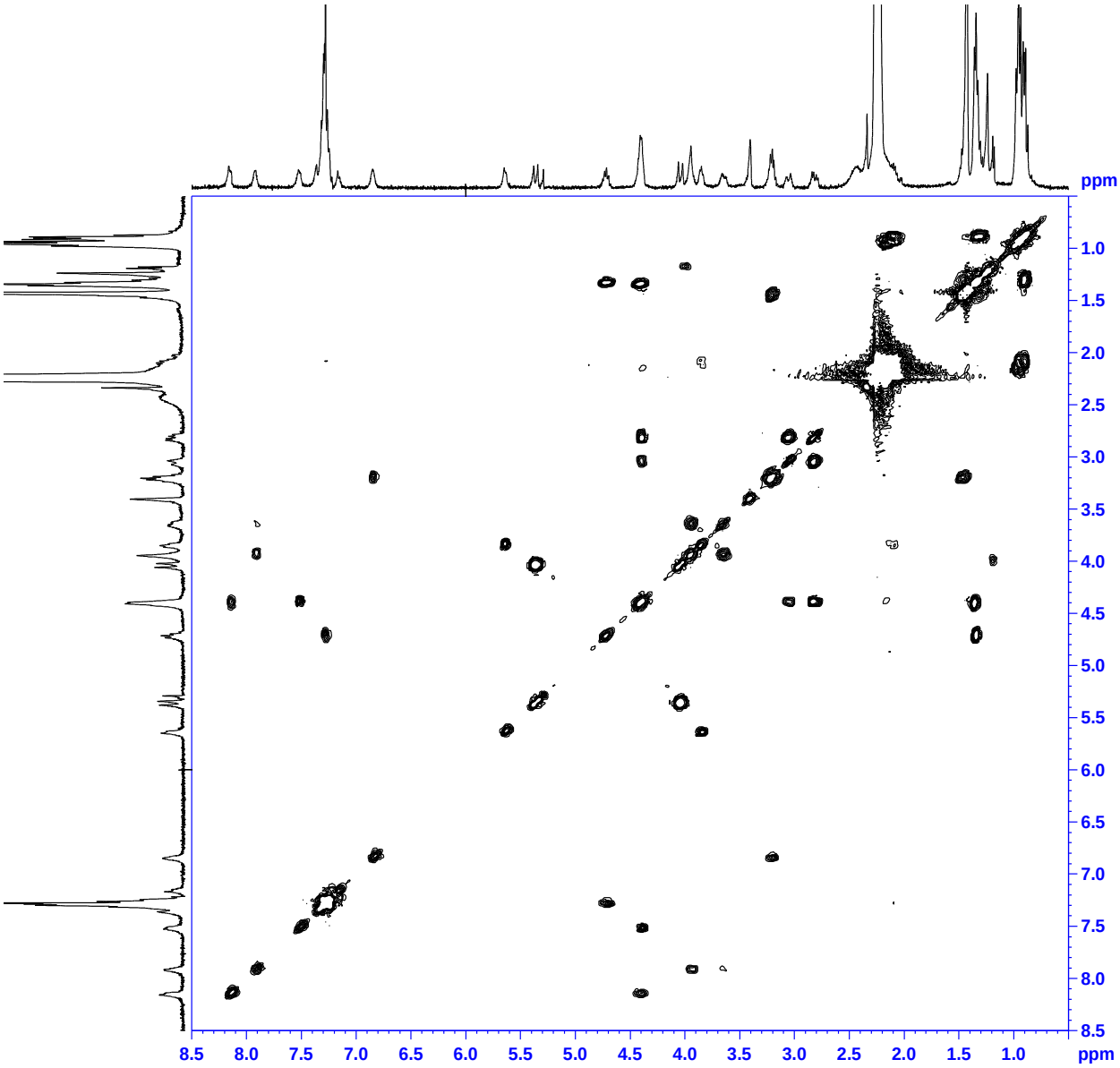

Figure XVI. COSY spectra of compound **95** (concentration 2 mM) in 5% CD_3OH-$CDCl_3$ at 25 ℃.

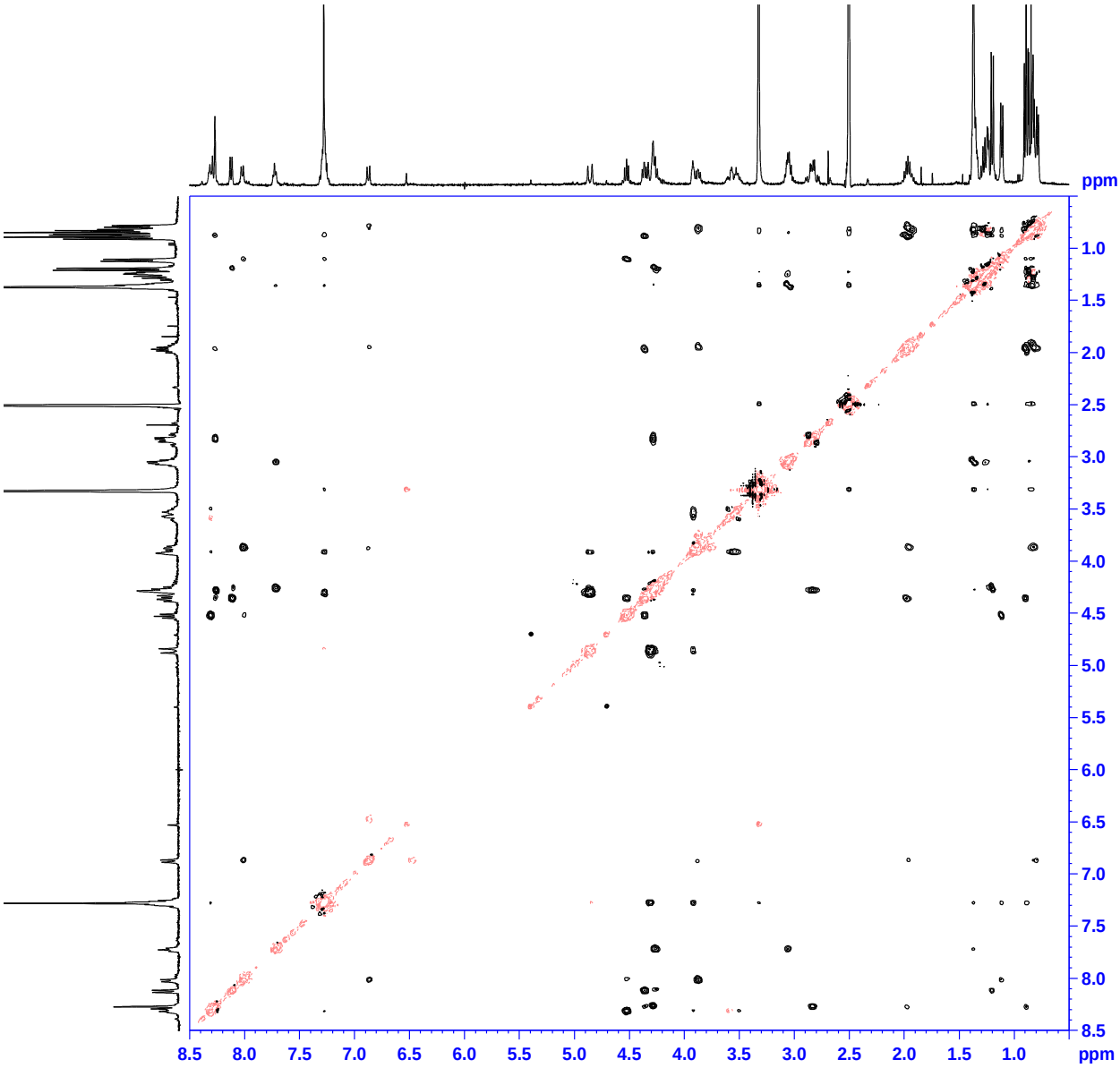

Figure XVII. ROESY spectra of compound **95** (concentration 2 mM) in DMSO-d_6 at 25 ℃, p15 = 400 ms. ROESY data collected with a roesytp pulse program with 1024 data points in F2 and 256 data points in F2.

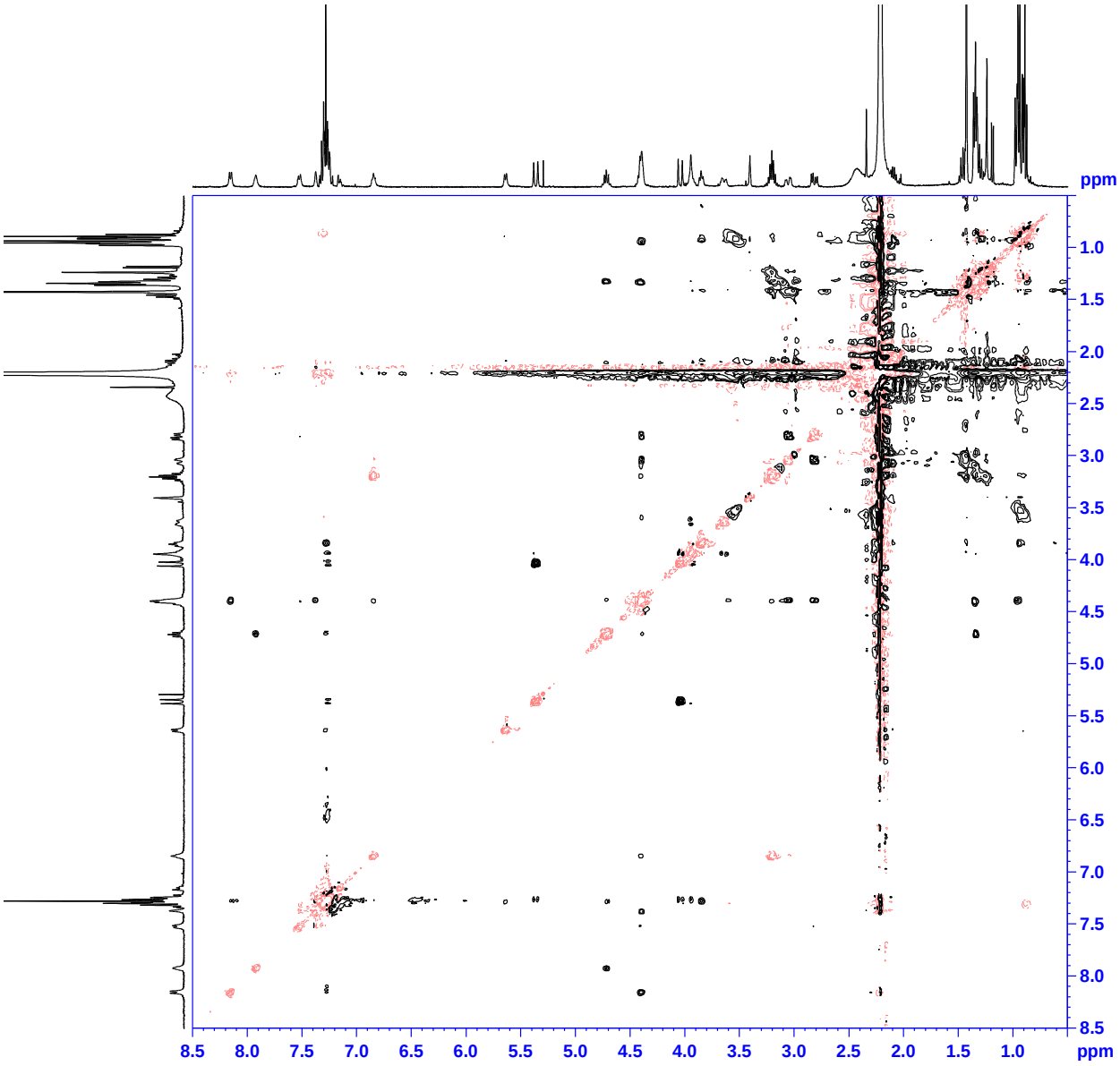

Figure XVIII. ROESY spectra of compound **95** (concentration 2 mM) in 5% CD_3OH-$CDCl_3$ at 25 ℃, p15 = 400 ms. ROESY data collected with a roesytp pulse program with 4096 data points in F2 and 256 data points in F2.

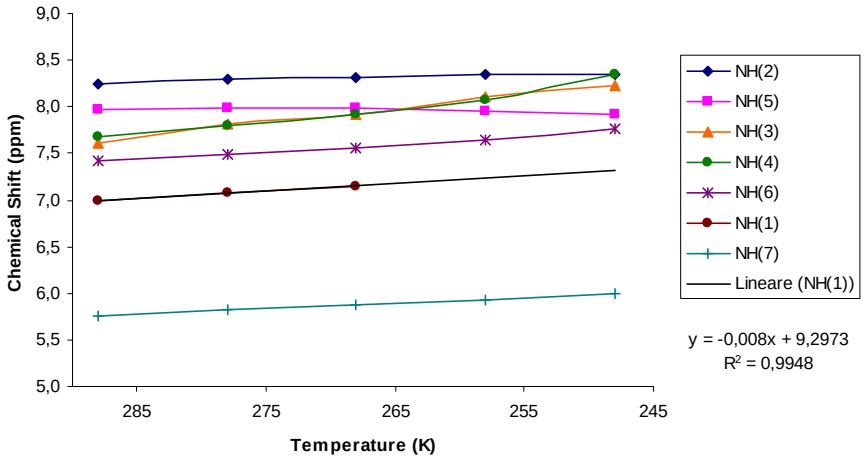

Figure XIX. Temperature dependence of NH chemical shifts of compound **95** (concentration 2 mM) in 5% CD_3OH-$CDCl_3$.

V. CONFORMATIONAL STUDIES OF COMPOUND 96:

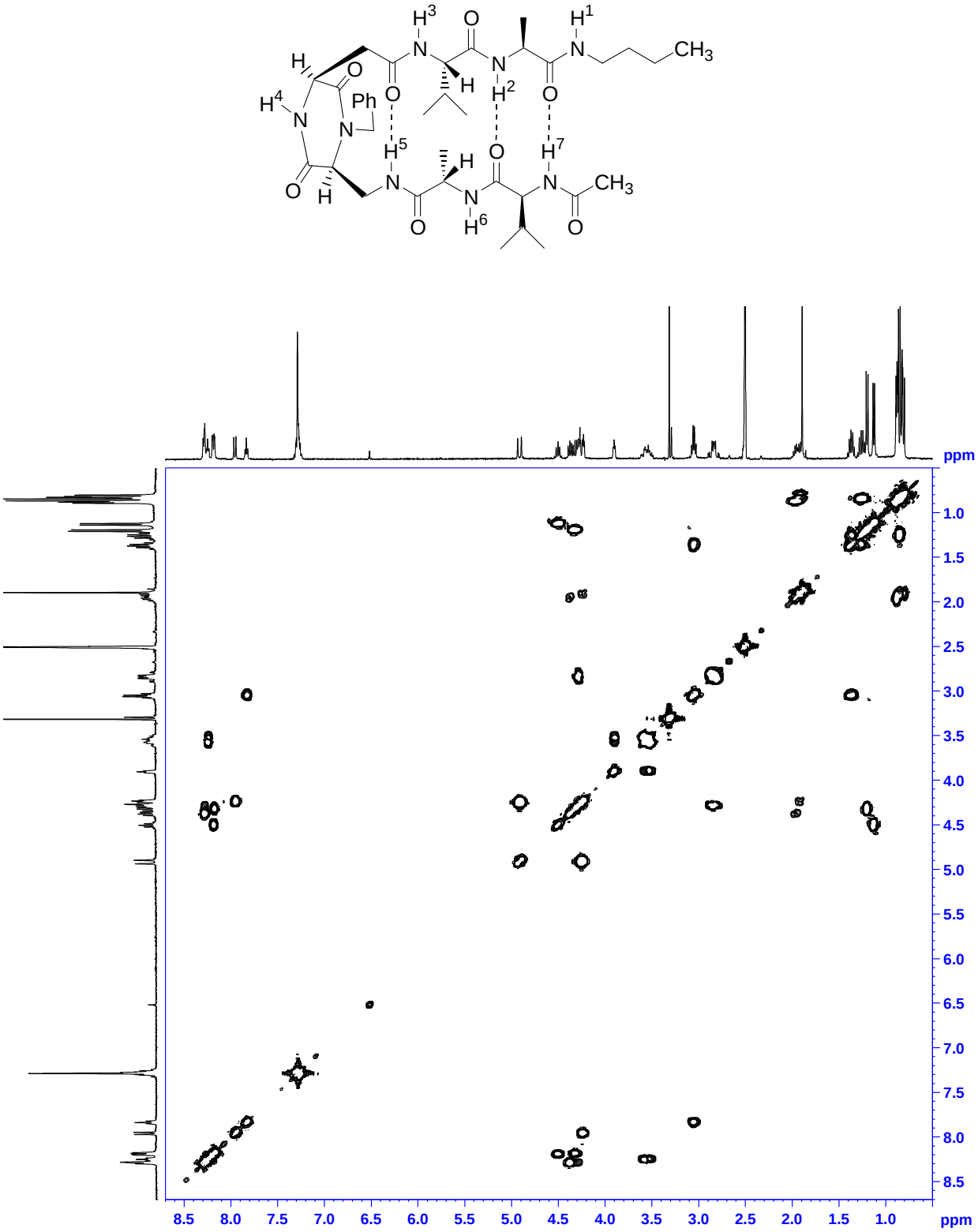

Figure XX. COSY spectra of compound **96** (concentration 2 mM) in DMSO-d_6 at 25 ℃.

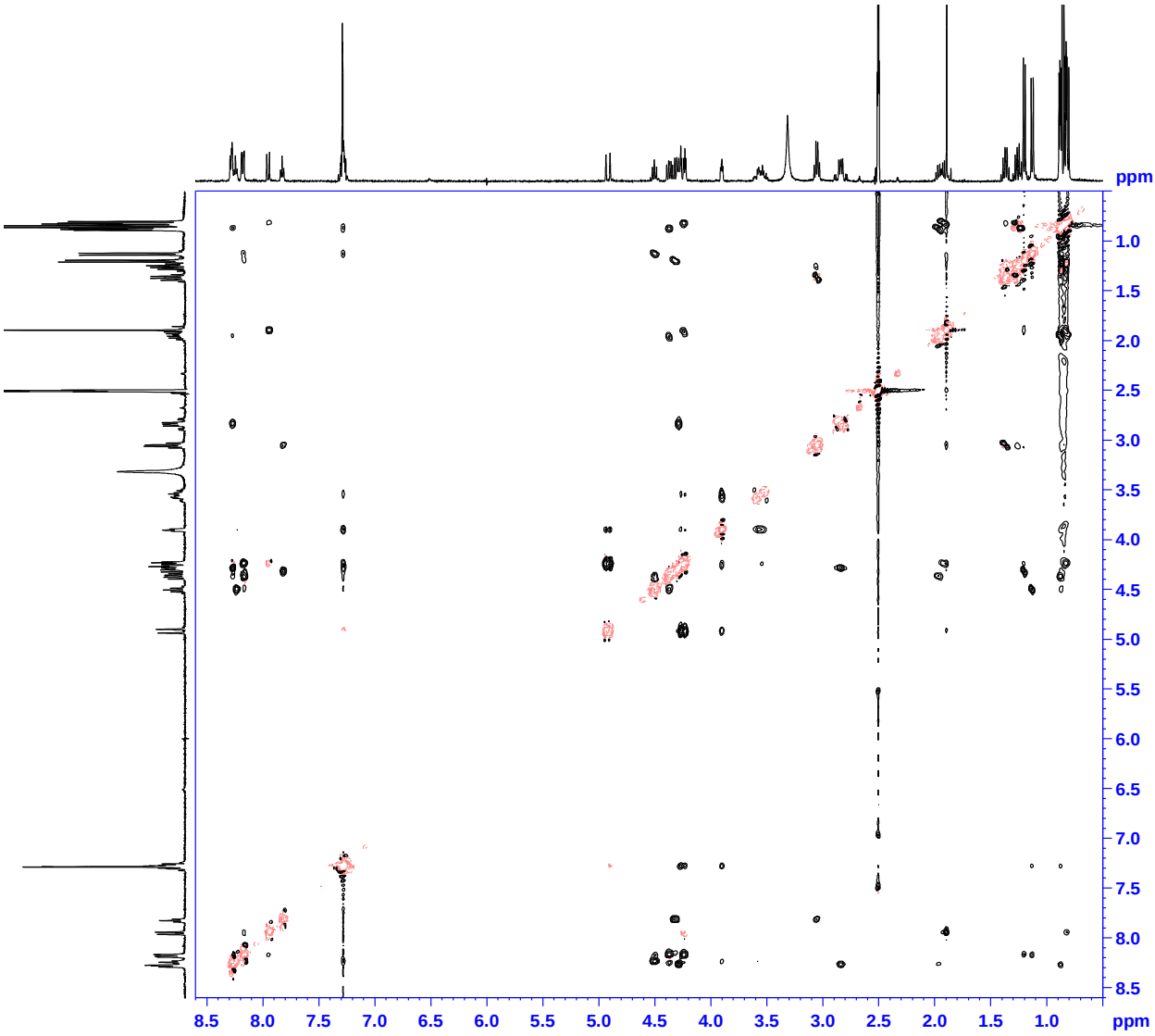

Figure XXI. ROESY spectra of compound **96** (concentration 2 mM) in DMSO-d_6 at 25 ℃, p15 = 400 ms. ROESY data collected with a roesytp pulse program with 1024 data points in F2 and 256 data points in F2.

Table III. ^{1}H-NMR data for the amide protons in compounds **95** and **96**.

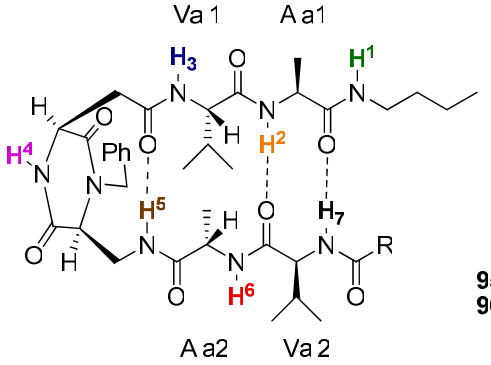

95 R = O-*t*Bu
96 R = CH_3

	95				**96**	
	$\delta^{a,b}$ (ppm)	$\Delta\delta/\Delta T^{a,c}$ (ppb/K)	$^{3}J_{NHCH\alpha}{}^{a,d}$	$^{3}J_{NHCH\alpha}{}^{e,f}$	$\delta^{e,f}$ (ppm)	$^{3}J_{NHCH\alpha}{}^{e,f}$
NH^{1}	6.99	-8.0	5.7	5.6	7.83	5.6
NH^{2}	**8.24**	**-2.5**	**7.7**	**7.4**	**8.19**	**7.9**
NH^{3}	7.61	-15.5	8.0	8.1	8.29	7.2
NH^{4}	7.68	-16.5	-[g]	-[g]	8.28	-[g]
NH^{5}	**7.97**	**-1.3**	**-[g]**	**-[g]**	**8.25**	**-[g]**
NH^{6}	7.42	-8.5	8.0	7.8	8.18	7.8
NH^{7}	5.76	-6.0	6.8	9.1	7.96	8.9

a) Concentration 2.0 mM in 5% CD_3OH-$CDCl_3$; b) at 288 K; c) determined between 248 and 288 K; d) at 278 K; e) Concentration 2.0 mM in DMSO-d_6; f) at 298 K; g) broad signal.